UNIVERSIDAD AUTONOMA
DE MADRID

BIOCHEMISTRY DEPARTMENT

Role of *Smad2* in the processes of neuroplasticity related to hippocampal-dependent spatial learning and memory

DOCTORAL THESIS

Simona Gradari

Madrid, 2017

Biochemistry Department
Faculty of Medicine
Universidad Autónoma de Madrid

Role of *Smad2* in the processes of neuroplasticity related to hippocampal-dependent spatial learning and memory

Simona Gradari
Biology, B.Sc.
Neuroscience, M.Sc.

Director: Dr. José Luis Trejo
Tutor: Dr. Juan Bernal Carrasco

Madrid, 2017

Instituto Cajal (CSIC)

Memoria presentada por **SIMONA GRADARI** para optar al grado de DOCTORA por la UNIVERSIDAD AUTÓNOMA DE MADRID en el PROGRAMA DE DOCTORADO EN BIOQUÍMICA, BIOLOGÍA MOLECULAR, BIOMEDICINA Y BIOTECNOLOGÍA (BIOCIENCIAS MOLECULARES).

JOSÉ LUIS TREJO, Doctor en Ciencias Biológicas y Científico Titular del CSIC,

AUTORIZA la presentación de la Tesis Doctoral titulada "Role of S*mad2* in the processes of neuroplasticity related to hippocampal-dependent spatial learning and memory",
de la que es autora **SIMONA GRADARI**, licenciada en Ciencias Biológicas, y que ha sido realizada bajo mi dirección en el Instituto Cajal, Madrid.

Y para que así conste a los efectos oportunos, firmo el presente certificado en Madrid, el día 23 de Enero de 2017.

Fdo. José Luis Trejo
Instituto Cajal (CSIC)
Madrid

Alla mia famiglia

AGRADECIMIENTOS

Me gustaría aprovechar este espacio para agradecer al Instituto Cajal todo el apoyo que me ha prestado durante estos años, ya que sin él me habría sido imposible llegar hasta aquí. Para mi ha sido un orgullo formar parte del centro de investigación neurobiológica más antiguo de España y contribuir, con este trabajo, a añadir mi gota en el océano de la investigación científica.

Por la misma razón, agradecer en primer lugar a mi director de tesis, el Dr. José Luis Trejo, por guiarme en este trabajo con su capacidad y experiencia científica en un marco de confianza, afecto y amistad, fundamentales para la realización de este trabajo.
Gracias José Luis por tu constante apoyo.

Agradezco al Dr. Sebastián Pons por permitir el desarrollo de esta tesis doctoral acogiéndome durante una breve, pero intensa e imprescindible, estancia en su laboratorio en Barcelona. Y, por supuesto, no puedo no mencionar al Dr. Antonio Herrera y su inconmensurable ayuda para alcanzar los objetivos de mi estancia.
Gracias por vuestra ayuda y amabilidad.

Agradezco de manera especial a la Dra. María De Ceballos que ha representado para mi una referencia, a lo largo de todo mi doctorado, demostrando una generosidad y un altruismo admirable.
Gracias María por toda tu ayuda, tanto material como científica.

Agradezco a la Dra. Laura López Mascaraque por todo el apoyo, ayuda y oportunidades ofrecidas a lo largo de este trabajo.
Gracias Laura y gracias a todos los miembros de tu laboratorio por vuestra continua colaboración.

Quiero agradecer a toda la gente que me ha mostrado su apoyo para sacar adelante este trabajo. Las dificultades se vuelven más sencillas si estás rodeado de buenos compañeros, pero se convierten en experiencias inolvidables si estás rodeado de buenos amigos.

Gracias Paloma por haber hecho de mi doctorado una experiencia tan especial. Hemos caminado mano en la mano en nuestras primeras etapas como investigadoras. Has sido una compañera de trabajo impresionante y, sobre todo, una amiga inolvidable.
Gracias por todo lo que me has dado, por todo lo que me has enseñado y por todo lo que has compartido conmigo.

Agradezco a Ángela por haberme demostrado como la perseverancia, la pasión y la organización en lo que haces da sus resultados. Tenerte al lado ha contribuido a mejorar mi trabajo desde el punto de vista científico, y a desconectar de él cuando hacía falta.
Gracias por tu colaboración y tu energía.

Agradezco a Kerry por su continua disponibilidad en ayudar hasta en los momentos más complicados y frenéticos de la vida de laboratorio. Este trabajo ha sido posible también gracias a ti. Tu tenacidad es de inspiración.
Gracias Kerry por tu amistad, eres una compañera fantástica.

Agradezco a Anna, que con su curiosidad y sus preguntas científicas ha contribuido en desarrollar la comprensión de esta tesis.
Gracias además por tus risas que han contribuido a aliviar mi último año en el laboratorio.

Agradezco a Clara, la maga de los Western Blots, que me ha ayudado en las etapas finales de mi trabajo. Sin ti, estaría todavía peleándome con membranas y proteínas.
Gracias por todo el tiempo que me has dedicado y por compartir conmigo tus conocimientos.

Agradezco a Eva y a Silvia que me han ayudado en la parte de cultivos celulares. Gracias Eva por haber sido tan disponible conmigo. Y gracias Silvia por correr siempre en mi ayuda en los momentos de desesperación. Eres sin duda una de las joyas que me ha regalado este doctorado.

Gracias Sonia, gracias Manu y gracias Dani por haber compartido conmigo tanto, sobre todo hacía el final de cada día de trabajo, cuando lo único que quieres es apagar el ordenador y compartir buenos momentos con buenos amigos. Habéis sido una parte fundamental de este trabajo, gracias a vuestros consejos científicos y a vuestra amistad.

Gracias Manolo: esta tesis empezó porque nuestros caminos se cruzaron hace unos años.
Gracias por haber estado al principio, gracias por haberme soportado y animado en estos años, y gracias por estar a mi lado para celebrar el final.

Y finalmente…
Grazie alla mia famiglia, che mi ha dato tutto e a cui dedico questa tesi.

Summary

Resumen

SUMMARY

The hippocampus is an essential structure of the brain involved in the formation of spatial learning and memory. Moreover, the subgranular zone of the dentate gyrus of adult mammals is a neurogenic niche, where new neurons born from stem cells. Previous evidences suggested a relationship between newborn cells and hippocampal-dependent spatial learning and memory. Neurogenesis is a highly regulated process where external influences, as physical exercise, and internal factors, as transcription factors, have a role in each cell developmental stage. The focus of this thesis is to analyse the role of *Smad2* gene in the regulation of adult hippocampal neurogenesis and its implication in spatial learning and memory. In fact, *Smad2* is an actor of an important cytokine signaling pathway, controlling many processes during development. However, the expression of this gene is very high in the adult dentate gyrus, suggesting a role also in this phase.

The expression of *Smad2* was manipulated in granule cells using genetic modified lentiviral constructs inoculated by means of stereotaxic injections into the dentate gyrus. The results show that *Smad2* is a modulator of plasticity of mature neurons and that it regulates the late-stages of adult hippocampal neurogenesis. A decrease in the expression of *Smad2* leads to a deficit in spatial learning and memory, however a moderate physical exercise is able to improve the behavioural performance. A molecular analysis was also carried out in order to describe epigenetic changes in the hippocampus induced by exercise. Finally, an extensive analysis was realised in order to describe the relationship between adult born neurons and the parameters studied in the Morris Water Maze. The most important findings reveal that: i) there is a negative correlation between task acquisition and behaviour persistence; ii) specific subpopulations of immature cells have a crucial role in the behavioural performance and the decrease in the expression of *Smad2* alters these correlations.

RESUMEN

El hipocampo es una estructura del cerebro que desempeña un papel esencial en el aprendizaje espacial y en la formación de la memoria. La zona subgranular del giro dentado del hipocampo de mamíferos adultos es un nicho neurogénico y ahí reside una población de células progenitoras con funciones de célula madre neural. Evidencias previas sugieren una relación entre las nuevas neuronas y el aprendizaje espacial y la memoria. La neurogénesis adulta es un proceso altamente regulado donde influencias externas, como el ejercicio físico, y factores internos, como los factores de transcripción, tienen un papel en cada etapa del desarrollo celular. Esta tesis se focaliza en analizar el papel del gen *Smad2* en la regulación de la neurogénesis hipocampal adulta y su implicación en el aprendizaje espacial y en la memoria. *Smad2* es un actor de la vía de señalización de una importante citoquina que controla procesos celulares durante el desarrollo. La expresión de este gen es muy alta en el giro dentado de individuos adultos, sugiriendo una función también en esta fase.

Se ha manipulado la expresión de *Smad2* en las células granulares usando constructos lentivirales genéticamente modificados, inoculados en el giro dentado mediante inyecciones estereotáxicas. Los resultados demuestran que *Smad2* es un modulador de la plasticidad de las neuronas maduras y que regula los estadios más tardíos de la neurogénesis hipocampal adulta. Una disminución en la expresión de *Smad2* lleva a un déficit en el aprendizaje espacial y en la memoria, sin embargo el ejercicio físico moderado es capaz de mejorar el rendimiento. Se ha llevado a cabo también un análisis molecular para describir cambios epigenéticos en el hipocampo inducidos por el ejercicio físico. Finalmente, se ha realizado un exhaustivo análisis para describir la relación entre las nuevas neuronas y los parámetros medidos en el laberinto acuático de Morris. Los resultados más importantes revelan que: i) existe una correlación negativa entre la fase de adquisición y la persistencia conductual; ii) ciertas subpoblaciones de células inmaduras tienen un papel crucial en los resultados conductuales y la disminución de la expresión de *Smad2* altera estas correlaciones.

Table of contents

Table of contents

List of abbreviations

LIST OF ABBREVIATIONS

AC, Activity Cage
AHN, Adult Hippocampal Neurogenesis
ALK5, Activin-Like Kinase 5
ANOVA, ANalysis Of Variance
AS, Acquisition Score
B, Basket cell
BCA, BiCinchoninic Acid
BDNF, Brain-Derived Neurotrophic Factor
BLBP, Brain Lipid-Binding Protein
BrdU, 5-Bromo-2'-deoxyUridine
BSA, Bovine Serum Albumin
bw, body weight
C, Control
CA, Cornu Ammonis
cDNA, Complementary Deoxyribonucleic Acid
CldU, Chloro-2'-deoxyUridine
CLR, Calretinin
CNS, Central Nervous System
C_T, Threshold Cycle
DAPI, 4',6-DiAmidino-2-PhenylIndole
DCX, Doublecortin
DG, Dentate Gyrus
DNA, DeoxyriboNucleic Acid
EF1-α, Elongation Factor1-α
EPM, Elevated Plus Maze
EX, Exercised
Ext, Extinction
FST, Forced Swim Test
GABA, Gamma Aminobutyric Acid
GAD, Glutamic Acid Decarboxylase
GDNF, Glial cell line-Derived Neurotrophic Factor
GFAP, Glial Fibrillary Acidic Protein
GFP, Green Fluorescent Protein
GC, Granule Cell
GCL, Granule Cell Layer
HDAC1, Histone DeACetylase 1
HEK 293T, Human Embryonic Kidney 293T cell line
IdU, 5-Iodo-2'-deoxyUridine
IGF-I, Insulin-like Growth Factor 1
LB, Lysogeny Broth
LP, Learning Profile
LPP, Lateral Perforant Path
LTP, Long Term Potentiation
LV, LentiVirus
M, glutamatergic Mossy cell
MAPK, Mitogen-Activated Protein Kinases
MCF, Mossy Cell Fibres
MCM2, Mini-Chromosome Maintenance protein 2
MH1/2, Mad-Homology Domain 1/2
ML, Molecular Layer
MPP, Medial Perforant Path
mRNA, Messenger RiboNucleic Acid

MWM, Morris Water Maze
NeuN, Neuronal Nuclei
NLS, Nuclear Localization Signal
NPC, Neural Precursor Cell
NSC, Neural Stem Cell
NT3, Neurotrophin Type-3
P, Pyramidal Neuron
P/PQ, Platform/Platform Quadrant
Pax6, Paired Box 6
PB, Phosphate Buffer
PBS, Phosphate Buffer Saline
PBTBSA, Phosphate Buffer/Triton X-100/Bovine Serum Albumin
PCNA, Proliferating Cell Nuclear Antigen
PerCross, Persistence Crossing over the platform location
PerPlat, Persistence in the Platform quadrant
PFA, ParaFormAldehyde
pH3, phospho-Histone 3
Prox1, Prospero homeobox protein 1
PrT, Probe Test
PSA-NCAM, Polysialylated Neural Cell Adhesion Molecule
pSMAD2, phospho SMAD2
PVDF, PolyVinylidene DiFluoride
qPCR, Quantitative Polymerase Chain Reaction
RNA, Ribonucleic Acid
RT, Room Temperature
RT-PCR, Reverse Transcription Polymerase Chain Reaction
S, Somatostatin
SARA, Smad Anchor for Receptor Activation
SBE, Smad Binding Element
SDS-PAGE, Sodium Dodecyl Sulphate - PolyAcrylamide Gel Electrophoresis
SED, SEDentary
Ser, Serine
SGZ, SubGranular Zone
shRNA, Short Hairpin Ribonucleic Acid
Smad, Mothers Against Decapentaplegic Homolog
Sox2, Sex determining region Y-box 2
SVZ, Subventricular Zone
TAE, Tris base/Acetic acid/EDTA buffer
Tbr2, T-box brain protein 2
TBS, Tris-Buffered Saline
TGF-β, Transforming Growth Factor-β
TβRI/II, Transforming Growth Factor-β Receptor Subunit I/II
VEGF, Vascular Endothelial Growth Factor
vGlut, Vesicular Glutamate Transporter

Introduction

INTRODUCTION

1. Anatomy of the hippocampus

The hippocampus is a bilateral structure found within the temporal lobes of the hemispheres and it is part of the limbic system (Kandel et al, 2000). It belongs to the philogenetically primitive part of the cortex, the allocortex, with its subdivision called archicortex. It is a three-layered structure, in contrast to the six layers of the neocortex, with a deep plexiform layer, a band of principal neurons and a superficial fibre layer. The name *hippocampus* was given by the italian anatomist Giulio Cesare Aranzio in 1587, who first described the structure, observing the resemblance with the silhouette of a seahorse. The hippocampus itself is divided into two major U-shaped interlocking sectors: the *fascia dentata* (o area dentata, dentate gyrus, DG) and the hippocampus proper (*cornu ammonis*, CA). In 1934, the spanish anatomist Lorente de Nó divided the hippocampus proper into four fields, CA1-4 (De Nó, 1934). He called CA1 the equivalent zone historically named hippocampus *regio superior* by Ramón y Cajal and subdivided the *regio inferior* into CA2 and CA3. CA4 designated the scattered cells inside the hilus of the dentate gyrus. Although these cells are not lined up like the pyramidal cells of CA3, they were included in the hippocampus proper because they have pyramid-like characteristics, they receive the mossy fibres and send their axons into the fimbria. However, unlike the CA3 pyramids, they do not receive an input from the basket cells. The CA2 field consisted of CA3-type pyramids that do not receive the mossy fibres of the dentate granule cells (O'Keefe and Nadel, 1978). In addition, there are two more regions: the subiculum, the most inferior component of the hippocampal formation that lies between the enthorinal cortex and the CA1 subfield; the presubiculum, a modified six-layered cortex between the subiculum and the main part of the parahippocampal gyrus.

Dentate gyrus and CA fields constitute the essentially trisynaptic core circuit of the hippocampus: 1. Afferents from the enthorinal cortex reach the dendrites of the granule cells in the DG through the perforant path, where they form the first synapse; 2. The axons of the granule cells build the

mossy fibre tract that reaches the pyramidal neurons in CA3; 3. The pyramidal neurons of CA3 project via the Schaffer collateral pathway to CA1, where the third synapse is located.

All mammals require the hippocampus for certain types of learning and as an emotional center (Isaacson, 1974). It is defined as the "gateway to memory" because it prepares and evaluates information before long-term storage takes place in neocortical regions (Kempermann, 2002; Redish, 1997). In this way, the hippocampus is not the primary storage area itself, but it is the region where declarative informations (i.e. the knowledge of facts and events) are processed and evaluated. This declarative content is elaborated by hippocampus, relating it in space and time, thus making memory episodic (Marr, 1970; Squire, 1992b). Human long-term memory of episodic contents is considered fundamental for consciousness and self-awareness.

2. Hippocampus-dependent spatial learning and memory: an overview

The hippocampus is part of a system of anatomically related structures in the medial temporal lobe that are important for mammalian memory (Squire, 1992a; Broadbent et al., 2004). Damages to this region lead to impaired performance on a variety of learning and memory tasks (Clark et al., 2000). Moreover, single-cell recording and neuroimaging techniques document changes in the hippocampal region during both learning and retention in humans (Suzuki and Eichenbaum, 2000).

The hippocampus is the region where cognitive maps are created (O'Keefe and Nadel, 1978). Cognitive maps refer to learning about the spatial relationship between cues. Hippocampus may contribute also to path integration that is a form of navigation in which an animal integrates self-movement cues (i.e. vestibular information) to locate its present position or to return to a starting location.

During the past years, evidences were published suggesting a relationship between adult hippocampal neurogenesis (AHN) and various types of learning and memory. This topic is still very controversial because most of the evidences are correlational and some of them do not agree. However, a great amount of data indicates a positive correlation between the number of

adult new-born neurons and the learning performance (Leuner et al., 2012). In fact, many studies have argued that adult generated neurons, having unique physiological characteristics, play a special role in hippocampus-dependent learning and memory (Epp et al., 2013). Hippocampus-dependent learning itself could be a regulator of AHN. In fact, the execution of hippocampus-dependent tasks, but not hippocampus-independent tasks, increases the number of 1-week-old cells born in the dentate gyrus. The Morris Water Maze (MWM), that is the most used and common spatial navigation and memory test, regulates AHN promoting the survival of cells born 7 days before the training and, at the same time, it induces apoptosis of cells born 3 days before. In this way, MWM learning induces the survival of relatively mature neurons, the apoptosis of more immature cells and the proliferation in the DG (Dupret et al., 2007). Many evidences, from experiments modulating AHN (for example, inhibiting apoptosis) suggest that learning itself selectively produces or removes adult-born neurons in the DG according to their function and state of maturation (Deng et al., 2010).

3. Adult neurogenesis

The adult neurogenesis is the production of new neurons under the conditions of the adult brain. New neurons born from stem cells residing in specific regions, called "neurogenic", and then they migrate, differentiate and mature into functioning and electrophysiological active cells. For this reason, neurogenesis is an elaborate process, not just the division of a precursor cell (Kempermann, 2006). This process takes place in regions of the brain characterized by an appropriate microenvironment and by the presence of diffusible elements that permit the neuronal development of intrinsic precursors.

The first control point of the process is the division of the precursor cell and that division can be symmetrical or asymmetrical (Zhong and Chia, 2008). The symmetric division gives birth to two identical daughter cells. The asymmetric one forms two different daughter cells. After the division, many factors are involved to determine when the progeny is to become a neuron. It means, a different gene expression, the migration of the cell from the

germinative layer to the final destination, the development of dendrites and axon that make connections and form synapses. The process of neurogenesis involves also the achievement of all the electrophysiological requirements and the ability to generate action potentials.

It is very important to define the word "adult": in this context, *adult* neurogenesis means the born of new neurons from the earliest stage of sexual maturation of the animals. It is different from the term *postnatal* because, even if the adult neurogenesis is of course a postnatal process, it happens only after the sexual maturation. While postnatal neurogenesis is considered as a direct continuation of embryonic and foetal neurogenesis, adult neurogenesis takes place in a cellular environment that has terminated its development. Another difference between postnatal and adult neurogenesis is that the first one can takes place in many parts of the brain while the second one only in specific regions. Considering only the Central Nervous System (CNS), the adult neurogenic regions discovered in mammals are two: the subventricular zone (SVZ) in the temporal walls of the lateral ventricles, that produces a progeny migrating over a long distance along the rostral migratory stream to the olfactory bulb (Mirzadeh et al., 2008; Fuentealba et al., 2012; Lim and Alvarez-Buylla, 2014); and the subgranular zone (SGZ), a granule cell layer in the dentate gyrus (DG) of the hippocampus (Kempermann et al., 2015) (Fig. 1).

A neurogenic region in the adult brain is defined for the presence of a germinative matrix with a significant production of new neurons throughout life and not only for the presence of neurogenic precursors. "Permissiveness" is an important concept to better define a neurogenic region: when a neural precursor cell (NPC) has been implanted in a neurogenic region, it should develop into a neuron while when it is grafted into a non-neurogenic region it should develop into a glial cell or die (Shihabuddin et al., 2000; Morrens et al., 2012). It is important the presence of precursor cells in the region but it is not the only requisite to define the "neurogenicity". It is also fundamental the presence of a microenvironment, consisting of cell-cell contacts and diffusible factors promoting neuronal development. A non-neurogenic region could contain precursors but, if there is not the permissiveness microenvironment, they cannot develop into neurons.

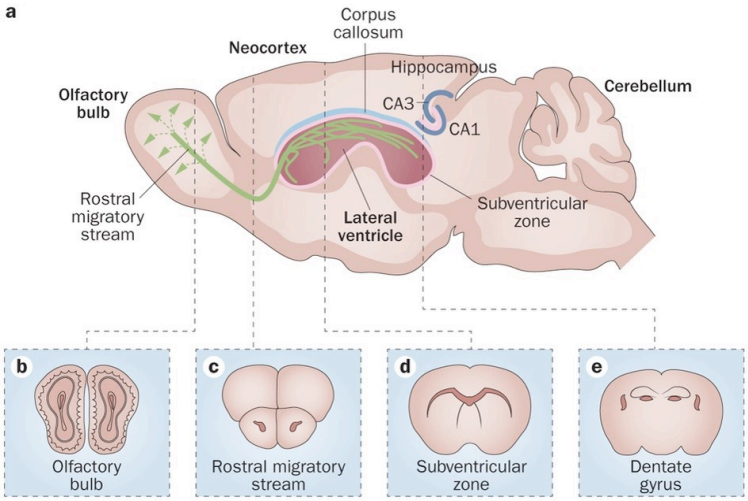

Fig. 1 Neurogenic regions in the adult mouse brain. A. Representation of a sagittal section of an adult mouse's brain. **B-C-D-E.** Coronal sections of regions involved in AHN: the olfactory bulb, the rostral migratory stream, the subventricular zone and the dentate gyrus (from Ziegler et al., 2015).

Precursor cells in the neurogenic zones are so inserted in such microenvironment with which they form a functional unit, called stem cell niche or germinative niche (Li and Xie, 2005). Niches are defined as local microenvironments that maintain and regulate stem cells; they provide nurturing factors and the interactions between stem cells and their neighbour cells determine many vital properties, including self-renewal, proliferation, differentiation and fate determination (Fuchs et al., 2004).

3.1 Neurogenesis in the adult hippocampus

The dentate gyrus consists of a densely packed granule cell layer (GCL), the molecular layer (ML) and the underlying polymorphic cell layer of the hilus. The granule cell (GC) is the principle cell type of the DG and it is part of the local circuitry (Fig. 2).

The precursor cells of the dentate gyrus reside in the SGZ, a narrow band of tissue between the granule cell layer and the hilus. Descriptively, the SGZ is defined as a layer about three cell nuclei wide (20 or 25 μm) and it provides the microenvironment permissive for neuronal development throughout life. So, it is recognized as a germinative matrix.

From their birth to their differentiation in the SGZ, the granular precursor cells proceed through a series of stages that can be identified by means of

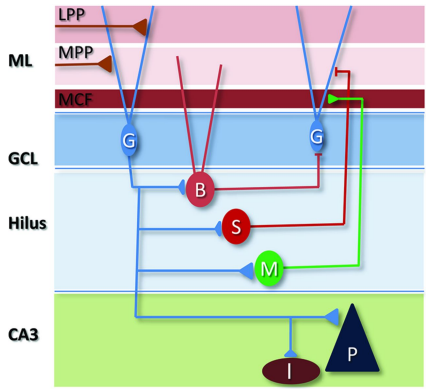

Fig. 2 Local circuitry of the dentate gyrus. Granule cells (G) extend their dendrites to the molecular layer (ML) and here they receive three primary bands of excitatory drive from proximal to distal mossy cell fibres (MCF), medial entorhinal cortical inputs through the medial perforant path (MPP) and lateral entorhinal cortex through the lateral perforant path (LPP). Granule cells send outputs to a number of cell types in the hilus, as the glutamatergic mossy cells (M), various GABAergic interneuron subtypes, as the basket cells (B) and dendritic targeting neurons expressing somatostatin (S). Cells from hilus project back to the GCL and project to the pyramidal neurons (P) and GABAergic interneurons (I) in the CA3 region (from Drew et al., 2013).

immunohistochemistry. The hippocampal neural stem cells are called type-1 cells and they generate type-2 and type-3 cells that are transiently amplifying populations of progenitors. It is possible to identify them based on morphology, marker expression and proliferation kinetics (Kempermann, 2006) (Fig. 3).

Type-1 cells have a unique radial process and ramified structure at their end. This population of cells draws attention because its morphology is reminiscent of radial glial cells that serve as NSCs during development. These cells also express *Glial Fibrillary Acidic Protein* (GFAP), *Nestin*, *Brain Lipid-Binding Protein* (BLBP) and *Sox2*, consistent with their conserved expression in radial glial cells. They have a triangular cell body and under physiological conditions, a type-1 cell is not so proliferative active (they are also known as quiescent neural progenitors). Recently, it has been suggested that the age-related decrease in hippocampal neurogenesis could be due to the conversion of the neural stem cells in mature hippocampal astrocytes after a rapid succession of asymmetric divisions (Encinas et al., 2011).

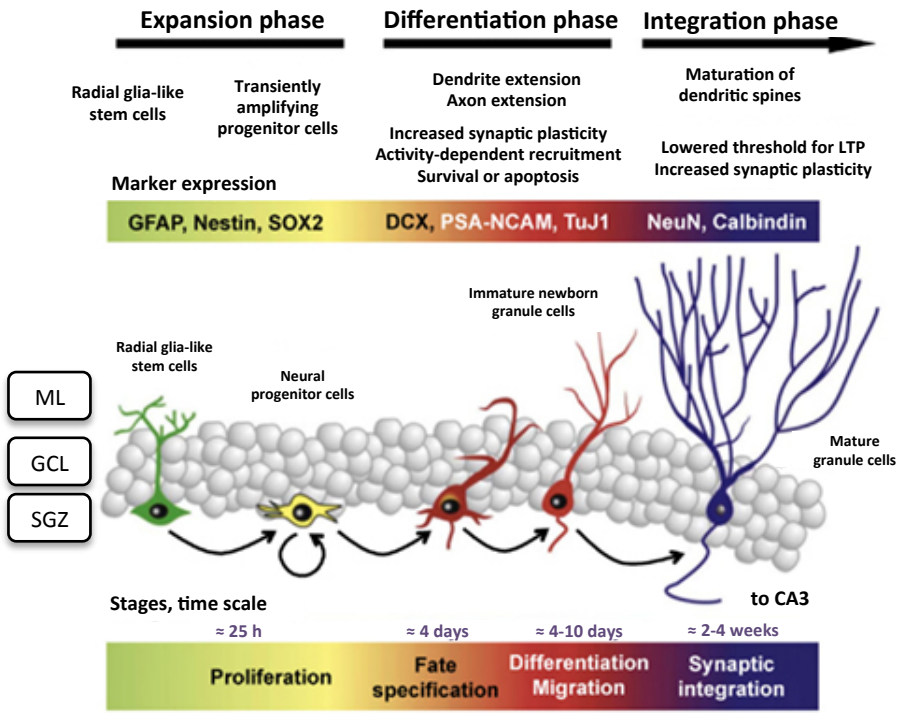

Fig. 3 Cells developmental stages in the adult hippocampus. Neural stem cells born in the SGZ of the DG. Here they proliferate, differentiate and start to migrate into the GCL (modified from Schouten et al., 2012).

Type-2 cells have either no process or a very short process. The morphology of this population of cells supports the possibility of a tangential migration during this stage and they have an irregularly shaped nucleus with dense chromatin. These non-radial cells maintain the expression of *Nestin* and *Sox2* but they do not express *Gfap*. Type-2 cells come in two subtypes, one negative (type-2a) and one positive (type-2b) for immature neuronal marker *Doublecortin* (DCX). Type-2 cells are highly proliferative (Kronenberg et al., 2003). The type-2 stage comprises the transition from a glia-like precursor cell to a neuronal determination.

Type-3 cells are the last identified type of proliferating cells. They can still divide, but less than type-2 cells. This stage is especially characterised by morphological changes. Type-3 cells have a horizontal orientation like type-2 cells, but often with longer horizontal processes. It is also possible to find cells at this stage with a more vertical orientation. The nucleus is rounded, so with a more definitive morphology. They are *Doublecortin* positive but *Nestin* negative. They invariably express *PSA-NCAM*. This is the stage of

radial migration into the granule cell layer. Sometimes radial migration begins at the stage of type-2b cells, but the migrating cells readily lose their *Nestin* expression when they reach the granule cell layer. Type-3 cells (and so type-2b) express the transcription factor *Prox1*, which remains expressed throughout granule cell development and in adult granule cells (Kronenberg et al., 2003). The type-3 stage comprises a transition from a potentially proliferative state to post-mitotic immature neuron.

The fate choice decision of new neurons come early and those cells that express neuronal markers, such as *NeuN*, are likely to become persistently integrated into the granular cell layer. The early post-mitotic stage of granule cell development during adult hippocampal neurogenesis is characterised by the transient expression of *Calretinin* (CLR). Brandt and colleagues reported studies about the founding in the adult murine SGZ of a number of cells expressing C*alretinin* and containing proliferation marker bromodeoxyuridine (BrdU) that had been injected into the animals 4 weeks earlier (Brandt et al., 2003). Cells switch the expression of *Calretinin* for *Calbindin* during the maturation process. The change in calcium-binding proteins occurs very rapidly and in mice takes place approximately 2 to 3 weeks after the cells have become post-mitotic. *Calretinin*-positive cells are localised in the SGZ and there are no distinguishable differences in the localization of *Calretinin*- or *Calbindin*-expressing newborn cells and cells expressing *NeuN*.

3.2 Effect of exercise on adult hippocampal neurogenesis

Adult neurogenesis is dynamically regulated by many factors, as environmental influences and psychotropic drugs. It is down-regulated by stress, aging, glucocorticoid hormones and drugs of abuse, whereas it is up-regulated by an enriched environment, exercise, hippocampal-dependent learning, estrogens, anti-depressant drugs, lithium, etc... (Lee and Son, 2009) (Fig. 4).

In recent years, physical exercise has emerged as the most effective way to prevent age-related neurodegenerative disease, to mitigate depression and to improve learning and memory, particularly in elderly populations (Cotman and Berchtold, 2007).

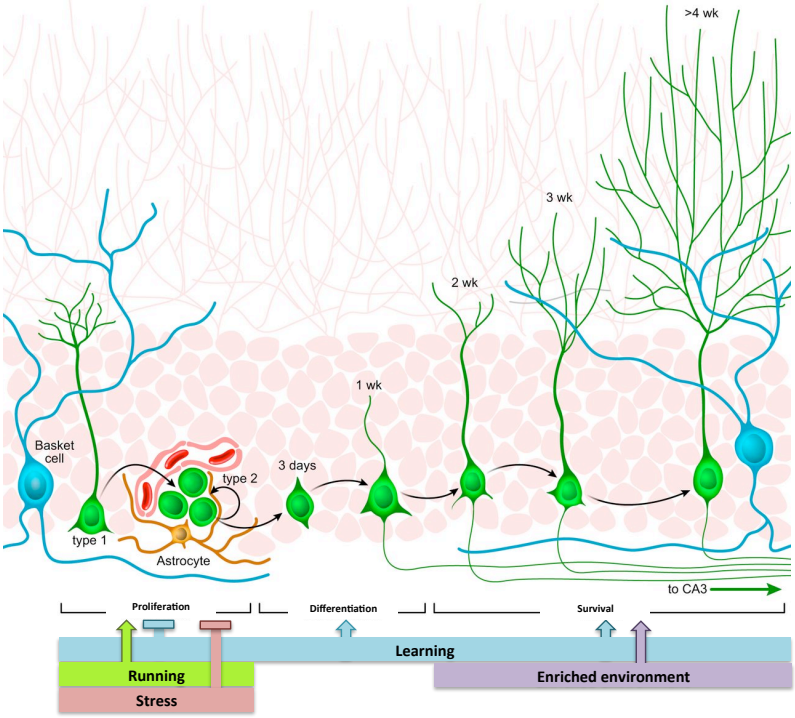

Fig. 4 Regulation of adult neurogenesis. Experiences as stress, learning, enriched environment and physical activity modulates adult hippocampal neurogenesis at many levels (modified from Aimone et al., 2014).

In fact, exercise increases synaptic plasticity and it reinforces processes as neurogenesis, metabolism and vascular function. So, it is commonly known that exercise regulates positively adult hippocampal neurogenesis.

For rodents, cognition is almost inseparable from locomotion. Physical activity, especially exerted over long periods of time, might indicate to the brain an increased chance of experience those situations rich in complexity and novelty that presumably benefit from more new neurons (Kempermann, 2008). Most investigations of exercise-induced neurogenesis in mice and rats have been performed using the running wheel paradigm. In this way, mice have free access to a running wheel located in their cage. Forced treadmill training has a similar up-regulating effect with the difference that in this way the time, the speed and the modality by which it is performed are controlled. Exercise protocols can vary widely across experiments, so it is necessary to find the optimal form, intensity and duration depending on the purpose (Leasure and Jones, 2008; Gradari et al., 2016b). There are several candidate molecules that could play a role in exercise-induced up-regulation of neurogenesis in the adult brain (Pérez-

Domper et al., 2013). Many factors have been shown to increase in both the circulation and the adult brain after physical exercise, among these it is possible to detect: β-endorphins (Koehl et al., 2008), the vascular endothelial growth factor (VEGF) (Olson et al., 2006), the brain-derived neurotrophic factor (BDNF) (Vaynman et al., 2004), the glial cell line derived neurotrophic factor (GDNF) (Chen et al., 2005), the neurotrophin type-3 (NT3) (Ickes et al., 2000), the insulin-like growth factor 1 (IGF-I) (Trejo et al., 2001) and serotonin (Ernst et al, 2006).

The relationship between physical activity and brain is very tight. The way the brain works changes along with the level of physical activity. These changes range from neural cell metabolism and gene expression, neuronal arborisation and spine density, blood-brain barrier properties and growth factor's concentration. Exercise itself can even be considered a form of stress. It has been proposed that under certain conditions exercise might even increase the susceptibility to glucocorticoid-induced suppression of neurogenesis (Stranahan et al., 2006). So, in some circumstances, exercise can induce negative effects representing a thermal, metabolic, hypoxic, oxydative or even a mechanical stress (Peake et al., 2015). For this reason, it has been introduced the hypothesis that exercise produces a hormetic response not only for physiological parameters, but also for brain health (Radak et al., 2008). Hormesis consists in a biphasic dose-response in which a low dose of a stressful stimulus activates an adaptive response that increases the resistance to a moderate-to-severe level of stress (Calabrese, 2008). In humans, many evidences from cognition performances after exercise show an inverted-U curve profile of the responses (Gómez-Pinilla and Hillman, 2013; Tomporowski, 2003): the increasing positive effects of physical exercise correlate with the intensity of the training protocol. When it reaches strenuous levels, the response starts to decline leading to detrimental effects or no effects at all. It is not completely predictable the effect of exercise because it depends not only on the intensity, but also on the duration of the training, on the previous individual's fitness level and on the motivation of the subject. In particular, the detrimental effects start when the activity reaches the anaerobic threshold. Intense exercise, above lactate threshold, induces brain mitochondrial dysfunction (Aguiar et al., 2008), it increases oxygen consume and it is associated to variation in

energy metabolism (Coyle, 2000).

Forced exercise can induce negative effects when performed after a deep brain surgery (Jun et al., 2012). Surgery leads to a decrease in the maximum positive response to exercise, reducing the hormetic zone (Calabrese, 2008).

A biphasic dose-response to exercise on cognition was observed also in animal models: memory retention in an object recognition task was significantly improved at low-moderate intensity exercise while high or very-high intensity protocols did not induce effects or lead to negative results on discrimination (García-Capdevila et al., 2009).

What is worthy of note is the increasing amount of evidences showing that both positive and negative effects of exercise are mediated by the same factors in a hormetic-like biphasic dose-response. For example, some positive effects of exercise correlate with an increase in levels of BDNF (Marosi and Mattson, 2014) and IGF-1 (Llorens-Martín et al., 2009). At the same time, high levels of these factors may induce negative effects on the brain (Ramsden et al., 2003). As vascular factors regulate neural plasticity, it has been suggested that exercise can indirectly modulate adult hippocampal neurogenesis in a biphasic dose-response way (for more details, see in Appendix Gradari et al., 2016b).

4. Effects of the growth factors on adult neurogenesis

During development, the growth factors play an important role in the differentiation and maturation process of the neurons. This process is characterized by a well-coordinated and sequential set of actions, mediated by the circulating molecules and the interaction with their transmembrane receptors in the targeting cell. The sequence of interactions and outcomes follow a continuous and circular diagram producing a situation previously described by our research group as “the chicken or the egg” dilemma (Fig. 5) (for further details, see Pérez-Domper et al., 2013).

However, in the adult brain, new neurons develop in a pre-existing circuit where interactions are already established. The survival-death decision modulated by growth factors is strictly dependent on the accessibility of the new neurons to those molecules in a competitive manner, as a function of

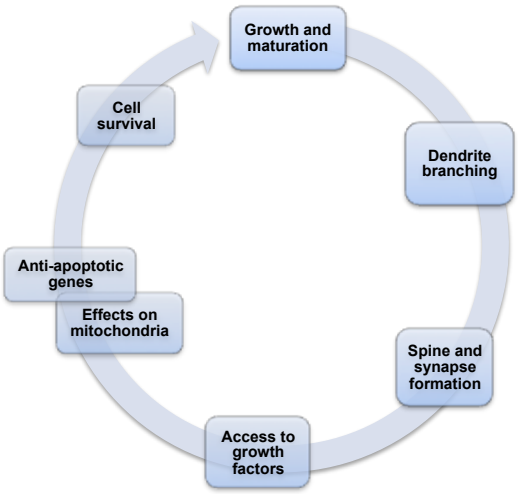

Fig. 5 Effects of growth factors on the development and differentiation of a neuron (modified from Pérez-Domper et al., 2013).

the system's necessities. These necessities are, in turn, dependent by the physical-cognitive activity of the individual. The growth factor-dependent fate of a neuron, in the adult hippocampus, is strictly connected with the entry of the granule cell dendrites in the two outermost thirds of the molecular layer, so with the arborisation development and spine formation. The survival decision in a pre-established circuit is very important because has to be meaningful and necessary for the system. For this reason, growth factors are fundamental for the selection of newborn neurons during adult hippocampus neurogenesis. During a short time window, the growth factors released by the pre-synaptic endings of entorhinal axons at the outer molecular layer of the dentate gyrus contributes to decide the survival of the new granule cells, promoting the formation of new contacts between cells (Fig. 6).

This thesis is focused on the role of one of the principle actor of the Transforming Growth Factor-β signal pathway, that is *Smad2*, and in the mechanisms by which the selection of the newborn neurons is achieved in the adult hippocampus.

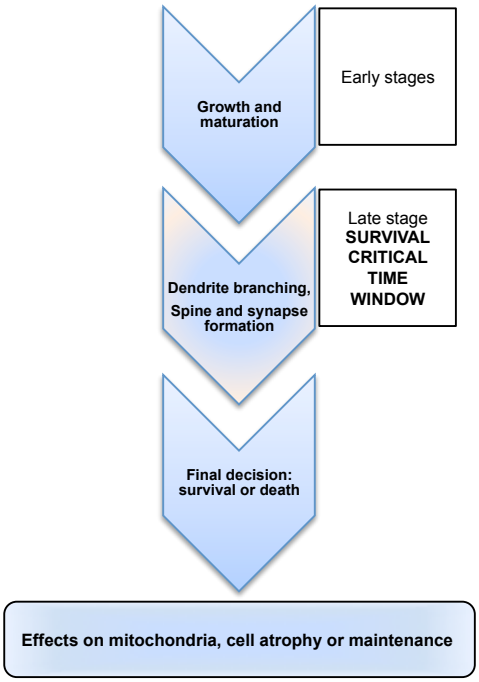

Fig. 6 During adult hippocampal neurogenesis, post-mitotic cells go through a critical time window during late maturation. Dendrite branching and spine formation is peaking around 2-4 weeks after cell birth at the two outer third of the molecular layers (from Pérez-Domper et al., 2013).

5. SMAD2 protein and the Transforming Growth Factor-β pathway

Smad2 is one of the main players of the Transforming Growth Factor-β (TGF-β) pathway that is a cytokine signaling pathway controlling many processes during development and tissue homeostasis. The flair of this pathway is its functional versatility being able to adapt to different functions, depending on the conditions. Cell proliferation, differentiation, migration and apoptosis are events controlled by TGF-β signal and elegantly coordinated by SMAD proteins. SMAD2 represents a node for signal integration acting as a transcription factor.

TGF-β molecules are produced and released by many parenchymal cell types and infiltrating cells such lymphocytes, monocytes, macrophages and platelets (Massagué et al., 2005). TGF-β acts through transmembrane serine/threonine protein kinase receptors (TβRI and TβRII): TGF-β binds the constitutively active TβRII that recruits TβRI forming a heterotetrameric complex. TβRII phosphorylates TβRI which, in turn, phosphorylates a number of proteins activating multiple downstream signaling pathway. TβRI phosphorylates the C-terminal of SMAD2 protein (a Ser-X-Ser motif). This

phosphorylation allows SMAD2 to bind other proteins, forming strategic complexes useful to enter into the nucleus, bind DNA and act as a transcription factor (Brown et al., 2007) (Fig. 7).

The *Smad* family is constituted by 3 functional groups: the receptor-activated Smads (R-Smads); the common mediator (Co-Smad); and the inhibitory Smads (I-Smads). In vertebrates, SMAD2 and SMAD3 are R-Smads phosphorylated in response to TGF-β and activin, whereas SMAD1, SMAD5 and SMAD8 are phosphorylated in response to the Bone Morphogenetic Proteins (BMPs). Thanks to the receptor-mediated phosphorylation, the R-Smad proteins can bind SMAD4 (a Co-Smad) and translocate to the nucleus. In order to prevent a persistent Smad signaling, one mechanism that provide regulation with negative feedback is represented by the I-Smad proteins, as SMAD6 and SMAD7, that inhibit R-Smads activation by competing for binding to TβRI. Smad proteins are characterized by two highly conservative regions: Mad-homology domain 1 (MH1) at the N-terminal and Mad-homology domain 2 (MH2) at the C-terminal. In a dephosphorylated state, R-Smads exist primarily as cytoplasmic monomers because they are auto-inhibited through an interaction between their own MH1 and MH2 domains. The Smad Anchor for Receptor Activation (SARA) is a protein associated with cell membrane containing an 80 amino-acidic Smad binding domain and a FYVE phospholipid-binding domain that strongly binds monomeric R-Smads (Di Guglielmo et al., 2003). Upon phosphorylation, SMAD proteins undergo a conformational change leading to a lower affinity for SARA. The phosphorylated R-Smads leave the anchor protein and form heteromeric complexes with SMAD4. Phosphorylation on Ser465 and Ser467 of SMAD2 allows the oligomerization with the common mediator. Mutations in one of these serines prevent the formation of SMAD2/SMAD4 complexes, leading to a decrease in nuclear concentration and a decrease in SMAD2 transcriptional activity in response to TGF-β.

The conformational change leads also to unmask the Nuclear Localization Signal (NLS) sequence contained in MH1. Although this sequence enables SMAD2 to enter inside the nucleus without any protein's help allowing the direct interaction with nucleoporins, as demonstrated in many cell cultures

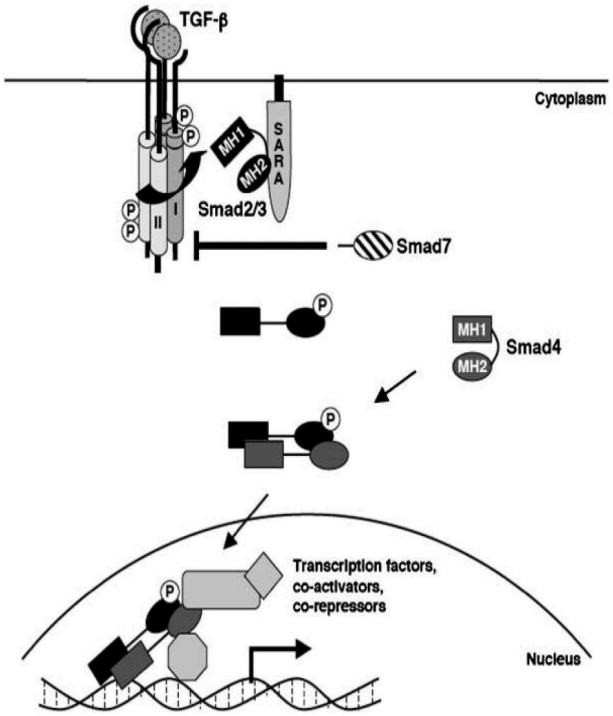

Fig. 7 Activation of TGF-β signaling and the SMAD pathway (from Brown et al., 2007).

studies (Fink et al., 2003; Calonge and Massagué, 1999; Liu F. et al., 1997), the nuclear translocation of SMAD2 alone is not sufficient to activate the transcriptional response. The association of the SMAD2/SMAD4 complex is essential for the transcriptional pathway but it can be formed either in the cytoplasm or in the nucleus. SMAD2/SMAD4 complexes have the ability to target different genes and activate or repress their expression. It is worth noting that SMAD4 and almost all the R-Smads can directly bind DNA, with one exception: in vertebrates, two spliced variants of *Smad2* are known. The most abundant SMAD2 protein contains an insert in the MH1 domain that prevents the binding with DNA (Shi et al., 1998). This insert is encoded by exon 3 so the lacking version of the protein is called SMAD2ΔE3. What is very interesting, but still unknown, is its function. In fact, while *Smad2*-null mice suffer an early embryonic lethal phenotype because *Smad2* has a crucial role in establishing the anterior-posterior axis within the epiblast and the formation of endoderm (Waldrip et al., 1998), mice engineered to exclusively express *Smad2ΔE3* are viable and fertile (Dunn et al., 2005).

The promoter regions of many Smad-responsive genes contain one or more Smad Binding Elements (SBE). However, SMAD2/SMAD4 complex has low

affinity for these regions. To improve the binding efficiency, many different co-factors are incorporated in the protein complex: in this way, the SMAD transcriptional complexes gain a higher affinity and selectivity for the target genes explaining the pleiotropic nature of the TGF-β signal. TGF-β can target several hundred genes in a specific cell but every SMAD complex activates or represses the transcription of few genes. So, a cell that does not express a particular SMAD2 partner, is not able to induce the response of the genes depending on that cofactor and this is determinant to confer cell specificity to TGF-β's response. However, it is still not so easy to understand how these complexes are able to manage hundreds of target genes in the same cell and at the same time. TGF-β signal promotes either cell proliferation or survival, among other activities, depending on the molecular circumstances.

The commitment of cell fates in the nervous system is deeply dependent on SMAD2 signaling cascade. However, many opposing results have been published on the role of *Smad2* for neuronal precursor proliferation and differentiation, indicating that SMAD2 action depends on local, temporal and contextual characteristics (Ueberham and Arendt, 2013).

5.1 *Smad2* expression in the nervous system

The development of the nervous system is strictly associated to SMAD proteins, from the earliest stages of neuralization of the ectodermal cells to the onset of neurological diseases. During neurulation, the suppression of *Smad2* signaling specifies neuroectoderm generation while the stimulation of this pathway blocks the neural induction and promote the non-neural fate of the cells (Chang and Harland, 2007). In the developing brain, the primary neurogenesis is also dependent on SMAD proteins because the neural stem cells need signals to decide their fate. So, while TGF-β promotes the differentiation of the radial glial cells toward astrocytes by activation of mitogen-activated protein kinases (MAPK) signal (Stipursky et al., 2012), neurogenesis depends on SMAD2 activity. The commitment of cell fate in the nervous system is closely arranged by SMAD2 signaling cascade, as well as the further differentiation steps (dendritic and axonal growth, myelination and synapse formation).

Previous experiments with homozygous mutant embyos (*Smad2*$^{-/-}$) showed that the organism fail to form an organized egg leading to a precocious death. About 20% of *Smad2* heterozygous embryos (*Smad2*$^{+/-}$) had sever gastrulation defects and lack mandibles or eyes, demonstrating that *Smad2* function is essential for early development and for several patterning processes in mice (Nomura and Li, 1998). Studies with mice lacking *Smad2* in the CNS (*Smad2*-CNS-KO) displayed behavioural abnormalities in motor coordination from an early postnatal stage: these animals showed aberrant cerebellar layers with an increased apoptotic cell death, delayed migration and maturation of granule cells and retardation of dendritic arborisation of Purkinje cells (Wang et al., 2011).

In the adult animal, it has been discovered that the brain has the highest Smad baseline activity among any other major organ. A study with SBE-luciferase reporter mice has shown that the highest activity is localized in the hippocampus and just lower signals were found in the neocortex, brainstem, thalamus and cerebellum (Luo et al., 2006). Moreover, the activated TGF-β pathway, identified using pSMAD2 as immunohistological marker (Massagué, 2000), is localized predominantly in neurons while no signals were detected in astrocytes or microglia. The presence of active SMAD2 in an adult neurogenic niche suggests that TGF-β could play an important role in the adult hippocampal neurogenesis. However, many contradictory results have been published about the function of *Smad2* on neuronal precursor proliferation and differentiation.

Previous studies demonstrated that the intracerebroventricular infusion of TGF-β1 in the brain of adult rat inhibits the proliferation of neural progenitor cells in the dentate gyrus and in the lateral ventricle wall (Wachs et al., 2006). In transgenic *TGF-β1* mice (expressing a constitutively active *TGF-β1* under a GFAP promoter), the over-expression of *TGF-β1* in glial fibrillary acidic protein positive cells reduced the proliferation of the NPCs (Buckwalter et al., 2006). This effect could be explained considering TGF-β signal responsible for sustaining the quiescent state of the stem cells and/or for supporting the survival of the newly generated neurons (Kandasamy et al., 2014; Kandasamy et al., 2010).

In the SGZ, most of the GFAP$^+$ cells as well as almost all the GFAP$^+$/Sox2$^+$ cells, MCM2$^+$ or Tbr2$^+$ progenitor cells are lacking pSMAD2 signal. About

95% of the pSMAD2$^+$ cells are mature NeuN$^+$ neurons and the remaining 5% are pSMAD2$^+$/DCX$^+$ cells. More than 95% of the pSMAD2$^+$/DCX$^+$ cells do not express the proliferative cell nuclear antigen PCNA, indicating post-mitotic immature neurons (He et al., 2014) (Fig. 8). The expression pattern of pSMAD2 in the hippocampal stem cell niche is primarily present in cells with neuronal commitment and neuronal identity, suggesting a function in the late-stages of neurogenesis.

Interestingly, also the other type of R-Smad, *Smad3*, is highly expressed in the DG. It is first expressed by the intermediate progenitors (type 2 cells) and the expression persists during the following developmental stages and in the mature neurons (Tapia-González et al., 2013).

The TGF-β canonical pathway involves the activation of the TGF-β type I receptor activin-like kinase 5 (TβRI or ALK5). The hippocampal neurogenesis was characterized in conditional knockout mice for *ALK5* (*ALK5*^{cKO}), with a 70% decrease in ALK5 and 20% in SMAD2 (He et al, 2014). The reduction of ALK5 does not affect the production of committed neurons from progenitors, but it reduces the survival of DCX$^+$ newborn neurons. A lentivirus-mediated knockout technique (LV-cre-eGFP) was used to acutely reduce *ALK5* expression in *CAMKIIa*-expressing cells in the adult dentate gyrus of *ALK5*$^{loxP/loxP}$ mice. Dividing cells were labelled with BrdU after the stereotaxic injections and the brains were analyzed 28 days later: the percentage of BrdU$^+$/NeuN$^+$ cells was decreased as well as the total number of DCX$^+$ and DCX$^+$/GFP$^+$ cells.

In the same way, the injection of a retrovirus expressing a shRNA against *ALK5* in the hippocampus leads to a decrease in the number of DCX$^+$/GFP$^+$ cells 14 days post-injection, suggesting that ALK5 is required for the survival of the newborn neurons in a cell-autonomous way. Moreover, the DCX$^+$/GFP$^+$ cells appeared with a shorter arborisation and a decelerated migration into the granular cell layer. On the other hand, the hippocampal neurogenesis was also studied in transgenic mice in which a constitutively active *ALK5* transgene and a reporter eGFP are expressed under a *CAMKIIa* promoter (*ALK5*^{CA}) (He et al, 2014). The transgenic modification induces the canonical TGF-β signaling in absence of the TGF-β ligand *in vivo*. *ALK5*^{CA} showed a 60% increase in the number of DCX$^+$ cells in the GCL, while there were no differences in the number of Sox2$^+$ neural stem cells. Moreover,

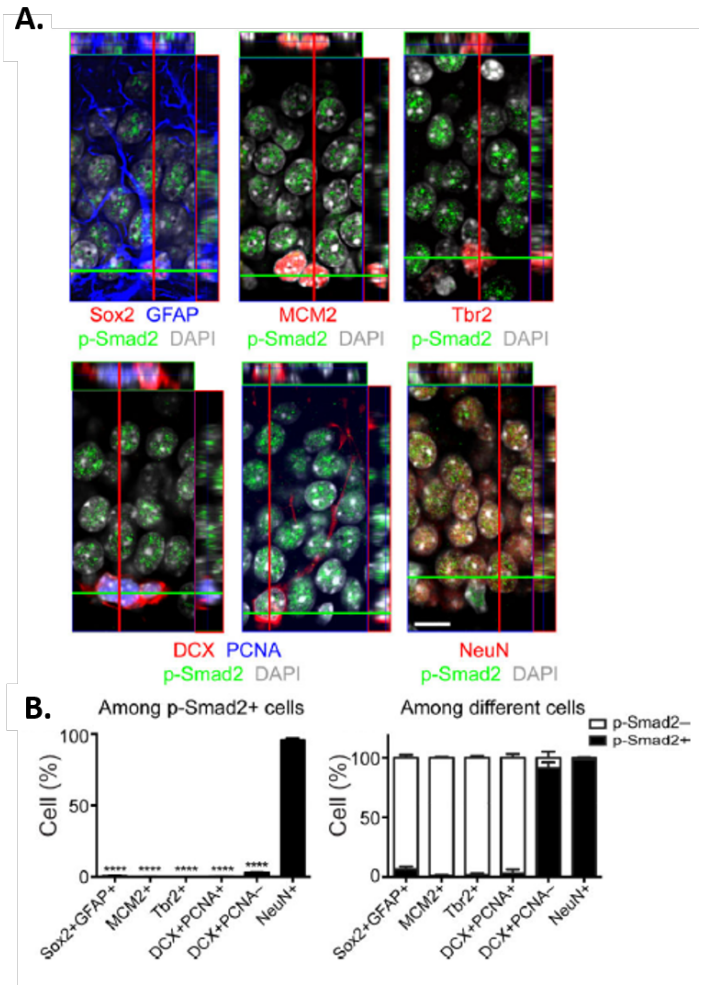

Fig. 8 **A.** Projections from confocal stack images of the DG of 2-month-old mice. **B.** Quantification of pSMAD2^{+} cells in the DG (modified from He et al., 2014).

treatments with analogues of thymidine suggest that cell proliferation and neuronal commitment are not altered by the activated TGF-β signaling. To determine how *ALK5* might increase the survival of neurons, the number of cells undergoing apoptosis and some proteins involved in cell death were assessed. *ALK5*^{CA} mice displayed three-fold fewer apoptotic cells in the SGZ and had two-fold more anti-apoptotic proteins than its control. Moreover, the newborn neurons in *ALK5*^{CA} mice show a higher *c-fos* expression and this increased activity lead to an improvement in hippocampus-dependent learning and memory tasks. The loss of *ALK5* in progenitor cells seems to affect the survival, the maturation and the migration of the immature neurons, while an increase in TGF-β signaling promotes the neuronal migration, maturation and survival antagonizing the apoptotic pathway. ALK5-dependent TGF-β signaling is so necessary to maintain wild-type

levels of neurogenesis in the dentate gyrus (He et al, 2014). Endogenous *Smad2* is constitutively activated in human and mouse hippocampal neurons. In granule neurons, at higher levels of *Smad2* corresponds lower levels of the modulator *SnoN* which strongly enhances axonal growth and neuronal branching. The constitutive expression of axonal growth inhibitors, as *Smad2* and *Smad3*, and the reduced expression of promoters, as *SnoN*, in terminally differentiated neurons creates a mechanism of control that allows a balance between a steady state and the neuronal plasticity (Ueberham et al, 2006; Ueberham et al., 2009; Stegmüller et al., 2008).
Generally, brains with a neurodegeneration show elevated levels of TGF-β1 and this condition might arrest NPC proliferation and neurogenesis. On the other hand, the inhibition of TGF-β signal might stimulate the progression of the neural precursor cell cycle. At the end, alterations in the levels of TGF-β, either increased or decreased, disturb brain structure and function. So, there is the possibility to stimulate NPC proliferation, using the TGF-β pathway as a target, to promote and preserve neurogenesis. In brains affected by Alzheimer's disease, the hyperphosphorylation of tau protein affects the neuronal SMAD2 localization, leading to a decrease in its nuclear concentration and disturbing its transcriptional functions (Ueberham et al, 2006; Lee et al., 2006). It was also suggested that the neurofibrillary tangle formations can disturb the neuronal transport mechanisms interfering with the retrograde Smad signaling in hippocampal neurons, but so far it was only demonstrated for Drosophila motor neurons (Chalmers and Love, 2007). Pathogenic decrease of neuronal SMADs can induce the activation of neuronal cell cycle, leading to apoptosis in neurons (Arendt et al., 2000). A disproportionate production of TGF-β factors causes chronic or congenital diseases, as cancer, fibrosis, disorders of fat-related metabolism and diseases of the immune system (Dreesen and Brivanlou, 2007; Luwor et al., 2008; Wan and Flavell, 2007), revealing the importance of the TGF-β system in the normal tissue homeostasis. For this reason, the understanding of TGF-β family signaling has also medical relevance and it represents a target for future therapeutic intervention (Romano, 2009). However, the targeting of this pathway is announced relevant, for the future, but difficult because more studies on stem cells are needed to generate a pharmaceutical or biotechnological cell-based therapy.

Aims

AIMS

1. The first aim of this thesis was to determine the role of *Smad2* in the neuroplasticity processes in the adult dentate gyrus of control mice.
The aim was composed by the following objectives:

- To generate a feasible technique to manipulate *Smad2* expression;
- To assess how *Smad2* modulates adult hippocampal neurogenesis;
- To investigate a role for *Smad2* at cell level measuring morphometric parameters;
- To verify if changes in *Smad2* expression affect hippocampus-dependent behaviours.

2. The second aim points to evaluate the effects of physical exercise mediated by *Smad2* on the adult dentate gyrus.
The aim was composed by the following objectives:

- To assess how *Smad2* modulates adult hippocampal neurogenesis after 2 weeks of moderate exercise;
- To investigate a role for *Smad2* at cell level measuring morphometric parameters in runner animals;
- To verify if physical exercise could improve hippocampal-dependent behaviours with an altered *Smad2* expression in the dentate gyrus.

3. The third aim was to define how two weeks of moderate exercise regulate *Smad2* in the adult dentate gyrus.
The aim was composed by the following objectives:

- To describe the effect of our protocol of physical exercise on adult hippocampal neurogenesis and hippocampal-dependent behaviours;
- To analyse molecular and biochemical changes in stem cell transcription factors in sedentary and runner mice, with a special focus on *Smad2*.

4. The purpose of **the fourth aim** was to deeply analyse the Morris Water Maze test, used in this thesis as spatial learning and memory test, evaluating the role of *Smad2* in the execution of the task.

The aim was composed by the following objectives:

- To evaluate the reliability of the learning curve to measure acquisition;
- To evaluate if the individual efficacy in learning a task is related to the individual response to the removal of reinforcement;
- To assess if the composition and number of newborn cell subpopulations of different age correlate with the score obtained in the learning and memory task;
- To explore if a decrease in *Smad2* expression in the dentate gyrus alters the correlations between adult hippocampal neurogenesis and spatial learning.

Materials and methods

MATERIALS AND METHODS

1. Animals and behaviour

1.1 Animals

All the experiments were performed using C57BL/6J mice (male, 2 months of age). For the learning and memory studies, data from (C57BL/6 X C3H) F1 mice and Swiss mice were also collected.

Animals were housed at 22±1 °C with a 12 hours light/dark cycle and ad libitum access to food and water. All the animals were handled in strict accordance with the Good Animal Practice guidelines defined by the national welfare bodies at the Cajal Institute and CSIC. The work was previously approved by the Bioethics Committee of the Cajal Institute and CSIC.

1.2 Thymidine analogues

The thymidine analogues were administered to the animals through intraperitoneal injections. 5-bromo-2'-deoxyuridine (BrdU, Sigma-Aldrich) was injected using a 50 mg/kg body weight (bw) dose prepared in 0.9% saline. 5-chloro-2'-deoxyuridine (CldU, Sigma-Aldrich) was prepared in 0.9% saline and the dose used was 42.75 mg/kg bw. 5-iodo-2'-deoxyuridine (IdU, Sigma-Aldrich) was injected at the dose of 56.75 mg/kg bw. These doses were based on equimolar doses of 50 mg/kg bw BrdU. IdU was prepared by using 0.1 M PBS with 2 drops of 5 N NaOH added per 10-15 ml phosphate buffered saline (PBS). This solution was then heated 2-3 times in a microwave oven without boiling and vigorously stirred manually (Llorens-Martín and Trejo, 2011). The thymidine analogs solutions were prepared just before the injection's session.

1.3 Physical and cognitive activities

1.3.1 Mild forced treadmill exercise

Animals were habituated to the treadmill (Cibertec). Each group of animal, sedentary and runner, was placed separately for 10 min in the inactive treadmill. Then, they start to run for 5 min at a speed of 0.1 m/s, and finally for 10 min at 0.2 m/s. The habituation phase was performed by both groups in order to avoid any effect due to the new environment. After 24 h,

the exercised animals started their training running for 40 min at a speed of 0.2 m/s, for 7 days/week over a period of 2 weeks, while the sedentary animals were placed in the treadmill for the same amount of time but without doing any running.

The apparatus has a shock grid incorporated at the end of the ramp to stimulate animals to run. To avoid any kind of stress for the mouse, the shock grid was turned off and a paperboard was placed at the end of the ramp to prevent the exit from the belt when animals run slower.

1.3.2 Forced swim test

Animals were placed in a cylindrical container filled with water (12 cm diameter and 29 cm tall, 24 °C) for 10 min each day on two consecutive days. Control animals were moved to the behavioural testing room along with swim test animals, where they remained in their cages for the duration of the test, in the same circumstances than experimental animals.

1.3.3 Activity Cage

The VersaMax Animal Activity Monitoring System was used to evaluate animal's level of general activity and locomotion. The apparatus consists of acrylic cages with infrared sensors. As the animal moves in the cage, it interrupts the infrared beams. The lower sensors monitor horizontal movements while the vertical sensors detect the rearing activity. So the number of broken beams is correlated with the amount of movement in the cage.

Animals were left in the cage for 5 min on two consecutive days. The activity was analysed minute by minute.

1.3.4 Elevated Plus Maze

The elevated plus maze (Cibertec) consists of a plus-shaped apparatus with two open and two enclosed arms, each with an open roof, elevated 40 cm from the floor. The room temperature was 22±1 °C, with a constant artificial white light.

This test consisted of a 5 min single trial per animal. Mouse was placed in the centre of the maze, in an open-arm direction and in opposite sense with

respect of the experimenter. During each trial, the mouse was allowed to move freely along the apparatus. If the animal fell to the floor, it was put another time in the centre of the maze and the accident was annotated. The movements of the animals were recorded with Tracking Interface software and analysed by using Video Maze software. During the execution of the behavioural task, the animals that did not perform elevated plus maze remained in their cage in standard conditions.

1.3.5 Morris Water Maze

The apparatus to perform the hidden version of the Morris Water Maze test consists of a 1 m diameter pool with a capacity of 120 l, containing water at a temperature of 22±1 °C, visual cues in the surface of the tank and an invisible methacrylate platform (Fig. 1).

The experiment consisted of three phases:

1. In the first session (habituation), the mouse was placed in the centre of the tank entering from the south side. After one minute session without platform, the animal returned to its cage. During this session, it was evaluated if the animals spent more time in one particular quadrant to avoid the positioning of the platform in that portion of the arena.
2. Right after the habituation, the animals began the acquisition sessions. The invisible methacrylate platform was placed in the south-east quadrant of the pool, submerged 1 cm below the water surface. Four daily trials were performed changing the entering side of the mouse in the pool. All the animals enter in the pool from the same side in the same trial. The order of the entering side was chosen randomly each day. The mice swam in the pool since they found the platform. With the help of a plastic cylinder, the animal stay up at the platform for 20 s, then return to their cage. If after 1 min they did not find the platform, the experimenter gently placed them on it. The number of acquisition days depends on the performance of each group, so the learning curve was monitored daily to avoid an overtraining effect.
3. The third session consisted of the probe trial. In almost all the

experiments presented in this thesis, the trial was performed just 1 h after the last acquisition, except for Experiment Formula (see Results, Ch. 4 fig. 1 A) where the probe was tested 24 h later. The platform was not placed in the pool. Each mouse was introduced in the centre of the tank entering from the south side. After 90 s swimming, the mouse was removed from the water and it returned to its cage.

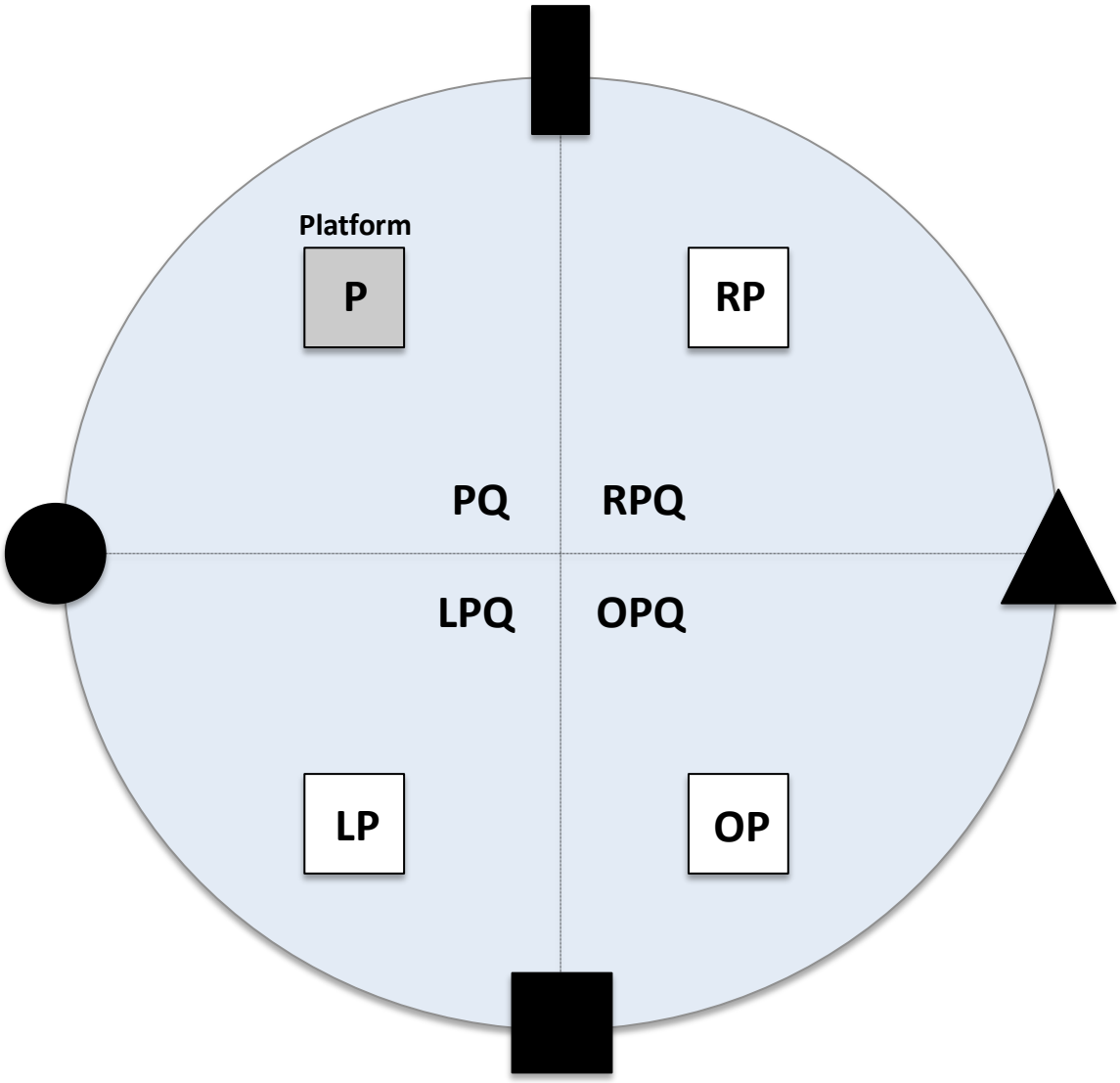

Fig. 1 Representation of the arena for the Morris Water Maze. P and PQ= Hidden Platform and Platform Quadrant; RP and RPQ= Right Platform (virtual position) and Right Quadrant; LP and LPQ= Left Platform (virtual position) and Left Quadrant; OP and OPQ= Opposite Platform (virtual position) and Opposite Platform Quadrant.

The time the animals spent to reach the platform (escape latency) was recorded with EthoVision XT 7 software. Daily mean escape latencies were measured to obtain the learning curve. Searching paths was video-recordered and EthoVision XT 7 software was used to obtain the time spent in every quadrant of the pool. The swim speed and path length were also recorded and compared between experimental groups throughout all the test to discard possible differences in locomotor capabilities and to analyse searching strategies, respectively.

1.3.6 T-Maze

The T-maze consists of a maze shaped like the letter T. During the 10 min training, one of the shorter arm was closed and the animals were free to explore the maze. After 4 h, the mice were put again for 10 min in the apparatus but this time all the arms were available to explore. The number of entries and the time spent exploring the new arm was calculated, recording the trial with the EthoVision XT 7 software. An index of discrimination for the time spent in each arm was obtained applying the following formula: $\frac{(T_{New\ Arm} - T_{Old\ Arm})}{T_{Tot}}$ (T= time).

1.4 Sacrifice

Animals were sacrificed by deep pentobarbital anesthesia (Euta-Lender). To obtain samples for histological analysis, mice were transcardially perfused with 0.9% saline followed by 4% paraformaldehyde in 0.1 M phosphate buffer (PB). Brains were removed and fixed again in the same fixative overnight at room temperature (RT).

To obtain samples for molecular and biochemical analysis, mice were transcardially perfused just with 0.9% saline. Brains were rapidly removed from the skull above an iced dish and the hippocampus formation was dissected, preserved in dry ice and store at -80 ºC as soon as possible.

2. Histology

2.1 Vibratome

Approximately 100 serial coronal sections 50 µm width of the hippocampal formation were obtained using an automatic vibratome (VT1000s, Leica)

and they were collected individually in 96-multiwell culture plates. The sections were stored at 4 ºC in 0.1 M PB.

2.2 Immunohistochemistry

Slices were initially preincubated for 5 min in 0.1 M PB with 0.5% Triton X-100 and 0.1% bovine serum albumin (BSA) (PBTBSA) used as a blocking solution. The antibodies were diluted in the same solution. The immunohistochemistries were performed to recognize (see Table 1):

- **BrdU, CldU, IdU**: the slices were preincubated in HCl 2 N for 30 min at RT. The primary antibodies used were a rat anti-BrdU (Abcam, 1:500), a rat anti-CldU antibody (Accurate chemicals, 1:500) and a mouse anti-IdU antibody (BD Biosciences, 1:500). The sections were left for 1 h at RT and then at 4 °C for 48 h. Primary antibodies were detected by using secondary alexa-conjugated antibodies: a 594 alexa-conjugated donkey anti-rat for BrdU (Invitrogen, 1:1,000), a 488 alexa-conjugated donkey anti-rat for the CldU antibody (Invitrogen, 1:1,000) and a 594 alexa-conjugated donkey anti-mouse for IdU (Invitrogen, 1:1,000), for 1 h at RT and then at 4 °C for 48 h.
- **phospho-Histone 3 (pH3)**: the primary antibody used was a rabbit anti-pH3 antibody (Chemicon-Millipore, 1:500) left over week-end at 4 °C. Then, a 594 alexa-conjugated donkey anti-rabbit (Invitrogen, 1:1,000) was added and left overnight at 4 °C.
- **Doublecortin (DCX)**: the primary antibody used was a goat anti-doublecortin antibody (Santa Cruz, 1:500), left for 1 h at RT and then at 4 °C over week-end. Doublecortin was recognized with a 594 alexa-conjugated donkey anti-goat (Invitrogen, 1:1,000) or a horse anti-goat biotinylated antibody (Vector, 1:1,000) combined with a 633 streptavidin-alexa antibody (Invitrogen, 1:1,000), incubated at 4 °C overnight.
- **Calretinin (CLR)**: the primary antibody used was a rabbit anti-calretinin antibody (Swant, 1:3,000), left for 1 h at RT and then at 4 ºC over week-end. Calretinin antibody was detected by a 488 alexa-conjugated donkey anti-rabbit antibody (Invitrogen, 1:1,000), incubated at 4 ºC overnight.

- **Fractin**: the primary antibody used was a rabbit anti-fractin antibody (Millipore, 1:500), left for 1 h at RT and then at 4 ºC over week-end. Fractin antibody was detected by a 594 alexa-conjugated donkey anti-rabbit antibody (Invitrogen, 1:1,000), incubated at 4 ºC overnight.
- **SMAD2**: the slices were preincubated for 1 h, at 80 ºC in citrate buffer pH 6 for antigen retrieval. Then, the slices were incubated with the primary antibody anti-SMAD2 (Cell Signaling, 1:500) for 1 h at RT and overnight at 4 ºC. To amplify the signal, the slices were incubated with a goat anti-rabbit biotinylated antibody (Sigma, 1:1,000) and then with a 633 streptavidin-alexa antibody (Invitrogen, 1:1,000), each of them for 1 h at RT and then overnight at 4 ºC.
- **Human SMAD2 (hSMAD2)**: the slices were incubated with the primary antibody rabbit anti-hSMAD2 (Cell Signaling, 1:500) for 1 h at RT and then overnight at 4 ºC. To detect the primary antibody, a 594 alexa conjugated donkey anti-rabbit antibody (Invitrogen, 1:1,000) was added and left overnight at 4 ºC.
- **Green Fluorescent Protein (GFP)**: to amplify the signal from the infected cells, the slices were incubated with a rat anti-GFP antibody (Nacalai Tesque, 1:1,000) or a rabbit anti-GFP (Life Technologies, 1:1,000) for 1 h at RT and then overnight at 4 ºC. The primary antibody was then detected by a 488 alexa-conjugated donkey anti-rat or anti-rabbit secondary antibody (Invitrogen, 1:1,000).
- **Neuronal Nuclei (NeuN)**: the slices were incubated with the primary antibody mouse anti-NeuN (Chemicon, 1:1,000) for 1 h at RT, and then for 48 h at 4 ºC. Then, a 594 alexa-conjugated donkey anti-mouse antibody (Invitrogen, 1:1,000) was added and left overnight at 4 °C.
- **Vesicular Glutamate Transporter (vGlut)**: the primary antibody used was a guinea pig anti-vGlut antibody (Chemicon, 1:2,500), left 1 h at RT and at 4 °C over week-end. vGlut was recognized with a goat anti-guinea pig biotinylated antibody (Vector, 1:1,000) combined with a 633 streptavidin-alexa antibody (Invitrogen, 1:1,000), incubated for 1 h at RT and then at 4 °C overnight.
- **Glutamic Acid Decarboxylase (GAD)**: the primary antibody used was a mouse anti-GAD antibody (Hybridoma Bank, 1:500), left 1 h at RT and

at 4 ºC over week-end. GAD antibody was detected with a 555 alexa-conjugated donkey anti-mouse antibody (Invitrogen, 1:1,000) incubated for 1 h at RT and then at 4 ºC overnight.

Antibody	Dilution	Brand
Rat anti-BrdU	1:500	Abcam
Rat anti-CIdU	1:500	Accurate Chemicals
Mouse anti-IdU	1:500	BD Biosciences
Rabbit anti-pH3	1:500	Chemicon Millipore
Goat anti-DCX	1:500	Santa Cruz
Rabbit anti-CLR	1:3,000	Swant
Rabbit anti-Fractin	1:500	Millipore
Rabbit anti-SMAD2	1:500	Cell Signaling
Rabbit anti-human SMAD2	1:500	Cell Signaling
Rat anti-GFP	1:1,000	Nacalai Tesque
Rabbit anti-GFP	1:1,000	Life Technologies
Mouse anti-NeuN	1:1,000	Chemicon
Guinea pig anti-vGlut	1:2,500	Chemicon
Mouse anti-GAD	1:500	Hybridoma Bank
594 alexa conjugated donkey anti rat	1:1,000	Invitrogen
488 alexa conjugated donkey anti rat	1:1,000	Invitrogen
594 alexa conjugated donkey anti mouse	1:1,000	Invitrogen
555 alexa conjugated donkey anti mouse	1:1,000	Invitrogen
594 alexa-conjugated donkey anti-rabbit	1:1,000	Invitrogen
488 alexa-conjugated donkey anti-rabbit	1:1,000	Invitrogen
594 alexa-conjugated donkey anti-goat	1:1,000	Invitrogen
Horse anti-goat biotinylated	1:1,000	Vector
633 streptavidin-alexa	1:1,000	Invitrogen
Goat anti-rabbit biotinylated	1:1,000	Sigma
Goat anti-guinea pig biotinylated	1:1,000	Vector

Table 1. List of primary and secondary antibodies used for immunohistochemistry, with the corresponding dilution and brand.

Sections were counterstained finally with DAPI (4',6-diamidino-2-phenylindole, Calbiochem, 1:1,000) for 12 min in 0.1 M PB. The slices were then mounted on gelatin slides and coverslipped by using Gerbatol (Sigma-Aldrich) mounting medium.

2.3 Nissl stain

Slices were mounted on gelatin slides without cover allowing them to dry for 48 h. Then:

- Dried slices were put in a toluidine blue solution (tolonium chloride) for 14 min;
- Then they stay for 10 s in milli-RO water to eliminate the surplus dye;
- For 2 min in 70% ethanol;
- For 2 min in 96% ethanol;
- For 4 min in 100% ethanol;
- For 3 min in xylene.

The slides were then coverslipped by using DePeX mounting medium (Sigma-Aldrich) and analysed with an optical microscope.

3. Anatomical measures

The area of the subgranular zone (SGZ) and the volume of the granular layer (GCL) were calculated considering the thickness of the slices (50 μm) and measuring the longitude of the SGZ and the area of the GCL using Nissl staining and the support of an optical microscope with Neurolucida software. For each animal, a total of 8 series of slices were obtained and one was randomly chosen and measured.

The length of the SGZ was measured in each slice of a series and then the total area of the SGZ was obtained applying the following formula:

$$Area\ SGZ = \left(\sum L * t\right) * 8$$

where L is the length of the SGZ in each slice and t is the thickness of the slice.

The volume of the GCL was obtained measuring the area of the GCL of each slice and then applying the following formula:

$$Volume\ GCL = \left(\sum A * t\right) * 8$$

where *A* is the area of the GCL of each slice and *t* is the thickness of the slice.

4. Stereology

Serial coronal sections 50 µm width were obtained with a Leica vibratome and collected in 96-multiwell culture plates for each hemisphere. One random series, constituted by one slice every 8, was chosen for each immunohistochemistry. To estimate the total number of $BrdU^+$, $CldU^+$, IdU^+, $pH3^+$ and $Fractin^+$ cells present in the dentate gyrus, it was applied the physical multi-stage fractionator technique. Briefly, the number of cells counted in all the sections of a series, using an inverted fluorescent microscope (Leica DMI6000B, 40X objective), was multiplied 8 times to obtain the total number of positive cells in the dentate gyrus, applying the following formula:

$$Cells\ total\ number = \sum Counted\ cells * 8$$

To study the hippocampal rostral gradient of $BrdU^+$ and $pH3^+$ cells, cells were counted in every section of a series comprised between -0.94 mm and -2.8 mm from bregma (references from the Paxinos and Franklin's Mouse Brain Atlas).

The number of DCX^+/GFP^+ cells were also obtained applying the fractionator method. Cells were counted in an optical microscope using a double cube filter allowing the detection of double staining cells. The number of cells counted was multiplied 8 times to obtain the total number.

Given the high number of immature cells in the dentate gyrus, DCX/CLR immunohistochemistry needed a different method of analysis. The total number of immature cells were analysed by applying a physical disector method developed for confocal microscopy (Leica TCS SP5, oil immersion

63× objective). The 3D-U-disector (Llorens-Martín et al., 2006) is a modified version from the basic "unbiased brick" proposed by Howard and Reed in 1998, in which optical sections were obtained thanks to the continuous scan along the z axis of the confocal microscope. In the present work, a modification called "physical disector" was employed, instead of the "optical disector": briefly, it consists in successive series of confocal images that can be efficiently saved, stored and used to count cells with the support of a computer without a confocal microscope. For each animal, 6 stacks were analysed (3 stacks in the suprapyramidal blade of the DG and 3 stacks in the infrapyramidal blade). Each stack consisted of 11 images (100 µm x 100 µm) with z≈ 17 µm. The images were taken with a 512 resolution and a 2.46 zoom. Each stack represents the U-physical disector.

Cells in each pair of confocal sections were counted using the first as a reference section. Cellular count was performed with the support of ImageJ software v. 1.49, applying the Cell Counter plugin: cells were marked and they were then identified in successive images of the disector, ensuring that each cell was counted just once (Fig. 2).

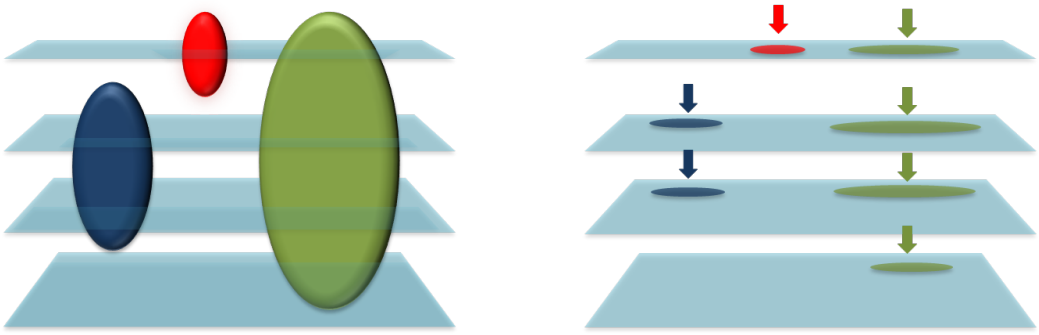

Fig. 2 Particles of different sizes generate different profiles in the sections. A bigger cell can be seen in more than one section, while smaller cells appears less. Also the orientation of the slice influences the number of sections where the cell does appear. Counting every single profile on sections would give an obvious overestimation of cell number (modified from Kaplan et al., 2012).

In each stack, the three different subpopulations of immature neurons were counted: DCX^+/CLR^-, DCX^+/CLR^+ and DCX^-/CLR^+. The number of immature neurons counted was divided by the area of the SGZ in the stack. In this way, it was possible to obtain a reliable estimate of cell density by "unit of

SGZ area". The total number of immature cells was obtained by multiplying the cell density by the total extension of the SGZ area, as follows:

$$Immature\ cells\ total\ number = \frac{Counted\ cells}{Stack\ Area} * Area\ SGZ$$

The total number of mature granule cells was counted using the DAPI stain. Due to the high density and number, cells were counted applying a physical disector. For each animal, three stacks were analysed. Each stack consisted of 6 images (33 μm x 33 μm) with z≈ 10 μm. The images were obtained with a confocal microscope (Leica TCS SP5, oil immersion 63× objective) and a 7.45 zoom. The number of cells in each image was counted using the Cell Counter plugin of ImageJ. Then, the mean density was calculated and the total number of cells was obtained multiplying it for the volume of the GCL.

$$Granule\ cells\ total\ number = \frac{Counted\ cells}{Stack\ Volume} * Volume\ GCL$$

vGlut and GAD positive boutons can be detected along dendrites. To quantify the percentage of area covered by each synapse, three images of the molecular layer of each sample were obtained with a confocal microscope (Leica TCS SP5, oil immersion 63× objective). Using the ROI Manager tool of ImageJ, a 100 x 100 circle was created and localized in the inner part of the molecular layer, near the upper limit of the granular layer. A threshold was assessed for each image and for each channel and then the total area occupied by the positive boutons was automatically calculated.

5. Morphometrical analysis

5.1 Morphometry of dendritic trees

The morphology of the granule neurons was studied on the GFP^+ cells. The cells chosen for the study were positive for NeuN marker and negative for DCX, in order to analyze just the mature neurons. Cells were also chosen based on a previous observation of the dendritic tree (no evident cut of the dendrites due to the vibratome) and based on the relative isolation from

other GFP positive cells, in order to simplify the reconstruction of the single neuron. Images were obtained scanning the entire cell every 0.8 μm with a confocal microscope (Leica TCS SP5, oil immersion 40× objective) and the analysis was performed on the final projection. The length of the dendrites was measured using the NeuronJ plugin of ImageJ. The Sholl analysis was performed applying concentric and equidistant circles, which were centered in the cell body, using the Concentric Circles plugin of ImageJ. Twenty to thirty cells for each experimental group were analysed.

5.2 Spines quantification

To quantify spine's density, a specific set up of parameters were applied in order to obtain the higher quality resolution in the confocal microscope from the immunofluorescent images. Spines were counted on tertiary dendrites, located in the molecular layer. Using an oil immersion 63x objective in a confocal microscope, and a 3.5 zoom, the dendrites were scanned taking an image every 0.13 μm. The 16-bits images, with a 2048 x 512 resolution, were subjected to a deconvolution process to deblur the image using the Leica LAS AF 2.6 software. Spines were then counted and the length of the dendrite was measured using the NeuronJ plugin of ImageJ in order to determine the spine's linear density.

6. Epigenetic analysis: DNA methylation

6.1 DNA extraction and purification

As mentioned before (par. 1.4), animals were sacrificed by means of a transcardiac perfusion with 0.9% saline to obtain samples for molecular analysis. DNA was extracted from the hippocampi previously dissected and stored at -80 ºC. To extract and purify DNA from the hippocampal tissue, it was used the DNeasy Blood and Tissue Kit (Qiagen): briefly, samples were first lysed using proteinase K. The lysates were loaded in perfect buffering conditions into the spin columns provided by the kit. During centrifugation, DNA selectively bounded to the column membranes while contaminants passed through. Remaining contaminants and enzyme inhibitors were removed in two wash steps and DNA was eluted in a proper buffer.

The efficiency of the process and DNA purity was measured with a spectrophotometer (ND-1000 NanoDrop, Thermo Scientific): a mean of 30 µg of DNA was extracted from each hippocampus from one hemisphere; in all the samples, the DNA extracted had A_{260}/A_{280} ratios of 1.8-2 and A_{260}/A_{230} ratios ≥1.

6.2 Methyl DNA restriction kit

To prepare genomic DNA for methylation analysis, it was used the EpiTect Methyl DNA Restriction Kit (Qiagen). It consists of a restriction digestion buffer and in two different enzymes: one is a methylation-sensitive and the other one is a methylation-dependent enzyme. These enzymes digest unmethylated and methylated DNA, respectively. First of all, it was necessary to prepare a reaction mix without enzymes, as follows (Table 2):

Component	Volume
Genomic DNA (1 µg)	Variable
Restriction Digestion Buffer 5X	26 µl
RNase-/DNase-free water	Variable
Final volume	**120 µl**

Table 2. Preparation of the reaction mix for the methyl DNA restriction process.

Then, each DNA sample was blended with the enzymes in order to perform 4 different restriction digestions (Table 3):

1. The product of a mock digestion (M_o, no enzymes added) contains all the input genomic DNA;
2. The product of the methylation-sensitive restriction enzyme digestion (M_s) contains hypermethylated DNA sequences;
3. The product of the methylation-dependent restriction enzyme digestion (M_d) contains unmethylated DNA sequences;
4. The product of a double digestion (M_{sd}, adding both enzymes) measures the background and the success of both digestions.

Component	M_o	M_s	M_d	M_{sd}
Reaction mix	28 µl	28 µl	28 µl	28 µl
Methylation-sensitive enzyme	–	1 µl	–	1 µl
Methylation-dependent enzyme	–	–	1 µl	1 µl
RNase-/DNase-free water	2 µl	1 µl	1 µl	–
Final volume	**30 µl**	**30 µl**	**30 µl**	**30 µl**

Table 3. Preparation of four different restriction digestions.

All the tubes were incubated overnight at 37 ºC in a heating block without shaking. The next morning, the reactions were stopped by heat, inactivating the enzymes at 65 ºC for 20 min. The product of the digestions was stored at -20 ºC until its analysis.

6.3 DNA methylation PCR arrays

To analyse the DNA methylation profiles in the CpG islands of specific genes of interest, it was used the EpiTect Methyl qPCR Array (Qiagen). The method consists in the detection by real-time PCR of remaining DNA after the cleavage with the restriction enzymes. Following digestion, the remaining DNA was quantified by PCR using primers that flank the promoter region of the gene. It was performed an array for 24 mouse stem cell transcription factors (cat. no. 335211 MeAM-511A), most of all being cell cycle regulators (see Table 4).

Gene symbol	Description	GenBank
Dnmt3	DNA methyltransferase 3B	NM_001003960
Ets1	E26 avian leukemia oncogene 1, 5' domain	NM_001038642
Fos	FBJ osteosarcoma oncogene	NM_010234
Foxa2	Forkhead box A2	NM_010446
Gata2	GATA binding protein 2	NM_008090
Hdac1	Histone deacetylase 1	NM_008228
Hif1a	Hypoxia inducible factor 1, alpha subunit	NM_010431
Jun	Jun oncogene	NM_010591
Myc	Myelocytomatosis oncogene	NM_010849
Neurog1	Neurogenin 1	NM_010896
Njya	Nuclear transcription factor –Y alpha	NM_001110832
Notch2	Notch gene homolog 2 (Drosophila)	NM_010928
Olig2	Oligodendrocyte transcription factor 2	NM_016967
Pax6	Paired box gene 6	NM_013627
Pcna	Proliferating cell nuclear antigen	NM_011045
Pparg	Peroxisome proliferator activated receptor gamma	NM_001127330
Rb1	Retinoblastoma 1	NM_009029
Runx1	Runt related transcription factor 1	NM_001111023
Runx2	Runt related transcript factor 2	NM_001145920
Smad2	MAD homolog 2 (Drosophila)	NM_010754
Sox2	SRY-box containing gene 2	NM_011443
Sp1	Trans-acting transcription factor 1	NM_013672
Stat1	Signal transducer and activator of transcription 1	NM_009283
Stat3	Signal transducer and activator of transcription 3	NM_011486

Table 4. List of the 24 stem cell transcription factors included in the methylation array.

To setup the PCR, a reaction was prepared for each of the 4 digestions as follows (table 5):

Component	M_0	M_s	M_d	M_{sd}
PCR Master Mix (SYBR Green)	330 µl	330 µl	330 µl	330 µl
M_0 digest	30 µl			
M_s digest		30 µl		
M_d digest			30 µl	
M_{sd} digest				30 µl
RNase-/DNase-free water	300 µl	300 µl	300 µl	300 µl
Final volume	**660 µl**	**660 µl**	**660 µl**	**660 µl**

Table 5. Setup of the PCR reaction mix.

Finally, 25 µl of each reaction was added in each well of the 96-well EpiTect Methyl Signature qPCR Array, where the primers were already present. The protocol used to run the PCR was as follows (Table 6):

Temperature	Time	Number of cycles
95 °C	10 min	1
99 °C	30 sec	3
72 °C	1 min	
97 °C	15 sec	40
72 °C	1 min	

Table 6. Thermocycling conditions for the PCR.

After the cycling program had completed, the C_T values were obtained and analysed. All the C_T values achieved were optimal as suggested by the trading house:

1. The C_T values of the mock digests were in the range of 18-29 cycles;
2. The C_T values of the M_s and M_d digests were between the values of the mock and double digests;
3. The C_T values of the double digests were higher than the C_T values of the mock digests.

Also the efficiency of the enzyme digestions were checked: the results were considered significant only if $\Delta C_T\,[M_{sd} - M_o] > 2$ that means that more than 75% of all DNA molecules in the samples were digested (Fig. 3).

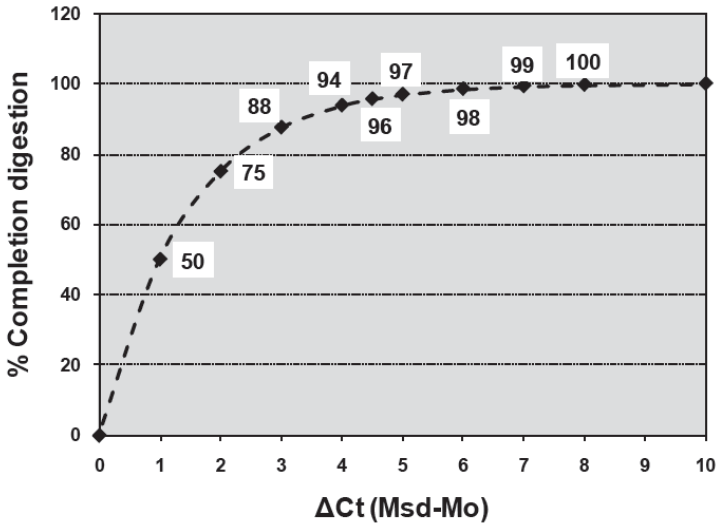

Fig. 3 Standard curve for the efficiency of the enzyme digestion.

The comparison between the C_Ts was performed by means of an Excel-based data analysis template provided with the kit. The fraction of DNA in each digest was calculated by normalizing the DNA amount to the amount of digestible DNA (the amount of digestible DNA was obtain in this way: C_{Mo}-C_{Msd}).

7. Genes expression analysis

7.1 RNA extraction

Total RNA was extracted from hippocampus using the QuickGene RNA tissue kit S II, following the instructions given by the manufacturer. The amount of tissue was determined and then it was homogenized in 400 µl of lysis buffer and 4 µl of 2-Mercaptoethanol with the help of a syringe with a 25 g needle and then with a 21 g smaller needle. Then, 200 µl of a solubilization buffer and 200 µl of ethanol 100% were added to the sample and it was mixed and centrifugated for 3 min at 15,000 rpm. The whole lysate from each sample was transferred to the corresponding cartridge column for the first pressured filtration. The cartridge filter was washed with 750 µl of wash

buffer and the solution was collected in a waste tube. A DNase solution was prepared according to the following table:

Component	Volume
Nuclease-free water	16 µl
10X Reactive Buffer	4 µl
DNase I	20 µl

Table 7. Preparation of the DNase solution to extract RNA.

The DNase solution was added directly into the filter of each cartridge and the treatment was left for 5 min at RT before proceed with the next two filtration processes.

The QuickGene kit consists in a porous membrane able to immobilize nucleic acid. So, the purified RNA remained trapped in the filter. 30 µl of elution buffer was added directly on the filter and left for 5 min at RT. The elution buffer changes the overall pH to release RNA from the column directly to a collection tube. Finally, the concentration and purity of RNA was measured in a spectrophotometer (ND-1000 NanoDrop, Thermo Scientific).

7.2 Reverse transcription polymerase chain reaction (RT-PCR)

RT-PCR is a technique to allow the reverse transcription of the RNA molecule of interest into its complementary DNA through the use of reverse transcriptase. The High Capacity RNA-to-cDNA Master Mix (Applied Biosystem) was used to synthesize cDNA following the protocol provided by the manufacturer. 1 µg of RNA was incubated with 4 µl of Complete Master Mix and it was added water up to a final volume of 20 µl. The thermal cycler conditions used were as followed (Table 8):

Temperature	Time
25 °C	5 min
42 °C	1 h
85 °C	5 min
4 °C	–

Table 8. Thermocycling conditions for the RT-PCR.

7.3 Primers design

The primers used in this work for quantitative PCR were created using the Primer Express 3.0 software.

Gene	Forward Sequence (5'-3')	Reverse Sequence (5'-3')
18S	ATG CTC TTA GCT GAG TGT CCC G	ATT CCT AGC TGC GGT ATC CAG G
Smad2	GAG ACC TTC CAT GCG TCA CA	GCG CAC TCC CCT TCC TAT ATG
Hdac1	GTG GCT ACA CCA TCC GGA AT	TCA TGT TGG AAG GGC TGA TGT
Gata2	CCC TAG AGG GCA GAG ACA ATT G	GGA GAC GTT TCC CCT TTC CA
Pax6	TGG AAA CAA ACG CCC TAG CT	CCG CCC TTG GTT AAA GTC TTC

Table 9. List of primers for qPCR.

The lyophilized primers were obtained from Invitrogen. The products were dissolved in milliQ water to a concentration of 100 µmol and then aliquots were prepared with a final concentration of 10 µmol.

7.4 Quantitative PCR (qPCR)

The level of expression of each gene was evaluated with a qPCR. First of all, a standard curve was generated to determine the optimal quantity of cDNA necessary for the reaction. Serial dilutions were prepared for each gene, from 1:2 to 1:8. Once established the optimal conditions, the quantitative PCR was carried out using SYBR Green (Applied Biosystems). A master mix was prepared using the following components (Table 10):

Component	Volume
SYBR Green	7.5 µl
Forward primer (10 µmol)	0.5 µl
Reverse primer (10 µmol)	0.5 µl
Water	5.5 µl

Table 10. Preparation of the SYBR Green master mix.

For the polymerase chain reaction, the master mix was added to the diluted cDNA of each gene:

Samples		Negative Control	
cDNA	3 µl	Water	3 µl
Master Mix	42 µl	Master Mix	42 µl

The reaction was prepared in triplicate for each sample in a 96-wells plate and the Applied Biosystems 7500 Real-Time PCR System was used with the following conditions:

Temperature	Time	Number of cycles
60 °C	30 sec	1
95 °C	10 min	1
95 °C	15 sec	40
60 °C	1 min	

Table 11. Thermocycling conditions for qPCR.

To analyse the results, the $2^{-\Delta\Delta Ct}$ method was applied: this is a widely used method to present relative gene expression comparing Ct values (Livak and Schmittgen, 2001).

8. Cloning techniques

The methods described in the "Cloning techniques" section were carried out during my PhD stage at the Molecular Biology Institute of Barcelona (CSIC), with Dr. Sebastián Pons's supervision.

8.1 Design of short hairpin RNAs against Smad2 mRNA (shRNAs-Smad2)

Smad2 mRNA sequence for Mus Musculus was found in GenBank and the shRNA sequences were designed with the help of the Shortcut OligoEngine software. The target sequence of each shRNA was composed by 19 bases, 100% complementary to a Smad2 mRNA sequence. To allow the insertion of the sequence inside a pSHIN vector, each shRNA was created with a BamHI and HindIII cohesive end. To guarantee the efficacy of the knock-down, four different shRNAs were designed and created as following, with a forward and reverse sequence (Fig. 4):

shRNA sequence 1 (G+C 47%):

5'-GATCCCCAATACGGTAGATCAGTGGGTTCAAGAGACCCACTGATCTACCGTATTTTTTTA-3'
5'-AGCTTAAAAAAATACGGTAGATCAGTGGGTCTCTTGAACCCACTGATCTACCGTATTGGG-3'

shRNA sequence 2 (G+C 47%):

5'-GATCCCCTTCACAGTCATCATGAGCTTCAAGAGAGCTCATGATGACTGTGAAGTTTTTA-3'
5'-AGCTTAAAAACTTCACAGTCATCATGAGCTCTCTTGAAGCTCATGATGACTGTGAAGGGG-3'

shRNA sequence 3 (G+C 47%):

5'-GATCCCCAGCAGGAATTGAGCCACATTCAAGAGATGTGGCTCAATTCCTGCTGTTTTTA-3'
5'-AGCTTAAAAACAGCAGGAATTGAGCCACATCTCTTGAATGTGGCTCAATTCCTGCTGGGG-3'

shRNA sequence 4 (G+C 42%):

5'-GATCCCCGCATGTCGTAAACCCATCATTCAAGAGATGATGGGTTTACGACATGCTTTTTA-3'
5'-AGCTTAAAAAGCATGTCGTAAACCCATCATCTCTTGAATGATGGGTTTACGACATGCGGG-3'

Fig. 4 Sequences of the shRNAs: in red, BamHI/HindIII restriction sites; in green, sense/antisense target sequences; in blue, hairpin sequences.

8.2 shRNA annealing

The lyophilized primers were obtained from Biomers. The products were dissolved in milliQ water to a final concentration of 100 nmol. To insert the shRNA inside an expression vector, it was necessary to anneal the oligos in a DNA double strand.

It was prepared a solution with 25 µg of the positive sequence, 25 µg of the negative sequence, 10 µl of a 10X Medium Restriction Buffer and it was added ultrapure water up to a final volume of 100 µl (final concentration= 0.5 µg/µl). The thermal cycler conditions used to allow the annealing were as follows (Table 12):

Temperature	Time
95 °C	3 min
68 °C	10 min

Table 12. Thermocycling conditions for shRNA annealing.

The DNA double strands were then stored at -20 ºC.

8.3 pSHIN-shRNA vectors

8.3.1 Linearization of the vector

pSHIN (also known as pG-SUPER) is a modified version of the commercial pSUPER vector (Fig. 5 A), obtained by Kojima Shin-Ichiro and gently donated by Dr. Elisa Martí from the Molecular Biology Institute of Barcelona. pSUPER is a commercial vector system (OligoEngine) for the expression of short interfering RNA. Shin-Ichiro and colleagues developed an improved vector to co-express the green fluorescent protein and the small hairpin RNA simultaneously to facilitate the analysis of silencing at the level of individual cells (Fig. 5 B) (Kojima et al., 2004).

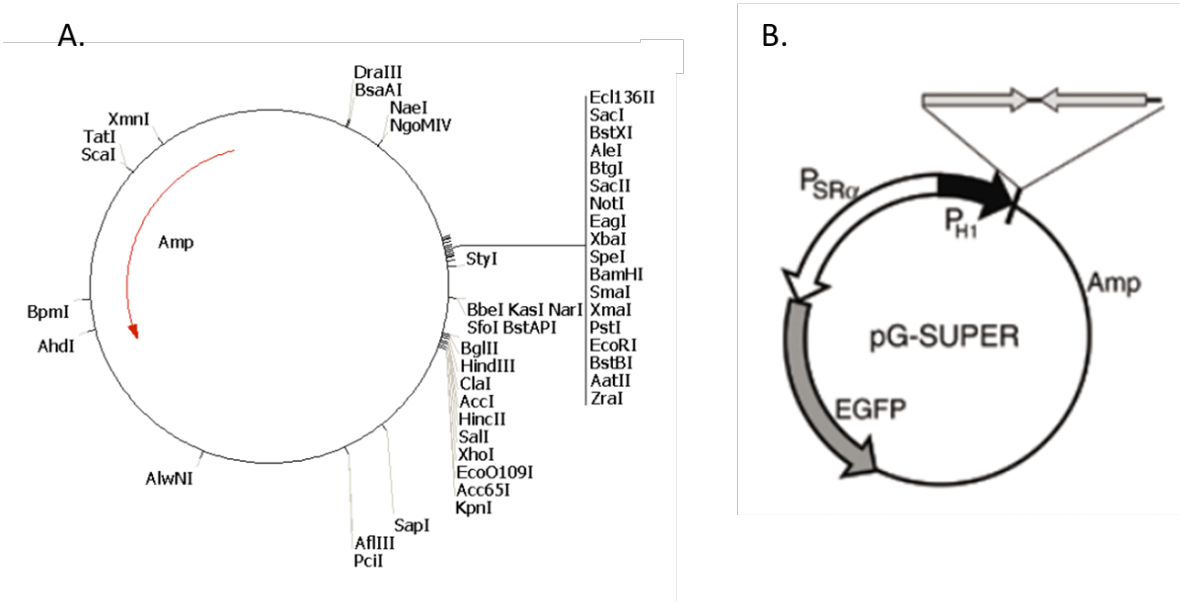

Fig. 5 **A.** p-SUPER vector's map; **B.** pG-SUPER, an improved hairpin small interfering RNA vector. Total nucleotide length is 3910 bp. Facing arrows represent oligonucleotide to be inserted after the H1 RNA promoter by BglII and HindIII (figure modified from Kojima et al., 2004).

The double strand oligo representing the shRNA was cloned into the vector between the unique BglII and HindIII enzyme sites and under the H1 promoter. So, first of all, the pSHIN vector was cut with specific restriction enzymes and conditions (Table 13). Then, the solution was incubated for 1 h at 37 ºC.

Component	Volume
pSHIN vector	1 µg
HindIII (Takara Bio)	1 µl
BglII (Takara Bio)	1 µl
Buffer K 10 X (Takara Bio)	2 µl
Water	Up to 20 µl

Table 13 Enzymatic restriction digestion.

8.3.2 Isolation and purification of the linearized pSHIN vector

Following digestion, the linearized vector was separated from any undigested circular plasmid on a 1% agarose gel. To prepare the gel, 1 g of agarose was dissolved in 100 ml of TAE 1X and heat up in a microwave until the complete dissolution. Once melted, 3 µl of SYBR Green (Invitrogen) was added to the compound and all the solution was poured into a casting tray containing a sample comb. The gel was allowed to solidify at RT. After the gel had solidified, the comb was removed and the tray was inserted inside a horizontal electrophoretic chamber, covered with buffer. To the 20 µl of vector sample, it was added 4 µl of Loading Buffer 6X. The sample was then pipeted in one of the well in the gel. In a lateral well, 10 µl of a marker (1 Kb Plus DNA Ladder, Invitrogen) were also charged.

A conventional agarose gel electrophoresis was used to separate DNA fragments (100 V for 1 h). Once electrophoresis ended, the linearized DNA fragment was visible and distinguishable from the circular DNA through an orange filter and a blue light (to avoid the employ of an ultraviolet mutagenic light).

The purification of the DNA molecules from the gel was obtained using the QIAquick Gel Extraction Kit (Quiagen), following the manufacturer's instructions. Briefly, the gel fragment containing the DNA of interest was removed and dissolved in a buffer. The mixture was applied to a spin column and centrifugated twice with a solution containing ethanol. With these conditions, DNA bound to the silica membrane and impurities were washed away. Pure DNA was then eluted with 50 µl of purified water.

8.3.3 Ligation into pSHIN vector

The oligo's concentration was led to 10 ng/µl. To assemble the cloning reaction, the following protocol was used (Table 14):

pSHIN vector + shRNA insert		**Negative Control**	
T4 DNA ligase buffer (Takara Bio)	2 µl	T4 DNA ligase buffer (Takara Bio)	2 µl
T4 DNA ligase (Takara Bio)	1 µl	T4 DNA ligase (Takara Bio)	1 µl
Linearized pSHIN vector	2 µl	Linearized pSHIN vector	2 µl
Oligos	15 µl	Water	15 µl

Table 14 Ligation reaction.

The reaction was incubated for 1 h at RT.

8.3.4 Transformation in Bacteria

The recombinant vector was transformed into competent DH5α cells (competence was previously induced in bacteria following a calcium chloride protocol). This procedure was performed under sterile condition. The transforming medium was prepared combining 100 µl of competent bacteria with 20 µl of the vector containing the insert. 20 µl of KCM buffer was added with water up to a final volume of 100 µl. The mix was left on ice for 20 min and then at RT for 10 min more. Finally, a volume of 800 µl of LB without antibiotics was added and left in a shaking incubator at 37 ºC for 1 h. Then, after a short centrifugation, the supernatant was eliminated, the pellet containing bacteria was resuspended, the cells were plated in a LB/ampicillin/agar plate and incubated at 37 ºC overnight. This process was repeated for every shRNA construct and for the negative control.

8.3.5 DNA miniprep

From each plate, six colonies were picked up and put in tubes with 4 ml of liquid LB with ampicillin. The tubes were incubated in a shaking incubator at 37 ºC for 7 h to allow the growth of the selected colony. Then, 1.5 ml of the medium was centrifugated for 1 min at 13,000 g and the pellet was isolated and resuspended with alkaline buffers: 100 µl of P1 buffer (containing Tris,

EDTA, HCl and RNasa A); 100 µl of P2 buffer (containing NaOH, SDS and water); finally, 100 µl of P3 buffer (containing potassium acetate and acetic acid). At the end of the process, DNA remained in the solution while the debris precipitated and it was eliminated with a centrifugation. The supernatant was put in a new tube and the addition of cold EtOH allowed DNA to precipitate with the help of a centrifugation. The supernatant was removed and the pellet was allowed to completely dry out. The plasmid pellet was then resuspended in 30 µl of pure water.

8.3.6 Diagnostic restriction digest

To verify the correct insertion of the sequence into the plasmid, it was carried out a diagnostic based on restriction enzymes. EcoRI and HindIII were the restriction sites chosen for the diagnostic. The digestion reaction was as follows (Table 15):

pSHIN vector + shRNA insert		**Negative Control**	
pSHIN+shRNA	6 µl	pSHIN	1 µl
EcoRI	1 µl	EcoRI	1 µl
HindIII	1µl	HindIII	1µl
Buffer M 1X (Takara Bio)	2 µl	Buffer M 1X (Takara Bio)	2 µl
Water	10 µl	Water	15 µl

Table 15 Preparation of the enzymatic digestion reaction for a diagnostic analysis.

The reaction was left at 37 ºC for 1 h. Then, the DNA fragments were separated by means of electrophoresis in a 2% agar gel and observed in an ultraviolet apparatus thanks to the presence of SYBR Green in the gel.

8.3.7 shRNAs efficiency

To quantify the efficiency of each shRNA to silence *Smad2*, fibroblasts from the 3T3 cell line were electroporated with each construct. After 24 h and 48 h post-electroporation, all the cells from each plate were rescued and lysate. SMAD2 protein was quantified by Western Blot. The sequence shRNA4 resulted as the more efficient to reduce the levels of SMAD2

protein, so it was chosen to execute the experiments presented in this thesis (Fig 6).

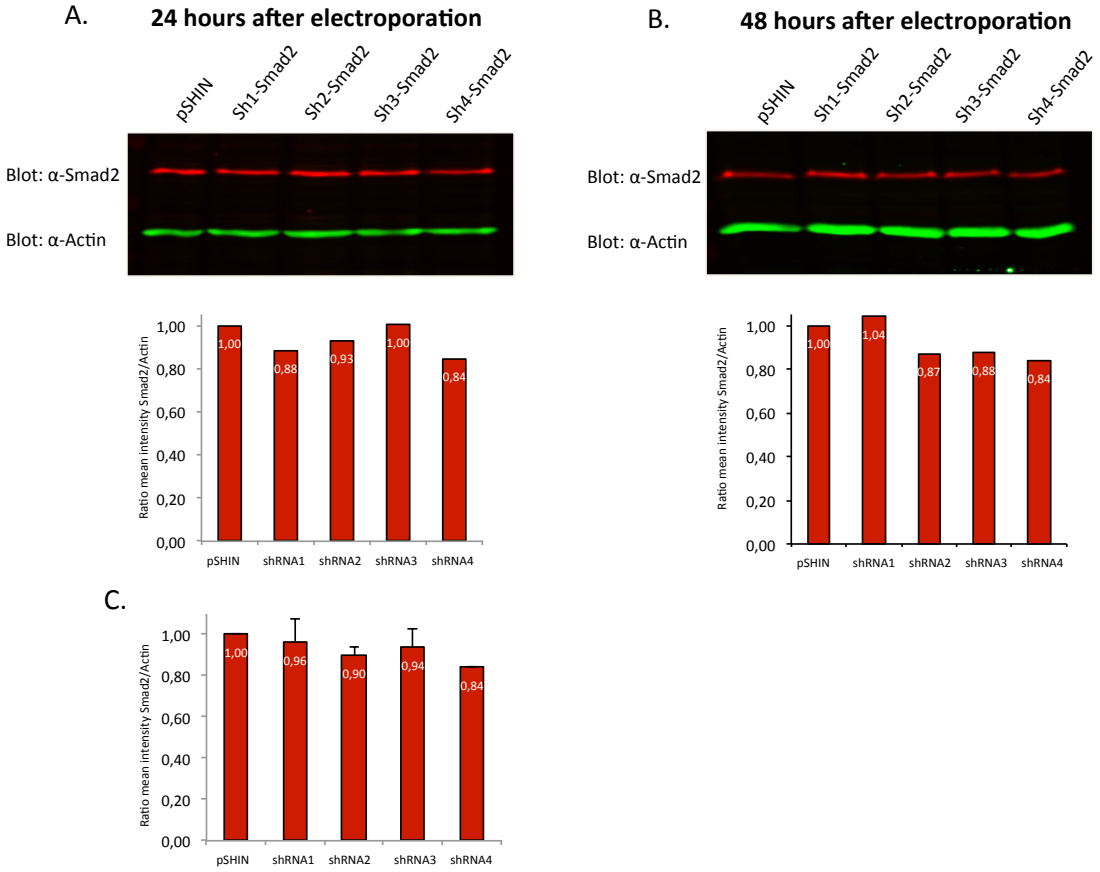

Fig. 6 SMAD2 protein quantification by Western Blot. A. SMAD2 quantification after 24 h post-electroporation; **B.** SMAD2 quantification after 48 h post-electroporation; **C.** SMAD2 quantification as a mean between 24 h and 48 h.

8.4 Lentiviral vectors

8.4.1 pLVTHM-shRNA-Smad2

pLVTHM is a second generation lentivector expressing shRNA from H1 promoter and GFP (created by Didier Trono lab, in Lausanne, Addgene plasmid #12247. Wiznerowicz M. And Trono D., 2003) (Fig. 7).

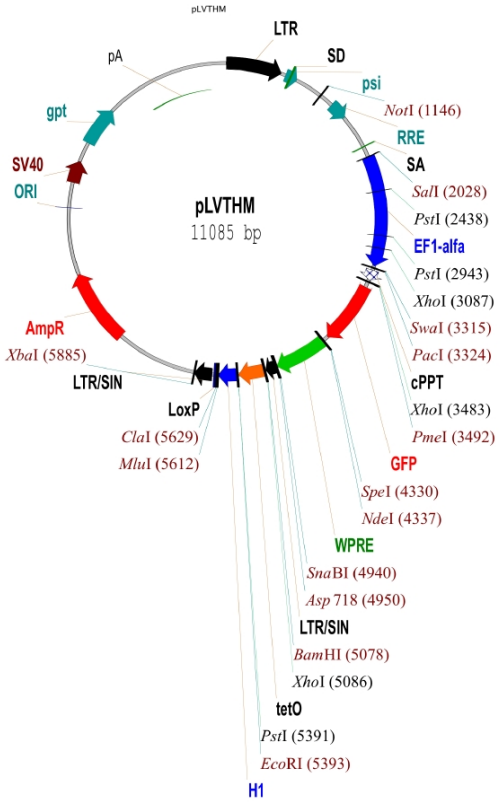

Fig. 7 Map of the vector pLVTHM.

The strategy used to insert the shRNA sequence from pSHIN vector to pLVTHM was to cut both plasmids in the same restriction sites (ClaI and EcoRI) in order to export also the H1 promoter.

The first reaction was as follows (Table 16):

pSHIN-shRNA-Smad2		**Negative Control**	
pSHIN-shRNA-Smad2	10 µl	pSHIN	1 µl
ClaI	1 µl	ClaI	1 µl
Tango Buffer 10X (Thermo Scientific)	2µl	Tango Buffer 10X (Thermo Scientific)	2µl
Water	7 µl	Water	16 µl

Table 16 Preparation of the digestion reaction to linearize pSHIN vector.

The reaction to linearize pLVTHM and eliminate the H1 sequence was (Table 17):

pLVTHM	
pLVTHM	2 µl
ClaI	1µl
Tango Buffer 10X (Thermo Scientific)	2 µl
Water	15 µl

Table 16 Preparation of the digestion reaction to linearize pLVTHM vector.

The digestion was left for 1 h at 37 ºC. Then, the second endonuclease was added (1 µl of EcoRI) and incubated for another hour at 37 ºC. DNA molecules were separated for electrophoresis in a 2% agar gel and purified with QIAquick Gel Extraction Kit (Quiagen).
H1-shRNA-Smad2 sequence was then inserted into the pLVTHM vector through the ligation process for 1 h at RT (Table 17):

Linearized pLVTHM (w/o H1)	2 µl
shRNA-Smad2	15 µl
T4 DNA ligase (Takara Bio)	1 µl
T4 DNA ligase buffer (Takara Bio)	2 µl

Table 17 Reaction to insert the shRNA sequence inside pLVTHM vector.

The new cloned vectors pLVTHM-shRNA-Smad2 were then isolated and purified with the same protocol.

8.4.2 pWPI-Flag-hSmad2

8.4.2.1 *hSmad2* gene

The *hSmad2* gene was obtained from the pCIG-Flag-hSmad2 expression vector, gently donated by Dr Elisa Martí. The transgene was cloned between XhoI and EcoRI sites in the multiple cloning site. So to obtain the sequence, the vector was cut in the same restriction sites. The following enzymatic digestion reaction was established and let for 1 h at RT (Table 18):

pCIG vector	1 µg
XhoI (Takara Bio)	1 µl
EcoRI (Takara Bio)	1 µl
Buffer H 10X (Takara Bio)	2 µl
Water	

Table 18 Enzymatic digestion reaction to open the vector and to extract *Smad2* sequence.

8.4.2.2 Isolation and purification of *hSmad2* gene

The linearized vector and the *hSmad2* DNA fragment were separated and isolated by means of electrophoresis in a 1% agar gel. The separation process gave two very distinct bands: the linearized pCIG vector (6280 bp) and the *Smad2* sequence (1400 bp). The lower band was isolated and purificated using QIAquick Gel Extraction Kit (Quiagen).

To allow the insertion of the sequence inside the pWPI vector, it was necessary to transform the sticky ends (produced by XhoI and EcoRI digestion) into blunt ends, as follow:

5’ TCGAG------G**AATT** 3’

3’ **AGCT**C------CTTAA 5’

To obtain this result, it was used the Klenow fragment (Large Fragment of DNA Polymerase I, Invitrogen) that conserves the 3’-5’ exonuclease activity of the DNA polymerase I. The following reaction was performed (Table 19):

dATP, dCTP, dGTP, dTTP	0.5 mM
Large Fragment of DNA polymerase I	1 µl
React 2 Buffer 10X (Invitrogen)	5 µl
Smad2 DNA sequence	1 µg

Table 19 Klenow reaction.

The reaction was briefly centrifugated and incubated for 15 min at RT. To isolate the blunt ended sequence, it was performed an electrophoresis in a 1% agar gel and then the DNA molecule was purified following the same protocol as before.

8.4.3 pWPI

pWPI is a second generation lentiviral vector (created by Didier Trono lab, in Lausanne, Addgene plasmid #12254) that allows the simultaneous expression of the transgene (in this case, *hSmad2* gene) and the GFP marker, under the Elongation Factor1-α (*EF1-α)* promoter (Fig. 8). The lentiviral vector was gently donated by Dr. Ramón Trullá from the Biomedic Research Institute of Barcelona (IDIBAPS).

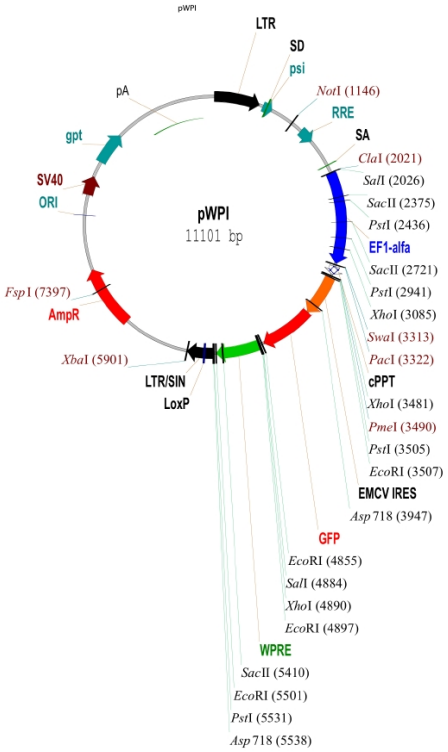

Fig. 8 Map of the pWPI vector.

8.4.3.1 Linearization, isolation and purification of pWPI vector

The pWPI vector was cut with the restriction endonuclease PmeI that produces blunt ends (Table 20).

pWPI vector	1 µg
PmeI	1 µl
Buffer B 10X	2 µl
Water	Up to 20 µl

Table 20 Reaction to linearize the pWPI vector.

The reaction was left for 1 h at RT. The linearized vector was separated from the undigested DNA molecules by electrophoresis in a 1% agar gel, adding 3 µl of phosphatase to inhibit the re-circularization of the vector. The correct band (11,000 bp) was then purified using QIAquick Gel Extraction Kit (Quiagen), as before.

8.4.3.2 Ligation into pWPI vector

Smad2 sequence was inserted into the pWPI vector thanks to a ligation reaction, left for 1 h at 37 ºC (Table 21):

T4 DNA ligase buffer (Takara Bio)	2 µl
T4 DNA ligase (Takara Bio)	1 µl
Linearized pWPI vector	2 µl
Smad2 DNA sequence	15 µl

Table 21 Ligation reaction.

Once *Smad2* was inserted inside the vector, the same protocol used for pLVTHM-shRNA-Smad2 was applied to amplify and analysed pWPI-hSmad2 (see par. from 8.3.4 to 8.3.6).

8.5 DNA sequencing

To guarantee the correct cloning of the inserts inside the vectors, a DNA sequencing was performed. Primers (Biomers) were designed using Oligo Explorer Software. The main characteristic for the forward primers was to be complementary with a sequence of the plasmid situated previous to the insert, while the reverse primers were random (Table 22).

Primer name	Forward Sequence (5'-3')	Reverse Sequence (5'-3')
pLVTHM vector	GTC GAG TTT ACC ACT CCC TA	AGA GAG ACC CAG TAC AAG CA
pWPI vector	GTA CAG TGC AGG GGA AAG AA	CAA CTC ACA ACG TGG CAC TG

Table 22 List of primers for DNA sequencing.

9. Lentiviral particles

9.1 Lentivirus production

Human Embryonic Kidney 293T cell line (HEK 293T) was used to produce the lentiviral particles. Cells were maintained in an appropriate culture medium (Table 23):

Product	Concentration
DMEM High glucose, Na-Pyruvate, no glutamine (Gibco)	1X
Fetal Bovine Serum (FBS) (Gibco)	12%
L-Glutamine (Gibco)	4 mM
Penicillin-Streptomycin (Gibco)	1%

Table 23 Culture medium for HEK 293T cells.

The day before the transfection, 6.0 x 10^6 cells were seed in a 10-cm plate and 6 plates were prepared for each virus.

A three-plasmid system was used to produce the lentiviral particles. The two helper plasmids were as follows: psPAX2 (second generation lentiviral packaging plasmid) and pMD2.G (VSV-G envelope expressing plasmid). The two helper plasmids (gently donated by Dr. Ramón Trulla, from IDIBAPS) were co-transfected with the engineered modified plasmid of interest using Lipofectamine 2000 (Invitrogen). The amount of reagents and plasmids used per 10-cm plate were as follows (Table 24):

Reagents	Quantity/10-cm plate
Expression vector	15 µg
psPAX2	9.7 µg
pMD2.G	5.3 µg
Lipofectamine 2000	30 µl
Opti-MEM (Gibco)	3 ml
293T cells/volume of medium	1.0x10^7/5 ml

Table 23 Reagents for transfection.

Briefly, the protocol consisted in gently mix 30 µl of Lipofectamine 2000 with 1.5 ml of OptiMEM and incubate it at RT for 5 min. Meanwhile, the appropriate volumes of plasmids were mixed with 1.5 ml of OptiMEM. The mix Lipofectamine-OptiMEM was added, drop by drop, to the mix DNA-

OptiMEM and incubate at RT for 20 min to allow DNA and the lipid molecules to form complexes. In the meantime, the overnight culture medium was replaced with 5 ml of DMEM with 10% FBS without antibiotics. The mix DNA-OptiMEM was finally add to the cells, drop by drop. The media was replaced 15 h post-transfection with new medium (Table 22). The supernatant was collected 48 h and 72 h post-transfection, filtrated using a 0.45 µm filter to eliminate small debris and storage at -80 ºC until the ultracentrifugation step.

9.2 Concentration

The supernatant containing the lentiviral particles was centrifugated in a BeckMAN centrifuge. A SW32 rotor was loaded and spun at 22,000 rpm at 4 ºC for 2 h. At the end of the spin, the tubes were quickly retrieved, the supernatant was removed by suction and without touching the viral pellet at the bottom of the tube.

In each tube, 50 µl of cold TBS-5 buffer were added. The tubes were closed with parafilm and put in a rack on ice at 4 ºC overnight. After soaking, the viral pellet was resuspended in the same buffer and aliquoted in 0.2 ml tubes. The viral aliquots were then stored at -80 ºC.

9.3 Titering

Titering was performed by transduction of HEK 293T cells using 10-fold dilutions of the virus. For each aliquot to be titer, six dilutions of the virus were prepared, from $1:10^2$ to $1:10^7$, adding 100 µl of cell suspension at a concentration of $1x10^6$ cells/ml. Each dilution was then seeded in the appropriate medium and cells were let grow for three days. After this period, cells were confluent but not overgrown.

The fluorescent clones were counted using an inverted fluorescent microscope (Leica) and a 10x objective. Clones were counted in a well with more than 10 but less than 200 clones. Then, the number of clones counted in a well was multiplied for the dilution factor and the initial volume.

The following titers were obtained for each construct:

pLVTHM-GFP: 18 x 10^9 TU/ml

pLVTHM-GFP-shRNA-Smad2: 11 x 10^9 TU/ml

pWPI-GFP: 17 x 10^9 TU/ml

pWPI-GFP-hSmad2: 16.4 x 10^9 TU/ml

10. Stereotaxic injections

To perform the stereotaxic injections, animals were deeply anaesthetized with isofluorane (Isoflo, Esteve) and placed in the stereotactic device (David Kopf Instruments) (Fig. 9 B). To avoid any damage to the eardrums, jaw holder cuffs (Stoelting) were used to securely clamp the zygomatic processes of the skull (Fig. 9 B). This technique provided an alternative non-invasive means to immobilize animal's head, avoiding let the mice deaf and therefore modifying the results from the behavioural tests.

The lentiviral vectors were administered with a 2 µl Hamilton micro-syringe. Each animal was injected bilaterally in the dentate gyrus of the hippocampus. In each hemisphere, two different injections were performed to guarantee infection all along the rostro-caudal axis. The stereotaxic coordinates were (from Paxinos and Franklin, 2004) (Fig. 9 A):

- Rostral injection: from bregma, antero-posterior -1.34 mm; medio-lateral, ±0.5 mm; dorso-ventral, -2 mm.
- Caudal injection: from bregma, antero-posterior -3.4 mm; medio-lateral, ±2.5 mm; dorso-ventral, -3 mm.

The Hamilton micro-syringe was inserted in the appropriate coordinates and left for 5 min. Then, 2 µl of lentivirus was injected at a rate of 0.2 µl/min using a micro-injector. Once the infusion finished, the Hamilton syringe was left *in loco* for other 15 min. Pilot studies showed that this dose of lentivirus led to long-term, constant expression of the transgenes, without causing an extended inflammatory reaction.

When the four injections were completed, animals were kept alone in a cage placed over a heating pad until they woke up. Animal's health conditions were monitored during all the experiment.

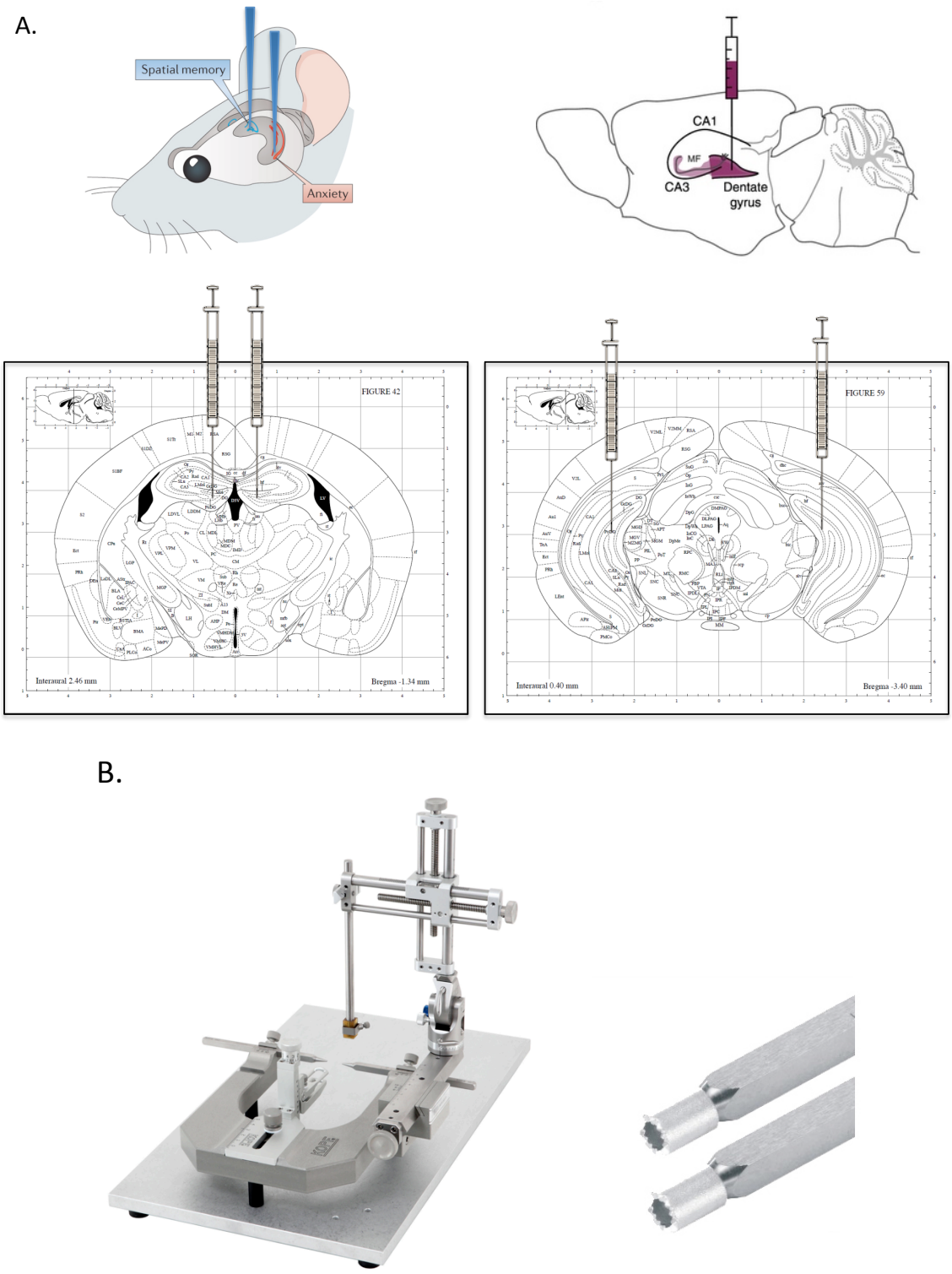

Fig. 9 **A.** Illustrations of the cerebral injections and schematic representation of the rostral and caudal coordinates (modified from Bannerman et al., 2014; modified from Paxinos and Franklin, 2004); **B.** Photo of the stereotactic device and of the jaw holder cuffs.

11. Protein quantification: Western Blots

11.1 Protein extraction

Samples for biochemical analysis were obtained after the sacrifice of the animals by means of transcardial perfusion with 0.9% saline and storing the tissue at -80 ºC. Each hippocampus was diluted in a lysis buffer (Table 24), adding a volume (µl) 10 times its weight (mg).

Component	Final concentration
HEPES pH 7,9	20 mM
NaCl	100 mM
EGTA	1 mM
EDTA	1 mM
Triton X-100	1%
DTT	5 mM
Na Orthovanadate	1 mM
NaF	2 mM
Protease Inhibitor	1X
Pure Water	Up to final volume

Table 24 Composition of the lysis buffer.

The tissue was sonicated until its complete lysis, centrifugated at 18,000 rpm for 15 min and the supernatant containing the proteins was collected.

11.2 Protein quantification and sample preparation

To determine the total protein concentration in each sample, it was applied the bicinchoninic acid (BCA) assay (Pierce™ BCA Protein Assay Kit, Thermo Fisher Scientific). This method combines the reduction of Cu^{2+} to Cu^{1+} by protein in an alkaline medium with a highly sensitive colorimetric detection using BCA. It was followed the protocol suggested by the manufacturer and the purple-colored reaction product, exhibiting a strong absorbance at 595 nm, was measured with a spectrophotometer (ND-1000 NanoDrop, Thermo Scientific).

The concentration of protein was determined for each sample and 50 µg of protein was diluted in a reducing buffer (Table 25). Proteins were then denatured by heating the sample at 95 ºC for 5 min.

Component	Concentration
Tris pH 6,8	1M
Glycerol	10%
SDS	5%
Bromophenol Blue	0.5%
β-mercaptoethanol	1M

Table 25 Composition of reducing buffer for protein denaturation.

11.3 Electrophoresis and transfer blot

Protein samples were put in a 4% SDS-PAGE gel (Sodium Dodecyl Sulphate - PolyAcrylamide Gel Electrophoresis, stacking gel) and separated on 10% SDS-PAGE gels. Samples ran for 40 min at 80 V and then for 1 h and 30 min at 120 V in a running buffer (Table 26).

Component	Concentration
Tris base	25 mM
SDS	0.1%
Glycine	192 mM

Table 26 Composition of the running buffer.

Proteins were transferred from the SDS-PAGE gel into a polyvinylidene difluoride (PVDF) membrane for 30 min at 25 V and 1 A using a semi-dry system (Trans-Blot Turbo Blotting System, BioRad). Previously, the PVDF membranes were equilibrated in methanol for 1 min, in water for 2 min and in Towbin transfer buffer for 10 min (Table 27).

Component	Concentration
Tris base	25 mM
Methanol	20%
Glycine	192 mM

Table 27 Composition of the Towbin transfer buffer.

11.4 Immunoblot

After washing twice with water, membranes were incubated with gentle agitation throughout the steps. After 1 h in blocking solution (Table 28), membranes were incubated with primary antibody for 2 h at RT and then overnight at 4 ºC. Membranes were then washed and incubated with appropriate secondary antibody for 1 h at RT (Table 29).

Component	Final concentration
Tris base	25 mM
NaCl	150 mM
Tween-20	0.1%
Non fat dry milk / BSA	5% / 3%

Table 28 Composition of the blocking solution.

Antibody	Dilution	Brand
Rabbit anti-SMAD2	1:2,000	Cell Signaling Technology
Rabbit anti-pSMAD2 (Ser465/467)	1:500	Cell Signaling Technology
Rabbit anti-HDAC1	1:500	Cell Signaling Technology
Rabbit anti-β-III-Tubulin	1:10,000	Abcam
Peroxidase-AffiniPure Donkey Anti-Rabbit IgG	1:10,000	Jackson Immuno Research Laboratories

Table 29 List of primary and secondary antibodies used for immunoblot.

To detect the proteins, the Super Signal West Pico Chemiluminescent Substrate (Thermo Scientific) was applied to the membranes and the results were visualized in a dark room applying the appropriate exposure times. To detect a second protein in the same membrane, a stripping protocol was followed. Membrane was left for 30 min at 70 ºC in a stripping buffer (Table 30):

Component	Final concentration
Tris HCl pH 6,8	62.5 mM
SDS	2%
β-mercaptoethanol	100 mM
Water	Up to final volume

Table 30 Composition of the stripping buffer.

Quantification of protein's levels was measured scanning the bands in a densitometer and analysing the images with the Quantity One software (Bio-Rad). Data were normalized using β-III-Tubulin protein as loading control.

12. Data analysis

Statistical analysis was performed using IBM SPSS Statistics software package v. 23. Different statistical tests were applied depending on groups and variables.

To compare a mean value of two groups, a Mann-Whitney U test was applied. A repeated measure ANOVA was chosen to compare the repeated measure factor within a same group. A Wilcoxon signed-rank test was used to compare two sets of scores coming from the same group.

An extensive data analysis was performed to evaluate the results presented in Chapter 4 in the Results section (for more details, see Gradari et al., 2016a). It should be emphasized that the massive data analysis was carried out by the exploratory software AutoDiscovery (Butler Scientifics). Thanks to this software, it was possible to consolidate the data related to the hippocampal neurogenic cell populations, the MWM test and the EPM test into a single dataset. The discovery process consisted of evaluating all the potential structural relationships between the variables, especially for those involved in different protocols. AutoDiscovery calculated the Spearman's rank correlation coefficients for each pair of numerical variables and every possible ratio between variables. Only those correlations evaluated in a data subset with $n \geq 5$ and $p < 0.05$ and Spearman's Rank correlation coefficient $\varrho \geq 0.7$ were considered in the analysis.

In the following table (Table 31), the new variables created to analyse behavioural parameters (Results, Ch. 4) are defined and summarized with the corresponding formula used to obtain them.

The mathematical formula for data adjustment to represent the mean group learning in the MWM was developed with MatLab software.

A p-value < 0.05 was considered significant (* 0.01 < p < 0.05; ** 0.001 < p ≤ 0.01; *** p ≤ 0.001). A p-value between 0.05 and 0.099 was considered as a tendency (#) toward significance.

PHASE DURING THE MORRIS WATER MAZE	VARIABLE	DEFINITION
Acquisition phase	**AS**: Acquisition Score	$1 - \frac{Escape\ Latency\ (s)}{60\ (s)}$ e.g. **AS5**: acquisition score on day 5; **ASRev**: acquisition score in the reversal trial.
	LP: Learning Profile	**LP1**: finding the platform early by chance on acquisition day 1; **LP2**: long latencies in finding the platform both on acquisition day 1 and day 2; **LP3**: a long latency on acquisition day 1 and a shorter one on day 2.
	Early Profile	$AS2 - AS1$ Represents the variation in the score between day 1 from that on day 2.
Probe trial	**Behavior Persistence**	During the probe trial, repeated swimming around the position where the animals learnt the platform was.
	Novel Behavior	Weaker persistence. Searching for the reinforcer (the platform) at novel location.
	Extinction Burst	Stronger persistence. Time spent around the virtual position.
	PerPlat: Persistence in the Platform quadrant	Time spent swimming in the platform quadrant.
	PerCross: Persistence Crossing over the platform location	Crossings over from the platform's virtual position.
Extinction phase	**Ext:** Extinction	Percentage of time spent swimming in the platform quadrant during the Full-Extinction experiment. e.g. **Ext1** is the percentage of time spent in the platform quadrant on day 1 as mean of four daily trials.

Table 31 List of abbreviations and their definitions for the different behaviours in the Morris Water Maze.

Results

CHAPTER 1
Effects of *Smad2* loss- and gain-of-function in the adult dentate gyrus of sedentary animals

1. Delivery of the lentiviral particles into the dentate gyrus

1.1 Time course of GFP expression

To determine the expression's time course of lentivirus, animals (n= 2 for each end point, for each construct) were subjected to a stereotaxic operation injecting the control constructs into the dentate gyrus. Mice were sacrificed at 12 h, 24 h, 48 h, 72 h and 7 days post-injections (Fig. 1 A) and the expression of GFP was qualitatively observed. GFP signal was not found in animals sacrificed before 72 h post-injection, while in the other end points it was possible to observe the infection. For this reason, in the following experiments in which the lentiviral particles were injected, at least three to four days were left between the surgical operation and the experimental procedure in order to allow a recovery period for the animals and to give the time for the lentiviral constructs to express.

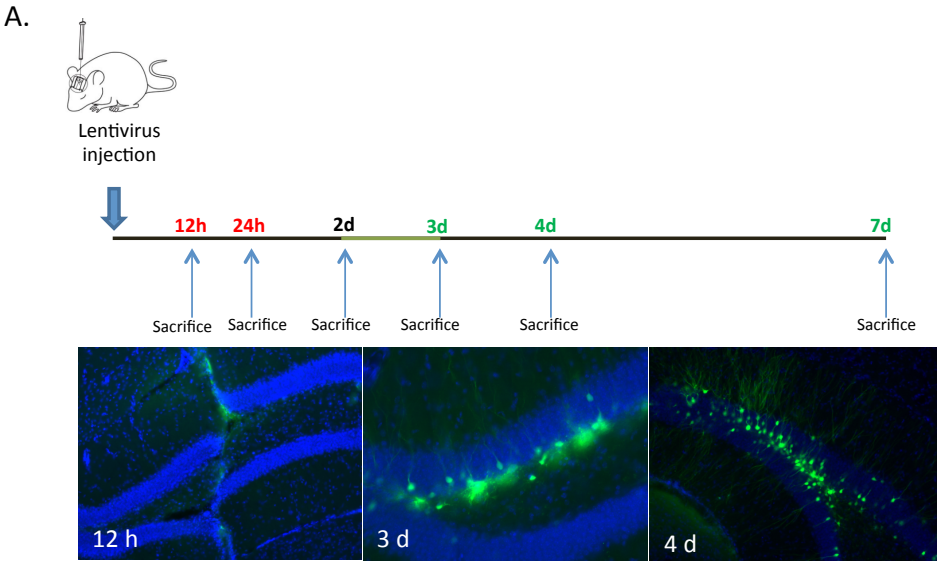

Fig. 1 **A.** Experimental design. To evaluate the lentivirus's expression time course, mice were operated with stereotaxic surgery, delivering lentiviral particles inside the dentate gyrus. They were sacrificed in different end points and the brain slices were observed with a fluorescent microscope in order to find GFP signal. GFP^+ cells were found in animals sacrificed not before 3 days from the operation.

Three weeks after the operation, virus expression (as GFP signal) was still visible and the double bilateral injections turned out to be an efficient strategy to ensure an extensive infection along the rostro-caudal axis of the dentate gyrus (Fig. 1 B).

B.

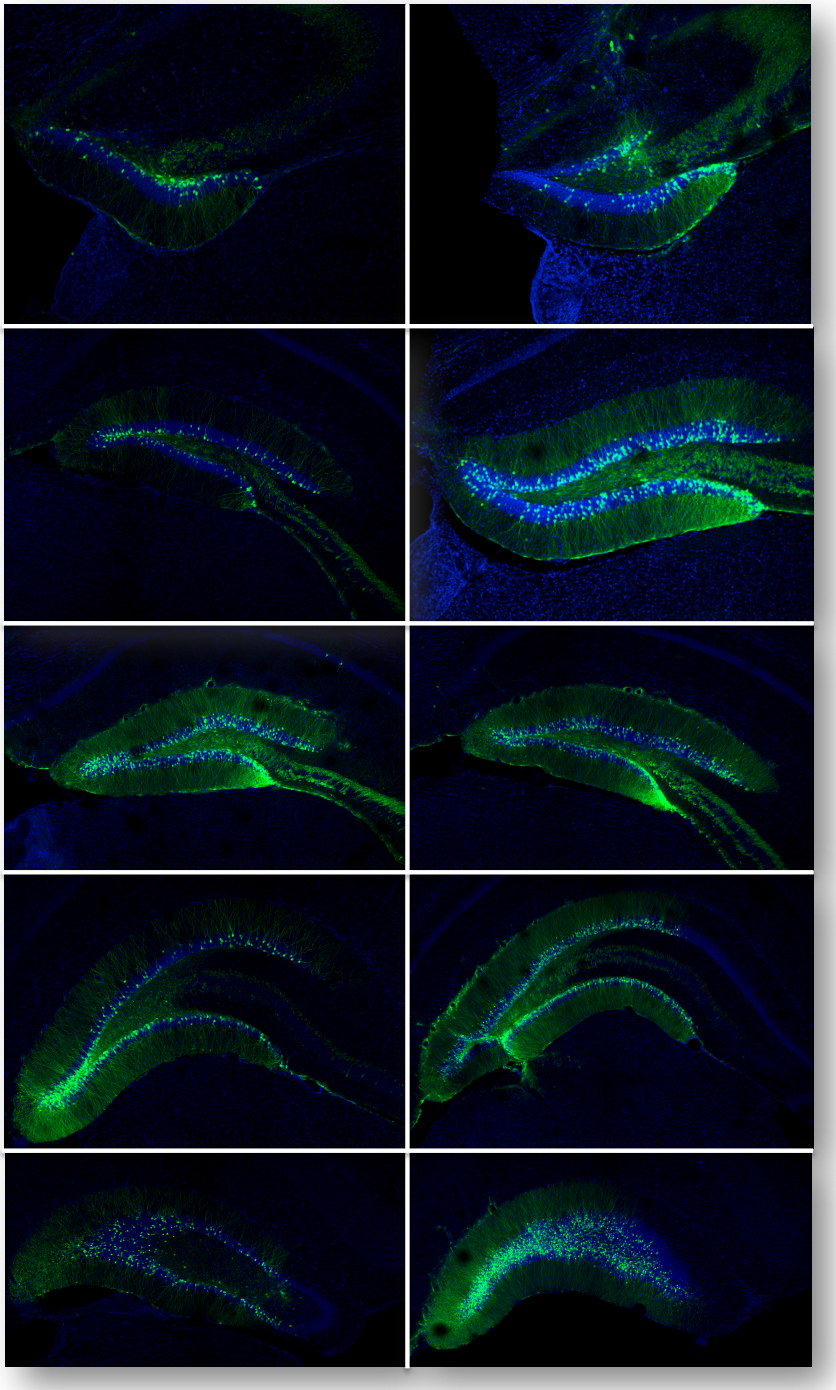

Fig. 1 B. Three weeks after the stereotaxic operation, lentivirus expression was observable along all the rostro-caudal axis of the DG with a high efficiency of infection. (Green, GFP marker; blue, DAPI staining).

1.2 Quantitative levels of SMAD2 protein as effect of the lentiviral vector's expression

To assess the efficacy of the genetic manipulation, mice were subjected to a double bilateral stereotaxic injection and sacrificed 3 weeks later. The total amount of SMAD2 protein was quantified in the hippocampus by means of Western Blot analysis. The levels of protein decreased almost 60% in the hippocampus injected with the shRNA construct (p-value= 0.002). The over-expression construct led to duplicate the quantity of protein in the hippocampus (p-value= 0.005) (Fig. 2).

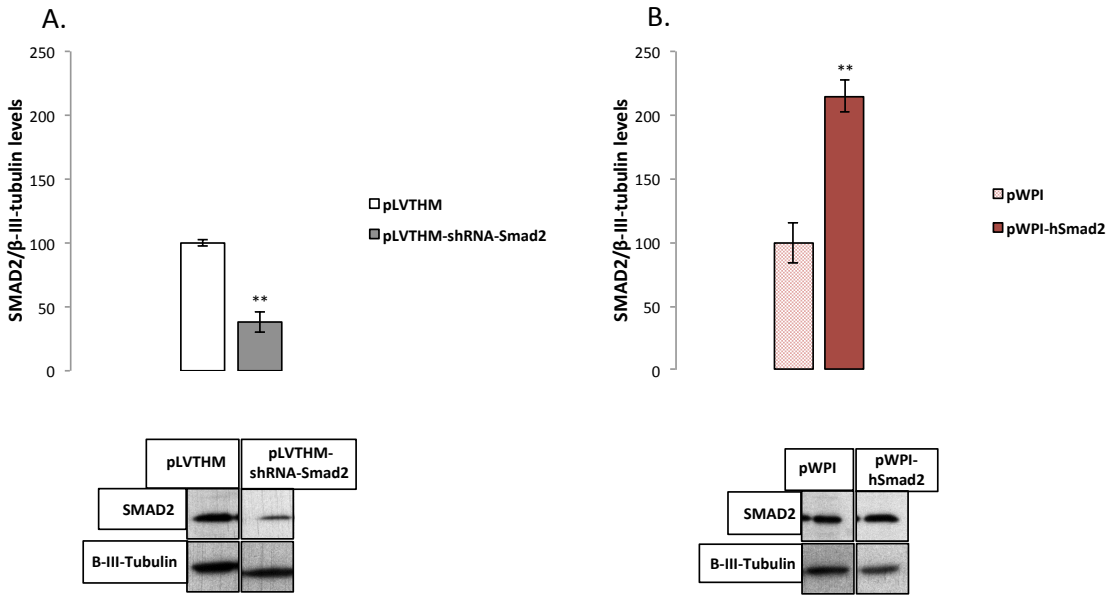

Fig. 2 SMAD2 protein quantification. Effect of different lentiviral constructs on the hippocampal level of SMAD2 protein, quantified by Western Blot. **A.** Silencing *Smad2* with pLVTHM-shRNA-Smad2; **B.** Over-expressing with pWPI-hSmad2.

2. *Smad2* loss- and gain-of-function produces histological modifications in the adult dentate gyrus

Smad2 is a gene expressed by the immature post-mitotic and mature neurons of the DG (Fig. 3) (see Introduction, par. 5.1 and Fig. 8).

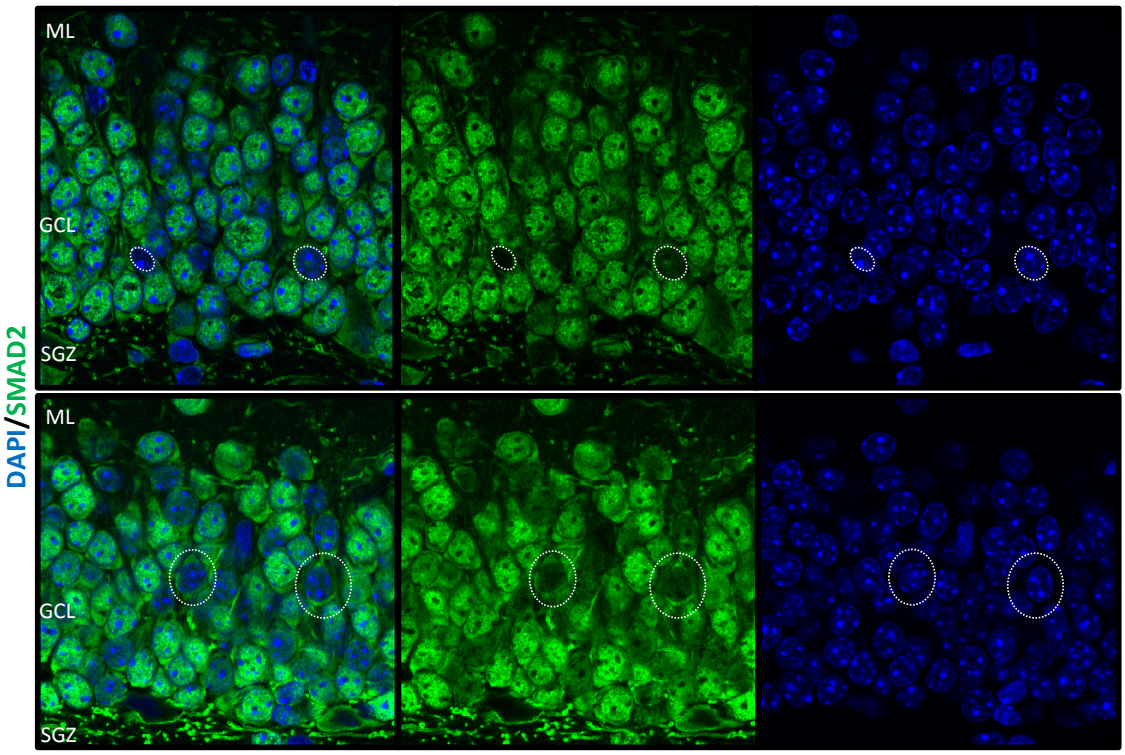

Fig. 3 SMAD2 immunohistochemistry in the DG. *Smad2* is highly expressed in the DG. However, not all the granule cells express *Smad2* and when the protein is in an unphosphorylated state the protein is located just in the cytoplasm. (Blue, DAPI staining; green, SMAD2 marker).

So, in order to study the function of *Smad2* in these cells of the dentate gyrus, animals were subjected to double bilateral stereotaxic injections with lentiviral constructs to silence or to over-express *Smad2* (n= 8-10 in each group). To assess the survival of the newborn cells in the granule cell layer, BrdU was injected for 4 consecutive days, once a day. The first BrdU dose was injected three or four days after the surgical operation. Two weeks after the first BrdU injection, animals were subjected to a set of behavioural task: the activity cage, the elevated plus maze and the Morris water maze. The day after the probe, animals were sacrificed and the histology of the brain was analysed (Fig. 4).

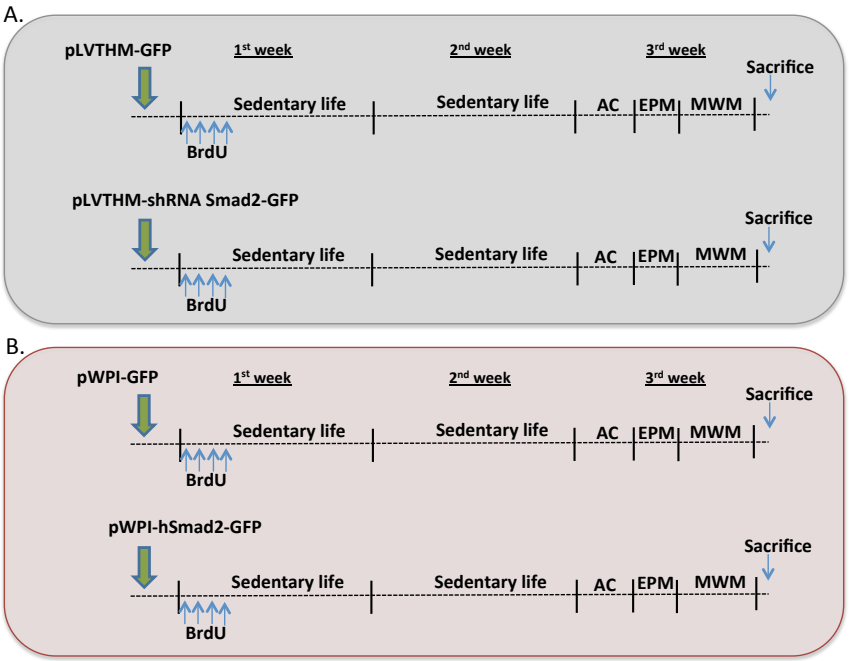

Fig. 4 Experimental design. A. *Smad2* loss-of-function study; **B.** *Smad2* gain-of-function study. AC= Activity Cage; EPM= Elevated Plus Maze; MWM= Morris Water Maze.

2.1 Anatomical analysis of the hippocampus

No differences were found in the volume of the GCL in animals with a lower or higher *Smad2* expression compared to their controls. On the other hand, it was noticed an increase in the area of the SGZ in animals where shRNA-Smad2 sequence was expressed (p-value= 0.005). This difference was not observed in the DG where *Smad2* was over-expressed (Fig. 5 A-D).

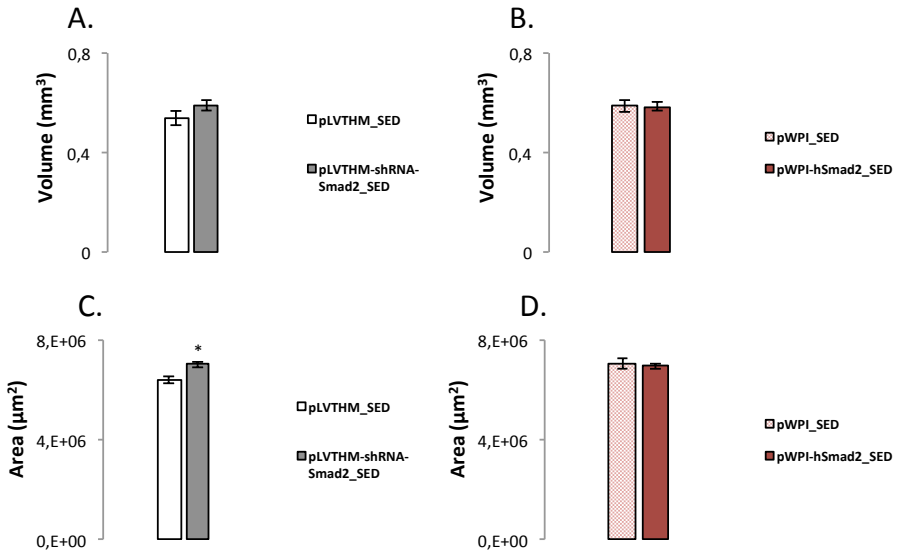

Fig. 5 Anatomical analysis. A-B. Volume of the DG in the silencing (A) and over-expressing (B) experiment; **C-D.** Area of the SGZ in the silencing (C) and over-expressing (D) analysis.

2.2 Modulation of the adult hippocampal neurogenesis

To study how the adult hippocampal neurogenesis process was affected by different levels of expression of *Smad2* gene, the first parameter analysed was the number of granule cells in the DG. Differences were found neither in the total number nor in the density of the cells, as effect of the genetic manipulation (Fig. 6 A-D).

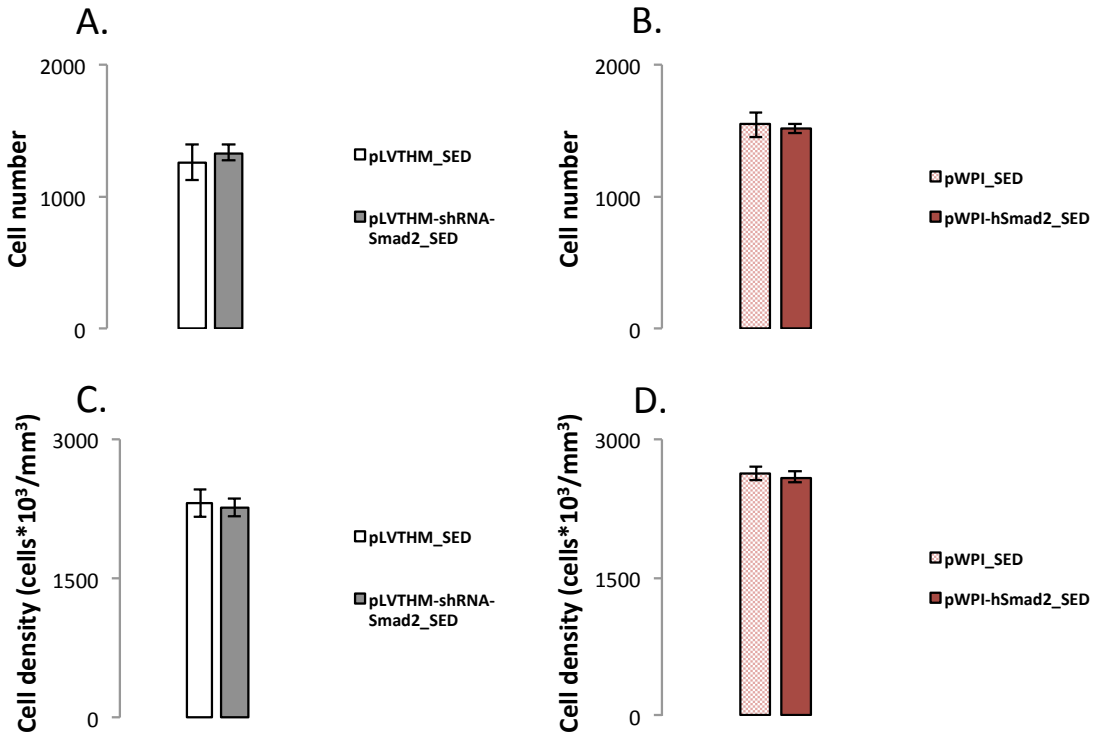

Fig. 6 Granule cells in the DG. A-B. Total granule cells number in the silencing (A) and over-expressing (B) experiment. **C-D.** Granule cell density in the DG of animals silencing (C) and over-expressing (D) *Smad2*.

It was observed an increase in the number of $pH3^+$ cells in the DG infected by the silencing lentivirus compared with its control (p-value= 0.003). This increase in proliferation was confirmed also observing the ratio between the number of $pH3^+$ cells and the total number of granule cells (p-value= 0.003) (Fig. 7 A and C). The over-expression of *Smad2* led to a downward trend in the number of $pH3^+$ cells (p-value= 0.077), and no differences were found comparing the ratio between the number of $pH3^+$ cells and the total number of granule cells (Fig. 7 B and D). To further analyse cell proliferation, the number of $pH3^+$ cells was estimated in the rostral part of the DG (to -2 from bregma). In fact, in the hippocampus where there were neurons silencing *Smad2*, there was a significant increased proliferation (p-

value= 0.011), in particular toward the rostral-medial dentate gyrus (at 1600 µm from bregma, p-value= 0.05; at 2000 µm from bregma, p-value= 0.017). In the rostral DG of animals over-expressing *Smad2*, the proliferation rate did not change compared to its control (Fig. 7 G-H).

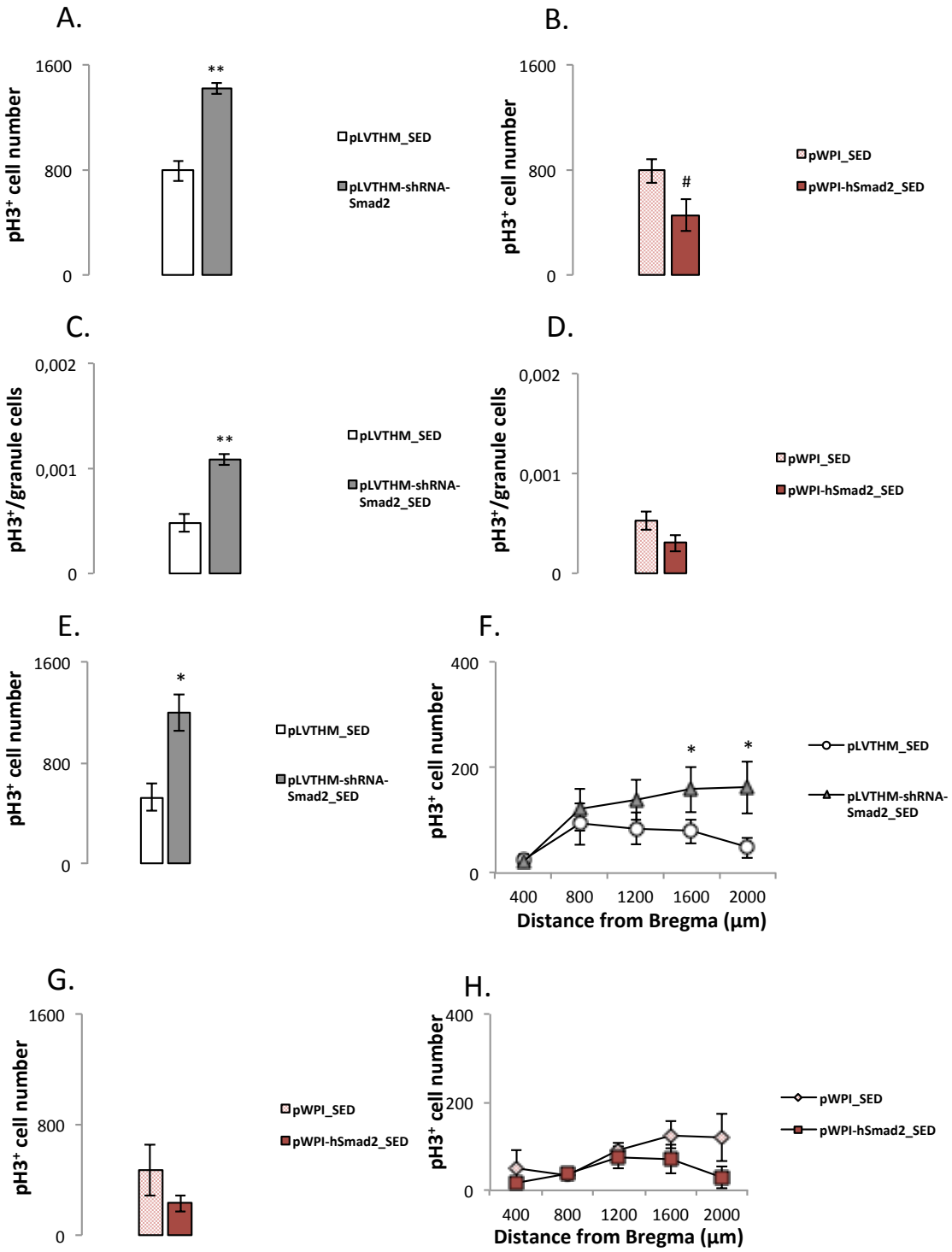

I.

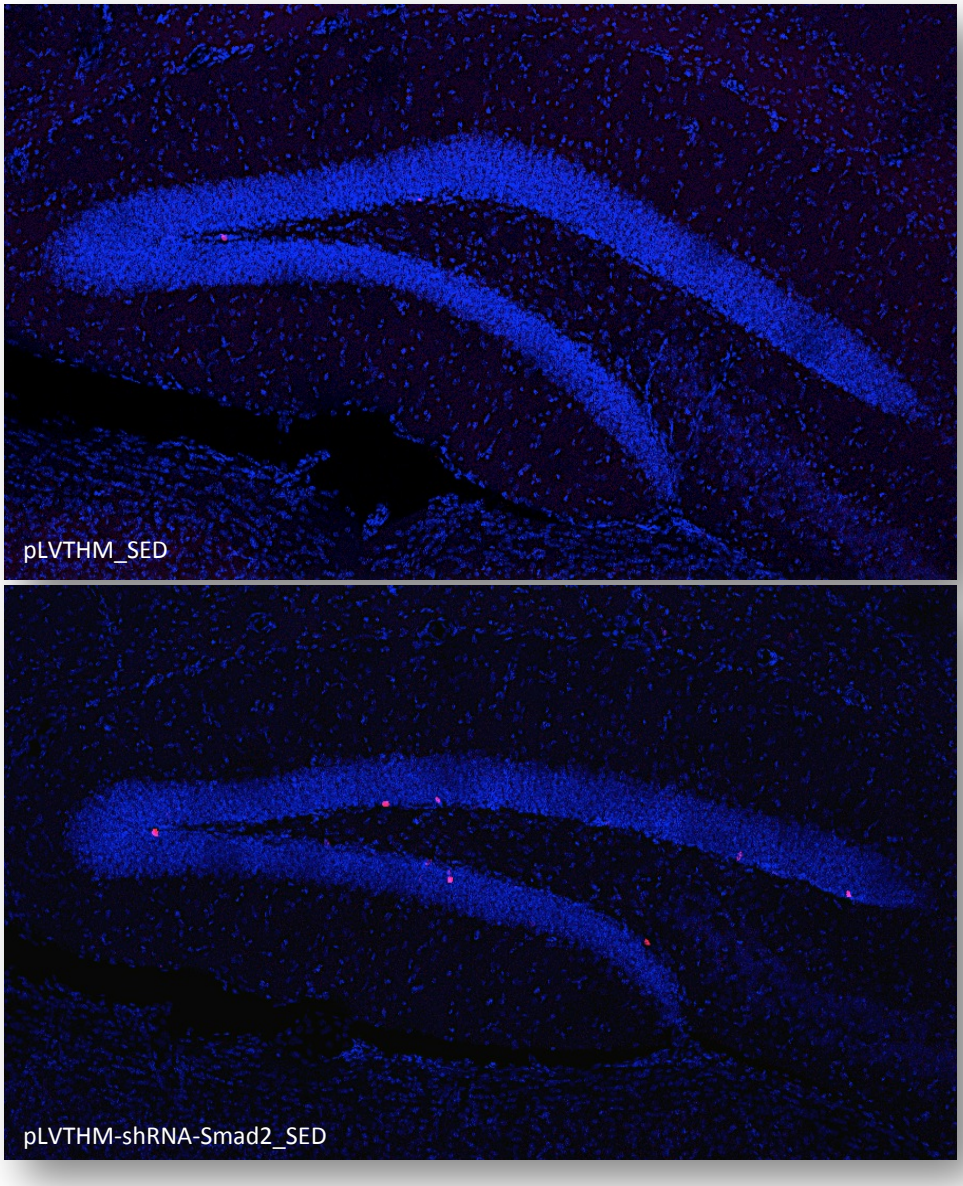

Fig. 7 Cell proliferation. Cells proliferating at the moment of the sacrifice was quantified by means of the pH3 marker. **A.** Total number of $pH3^+$ cells in the loss-of-function study. **B.** Total number of $pH3^+$ cells in the gain of function study. **C-D.** Ratio between the number of $pH3^+$ cells and the number of granule cells in the DG. **E-F.** Total number of $pH3^+$ cells in the rostral part of the DG infected by shRNA (from bregma to -2). **G-H.** Total number of $pH3^+$ cells in the rostral part of the DG over-expressing *Smad2*. **I.** pH3 immunohistochemistry representing the difference in the total number of proliferating cells at the moment of sacrifice in a control mouse and in a mouse operated with the silencing virus (red, $pH3^+$ cells; blue, DAPI staining).

At the time of the sacrifice, the $BrdU^+$ cells were 3 weeks old. So, the estimation of the total number of $BrdU^+$ cells was useful to assess the survival capacity of the newborn neurons in the DG. The silencing of *Smad2* led to an increase in the survival of the 3-weeks-old neurons (p-value= 0.007) while the *Smad2* over-expression decreased the number of $BrdU^+$ cells (p-value= 0.034). This modulation was confirmed analysing the ratio between the number of $BrdU^+$ cells and total number of granular cells (p-value= 0.007 for shRNA and p-value= 0.034 for the over-expression) (Fig. 8 A-D).

The influence of the differential gene expression on survival was observable also in the rostral region of the DG. There was a significant increase in the rostral regions where neurons expressed less *Smad2* (at 1600 μm from bregma, p-value= 0.018; at 2000 μm from bregma, p-value= 0.010), while, on the contrary, there was a significant decrease in the rostral DG where *Smad2* was over-expressed (p-value= 0.034) (Fig. 8 E-H).

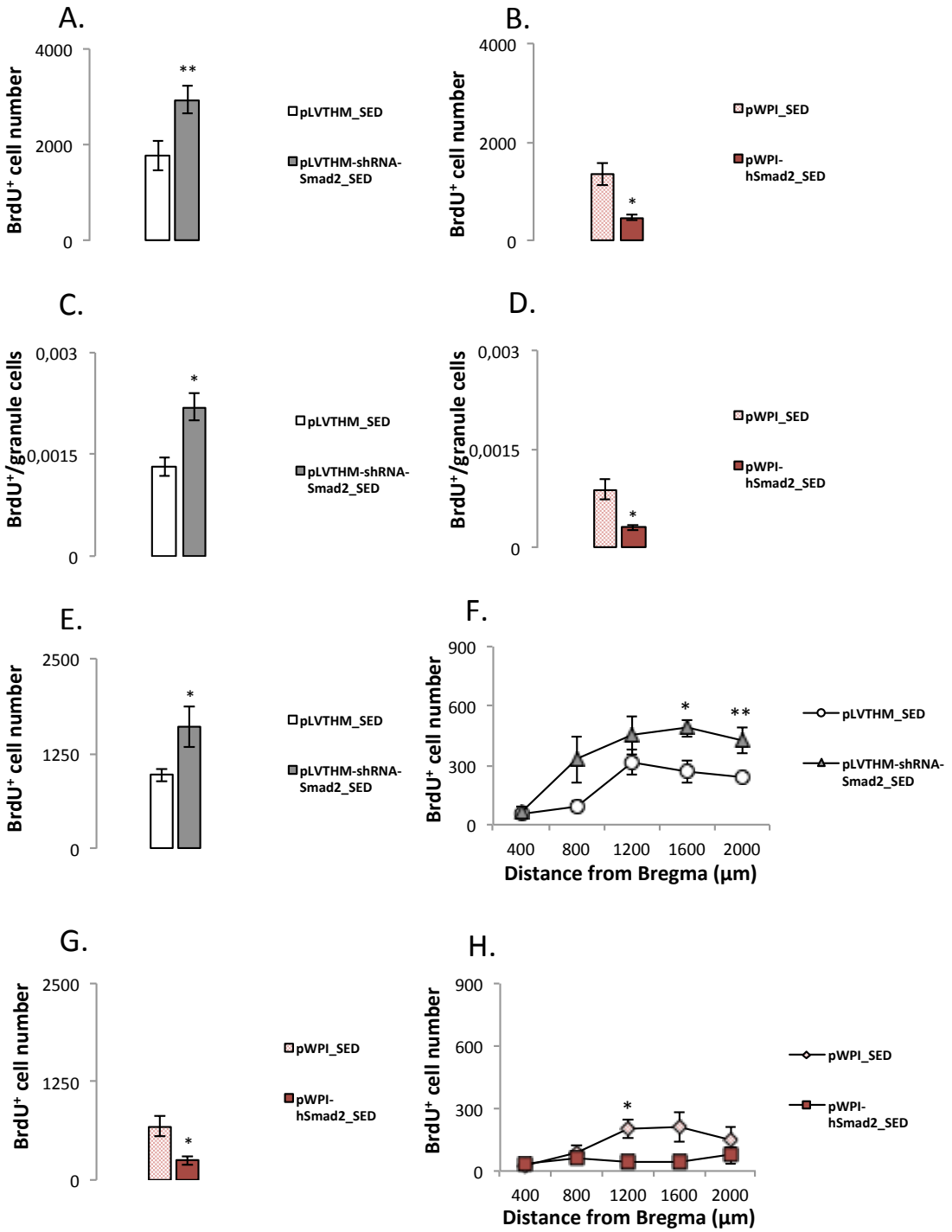

Fig. 8 BrdU⁺ cell survival. Cells 3-weeks-old were labelled with BrdU. **A.** Total number of BrdU⁺ cells in the loss-of-function study. **B.** Total number of BrdU⁺ cells in the gain of function study. **C-D.** Ratio between the number of BrdU⁺ cells and the number of granule cells in the DG. **E-F.** Number of BrdU⁺ cells in the rostral part of the DG infected by shRNA (from bregma to -2). **G-H.** Number of BrdU⁺ cells in the rostral part of the DG over-expressing *Smad2*. [Continues on next page]

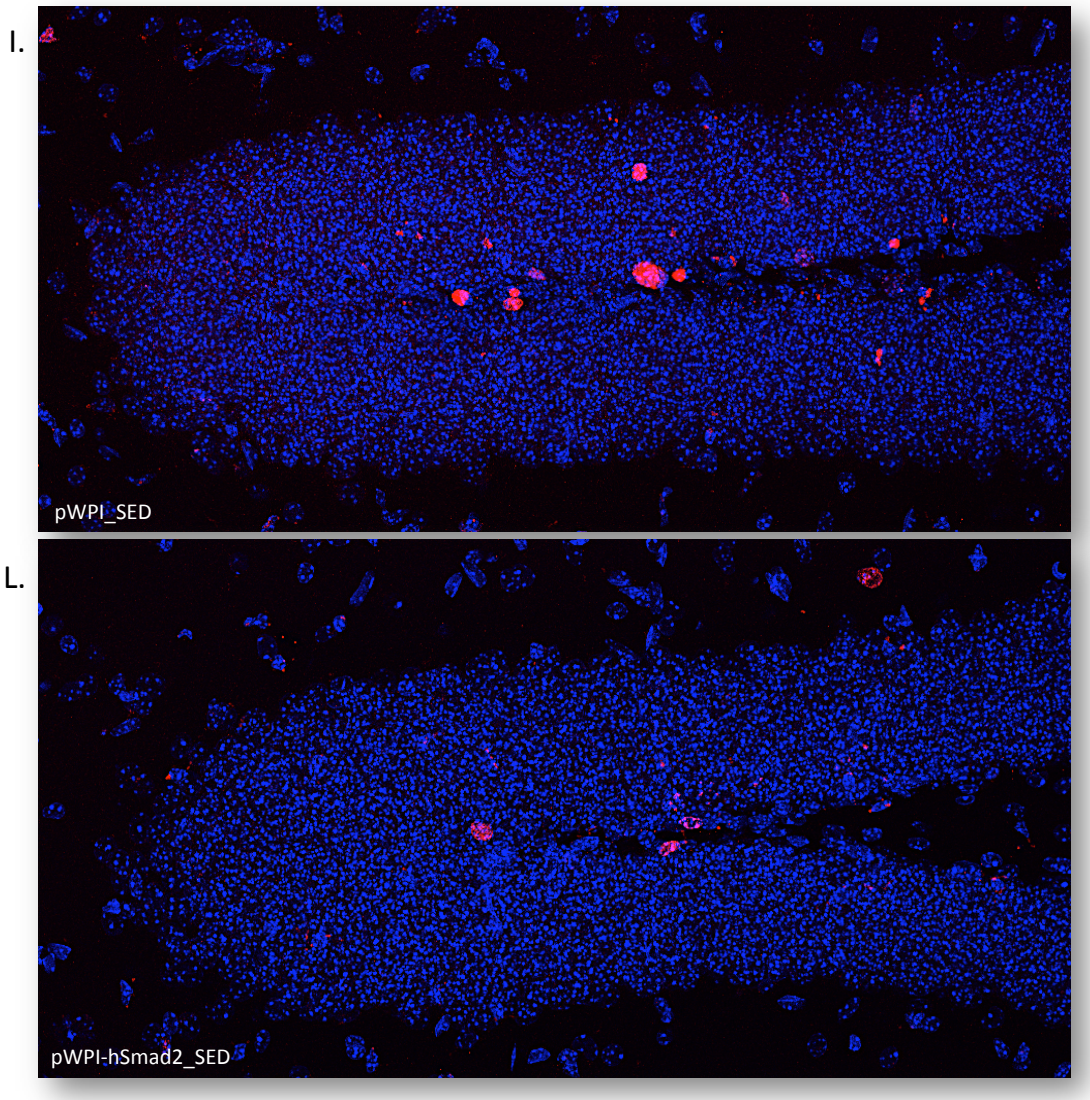

Fig. 8 BrdU$^+$ cell survival. Cells 3-weeks-old were labelled with BrdU. **I-L.** BrdU immunohistochemistry representing the difference in the total number of BrdU$^+$ cells in a control mouse (I) and in a mouse operated with the over-expression virus (L). Detail of the peak of the DG. (red, BrdU$^+$ cells; blue, DAPI staining).

The total number of cells representing the different subpopulations of immature neurons (DCX$^+$/CLR$^-$; DCX$^+$/CLR$^+$; total number of DCX$^+$ cells; %(DCX$^+$/CLR$^+$)/DCX$^+$) remained unchanged (Fig. 9 A-H), also when related to the total number of granule cells (Fig 10 A-F).

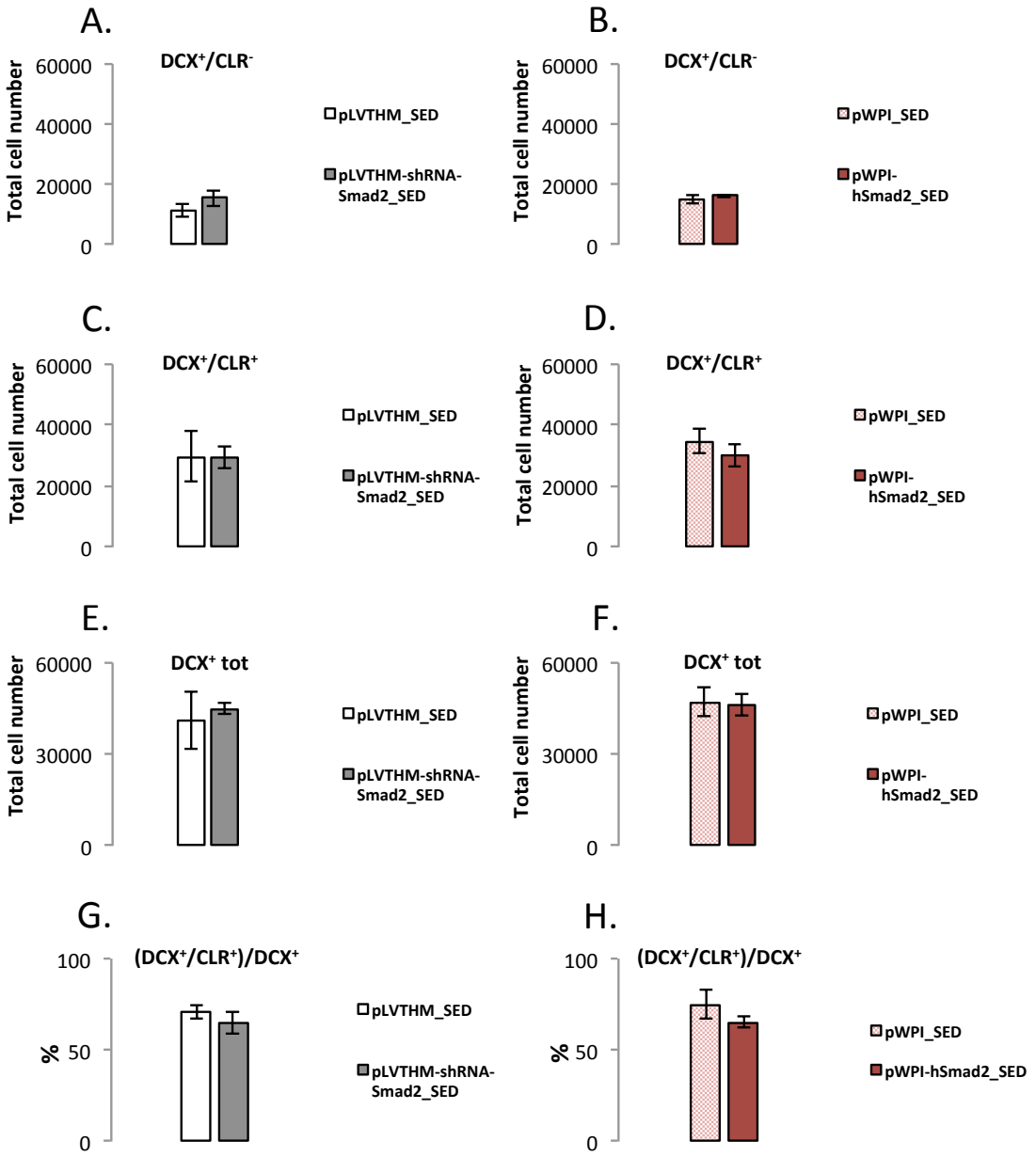

Fig. 9 Subpopulations of immature cells. Total number of DCX^+/CLR^- (**A-B**), DCX^+/CLR^+ (**C-D**) and DCX^+ cells (**E-F**) in the dentate gyrus. **G-H.** Ratios between DCX^+/CLR^+ cells and the total number of DCX^+ cells.

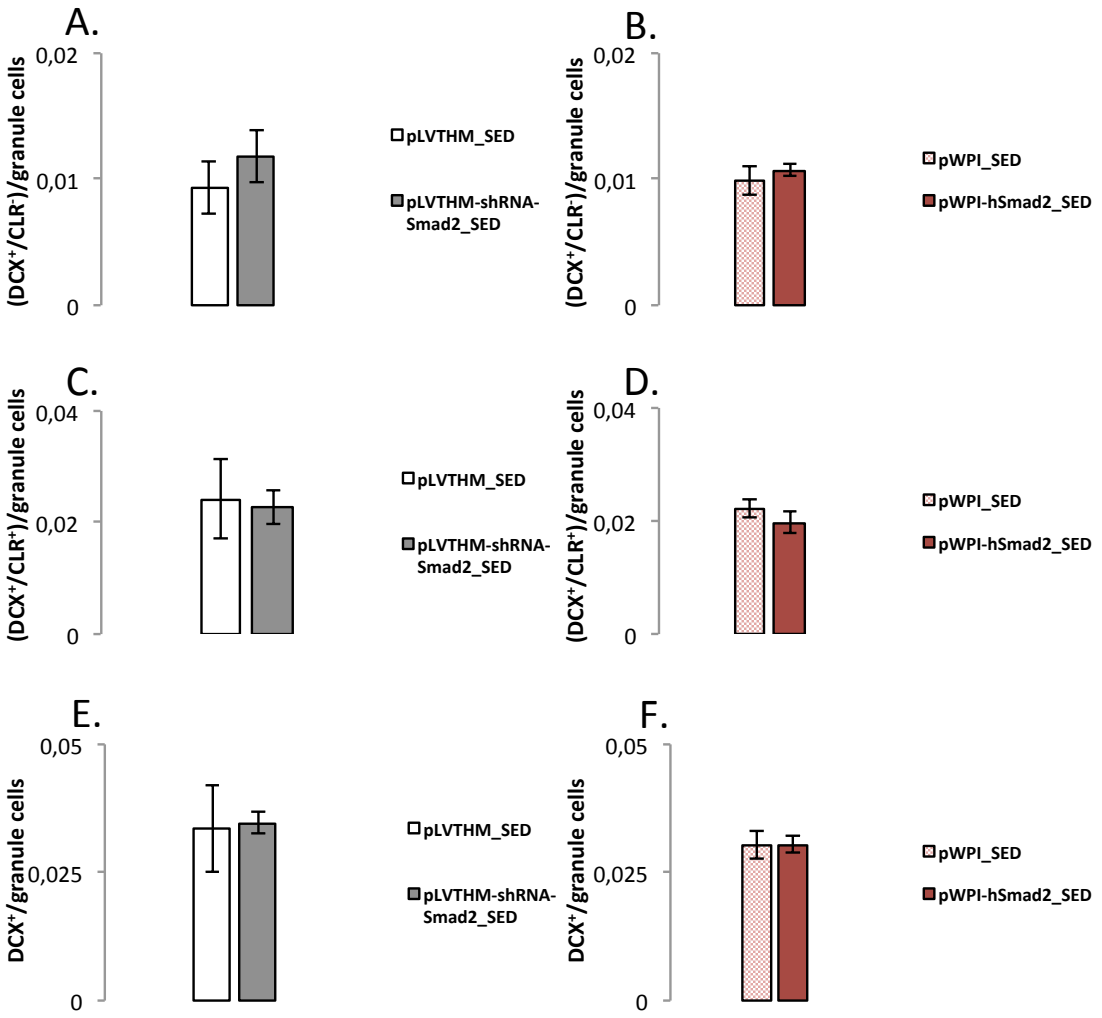

Fig. 10 Ratios between the different subpopulations of immature cells and the total number of granule cells.

Lentivirus infects all kind of cells in the DG, so the number of GFP^+ cells co-expressing DCX marker were counted in order to infer a role of *Smad2* in the maturation process of the neurons. The regions where the shRNA-Smad2 lentivirus was injected showed a higher number of DCX^+/GFP^+ cells, (p-value= 0.007), while, in the group of over-expression, there was a downward trend (p-value= 0.077) (Fig. 11 A-B).

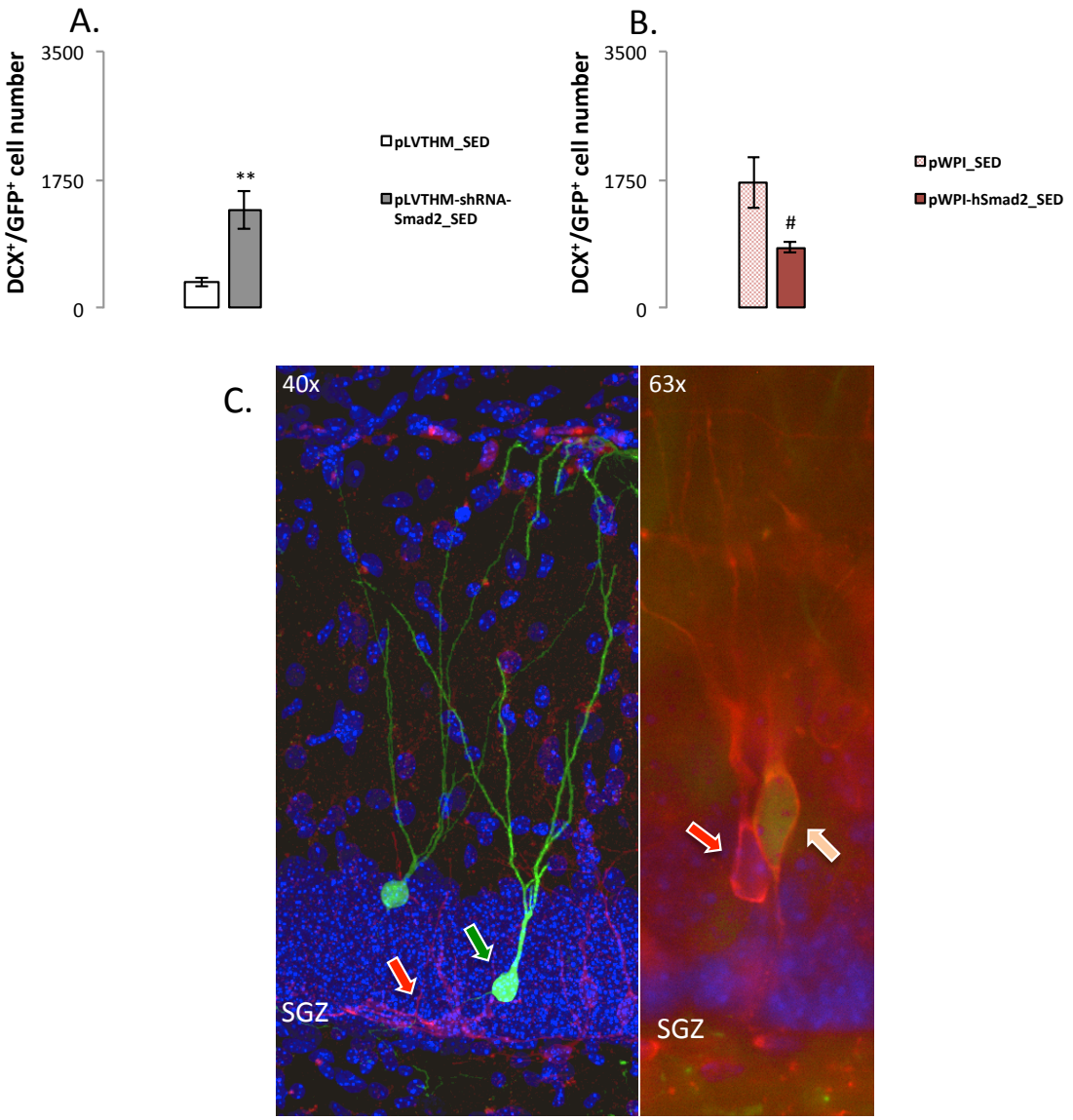

Fig. 11 DCX$^+$/GFP$^+$ cells. A. Number of GFP$^+$ cells (green) co-expressing DCX (red) in the silencing experiment and **B.** in GFP$^+$ cells over-expressing *Smad2*. **C.** Examples of DCX$^-$/GFP$^+$ cells (green arrow), DCX$^+$/GFP$^-$ cells (red arrows) and DCX$^+$/GFP$^+$ cells (orange arrow). (Blue, DAPI staining).

The area occupied by vGlut and GAD's synaptic boutons was measured in the inner part of the molecular layer. No co-localization of the excitatory and inhibitory boutons was found at any site. The percentage of area covered by the vGlut synapses did not change as effect of the genetic manipulation. It was noticed a decrease in the percentage of area covered by the GAD's inhibitory boutons in the DG expressing shRNA-Smad2 (p-value= 0.05) and an increase in the ratio vGlut/GAD (p-value= 0.027), while no changes were detected in the over-expression group (Fig 12 A-F).

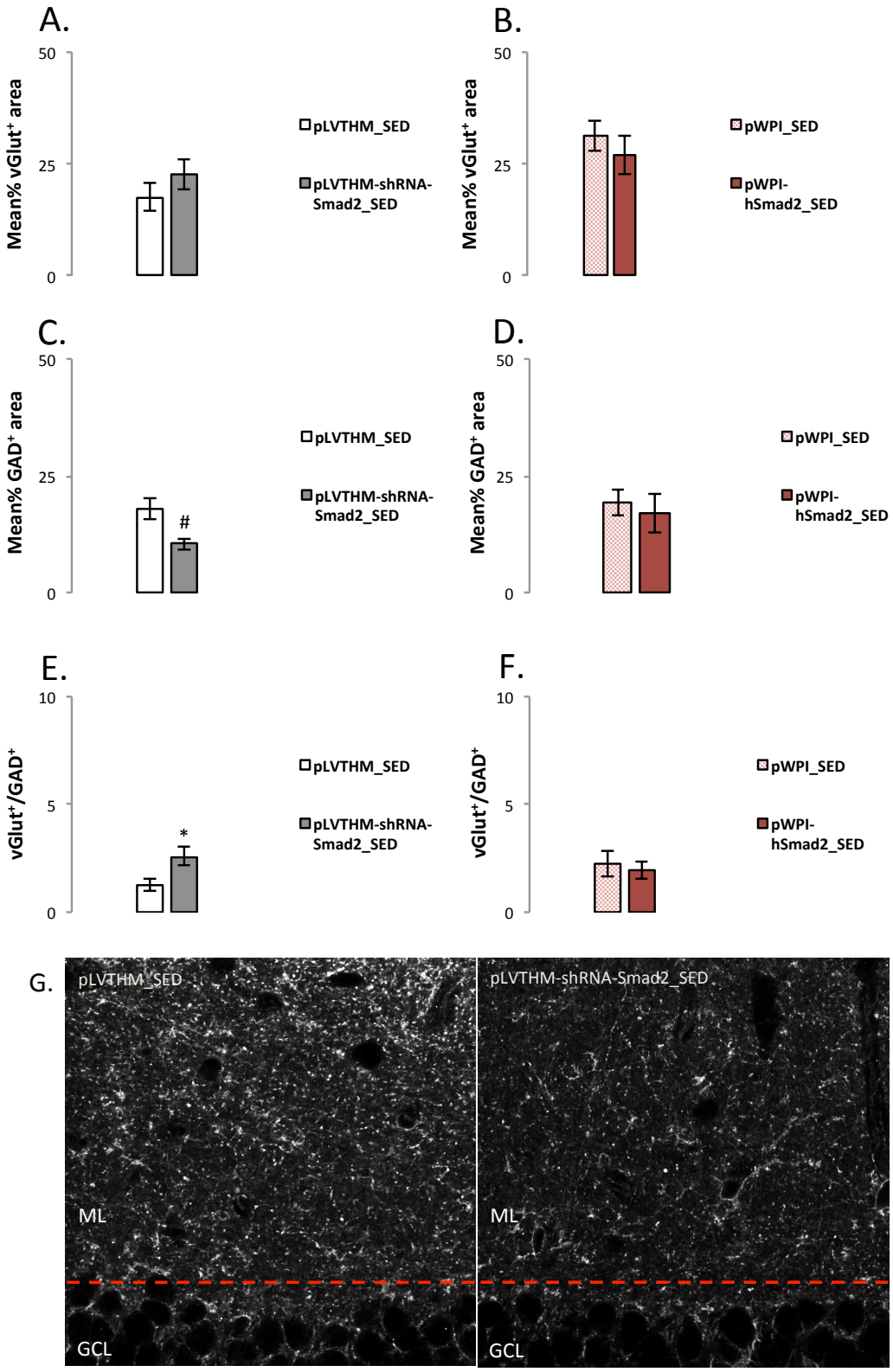

Fig. 12 vGlut⁺ and GAD⁺ areas. A-B. The vGlut⁺ area was measured in the inner part of the ML; **C-D.** The GAD⁺ area was measured and a tendency toward a lower mean percentage was found in animals infected with the shRNA; **E-F.** Ratios between vGlut⁺ and GAD⁺ areas. Animals expressing less *Smad2* showed a higher ratio. **G.** 8-bits images representing the different density of GAD's synaptic boutons in a control mouse (left) and in a mouse operated with the silencing virus (right).

2.3 Effects of differential *Smad2* expression on synaptic plasticity

The silencing of *Smad2* significantly decreased the arborisation complexity of the mature neurons. Sholl analysis of confocal z-stacks of GFP^+ cells revealed a decrease in the number of intersections and length compared to the control group (Fig. 13 A and C). It was observed a decrease in the length of the tertiary dendrites (p-value= 0.032), but no differences where found in the number of branch points (Fig. 14 A-C-E). Differences in the proximal dendrites were found analysing the GFP^+ cells over-expressing *Smad2* (Fig. 13 B and D; Fig. 14 B-D-F).

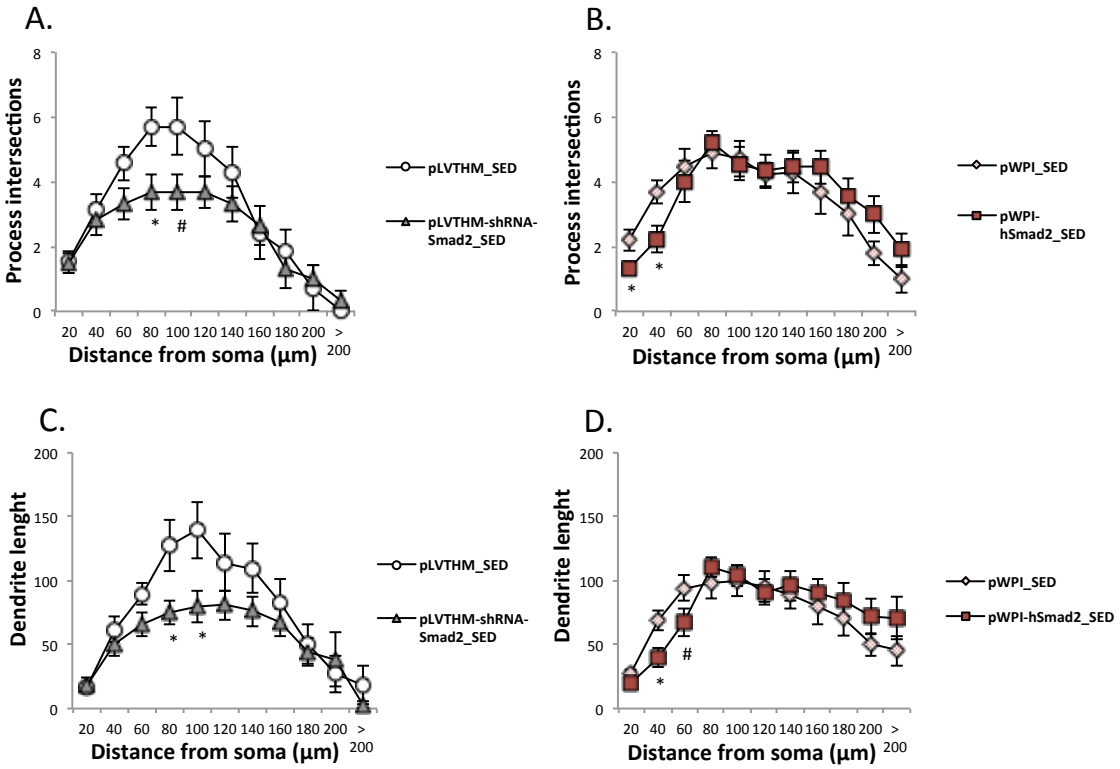

Fig. 13 Dendritic complexity analysed with a Sholl analysis. A. Number of dendritic intersections per shell in the GFP^+ cells silencing *Smad2* (p-values at 80 µm= 0.029 and 100 µm= 0.055); **B.** Number of dendritic intersections per shell in the over-expressing cells (p-values at 20 µm= 0.03 and 40 µm= 0.021); **C.** Mean measurement of the total dendritic length in each shell of the silencing cells (p-values at 80 µm= 0.025 and 100 µm= 0.025). **D.** Mean measurement of the total dendritic length in each shell of the over-expressing cells (p-values at 40 µm= 0.018 and 60 µm= 0.086).

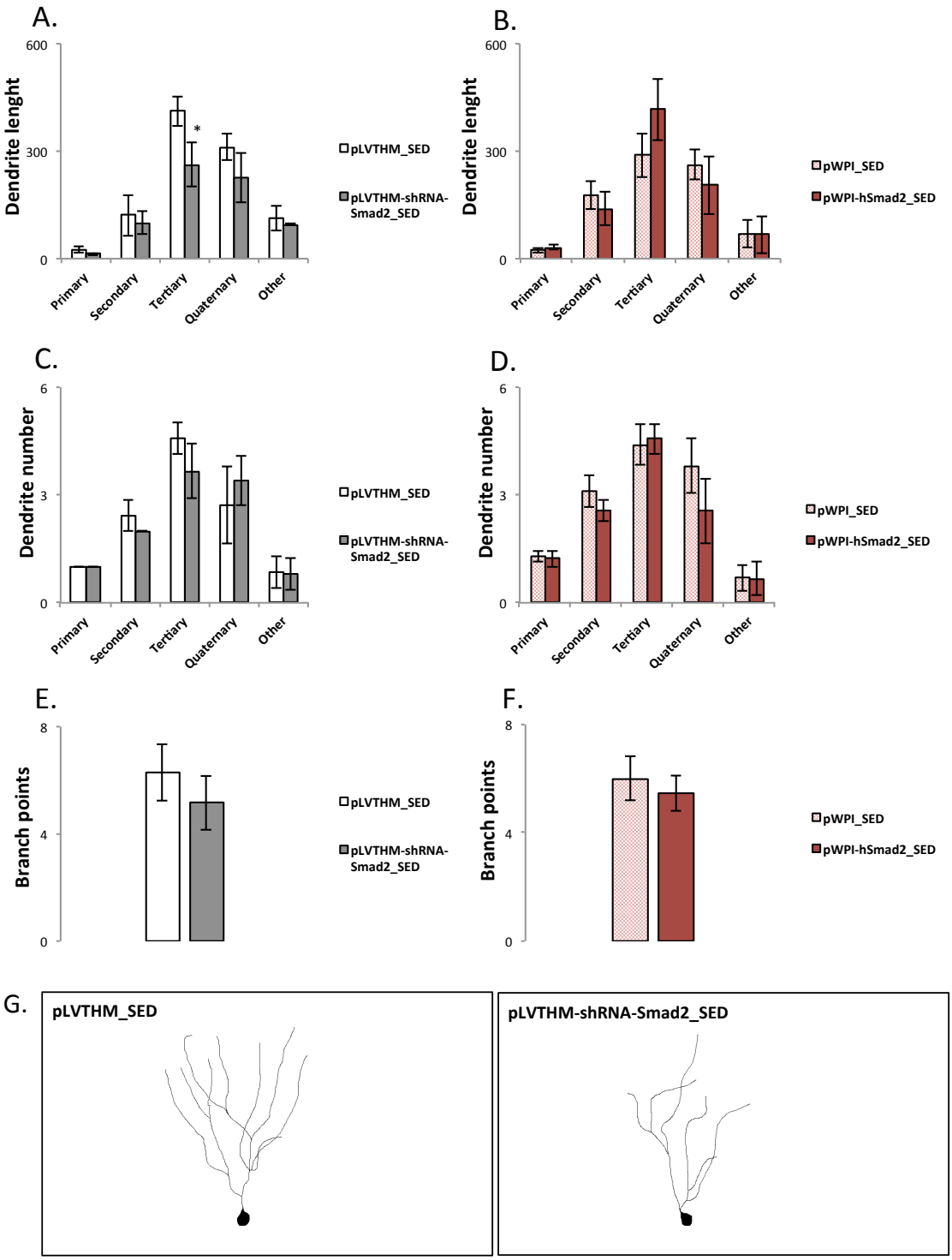

Fig. 14 Dendritic complexity. Parameters measuring the dendritic arborisation complexity of the GFP$^+$ cells. **A-B.** Mean length for each class of dendrites. **C-D.** Mean number of dendrites for each class of dendrites; **E-F.** Number of branch points. **G.** Drawings of DG granule cell dendritic tree from a representative control GFP$^+$ neuron and a GFP$^+$ neuron silencing *Smad2*.

Spines were quantified on projections of confocal stacks of tertiary dendrites, located in the molecular layer. The GFP^+ cells expressing shRNA-Smad2 showed a decrease in spine density compared to the cells expressing the control vector (p-value< 0.001). No differences in spine density were found between cells infected by the virus over-expressing *Smad2* and its control (Fig. 15).

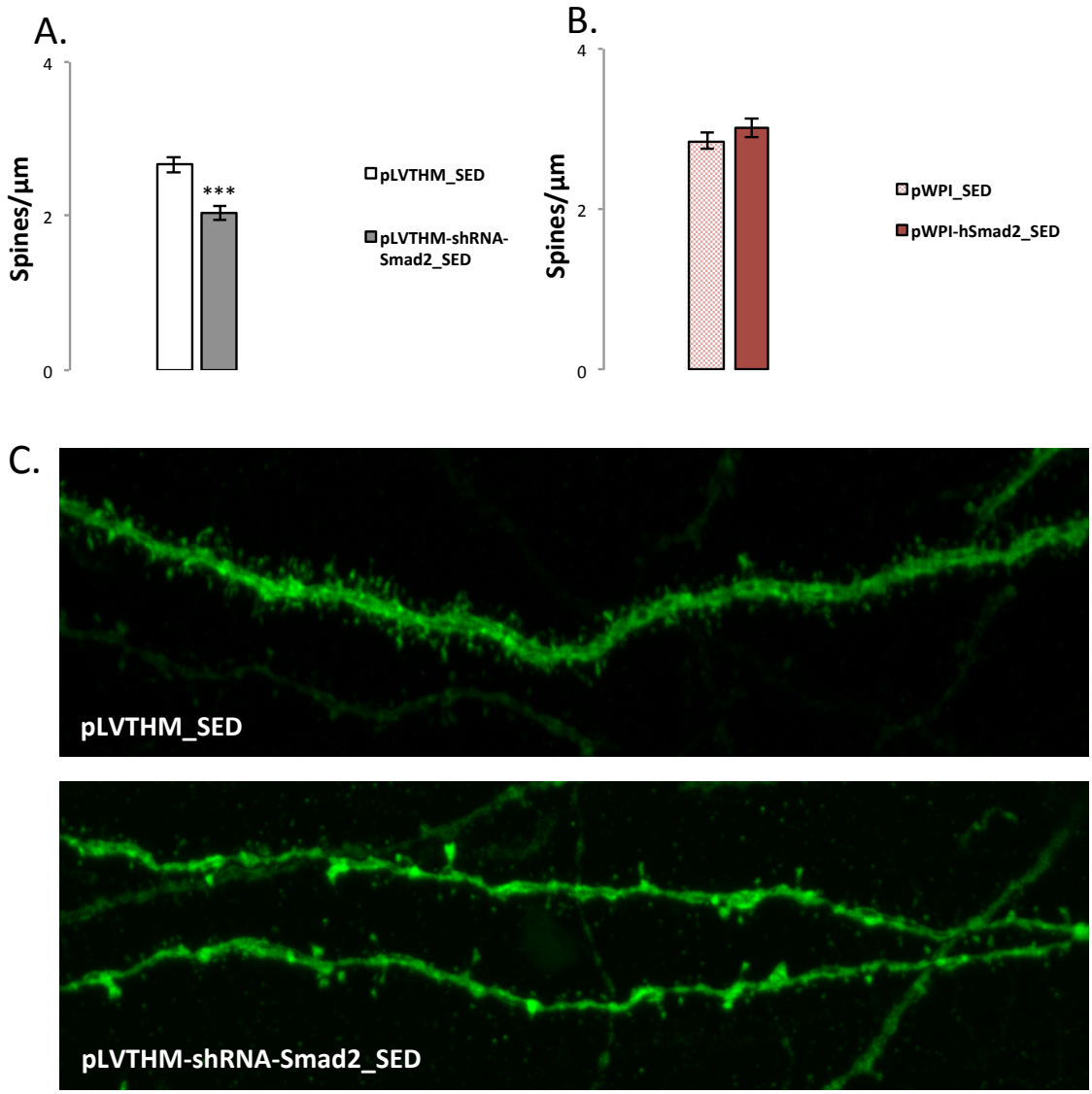

Fig. 15 Spine density. Spine density was quantified on confocal stacks of tertiary dendrites of GFP^+ cells silencing *Smad2* (**A**) or over-expressing it (**B**). **C.** Examples of the different spine density in a tertiary dendrite of a control neuron and of a neuron silencing *Smad2*.

3. Effects of *Smad2* loss- and gain-of-function on hippocampal-dependent behaviour

To assess if *Smad2* manipulation in the DG has an effect on behaviour, animals underwent to a battery of hippocampal-dependent tests before the sacrifice.

3.1 Activity

Animals were tested in an activity cage to exclude any kind of impairment in motor skills and/or activity, due to the surgical operation or the genetic manipulation. All the animals showed a normal activity's profile (Fig. 16).

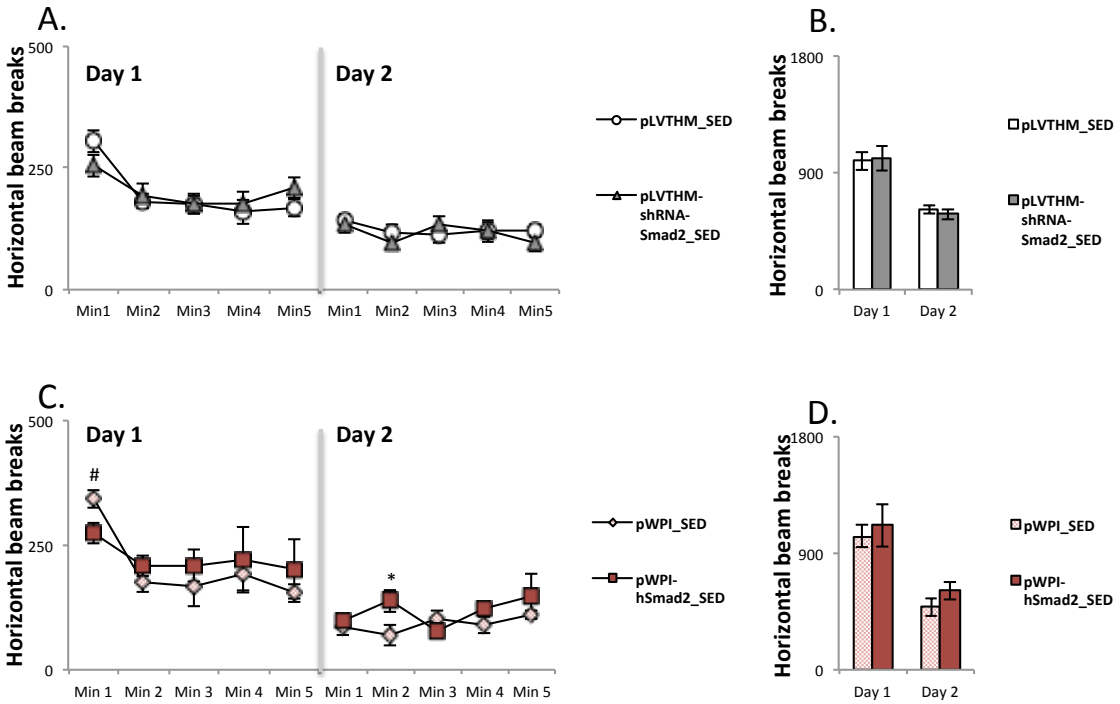

Fig. 16 Activity Cage. Motor activity was observed for 2 days and measured as the number of horizontal beam breaks. **A.** Representation of the horizontal beam breaks at each minute in the animals injected with the shRNA; **B.** Mean of the total horizontal activity at each day in the animals silencing *Smad2*; **C.** Horizontal beam breaks at each minute in the animals injected with the plasmid of over-expression; **D.** Mean of the total horizontal activity at each day in the animals over-expressing *Smad2*.

3.2 Anxiety

No differences were found in the elevated plus maze between groups. All the animals spent a similar average amount of time in the open arms,

independently of the different genetic expression. The parameters analysed showed that all the animals had a similar profile in an anxiety test (Fig. 17).

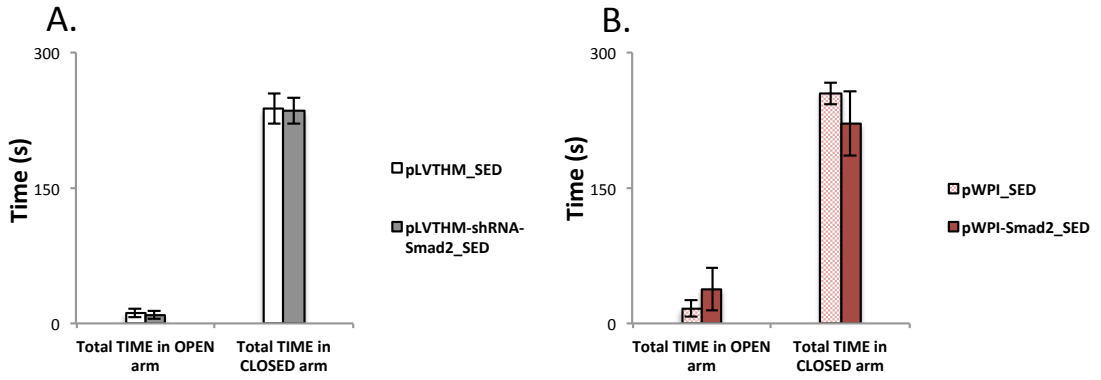

Fig. 17 Elevated Plus Maze. Total time spent in the open and closed arms in the experiment of loss-of-function (**A**) and gain-of-function (**B**).

3.3 Spatial learning and memory

3.3.1 Morris Water Maze

As further confirmation that the motor activity of the animals was the same, no differences were found comparing the velocity by which the mice swam in the pool during the Morris water maze test (data not shown). Nevertheless, mice injected with shRNA-Smad2 virus showed a deficit in learning the task, as it was possible to deduce observing the learning curve. The average time that the animals spent finding the platform at the 5th day of acquisition is generally longer compared to the time spent by the control group (p-value= 0.037) (Fig. 18 A). The slope obtained from the learning curve showed a worst performance for the shRNA-Smad2 group (p-value= 0.037) (Fig. 18 B).

However, the time spent in the platform quadrant during the probe was the same as the control when compared with the mean time spent in the other quadrants (p-value for pLVTHM_SED= 0.028 and for pLVTHM-shRNA-Smad2_SED p-value= 0.017) (Fig. 18 C). On the other hand, while the total time spent in the other quadrants is the same time spent in the only platform quadrant in the control animals, animals operated with the shRNA construct spent more time in the quadrants without the platform (p-value= 0.036) (Fig. 18 D).

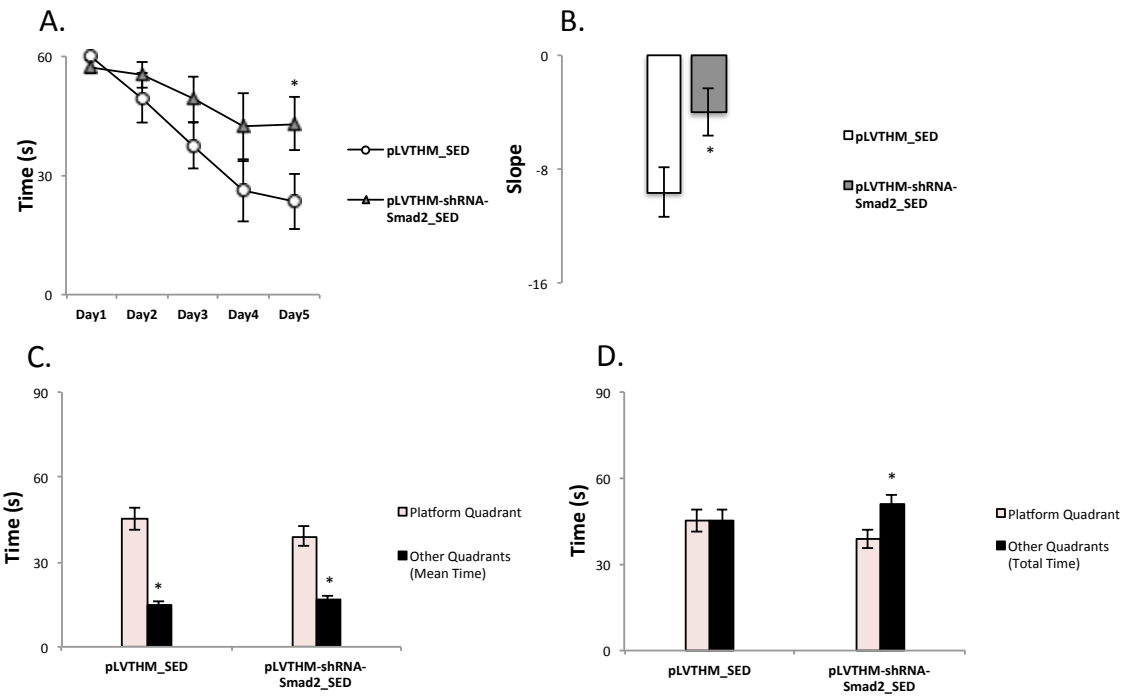

Fig. 18 Morris Water Maze in the loss-of-function experiment. A. The learning curve represents the mean escape latency at each day; **B.** Slope extrapolated from the learning curve; **C.** Probe test: mean time spent in the platform quadrant versus the mean time spent in the other three quadrants. **D.** Probe test: time spent in the platform quadrant versus the total time spent in the other three quadrants.

In the experiment where *Smad2* was over-expressed, no differences were found in the Morris water maze (Fig. 19).

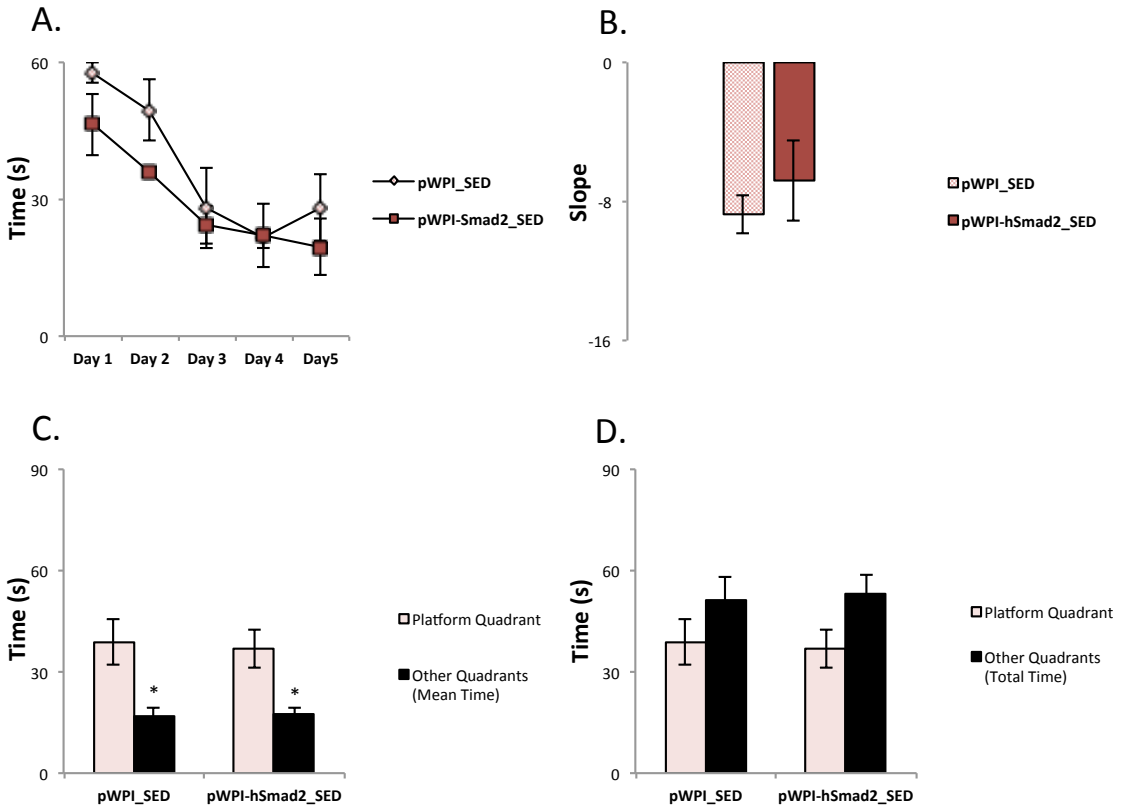

Fig. 19 Morris Water Maze in the gain-of-function experiment. A. The learning curve represents the mean escape latency at each day; **B.** Slope extrapolated from the learning curve; **C.** Probe test: mean time spent in the platform quadrant versus the mean time spent in the other three quadrants (p-value for pWPI_SED= 0.028 and for pWPI-hSmad2_SED p-value= 0.017). **D.** Probe test: time spent in the platform quadrant versus the total time spent in the other three quadrants.

3.3.2 T-Maze

To further investigate the role of *Smad2* in spatial learning and memory, a new set of animals was operated and injected with the modified lentiviral constructs. Twenty days after the stereotaxic operation, the mice were exposed to a T-Maze. During the test trial, the control animals and the over-expression group performed more entries and spent more time in the new arm while the pLVTHM-shRNA-Smad2_SED group spent the same amount of time visiting both arms (p-value for entries= 0.002; p-value for time= 0.007) (Fig. 20).

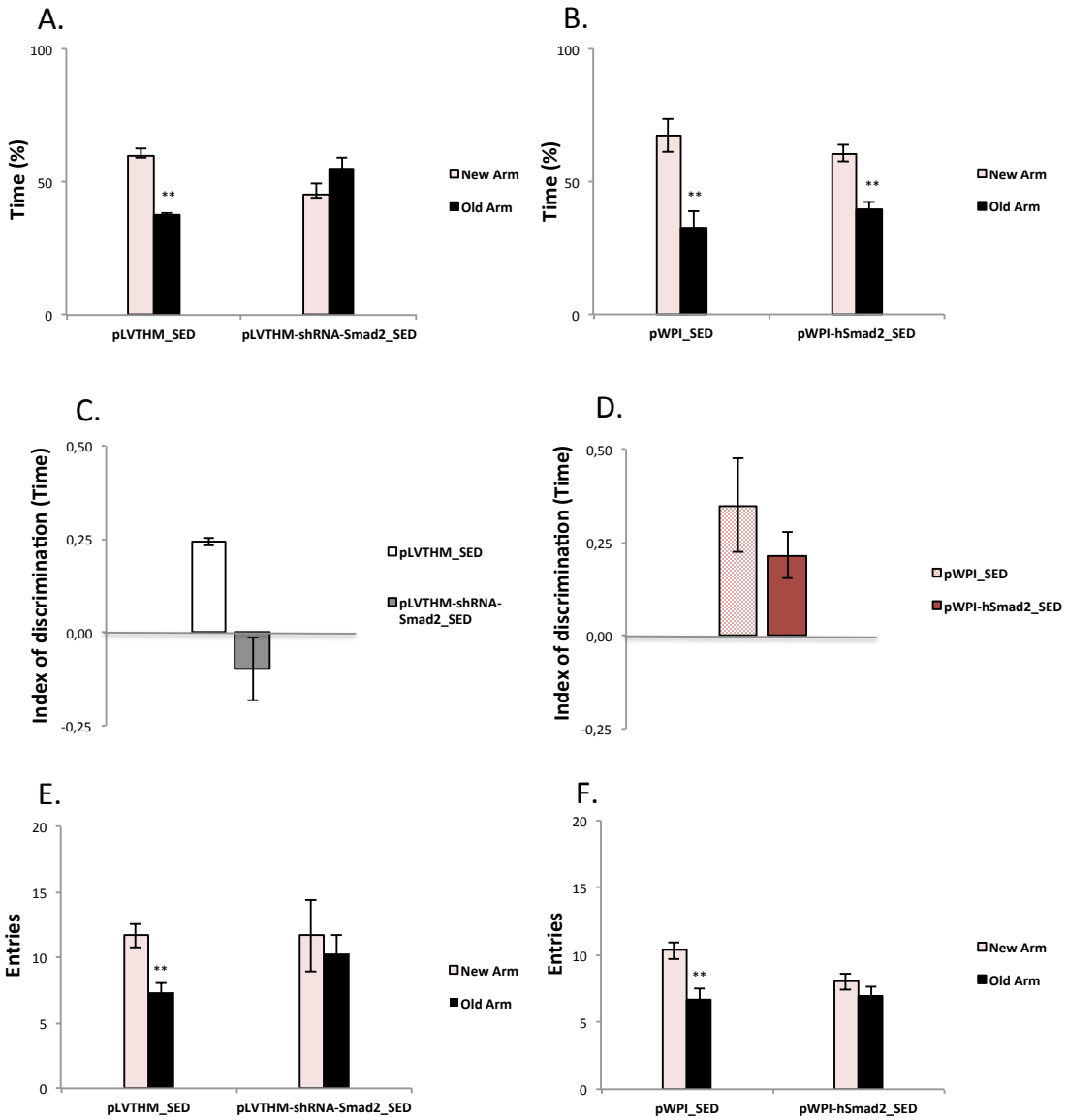

Fig. 20 T-Maze. A-B. Percentage of time spent visiting the new or old arm during the probe trial in the animals silencing *Smad2* (A) or over-expressing it (B). **C-D.** Index of discrimination calculated as the ratio between the difference in the time spent in the new and old arm, and the total time spent in both arms. **E-F.** Entries in each arm of the maze.

CHAPTER 2
Effects of *Smad2* loss- and gain-of-function in the adult dentate gyrus of runner animals

1. A study on the effects of exercise mediated by *Smad2* gene

In order to study the effects of exercise mediated by *Smad2*, animals were subjected to double bilateral stereotaxic injections with lentiviral constructs to silence or over-express *Smad2* (n= 8-10 in each group). After three to four days of recovery, animals started their training on a treadmill. To assess the survival of the newborn cells in the granule cell layer, BrdU was injected for 4 consecutive days, once a day, during the first days of running. Two weeks after the first BrdU injection, animals were evaluated in a set of behavioural task: the activity cage, the elevated plus maze and the Morris water maze. The day after the probe, animals were sacrificed and the histology of the brain was analysed (Fig. 1).

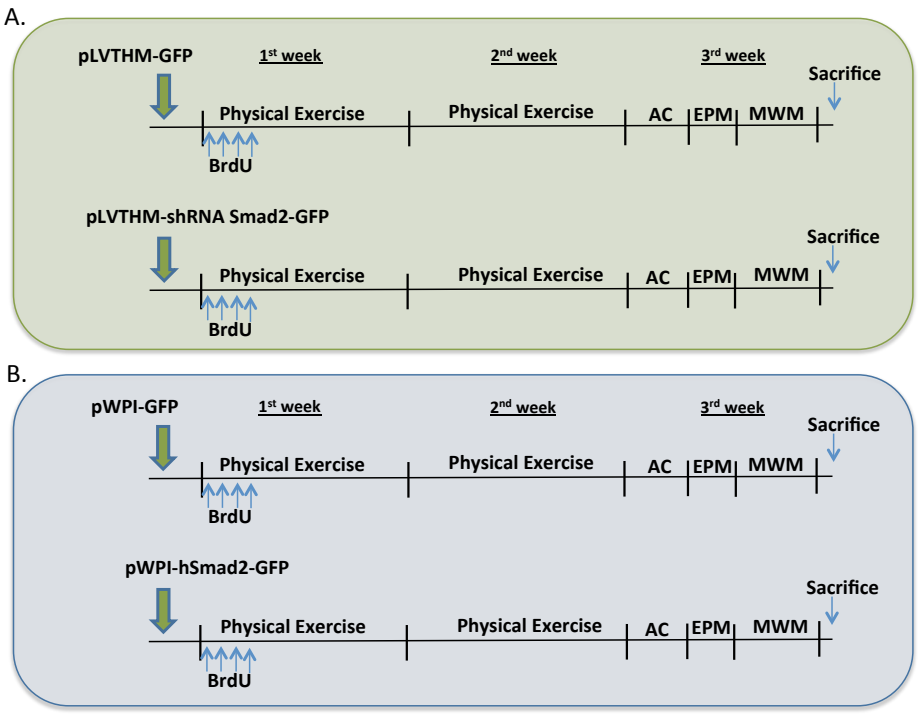

Fig. 1 Experimental design. A. *Smad2* loss-of-function study; **B.** *Smad2* gain-of-function study. AC= Activity Cage; EPM= Elevated Plus Maze; MWM= Morris Water Maze.

1.1 Anatomical analysis of the hippocampus

No differences were found in the volume of the GCL and in the area of SGZ in animals with a lower and higher *Smad2* expression compared to their controls (Fig. 2).

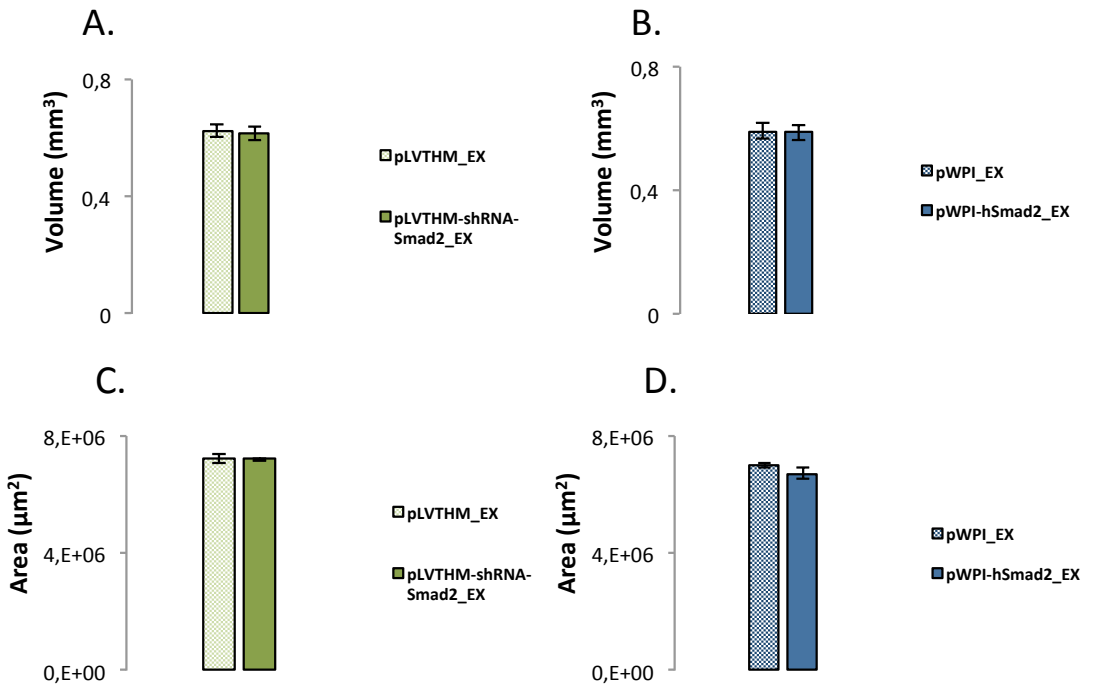

Fig. 2 Anatomical analysis. A-B. Volume of the DG in the silencing (A) and over-expressing (B) experiment; **C-D.** Area of the SGZ in the silencing (C) and over-expressing (D) analysis.

1.2 Modulation of the adult hippocampal neurogenesis

No differences were found neither in the total number nor in the density of granule cells in the DG, as effect of the genetic manipulation (Fig. 3).

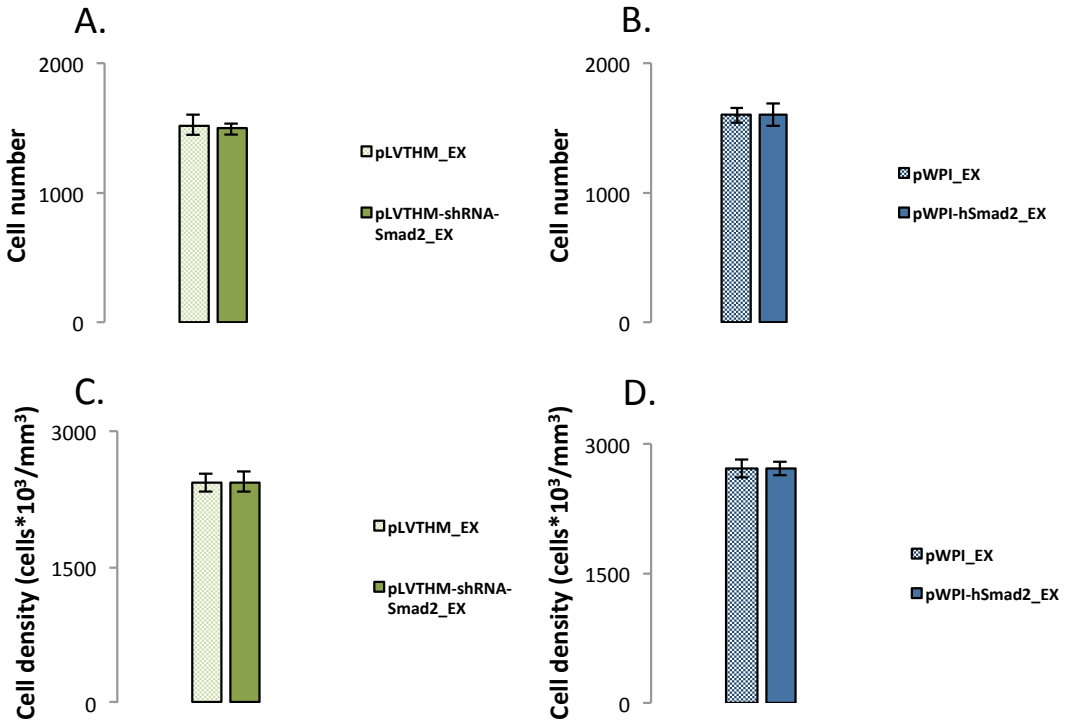

Fig. 3 Granule cells in the DG. A-B. Total granule cells number in the silencing (A) and over-expressing (B) experiment. **C-D.** Granule cell density in the DG of animals silencing (C) and over-expressing (D) *Smad2*.

In runner animals, it was not observed any difference in the number of $pH3^+$ cells in the DG due to the genetic manipulation. No differences were found neither relating the number of $pH3^+$ cells to the total number of granule cells (Fig. 4). Considering just the rostral portion of the DG (from bregma to 2000 μm), the distribution of positive cells was the same among groups, suggesting that no changes in proliferation occurred.

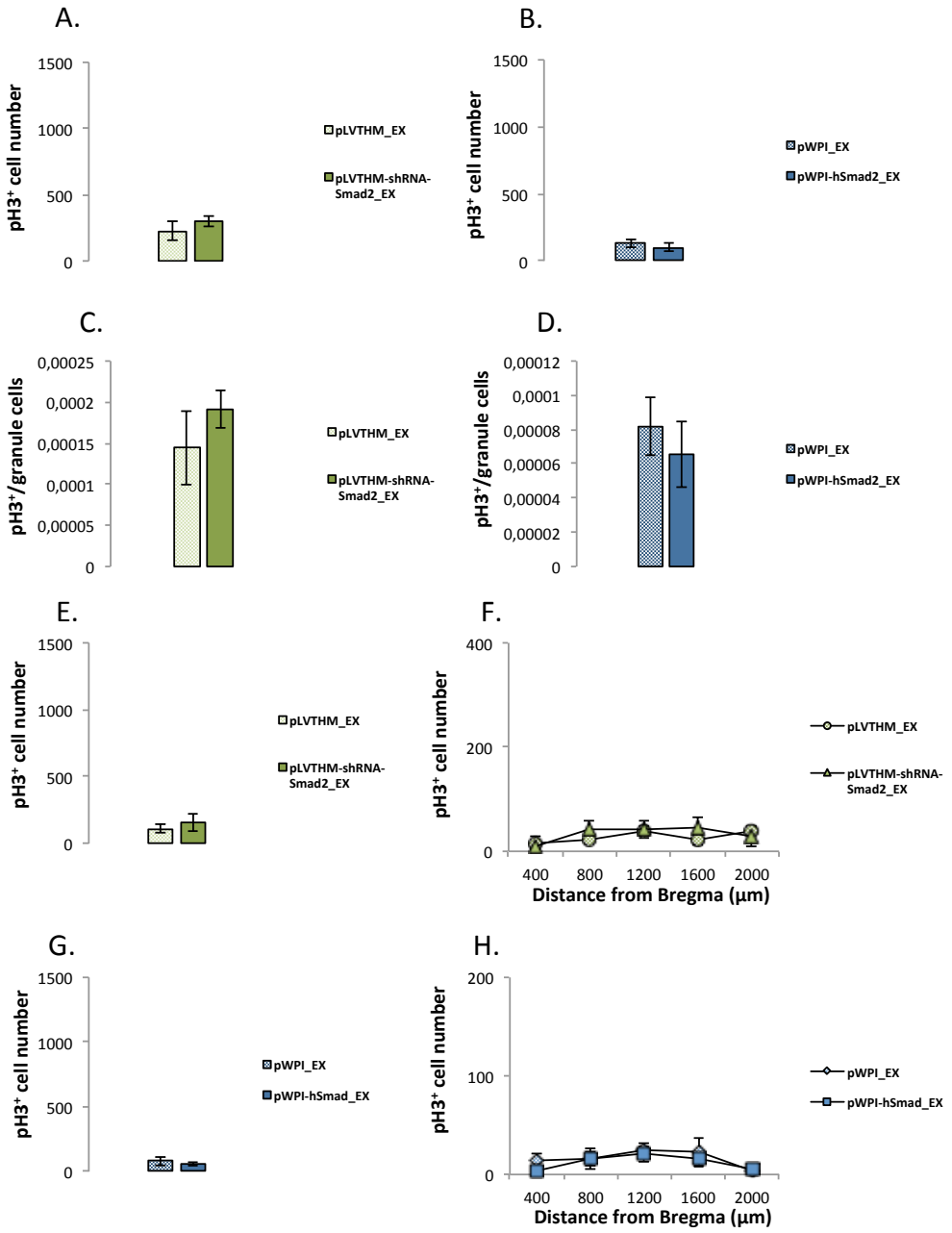

Fig. 4 Cell proliferation. Cells proliferating at the moment of the sacrifice were quantified by means of the pH3 marker. **A.** Total number of $pH3^+$ cells in the loss-of-function study. **B.** Total number of $pH3^+$ cells in the gain-of-function study. **C-D.** Ratio between the number of $pH3^+$ cells and the number of granule cells in the DG. **E-F.** Number of $pH3^+$ cells in the rostral part of the DG infected by shRNA (from bregma to -2). **G-H.** Number of $pH3^+$ cells in the rostral part of the DG over-expressing *Smad2*.

The total number of $BrdU^+$ cells was estimated to assess the survival of the three-weeks-old cells. The DG of those runner animals infected with the shRNA-Smad2 showed an increase in the survival (p-value= 0.022) (Fig. 5 A). An upward trend was detected if the number of $BrdU^+$ cells was related

to the total number of granule cells (p-value= 0.063) (Fig. 5 C). In the rostral portion of the DG, no differences were found in the distribution of $BrdU^+$ cells (Fig. 5 E-F) (at 800 μm from bregma, p-value= 0.045; at 1600 μm from bregma, p-value= 0.086).

No differences were observed in the survival of three-weeks-old cells in the over-expression study (Fig. 5 B-D-G and H).

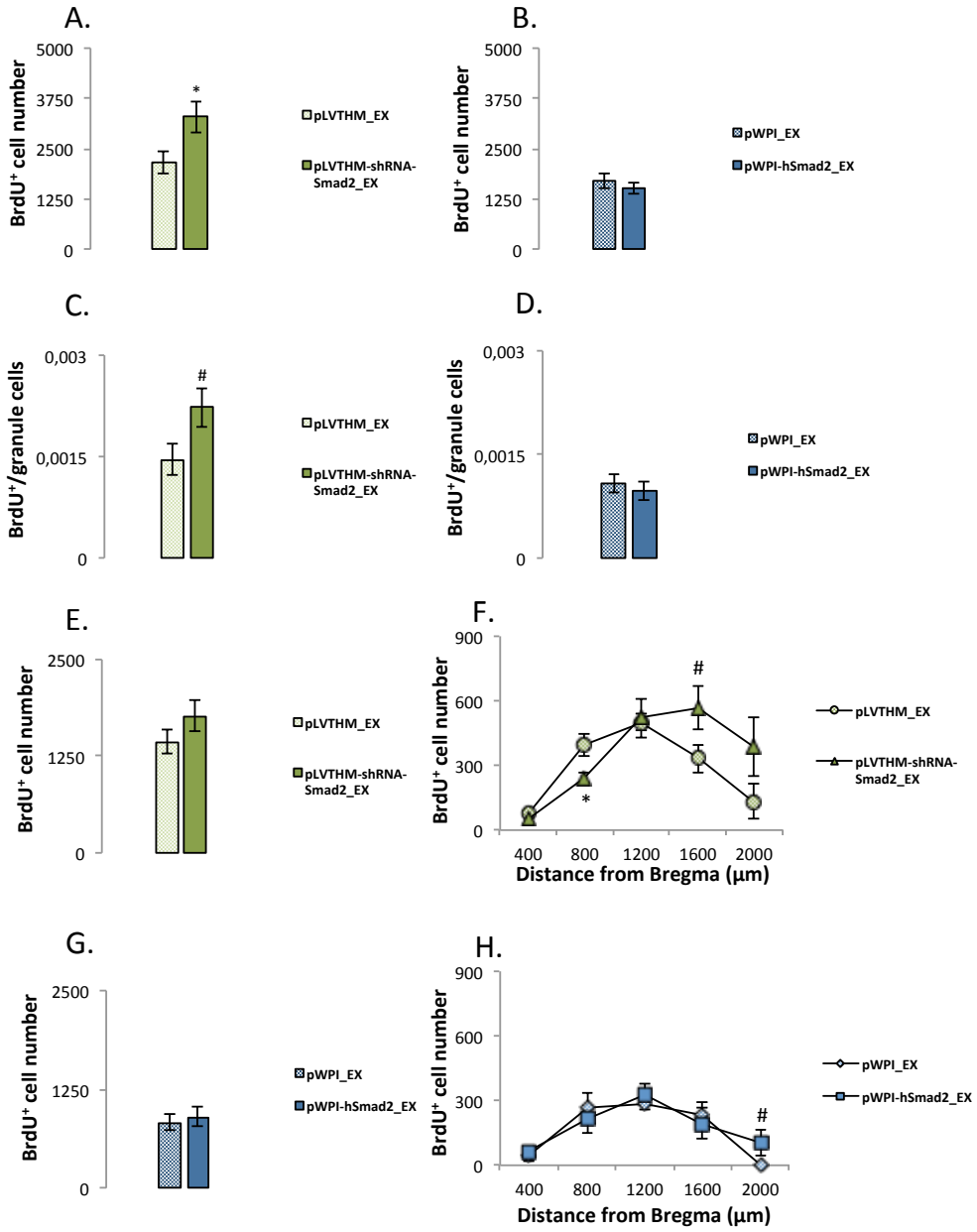

Fig. 5 $BrdU^+$ cell survival. 3-weeks-old cells were labelled with BrdU. **A.** Total number of $BrdU^+$ cells in the loss-of-function study. **B.** Total number of $BrdU^+$ cells in the gain of function study. **C-D.** Ratio between the number of $BrdU^+$ cells and the number of granule cells in the DG. **E-F.** Number of $BrdU^+$ cells in the rostral part of the DG infected by shRNA (from bregma to -2). **G-H.** Number of $BrdU^+$ cells in the rostral part of the DG over-expressing *Smad2*.

The total number of cells representing the different subpopulations of immature neurons (DCX^+/CLR^-; total number of DCX^+ cells; $\%(DCX^+/CLR^+)/DCX^+$) remained unchanged, except for the DCX^+/CLR^+ subpopulation that increases in the animals infected with the shRNA (p-value= 0.05) (Fig. 6) and the number of DCX^+ cells compared to the total number of granule cells in the dentate gyrus (p-value= 0.05) (Fig. 7).

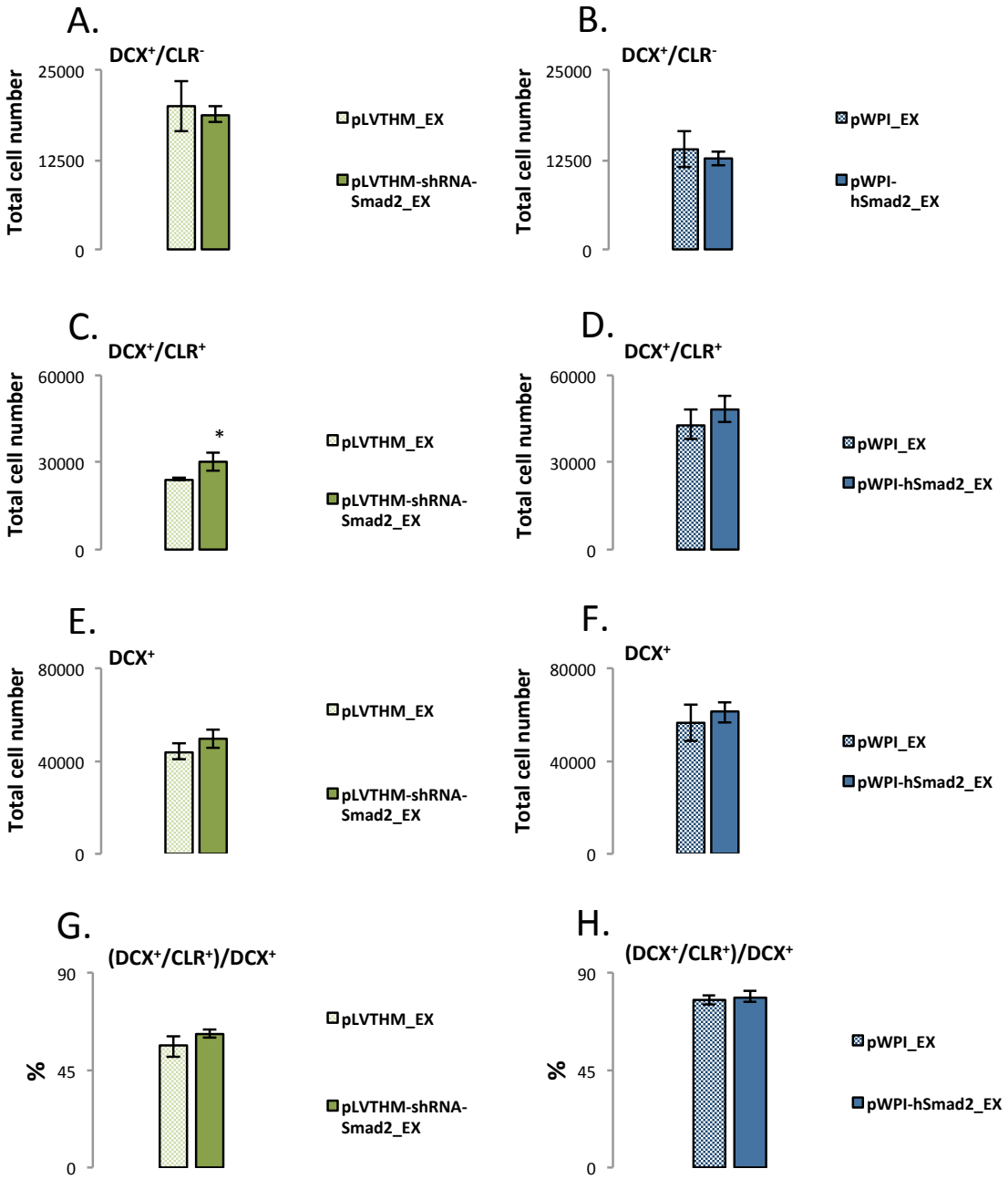

Fig. 6 Subpopulations of immature cells. Total number of DCX^+/CLR^- (**A-B**), DCX^+/CLR^+ (**C-D**) and DCX^+ cells (**E-F**) in the dentate gyrus. **G-H.** Ratios between DCX^+/CLR^+ cells the total number of DCX^+ cells.

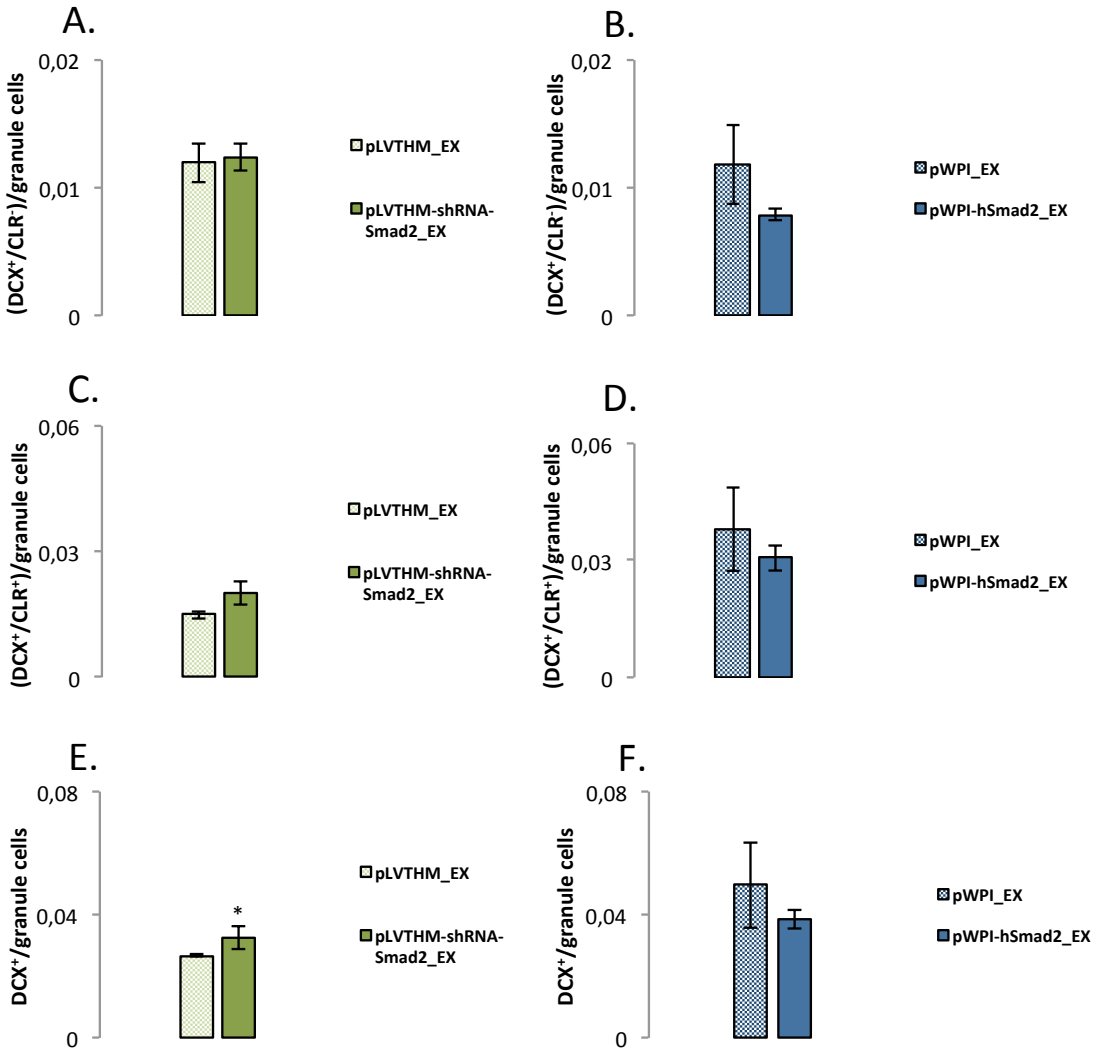

Fig. 7 Ratios between the different subpopulations of immature cells and the total number of granule cells.

The number of GFP^+ cells co-expressing DCX marker were counted in order to infer a role of *Smad2* in the maturation process of the neurons. The regions where the shRNA-Smad2 lentivirus was injected showed a higher number of DCX^+/GFP^+ cells (p-value= 0.003), while *Smad2* over-expression lead to a decrease of these subpopulations of cells (p-value= 0.009) (Fig. 8).

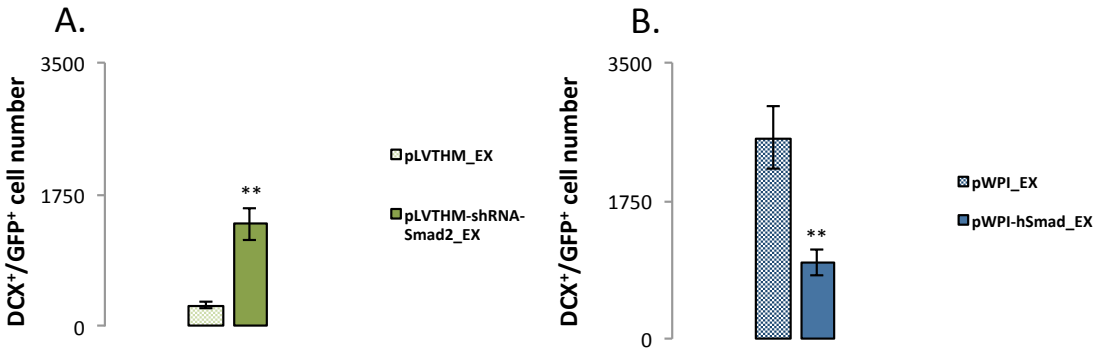

Fig. 8 DCX$^+$/GFP$^+$ cells. A. Number of GFP$^+$ cells co-expressing DCX in the silencing experiment and **B.** in the experiment of over-expression.

The area occupied by vGlut and GAD's synaptic boutons was measured in the inner part of the molecular layer. No co-localization of the excitatory and inhibitory boutons was found at any site.

The percentage of area covered by the vGlut synapses did not change as effect of the genetic manipulation. The percentage of area covered by GAD's inhibitory boutons increased in the DG where cells over-expressed *Smad2* (p-value= 0.001). So, the ratio between vGlut and GAD decreased in runner animals over-expressing *Smad2* (p-value= 0.002) (Fig. 9).

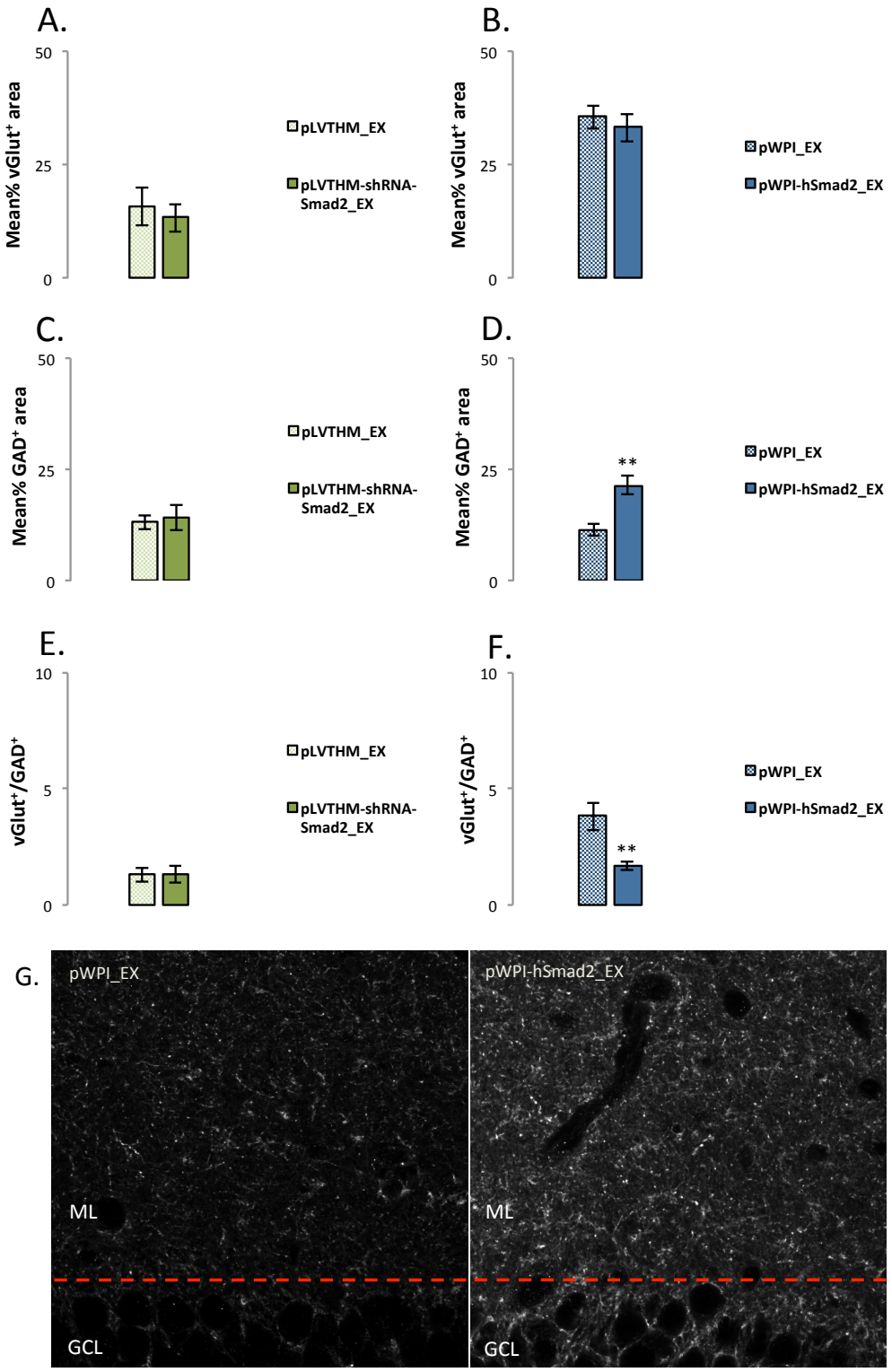

Fig. 9 vGlut$^+$ and GAD$^+$ areas. A-B. The vGlut$^+$ area was measured in the inner part of the ML; **C-D.** The GAD$^+$ area was measured and an increased GAD$^+$ area was found in the molecular layer of the hippocampus over-expressing *Smad2*; **E-F.** Ratios between vGlut$^+$ and GAD$^+$ areas. Animals expressing less *Smad2* showed a higher ratio. **G.** 8-bits images representing the different density of GAD's synaptic boutons in a control mouse (left) and in a mouse operated with the virus of over-expression (right).

1.3 Effects of differential *Smad2* expression on synaptic plasticity

As observed in sedentary animals (see Results, Ch.1, par. 2.3), the silencing of *Smad2* decreased the arborisation complexity of the cells infected by the lentivirus. The results of the Sholl analysis, showed a decrease in the number of intersections, in the length and in the number of dendrites. This is also the reflection of a decrease in branch points (p-value< 0.001) (Fig. 10-11). On the other hand, *Smad2* over-expression, combined with physical exercise, led to a significant increase in the arborisation complexity: a higher number of intersections, longer dendrites and higher number (Fig. 10-11).

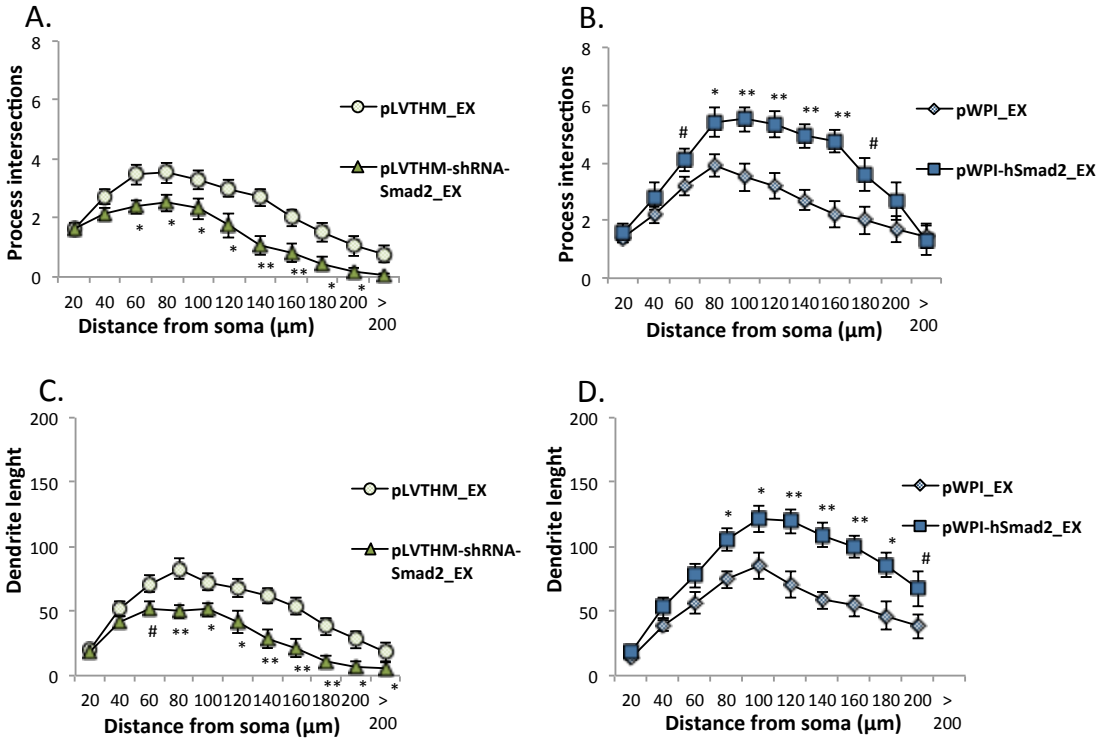

Fig. 10 Dendritic complexity analysed by Sholl analysis. A. Number of dendritic intersections per shell in the GFP$^+$ cells silencing *Smad2* (p-values at 60 µm= 0.018; at 80 µm= 0.045; at 100 µm= 0.043; at 120 µm= 0.014; at 140 µm= 0.002; at 160 µm= 0.006; at 180 µm= 0.015; at 200 µm= 0.036); **B.** Number of dendritic intersections per shell in the over-expressing cells (p-values at 60 µm= 0.082; at 80 µm= 0.031; at 100 µm= 0.009; at 120 µm= 0.007; at 140 µm= 0.002; at 160 µm= 0.002; at 180 µm= 0.051); **C.** Mean measurement of the total dendritic length in each shell of the silencing cells (p-values at 60 µm= 0.059; at 80 µm= 0.006; at 100 µm= 0.026; at 120 µm= 0.021; at 140 µm= 0.003; at 160 µm= 0.003; at 180 µm= 0.002; at 200 µm= 0.019; at more than 200 µm= 0.02). **D.** Mean measurement of the total dendritic length in each shell of the over-expressing cells (p-values at 80 µm= 0.012; at 100 µm= 0.021; at 120 µm=0.004; at 140 µm= 0.002; at 160 µm= 0.004; at 180 µm= 0.012; at 200 µm= 0.075).

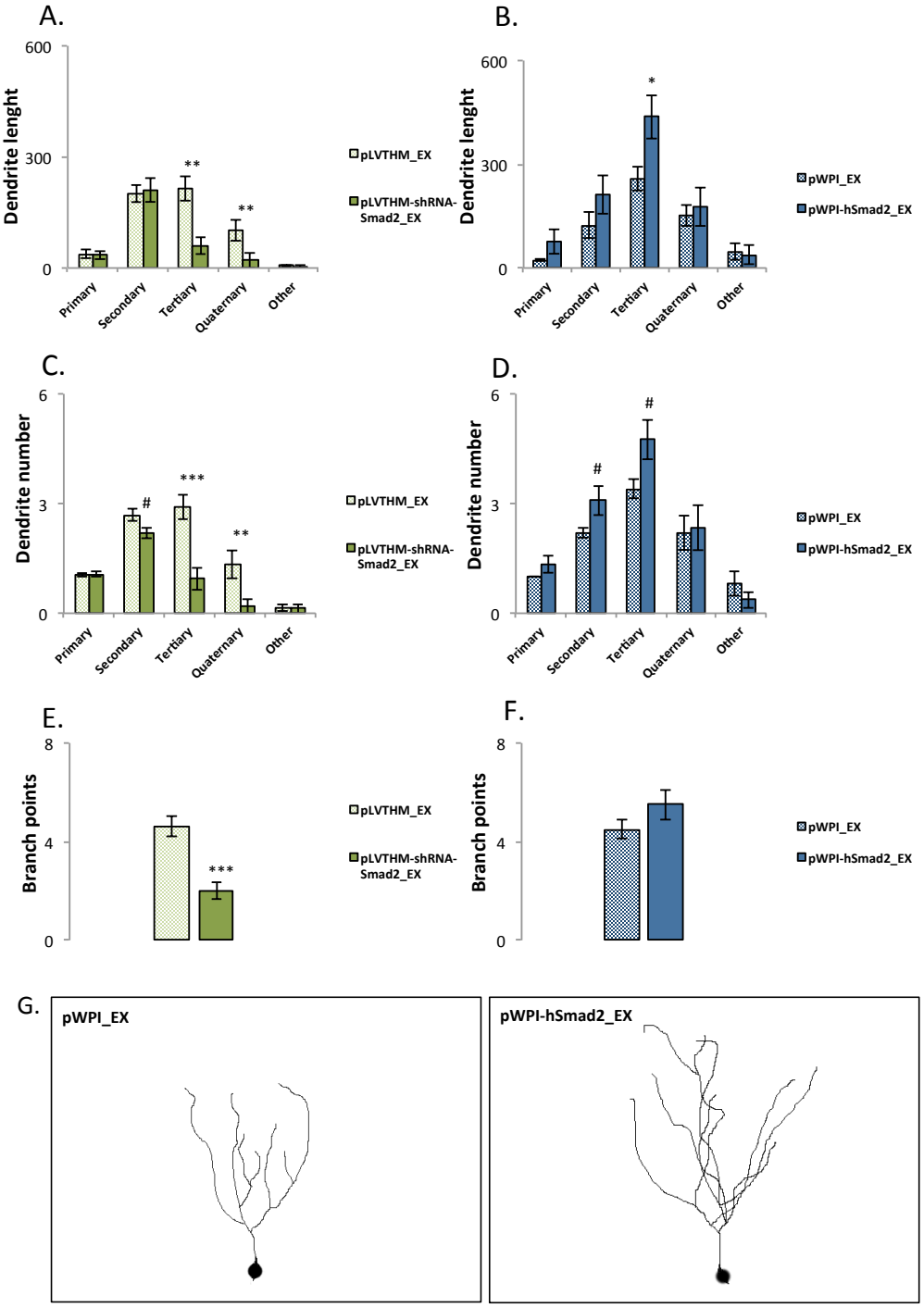

Fig. 11 Dendritic complexity. Parameters measuring the dendritic arborisation complexity of the GFP$^+$ cells. **A.** Mean length for each class of dendrites in the silencing experiment (p-values: tertiary length= 0.001; quaternary length= 0.004); **B.** Mean length for each class of dendrites in the over-expression experiment (p-values tertiary length= 0.025). **C.** Mean number of dendrites for each class of dendrites in the silencing experiment (p-values: secondary number= 0.072; tertiary number< 0.001; quaternary number= 0.004); **D.** Mean number of dendrites for each class of dendrites in the over-expression experiment (p-values: secondary number= 0.091; tertiary number= 0.056). **E-F.** Number of branch points. **G.**

Drawings of DG granule cell dendritic tree from a representative control GFP$^+$ neuron and a GFP$^+$ neuron over-expressing *Smad2* of runner mice.

Cells expressing shRNA-Smad2 had a lower spine density in the tertiary dendrites (p-value= 0.015), while neurons over-expressing *Smad2* showed a higher density compared to the control (p-value< 0.001) (Fig. 12).

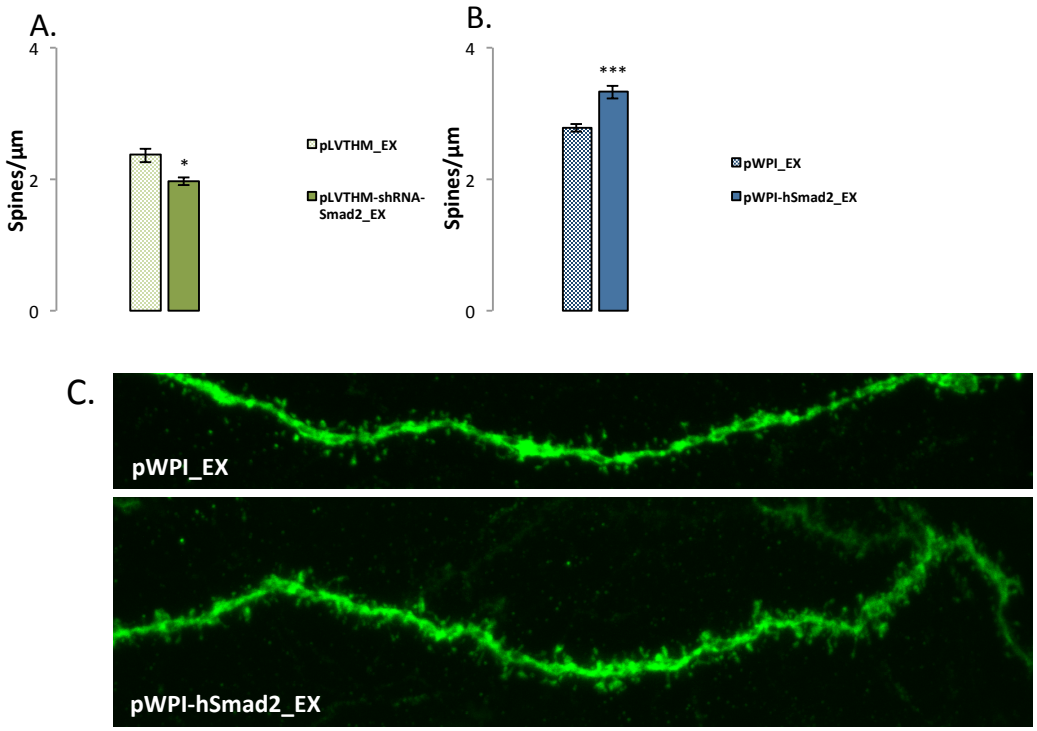

Fig. 12 Spine density. Spine density was quantified on confocal stacks of tertiary dendrites of GFP$^+$ cells silencing *Smad2* (**A**) or over-expressing it (**B**). **C.** Examples of the different spine density in a tertiary dendrite of a control neuron and of a neuron over-expressing *Smad2* in runner mice.

2. Effects of *Smad2* loss- and gain-of-function on hippocampal-dependent behaviour

To assess if *Smad2* manipulation in the DG could have an effect on behaviour, animals were evaluated in a battery of hippocampal-dependent tests before the sacrifice.

2.1 Activity

Animals were tested in an activity cage to exclude any kind of problem in motor skills and/or activity, due to the surgical operation or the genetic manipulation.

Mice over-expressing *Smad2* showed a slightly higher horizontal activity on day 2, but all the animals showed a normal activity's profile.

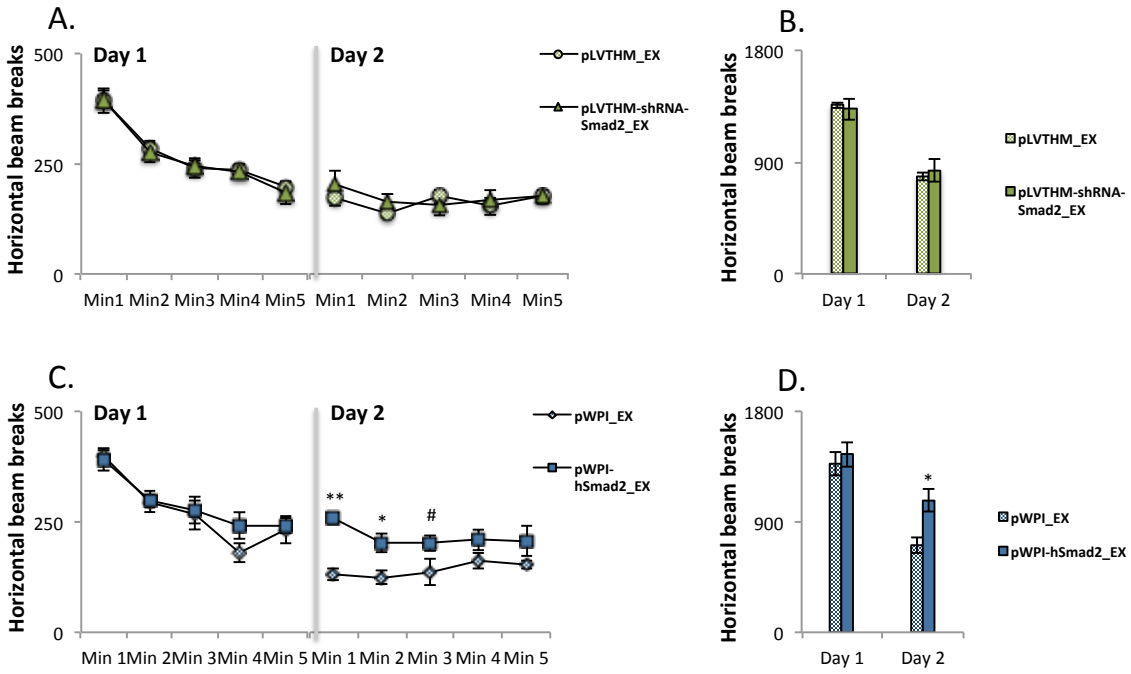

Fig. 13 Activity Cage. Motor activity was observed for 2 days and measured as the number of horizontal beam breaks. **A.** Representation of the horizontal beam breaks at each minute in the animals injected with the shRNA; **B.** Mean of the total horizontal activity at each day in the animals silencing *Smad2*; **C.** Horizontal beam breaks at each minute in the animals injected with the plasmid of over-expression (p-values on day 2: min1= 0.009; min2= 0.016; min3= 0.076 **D.** Mean of the total horizontal activity at each day in the animals over-expressing *Smad2* (p-value at day 2= 0.028).

2.2 Anxiety

No differences between the groups were found in the elevated plus maze. All the animals spent a similar average amount of time in the open arms. The parameters analysed showed that all the animals had a similar profile in an anxiety test (Fig. 14).

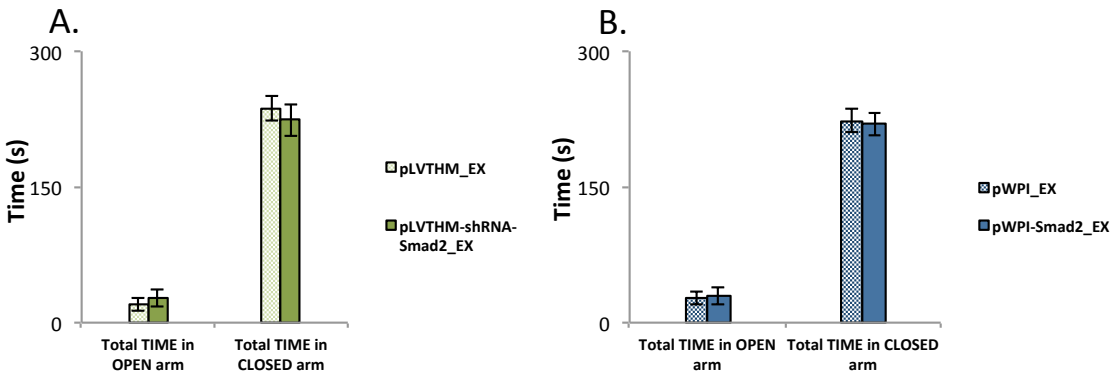

Fig. 14 Elevated Plus Maze. Total time spent in the open and closed arms in the experiment of loss-of-function (**A**) and gain-of-function (**B**).

2.3 Spatial learning and memory

No differences among groups were found analysing the swimming speed in the Morris water maze (data not shown). The silencing of *Smad2* in the DG, combining with physical exercise, led to rescue the deficit in learning observed in sedentary animals (see Results, Ch. 1, par. 3.3). However, the slope from the learning curve of the control group tends to be more negative than the silencing group (p-value= 0.063) (Fig. 15 A-B). The probe test confirmed that all the animals remember where the platform was during the test (Fig. 15 C-D).

No differences at all were observed in the over-expression study (Fig. 16).

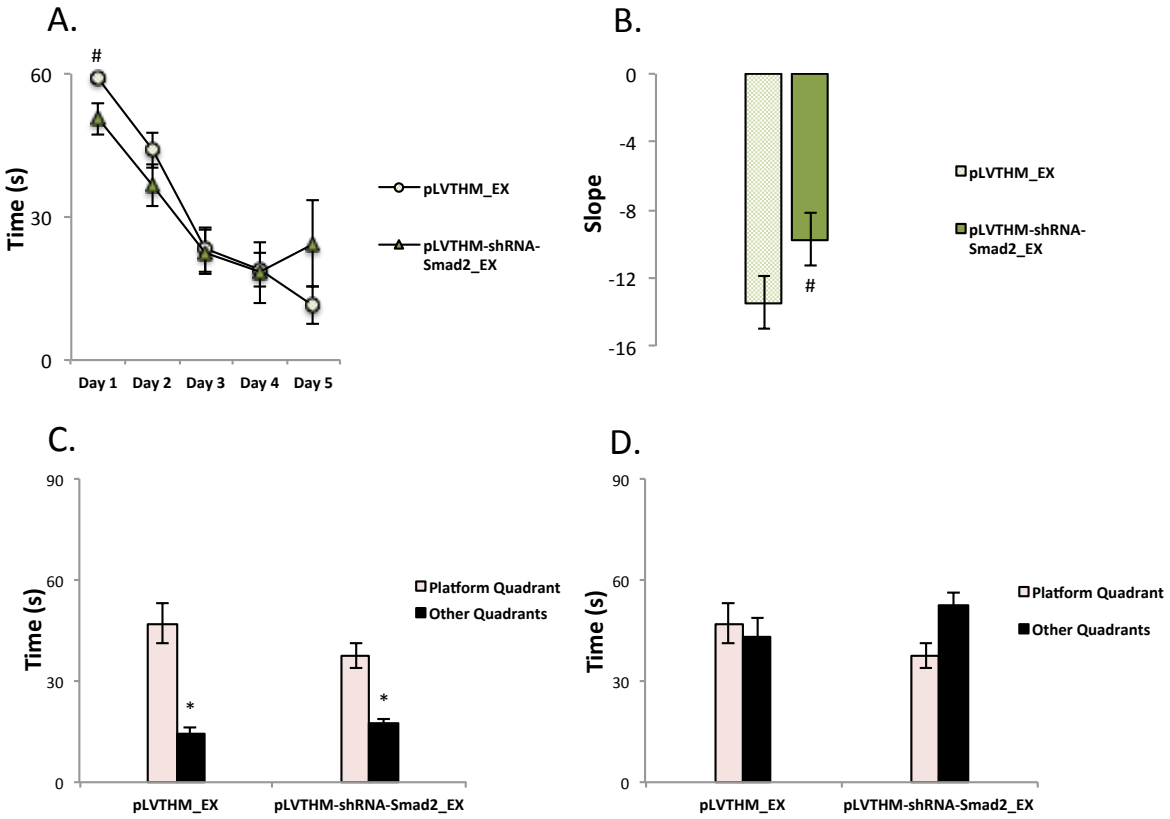

Fig. 15 Morris Water Maze in the loss-of-function study in runner animals. A. The learning curve represents the mean escape latency at each day; **B.** Slope extrapolated from the learning curve; **C.** Probe test: mean time spent in the platform quadrant versus the mean time spent in the other three quadrants (o-value for pLVTHM_EX= 0.018 and for pLVTHM-shRNA-Smad2_EX p-value= 0.028). **D.** Probe test: time spent in the platform quadrant versus the total time spent in the other three quadrants.

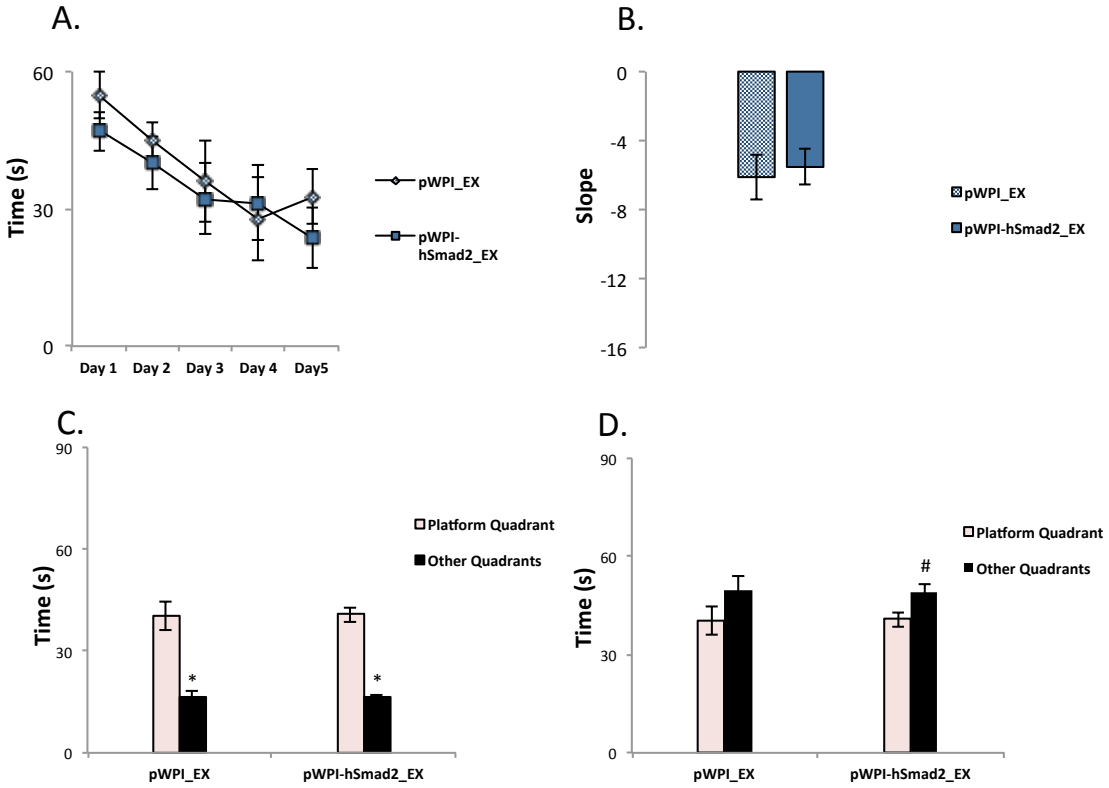

Fig. 16 Morris Water Maze in the gain-of-function study in runner animals. A. The learning curve represents the mean escape latency at each day; **B.** Slope extrapolated from the learning curve; **C.** Probe test: mean time spent in the platform quadrant versus the mean time spent in the other three quadrants (p-value for pWPI_EX= 0.043 and for pWPI-hSmad2_EX p-value= 0.043). **D.** Probe test: time spent in the platform quadrant versus the total time spent in the other three quadrants (p-value for pWPI-hSmad2_EX= 0.08).

CHAPTER 3
Physical activity modifies paths of epigenetic control during adult hippocampal neurogenesis

Physical exercise modulates the function of a great number of physiological processes in the body. One of the aim of this thesis was to define how two weeks of moderate, but forced, exercise regulate AHN through DNA methylation. In particular, the focus was on the effect of exercise on *Smad2* gene.

The first experiment was carried out to describe the effect of exercise on AHN in our laboratory conditions and mice strain. Once define the histological changes and their effects on hippocampal-dependent behaviours, molecular and biochemical analyses were performed to investigate differences in gene expression in the dentate gyrus of sedentary and runner mice.

1. Influence of exercise on AHN and its effects on behaviour

To evaluate the effects of a moderate exercise on AHN, a group of animals were trained for 2 weeks on a treadmill while another group remained sedentary, as control (n= 10 in each group). After 2 training weeks and before the sacrifice, all the animals were subjected to two behavioural tasks: the elevated plus maze and the Morris water maze. In order to assess the survival of the newborn cells, all the animals received one IdU injection for 4 consecutive days (Fig. 1).

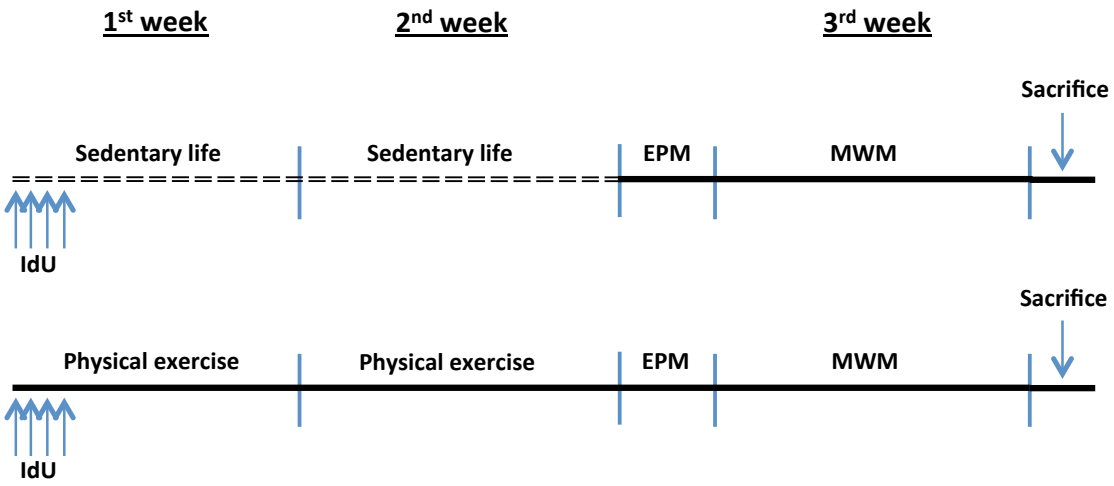

Fig. 1 Experimental design. Mice from the Control group remained for two weeks in their cages, while mice from the Runner group were trained every day, for two weeks, on a treadmill. EPM= Elevated Plus Maze; MWM= Morris Water Maze.

1.1 Modulation of the AHN as effect of exercise

Trained animals showed an increased proliferation in the DG with a higher number of $pH3^+$ cells (p-value= 0.029) (Fig. 2 A). Exercise increased also the survival of the 3-weeks-old neurons labelled with IdU (p-value= 0.003) (Fig. 2 B). While no differences were observed in the DCX^+/CLR^- subpopulation, the exercised animals showed an increase in the number of DCX^+/CLR^+ cells (p-value= 0.022) (Fig. 2 C-D). The apoptotic events, highlighted by the Fractin marker, were intensified in the DG by 2 weeks of exercise (p-value= 0.01) (Fig. 2 E).

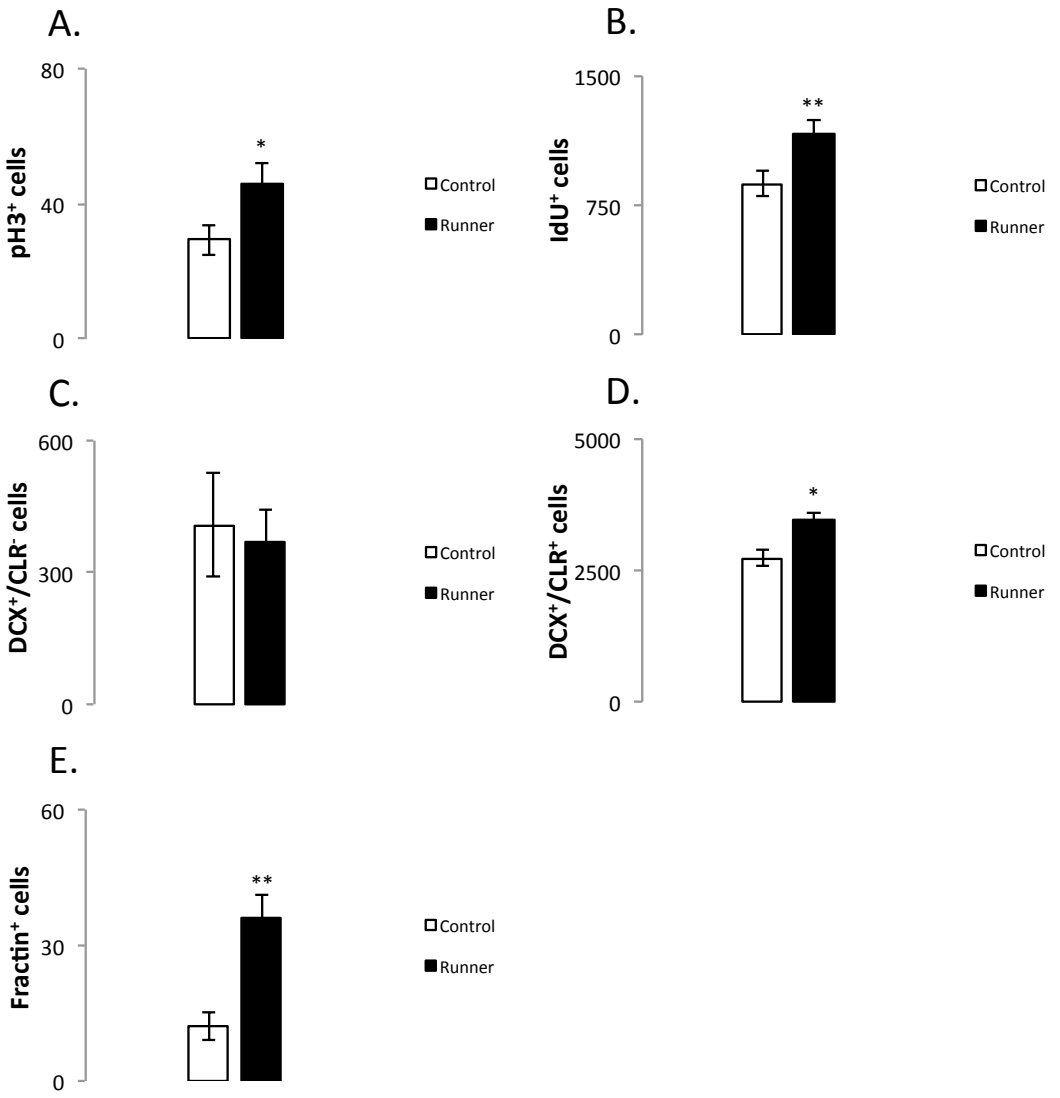

Fig. 2 Modulation of the adult hippocampal neurogenesis as effect of exercise. AHN was characterized labelling cells immunohistochemically with cellular markers. **A.** pH3 as a marker of cell proliferation; **B.** IdU to evaluate the survival of 3-weeks-old cells; **C-D.** Co-labelling of DCX and CLR to identify different subpopulations of immature neurons; **E.** Fractin antibody labels apoptotic cells.

1.2 Influence of exercise on behaviour

When mice performed the elevated plus maze, it was possible to observe a higher activity in the trained animals (Fig. 3 A) (p-value= 0.79). However, no difference was found in the time spent in open arms (Fig. 3 B).

No significant differences were found neither in the Morris water maze performance: runner animals seemed to achieve best scores every day, but no statistical differences were found in the learning curve nor in the probe (Fig. 3 C-D-E).

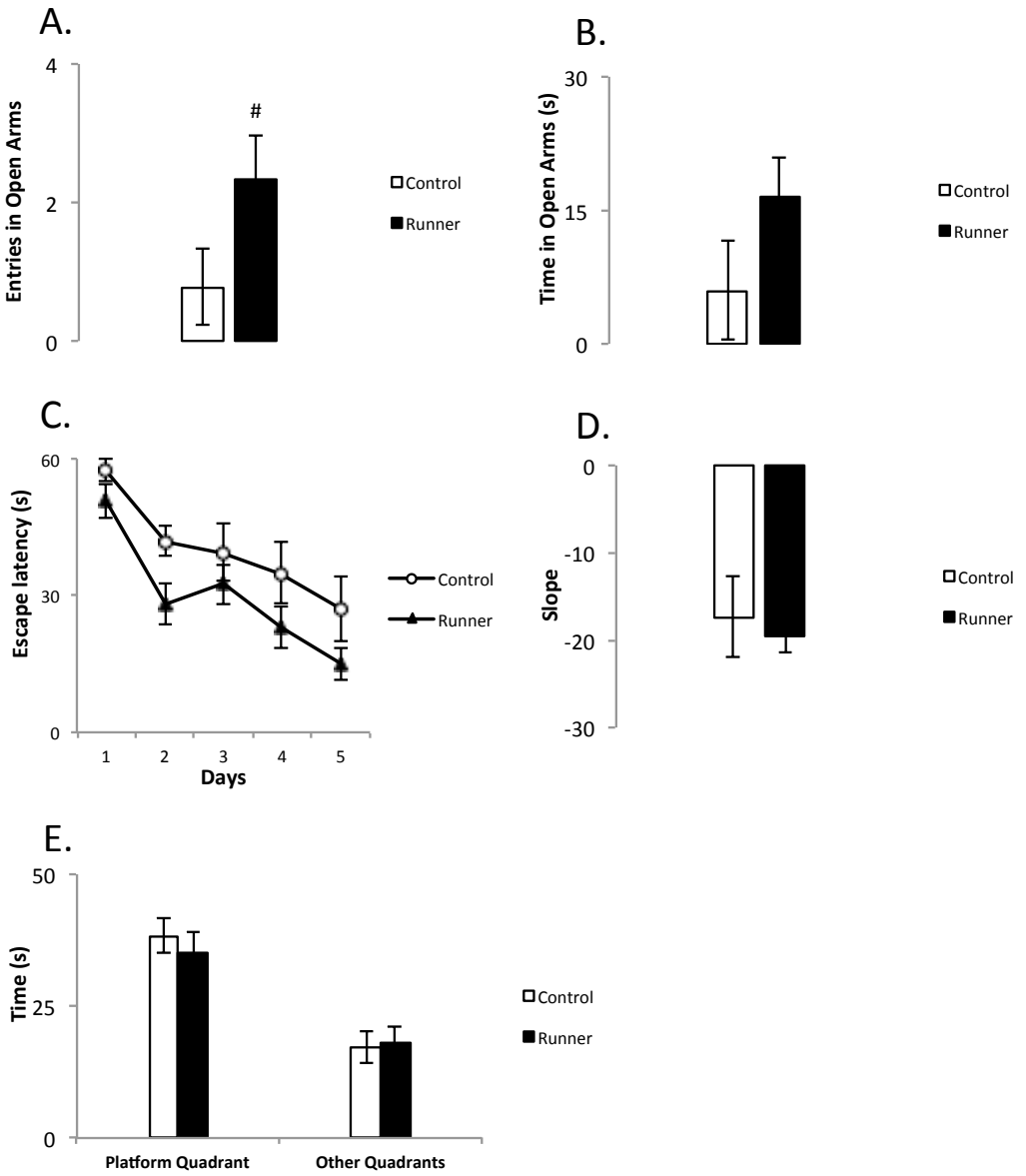

Fig. 3 Influence of exercise on behaviour. A. Number of entries in the open arms of the EPM; **B.** Time spent in the open arms of the EPM; **C.** Learning curve representing the mean escape latency at each day of the MWM; **D.** Slope extrapolated from the learning curve of the MWM; **E.** Probe test for the MWM: mean time spent in the platform quadrant versus the mean time spent in the other three quadrants.

2. Physical activity modifies the DNA methylation level of stem cell transcription factors in the adult DG

To evaluate if physical exercise could evoke epigenetics changes in order to produce molecular adaptive responses and contributes to determine cell fates, a group of mice were trained for two weeks on a treadmill, while the control group remained in sedentary conditions (n= 5 in each group). Animals were sacrificed the day after the last training session (Fig. 4). The

principle aim of this analysis was to figure out if *Smad2* gene could be influenced by exercise and if DNA methylation could be one of the regulatory mechanisms.

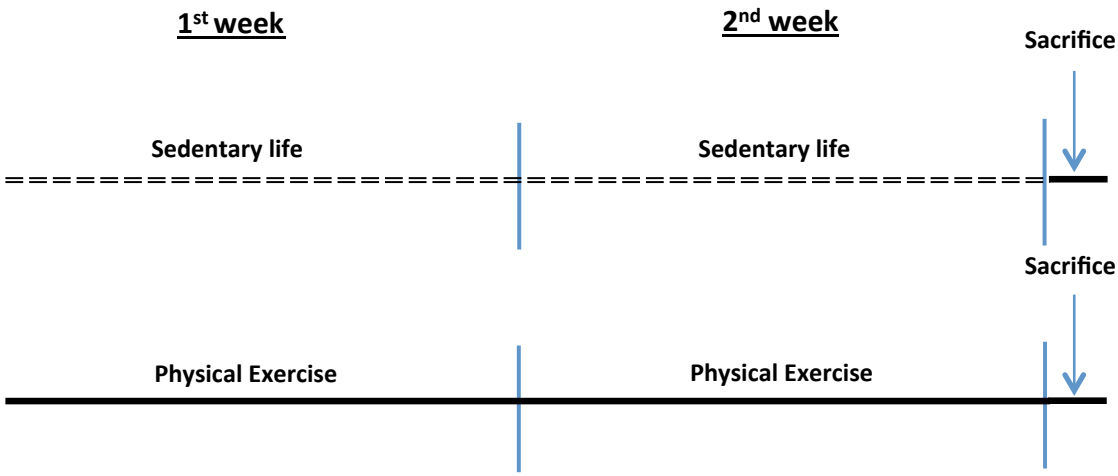

Fig. 4 Experimental design. Mice were divided into two groups: the Control group remained in its cage for two weeks, while the Runner group were trained, daily, for the same amount of time. Sacrifice occurred the day after the last treadmill session.

2.1 DNA methylation analysis in sedentary and runner animals: exercise induces modifications in *Smad2* gene

DNA methylation level in the CpG islands of 24 stem cell transcription factors, including *Smad2* gene, was analysed from the hippocampus of adult mice (Fig. 5). Generally, genes from runner animals showed a lower level of methylation compared to the sedentary mice. Exercise did not produce changes in the DNA methylation of the following genes: *Pax6, Dnmt3b, Ets1, Fos, Foxa2, Hif1a, Jun, Myc, Neurog1, Nfya, Notch2, Olig2, Pcna, Pparg, Rb1, Runx1, Runx2, Sox2, Sp1, Stat1 and Stat3*. A statistical difference in methylation was found for *Smad2, Hdac1* and *Gata2* gene (*Smad2*= 0.009; *Hdac1*= 0.009; *Gata2*= 0.047) (Fig. 6).

Values up to 10% were considered as hypermethylation. The majority of genes studied in this experiment were hypomethylated. It is worth noting that *Smad2* gene was found in a hypermethylated status in sedentary mice, while 2 weeks of physical exercise reduced the methylation level under the threshold value (from 30.89% ±2.74 to 5.73% ±0.33). Genes as *Hdac1* and *Gata2*, showed a similar methylation's profile as *Smad2* (*Hdac1*: from

37.28% ±5.75 to 6.09% ±1.68; *Gata2*: from 29.40% ±7.67 to 9.77 ±3.71).

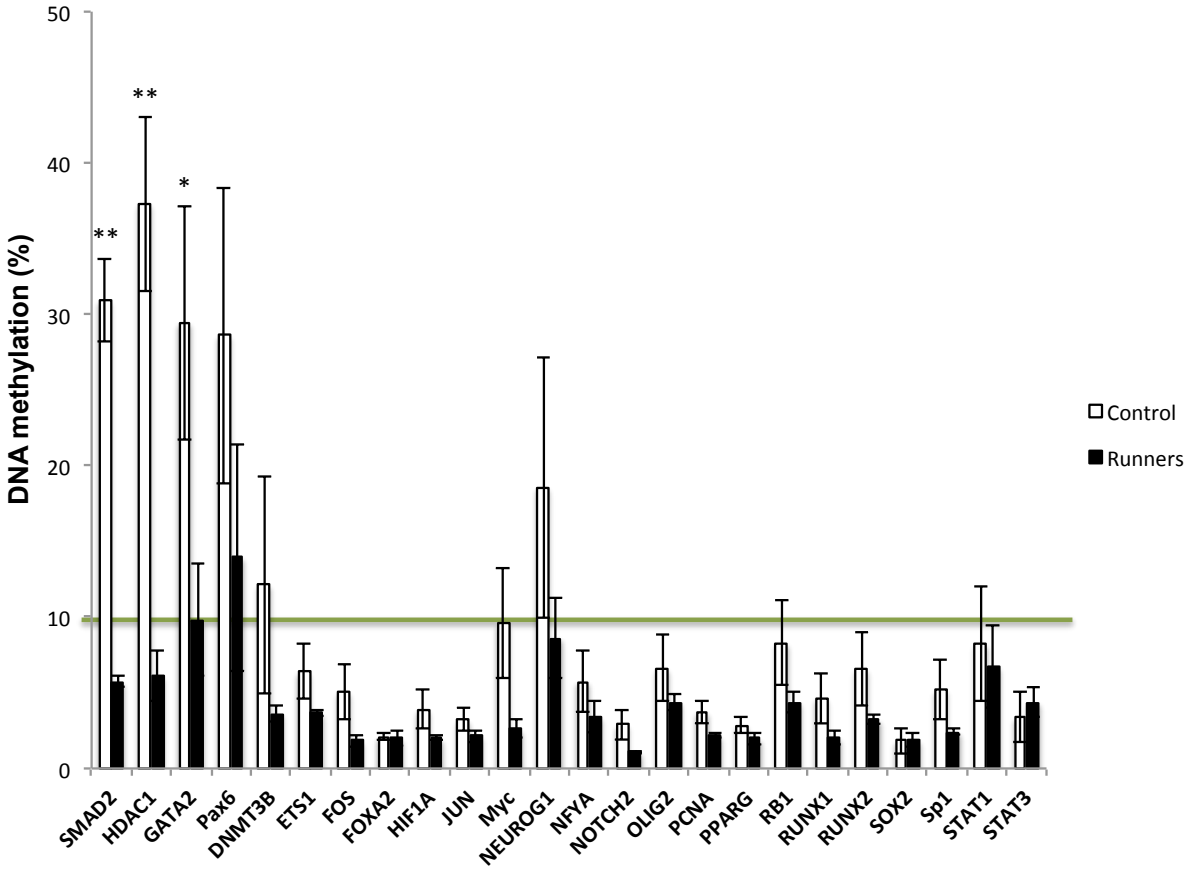

Fig. 5 DNA methylation array. The DNA methylation profile of 24 mouse stem cell transcription factors was defined in the hippocampus of sedentary and runner mice. The green line shows the threshold from where values up to 10% are considered as hypermethylation.

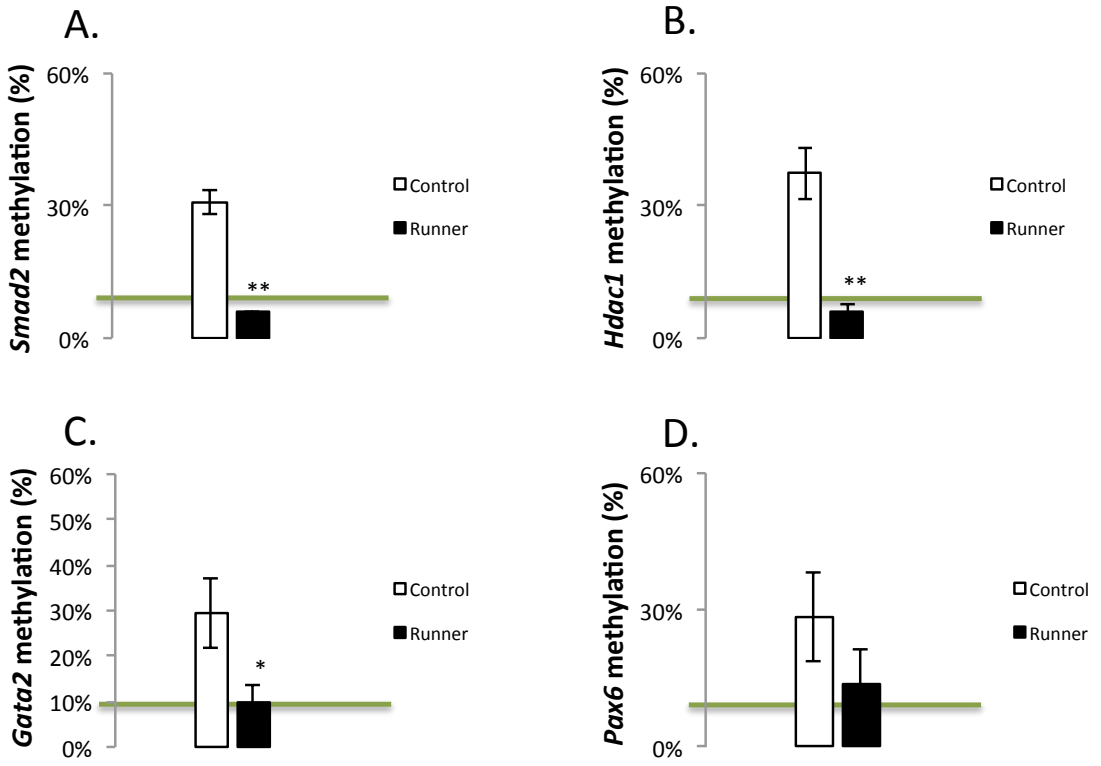

Fig. 6 DNA hypermethylation. The DNA hypermethylation of some genes is here shown more in detail. The green line shows the threshold from where values up to 10% are considered as hypermethylation. **A.** *Smad2* gene; **B.** *Hdac1* gene; **C.** *Gata2* gene; **D.** *Pax6* gene.

2.2 Gene expression in sedentary and runner animals: exercise induces the expression of *Smad2* gene

DNA methylation is related to gene silencing. So, a qPCR was performed to assess changes in the expression of *Smad2* and of those genes with a similar methylation profile. Morever, a qPCR analysis was also performed for *Pax6* representing a control gene without changes in DNA methylation. No differences were found in the mRNA levels of *Gata2* and *Pax6* in response to exercise (Fig. 7 C-D). The hypomethylation of *Hdac1*, as effect of exercise, resulted in an increased trend of gene expression (p-value= 0.052) (Fig. 7 B). Finally, *Smad2* mRNA levels increased significantly in runner animals (p-value= 0.02) (Fig. 7 A).

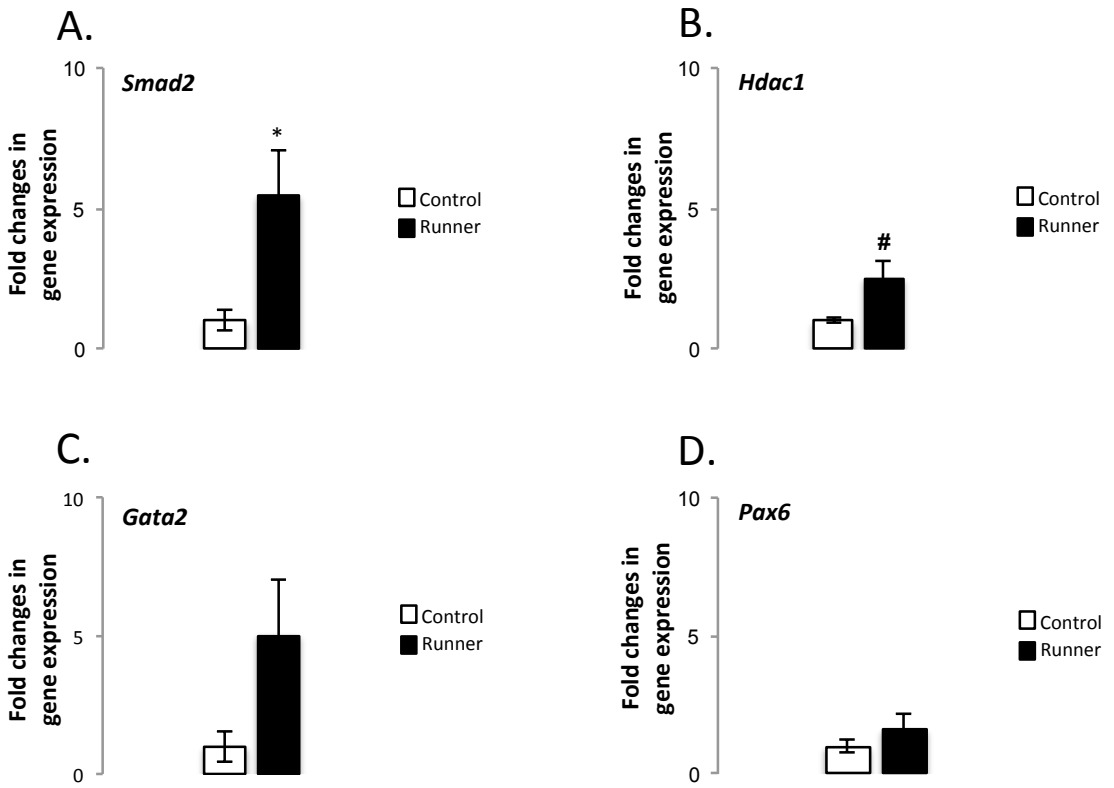

Fig. 7 mRNA quantification by qPCR. Different levels of mRNA in the hippocampus as effect of exercise. **A.** *Smad2* gene; **B.** *Hdac1* gene; **C.** *Gata2* gene; **D.** *Pax6* gene.

2.3 SMAD2 protein

SMAD2 protein's level was quantified by Western Blot in the hippocampus of sedentary and runner animals. No difference was found between the groups (Fig. 8 A). However, in runner animals it was found an increased ratio pSMAD2/SMAD2 indicating higher levels of activated protein (p-value= 0.043) (Fig. 8 B). What is worth of note is that the levels of HDAC1 protein decreased in runner mice, indicating a possible reduction in the formation of repressive transcription complex (p-value= 0.057) (Fig. 8 C).

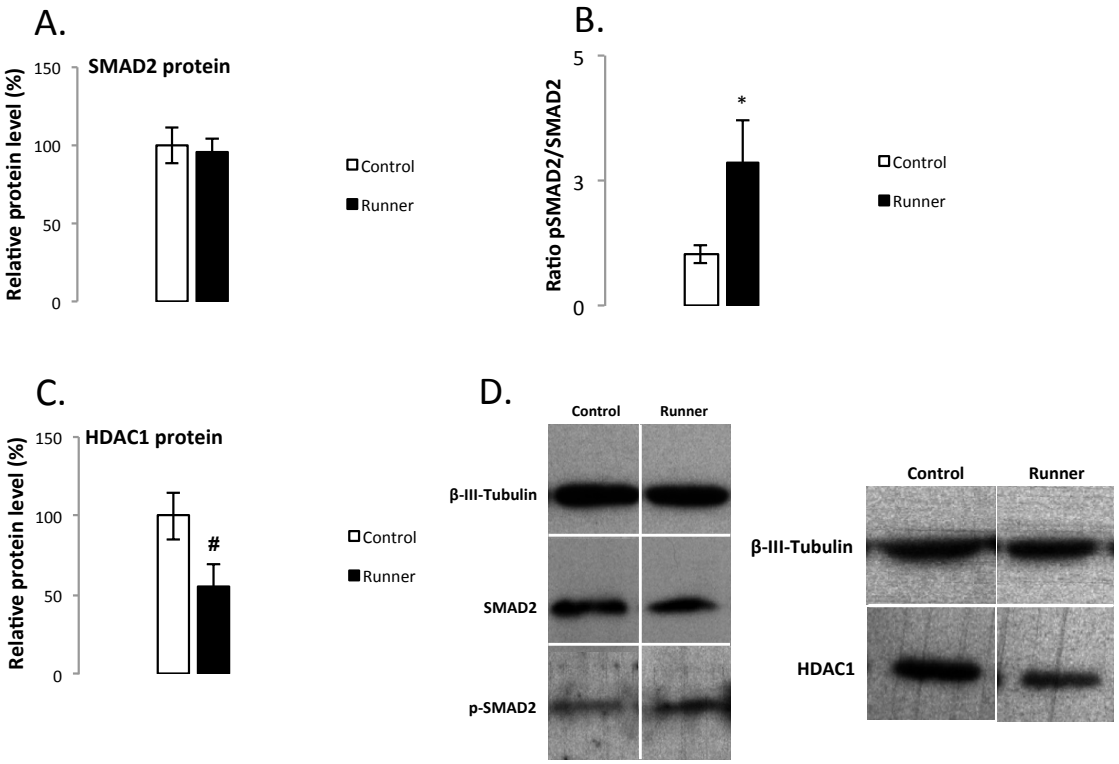

Fig. 8 Protein quantification by Western Blot. A. The amount of SMAD2 protein in the hippocampus does not change between control and runner mice; **B.** Exercise induces the phosphorylation of SMAD2 protein; **C.** In the hippocampus of runner mice, the level of HDAC1 protein decreases. **C.** Western Blot for SMAD2/pSMAD2 and HDAC1, using β–III-tubulin as loading control.

CHAPTER 4
The involvement of adult hippocampal neurogenesis in behavioural acquisition and persistence

Many evidences suggested a role for the newborn granule cells of the hippocampus in learning and memory tasks. The *par excellence* and most used test in behavioural and cognitive laboratories is the Morris Water Maze. Also in this thesis, the MWM was chosen to test the effects of the genetic manipulation in the DG, as it is a widely accepted test in the scientific community. Moreover, one of the aim of this work was to deeper analyse the test, exploring new correlations between the execution of the test and AHN and to generate new knowledge and understanding of the learning and memory mechanisms.

To evaluate the reliability of the learning slope to measure acquisition, a specific analysis was performed through a mathematical model. So, first of all, it was used a standard MWM protocol to analyse the learning profile of a large cohort of mouse from different strains (Fig. 1 A).

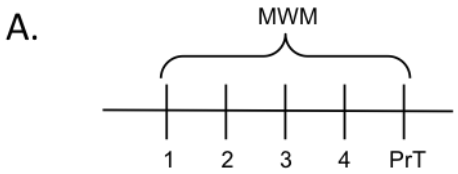

Fig. 1 Experimental designs. A. Experiment Formula. The Morris water maze was used over 4 acquisition days and a probe trial was performed the day after the last acquisition test. ["Experimental designs" continues on next page]

Then, a second set of experiments was performed to compare the acquisition score and behaviour persistence with the size of the newborn immature neuron subpopulations in the adult hippocampus. In this experiment, it was used a MWM protocol designed to maximize both the extinction bursts and novel search strategies during the probe trial (Fig. 1 B and C).

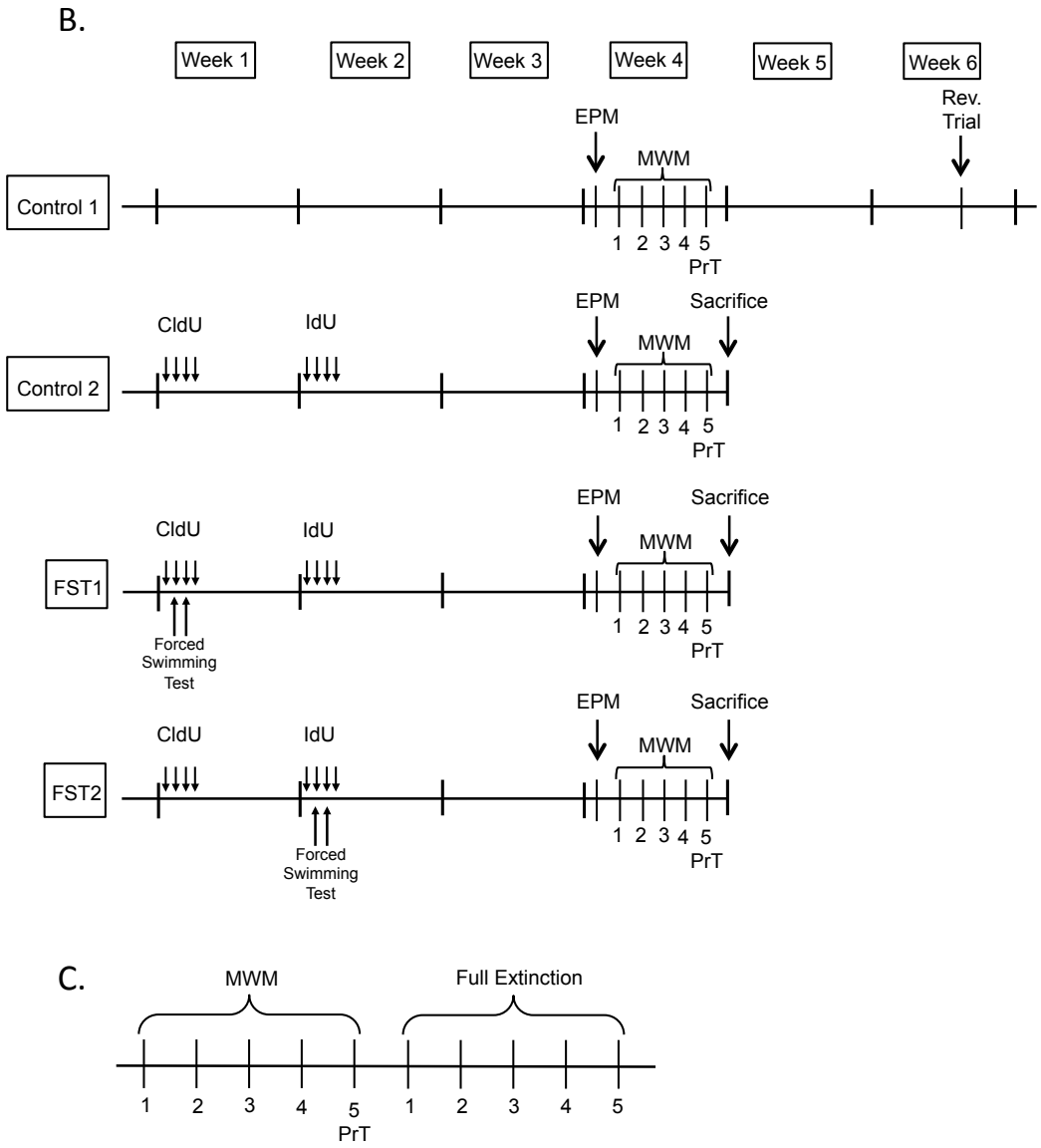

Fig. 1 B. Experiment Neurogenesis and Reversal. Mice received CldU injections on 4 consecutive days at the beginning of the experiment. Animals in the FST1 (Forced Swim Test 1) group were exposed to a Forced Swim Test (Porsolt test) on 2 consecutive days. One week later, all the mice received IdU injections on 4 consecutive days and the animals of the FST2 (Forced Swim Test 2) group were exposed to a Porsolt test on 2 consecutive days. One week before sacrifice, all the animals performed a 1-day Elevated plus Maze and a 5-day Morris Water Maze test and the probe trial was performed immediately after the last acquisition test (EPM, Elevated Plus Maze; MWM, Morris Water Maze; PrT, Probe Test). Some animals were not sacrificed at this time and remained in their cages for 12 more days till reversal trial was performed. **C. Experiment Full-Extinction.** The same Morris water maze protocol was used, but besides the animals followed a complete extinction protocol beginning the first day after the probe trial was finished.

In the first experiment, the probe trial was performed 24h after the last acquisition day, while in the second set of experiments the probe was carried out immediately after the last acquisition trial.
The correlations between neural resources and behaviour were applied also on the experiment of *Smad2* loss- and gain-of-function in sedentary animals (from Chapter 1). The same trends were found in mice infected with the control and over-expressing lentiviral constructs, while in those animals silencing *Smad2* in the DG there were opposite or no correlations.
All the new variables created for this work are defined in Materials and Methods, par. 12.

1. Experiment Formula

1.1 A mathematical formula to describe the temporal profile of water maze acquisition

In Experiment Formula, the learning curves of a great number of animals from different strains were analysed in order to discover a mathematical model to define the acquisition phase in a Morris water maze. It was found that the mean of the daily escape latencies for each group, independently from the strain, were well described for all the mice applying the following exponential equation:

$$\boldsymbol{t = a + be^{-c(day-1)}}$$

Where *a* represents the escape latency at the end of the test; *a*+*b* represents the escape latency on the first day of the test (acquisition day 1); *c* is the exponential factor. In this experiment, *a*= 21,5; *b*= 25,2; *c*= 0,64. So, the individual escape latencies followed an exponential function, although there was a strong inter-individual variability in the time profile of the learning curves (Fig. 2).

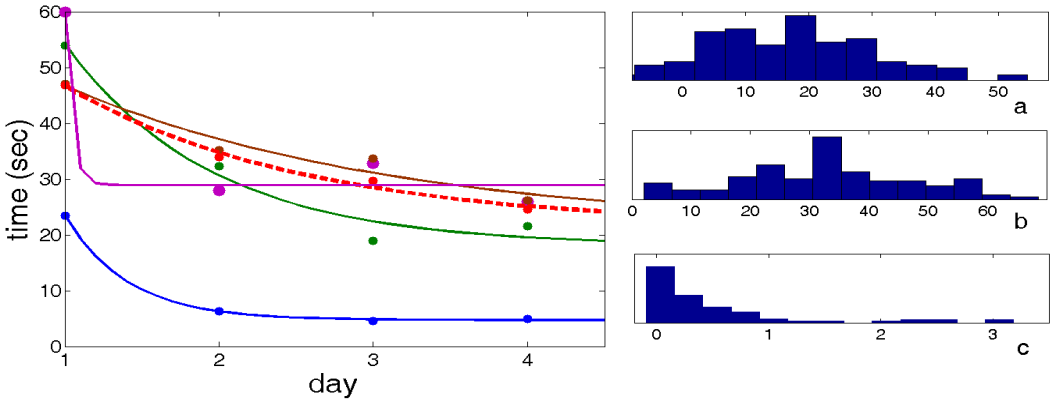

Fig. 2 The mean learning curves from 98 control mice were analysed. The time profile for the mean group learning follows an exponential curve (red dashed curve). Individuals show different time profiles, also following exponential curves but with very different parameters (colored curves). Histograms for parameters a, b, and c obtained from 98 individuals show a high variability in the individual time profiles.

1.2 Effect of the early variability in acquisition on test performance

According to the "Learning Profile" criterion (see Material and Methods, par. 12), it was worth noting that the performance on the first two days of acquisition could be different among the animals. So, in order to test if this difference could influence the performance of the rest of the behavioural test, it was generated an *Early Profile* variable through the data from Experiment Formula. As previously defined (see Material and Methods, par. 12), the *Early Profile* variable was obtained subtracting *AS1* to *AS2* and it was compared to *AS4*, *AS5* and to the probe trial's parameters *PerPlat* and *PerCross*. No significant correlations were found between the variables neither considering the entire group nor when the animals were grouped by strains (results not shown). For this reason, *AS4* and *AS5* were considered appropriate measures for acquisition.

2. Experiment Neurogenesis, Reversal and Full-Extinction

2.1 Correlation between task acquisition and behaviour persistence in control animals

To study the persistence behaviour after an acquisition phase of a water maze, a second set of experiments was performed. The control groups C1 and C2 were considered as an unique control group until the end of the

probe trial because animals were subjected to the same treatment. It is important to remember that for this MWM protocol, the probe was carried out immediately after the last acquisition trial. As expected, all animals learned the task in five days or less (according to the criterion of finding the platform in less than 20 seconds) (Fig. 3 A). Similarly, all the animals performing the probe trial showed to retain the acquired behaviour during the 90 seconds trial without the platform in the pool (Fig. 3 B).

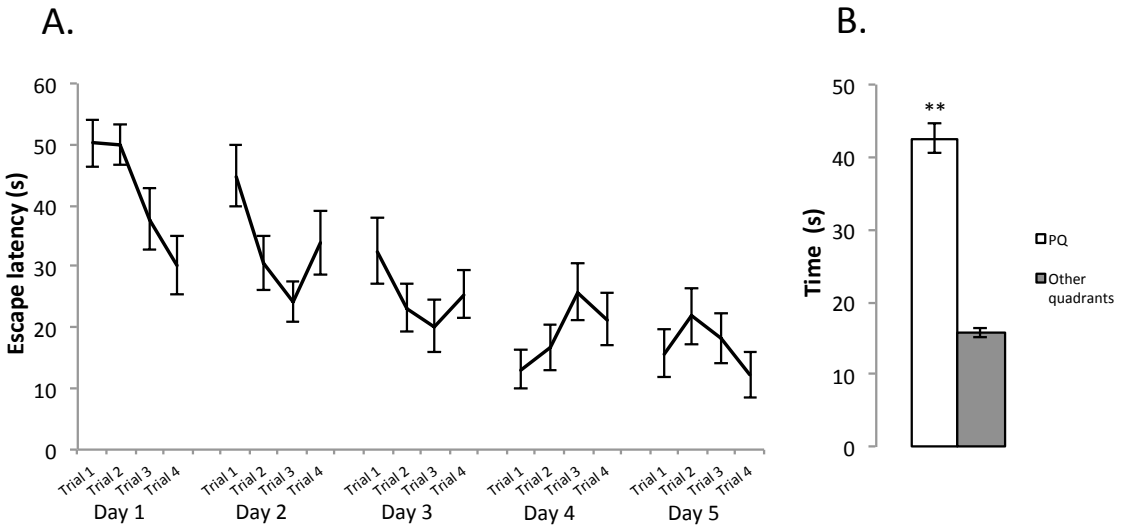

Fig. 3 A. Group mean escape latency for the 25 control mice from Experiment Neurogenesis and Reversal. **B.** Time spent into the four pool quadrants during the probe trial. All animals preferred the platform quadrant.

The most relevant result is that it was found a trend in the negative correlation between *AS4* and *PerPlat* (ρ= -0.74, p-value= 0.092), so the higher the acquisition score, the shorter was the persistence in the target quadrant (Fig. 4 A). A similar trend was observed when *AS4* was related to the *PerCross* variable, but no statistical significance was found (data not shown).

Animals from group C1 were subjected to a reversal trial 12 days after the probe (Fig. 1 B, Control 1 group). A positive correlation was found between *AS4* and *ASRev*, suggesting a stronger ability to find the platform located in a new quadrant distinct to that used during the acquisition phase (Fig. 4 B).

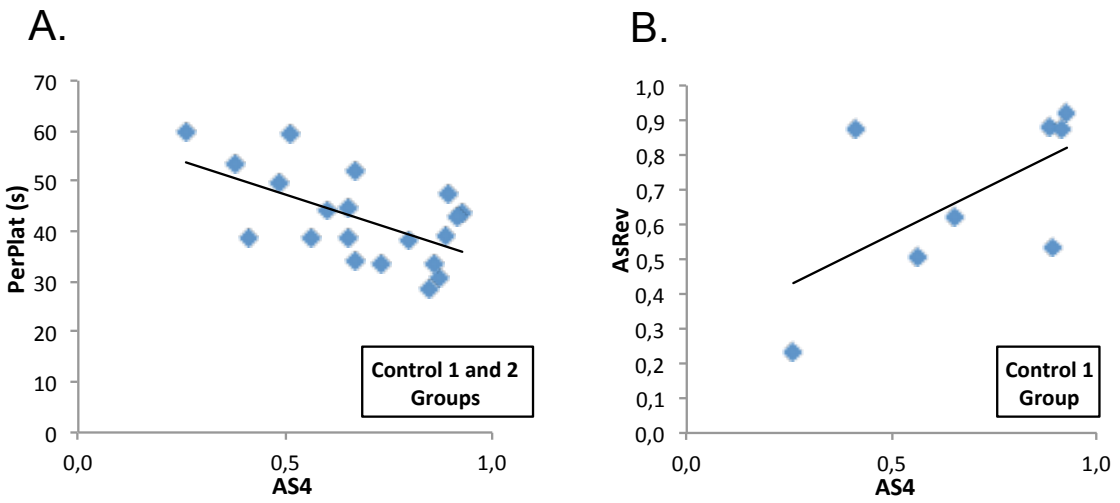

Fig. 4 **A.** Correlation comparing the score towards the end of the acquisition phase (AS4, when all animals have performed at least three consecutive trials escaping to the platform in at least 20 s) with the score during the probe trial (measured as the persistence of the behaviour in searching for the platform in the quadrant where it was located during the acquisition phase: PERPlat). **B.** Correlation comparing the acquisition score on day 4 (AS4) with the score on the reversal day (day 12 after completing the acquisition phase), showing a positive significant correlation, pointing to an influence of behaviour acquisition on late reversal trials.

In the Full-Extinction experiment (Fig. 1 C), a full extinction protocol was applied. All the animals "extinguished" their preference for the platform quadrant after 4 days. The animals with a longer time spent in the platform quadrant during the probe trial, spent shorter time in that quadrant at the end of the extinction protocol (Fig. 5). Interestingly, the animals spending shorter times in the platform quadrant during the probe trial, showed a highly variable searching profile in the other three quadrants at the end of the extinction (shorter or equal than 10% of the total time) (results not shown).

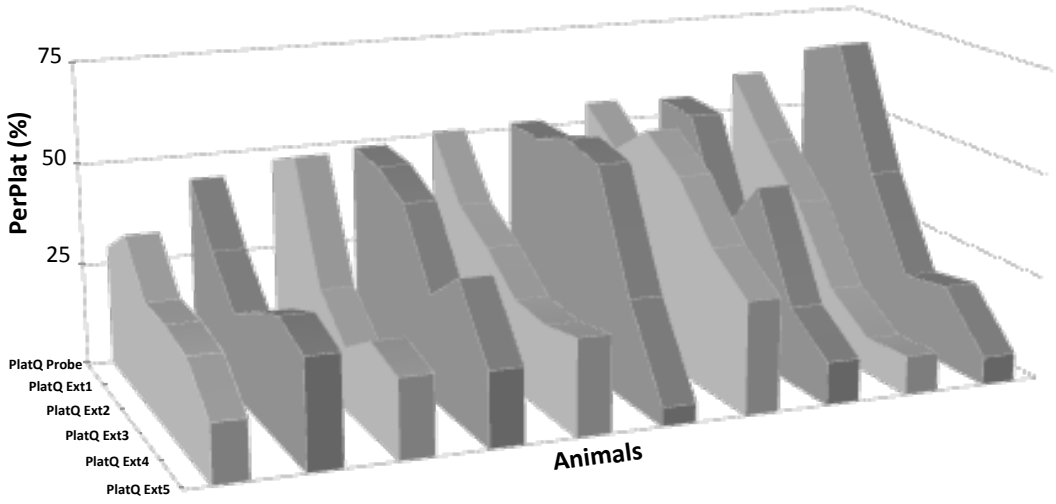

Fig. 5 Individual extinction curves in the Full-Extinction Experiment. The percentage time in the platform quadrant (PerPlat) decreases along time (from Probe to Ext5) for all animals. Mice with a stronger persistence in the probe trial (higher values to the right of the chart) spent shorter times at the end of extinction (Ext5), pointing to an influence of persistence parameters in late extinction behaviours in this test.

2.2 Flexibility of behaviour as a putative explanation

To test if the acquisition and persistence data obtained from the second set of experiments fitted with the "flexible behaviour hypothesis", animals with the best *AS4* and lowest *AS1* scores were deeply analysed. The hypothesis suggested to verify if these animals had a more flexible behaviour, showing a weaker persistence in the probe trial. Therefore, it was evaluated whether the probe trial score (*PerPlat*) of these animals was in the lower *PerPlat* tertile (≤38.6 s). A *Difference* variable ($PerPlat_i - 38.6\,s$) was created for each animal in order to determine if it was statistically ≤0. The 95% confidence interval for this analysis was in the range between -7.1 and +6.95, indicating that this subgroup of animals persisted in their acquired behaviour during the probe trial, irrespective of how they scored at the end of the acquisition phase.

2.3 Correlation between behavioural performance and the natural variability of adult hippocampal neurogenesis rate in control animals

The control group C2 received four injections of CldU and IdU (Fig. 8 A), respectively 4 and 3 weeks before the sacrifice (Fig. 1 B). In order to assess a relationship between the behaviour in the water maze and AHN, the number of 4-weeks-old ($CldU^+$) and 3-weeks old cells (IdU^+) were counted and related to the learning parameters. The number of $CldU^+$ and IdU^+ cells was significantly correlated with the performance in both the acquisition and probe trials. In particular, cell number was inversely correlated with behaviour acquisition: the higher the cell number, the worse the acquisition score (ρ= -0.7471, p-value= 0.06 for figure 6 A; ρ= -0.8986, p-value= 0.016 for figure 6 B) (Fig. 6 A and B). On the other hand, a positive correlation was found between cell number and persistence: the higher the cell number, the longer time spent in the virtual platform quadrant (ρ= 0.7675, p-value= 0.022) (Fig. 6 C).

Moreover, the number of $CldU^+$ and IdU^+ cells was closely related to the total number of immature DCX^+/CLR^+ neurons (ρ= 0.689, p-value= 0.082) (Fig. 6 D and Fig. 8 C-F).

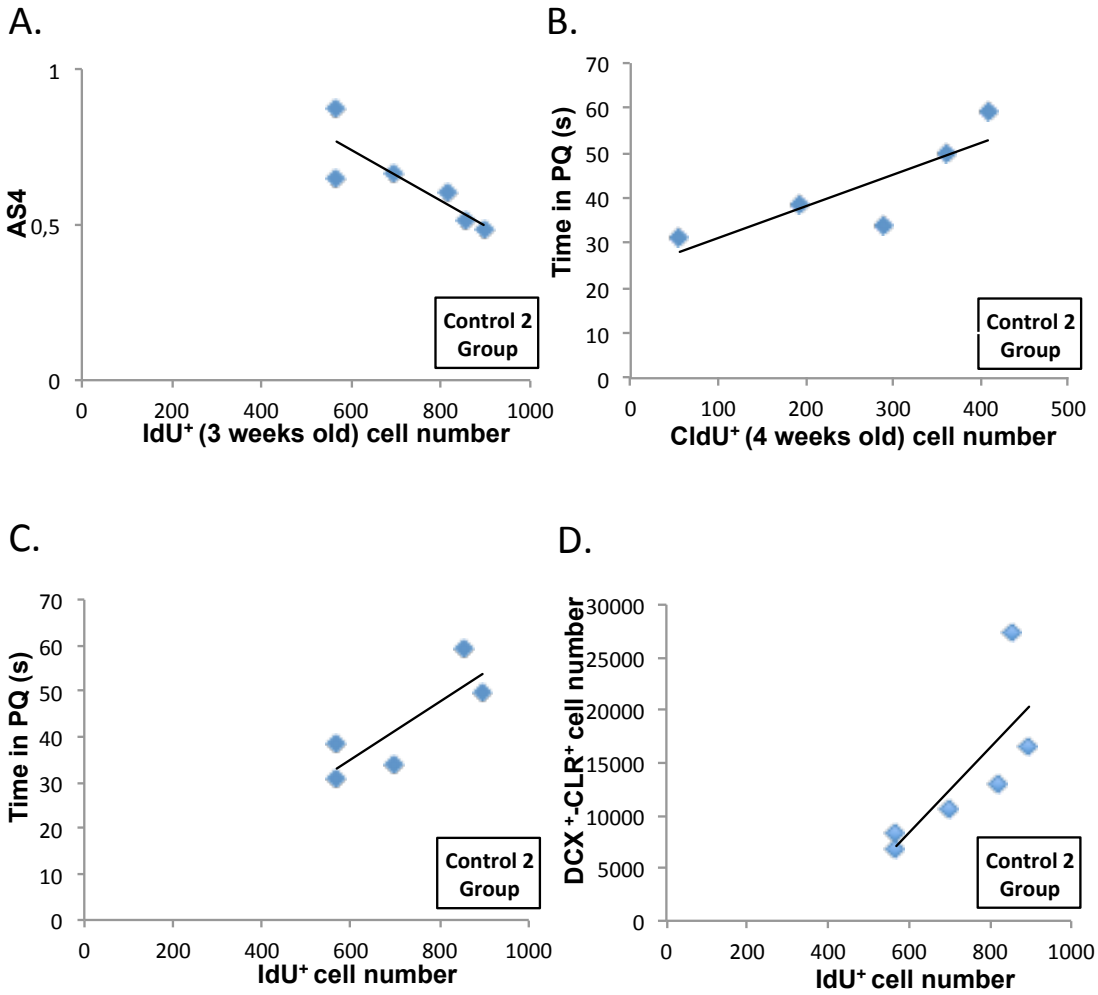

Fig. 6 A-C. Significant correlations between the number of specific immature neuron subpopulations with task acquisition and persistence. A. Negative correlation between IdU^+ neurons (3-week-old cells at the time of sacrifice) and AS4. **B.** $CldU^+$ neurons (4-week-old cells at the time of sacrifice) and the persistence of behavior as measured by the time spent swimming in the platform quadrant. **C.** It was found a positive correlation for this parameter also in the case of IdU^+ cells. **D.** Positive correlation between IdU^+ neurons and the number of immature DCX^+/CLR^+ neurons in the GCL. All animals are control mice from Experiment Neurogenesis.

2.4 Effect of an experimental decrease of adult hippocampal neurogenesis: the forced swim test

In Experiment Neurogenesis, the groups FST1 and FST2 were subjected to a forced swim test during the 2nd and 3rd day of CldU (FST1) or IdU (FST2) injections (Fig. 8 G-I) in order to induce cell death and a decrease in the number of some subpopulations of immature neurons. As expected, all animals learned the water maze task (Fig. 7 A) and retained the acquisition during the probe trial (Fig. 7 B). No differences in learning were found

between the groups. However, the day before the MWM, animals were tested in an elevated plus maze and both FST1 and FST2 groups showed a significant reduction in the time spent in the open arms comparing to the control group ($F(2.20)= 5.813$, p-value= 0.011; fig. 7 C) indicating the long-term persistence of the stress as consequence of the forced swim test. As expected, this stress affected hippocampal neurogenesis, as it was possible to detect observing the significant decrease in the number of $pH3^+$ cycling cells ($F(2.20)= 5.953$, p-value= 0.01; fig. 7 D). This decrease provoked a trend towards a reduced number of DCX^+/CLR^+ cells in FST2 mice ($F(2.20)= 2.72$, p-value= 0.093; fig. 7 E). On the other hand, other subpopulations of immature neurons were not affected (Fig. 7 F-G-H).
In addition, it was found a tendency towards a correlation between $CldU^+$ cells (4-weeks-old) and behaviour persistence in FST1 group: the higher the number of $CldU^+$ cells, the weaker the persistence ($\rho= 0.5093$, p-value= 0.047 for figure 7 I).

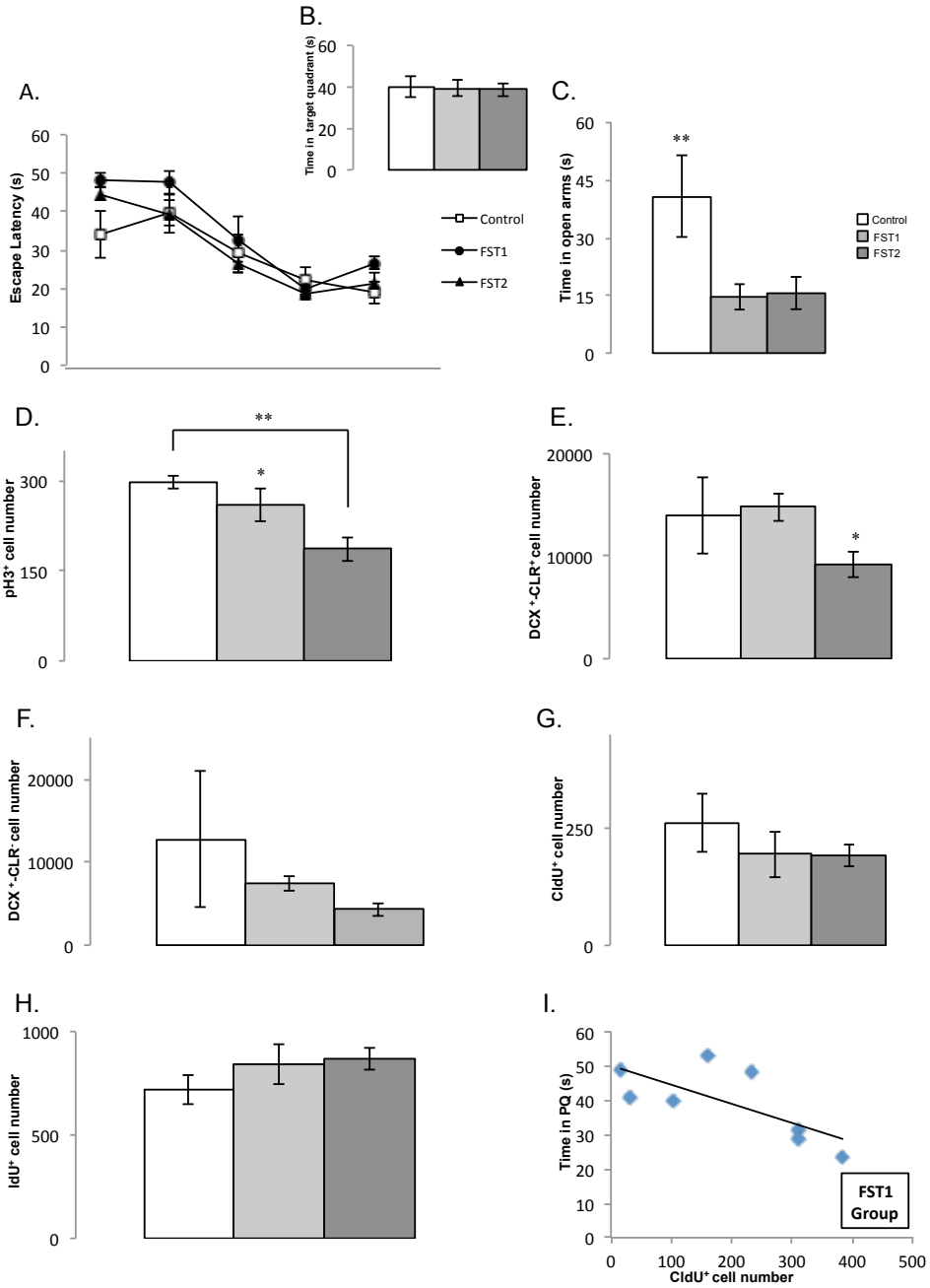

Fig. 7 Effects of forced swim test on behaviour and cell counting. **A.** Learning curves from the Morris Water maze. (Experiment Neurogenesis). A floor effect was found between AS4 and AS5, and no significant differences were found between the C, FST1 and FST2 groups, either during acquisition or retention during the probe trial **(B)**. **C. Elevated plus maze.** The time spent in the open arms was compared among groups and there was a significant decrease in the FST groups compared to the control animals. **D–I. Cell number. D.** The number of pH3-positive cells decreased significantly in the FST1 and FST2 groups compared to the control animals, as did the number of DCX^+/CLR^+ neurons **(E)**. By contrast, other subpopulations of immature neurons were less affected as no significant differences were found in DCX^+/ CLR^- neurons **(F)**, or in $CldU^+$ **(G)** or IdU^+ cells **(H)**. **I.** Negative correlation of $CldU^+$ cell number and the time spent swimming in the platform quadrant for FST1 animals, opposite to that found in control animals.

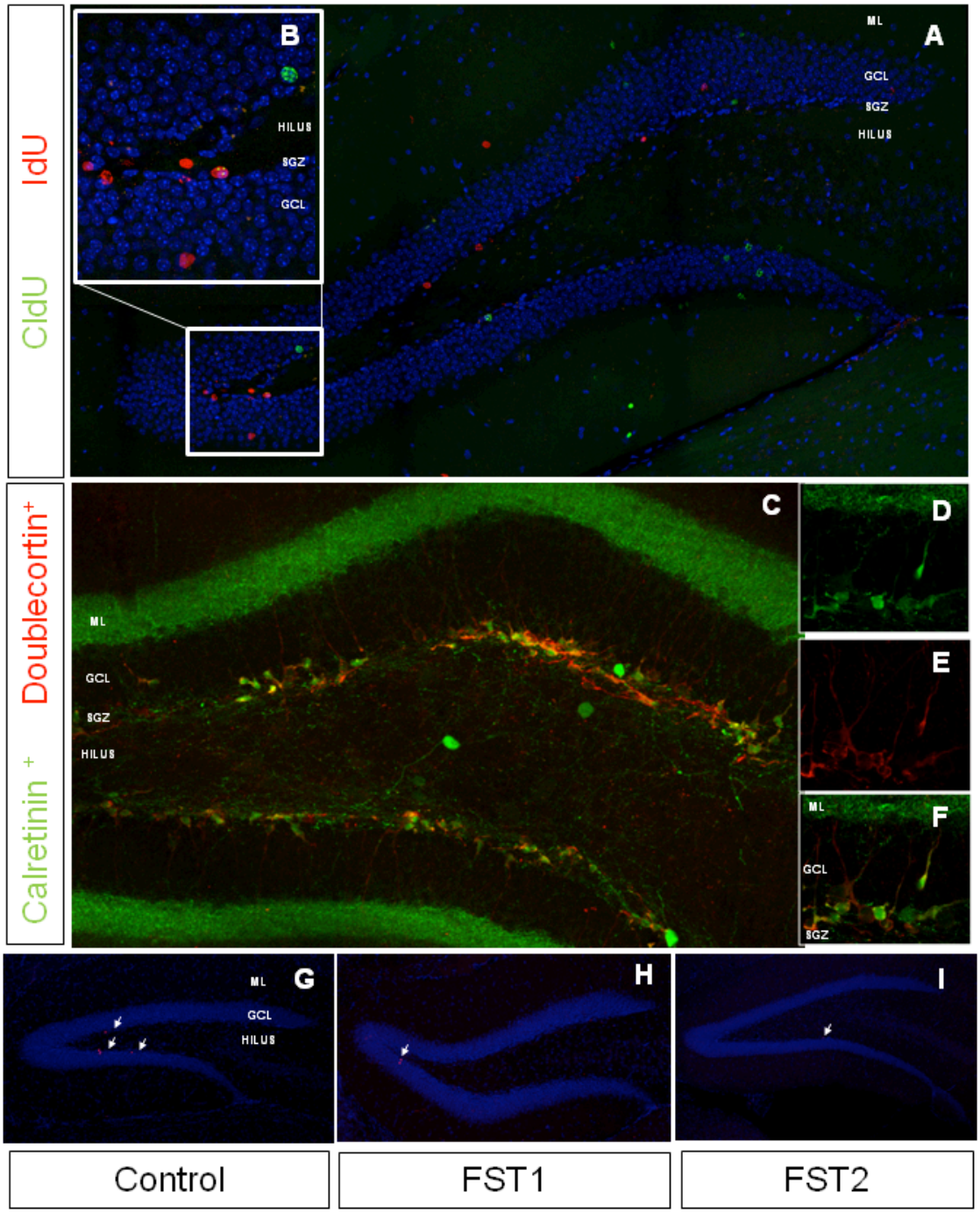

Fig. 8 **Representative images of cells labeled with different markers. A.** Thymidine analogues (green, CldU; red, IdU) in the DG of a control mouse; **B.** Detail of the different markers with a higher magnification; **C.** Immature neurons labeled with DCX (red) and CLR (green); **D-E-F.** CLR^+ cells, DCX^+ cells and merge image. **G-H-I.** $pH3^+$ cells (red) in control and FST groups. The Forced Swim Test reduced the number of proliferating cells. (Blue, DAPI staining).

2.5 Comparisons between cell numbers and ratios representing the relationship between acquisition and persistence

To further analyse the relationship between acquisition, persistence and neurogenesis, behavioural data from Experiment Neurogenesis were combined to create new variables. *PerPlat/AS4*, *PerPlat/AS5*, *PerCross/AS4* and *PerCross/AS5* are ratios that represent the relation between the performance during the acquisition phase and the persistence during the probe trial. No differences were observed for all these variables among the control, FST1 and FST2 group (Fig. 9 A-F).

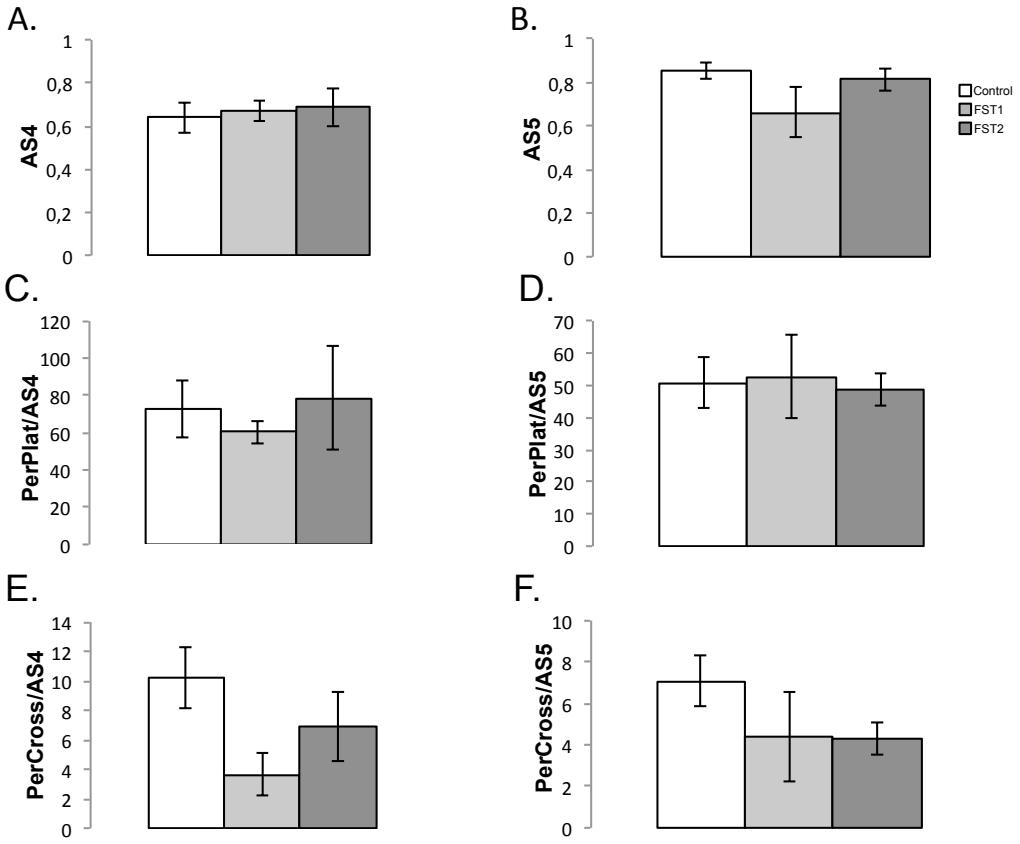

Fig. 9 The behaviour persistence/acquisition ratio. Four different ratios are shown in fig. from C to F analysing two different parameters for persistence (platform quadrant preference and platform crossings) on days 4 and 5 of acquisition.

Interesting results appeared searching correlations between the ratio variables and the size of the two subpopulations of immature neurons of known age. The number of $CldU^+$ cells was significantly and positively correlated with the *PerCross/AS4* ratio in control animals ($\rho = 1$, p-value= 0.016) (Fig. 10 A). This ratio represents the direct relationship between

behavioural persistence and acquisition in each animal, so the higher the number of immature cells that survived, the stronger the positive impact on persistence with respect to acquisition. On the other hand, the fewer the number of immature cells, the weaker the impact on persistence due to the positive impact on acquisition. The animals with the fewest immature cells in the FST1 group also had a low ratio (observe the two black circles in fig. 10 A). This correlation was also valid for the three-weeks-old cells (both AS4 and AS5) and for animals from the FST1 group (ρ= 0.8214, p-value= 0,034) (Fig. 10 B).

Moreover, the relationship was independent of the experimental group, so it was also valid for other grouping variables, as the learning profiles (for example, fig. 10 C represents Learning Profile 1 group: ρ= 0.7857, p-value= 0.048).

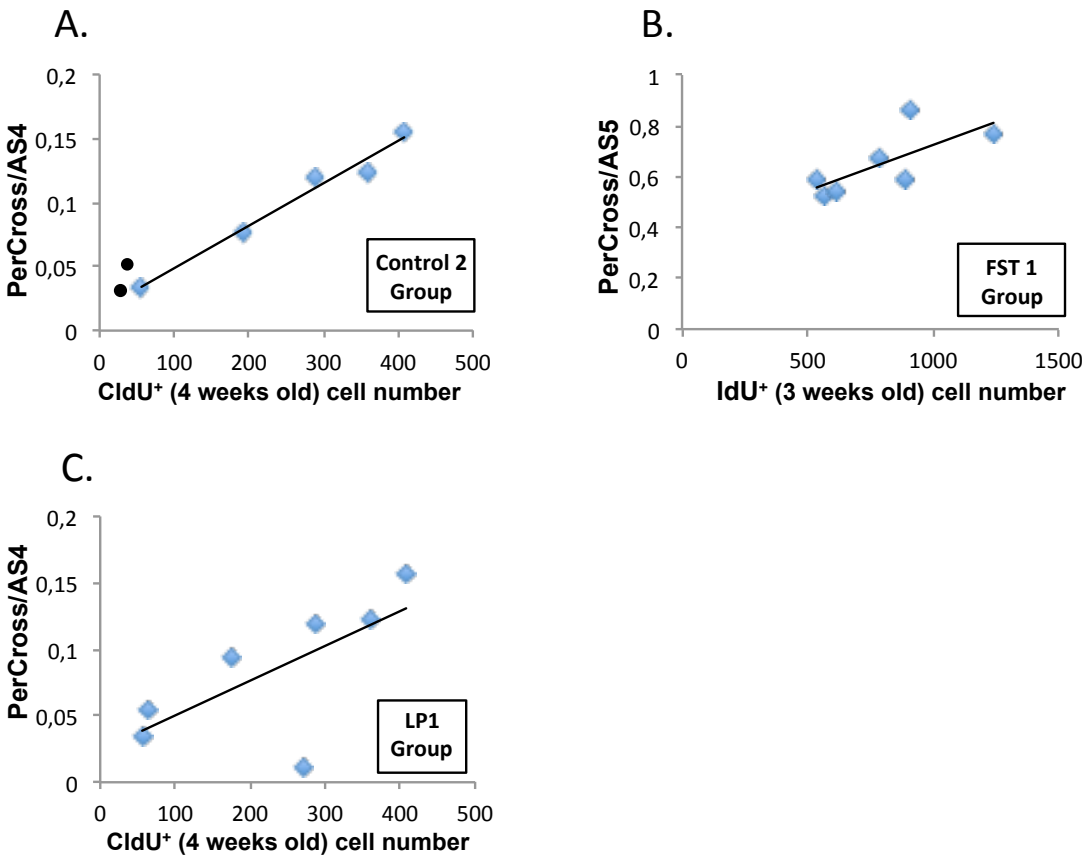

Fig. 10 Significant differences were found between PerCross/AS4 and AS5 with the number of specific immature subpopulations, both in control **(A)** and FST1 **(B)** animals and also for different grouping variables (LP1 group) **(C)**. In fig. A, the two black circles indicate the animals from group FST1 with the lowest number of $CldU^+$ cells.

2.6 The relationship between neural resources and behaviour

It was further analysed the role of the discrete subpopulations of immature post-mitotic neurons, interpreted as neural resources, in the different aspects of the learning task. The ratio DCX^+-CLR^+/AS5 represents the "cost" in newborn immature neurons of acquiring the behaviour. So, in other words, it reveals how many neurons might have been involved in obtaining such a score. In control animals, a higher number of 4- and 3-weeks old cells ($CldU^+$ and IdU^+, respectively) was associated to a higher ratio DCX^+-CLR^+/AS on day 5 and 4 ($CldU^+$ and DCX^+-CLR^+/AS5: ρ= 0.9429, p-value= 0.016; IdU^+ and DCX^+-CLR^+/AS4: ρ= 0.9267, p-value= 0.016; DCX^+-CLR^+/AS5: ρ= 0.8697, p-value= 0.033 (Fig. 11 A-B-C). So, as the number of CldU and IdU positive cells increases, the more cells are needed to achieve the same behavioural score. These correlations are consistent with all the experimental groups and for other grouping variables. For example, when groups LP1 and 2 are pooled it is still observed a positive correlation between $CldU^+$ cells and DCX^+-CLR^+/AS5 (ρ= 0.7903, p-value= 0.006) (Fig. 11 D).

Once again, when the probe test is considered using a persistence variable, it was obtained an inverse, but still valid and significant, result (IdU^+ cells and DCX^+-CLR^+/PerPlat: ρ= -0.8214, p-value= 0.034) (Fig. 11 E).

As a further confirmation that different subpopulations of immature neurons play distinct roles in the MWM, it was analysed the correlation between the ratio $CldU^+$/DCX^+-CLR^+ and AS5 (Fig. 11 F). As it was expected, the higher the proportion of the 4-weeks-old cells relative to the total immature subpopulation, the lower the acquisition score (ρ= -0.8857, p-value= 0.033).

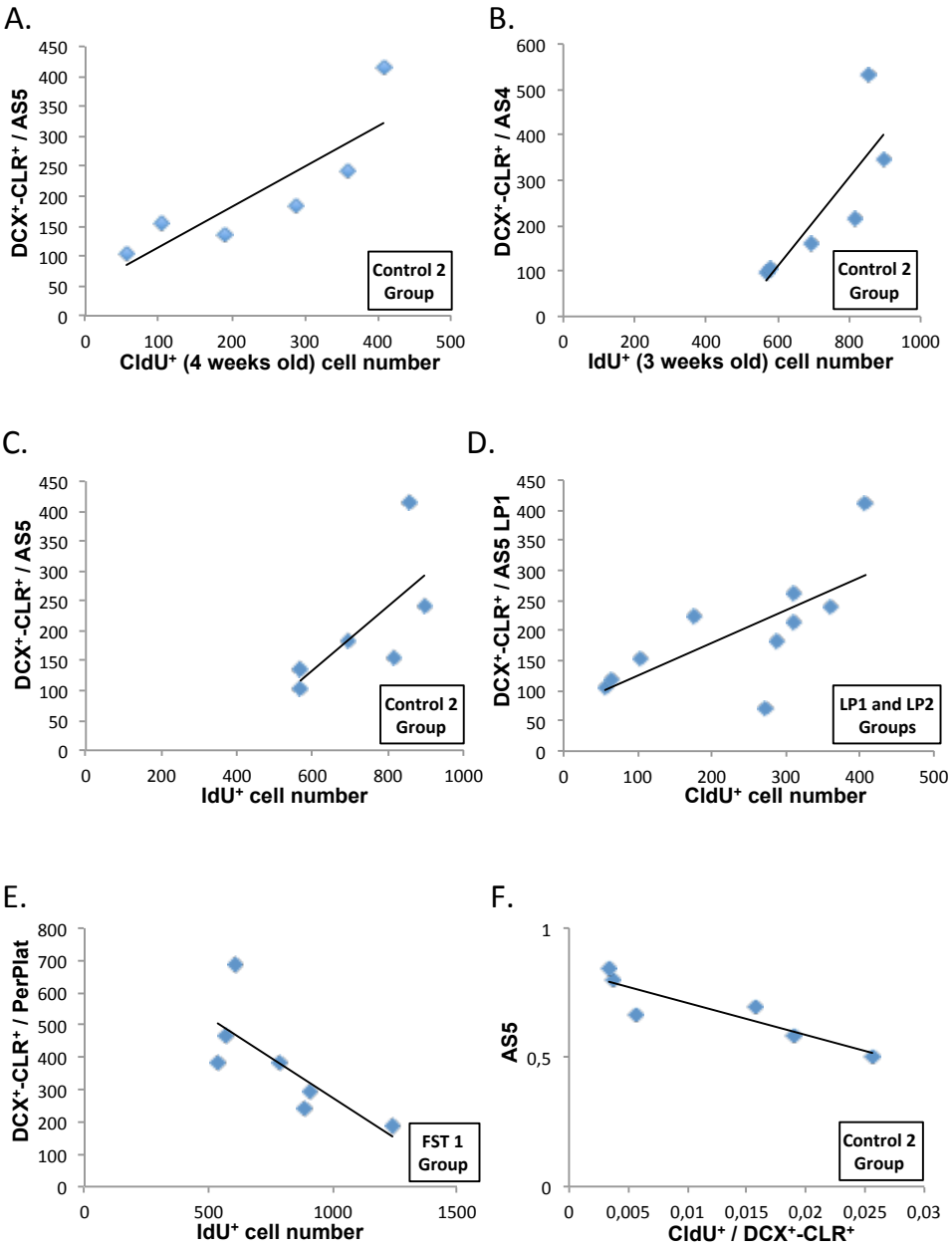

Fig. 11 Correlations of the newborn cell number with the different ratios representing the "cost" of neural resources to acquire and/or retain a task. A. A significant correlation was found between the $CldU^+$ cell number and the DCX^+-CLR^+/AS5 ratio, reflecting the total number of immature neurons in the GCL of the dentate gyrus (DCX^+ and CLR^+ neurons) and the acquisition score in the last day of the learning period (AS5). **B-C.** Similar significant positive correlations were found irrespective of the age of the newborn neurons, as IdU^+ cell number was also correlated with this ratio, irrespective of the day analysed (IdU^+ and the DCX^+-CLR^+/AS4 or AS5 ratio), and of the grouping variable (LP1-2 groups pooled) **(D)**. **E.** When the correlation was analysed with persistence instead of acquisition, a significant negative rather than positive correlation was evident. **F.** An interesting and unexpected negative correlation was found between the acquisition score at the end of the learning period (AS5) and the proportion of 4-week-old neurons related to the total number of immature newborn neurons.

2.6.1 The relationship between neural resources and behaviour when *Smad2* is silenced in the adult dentate gyrus

As animals with a lower expression of *Smad2* in the DG showed an impairment in the acquisition phase of the MWM (see Results, Ch. 1 fig. 18 A), it was analysed if this performance was due to a different contribution of the adult neurogenesis. First of all, it was checked if the correlation found in the Experiment Neurogenesis between 3-weeks-old cells (labelled here with BrdU) and AS was valid in all the sedentary control animals. Indeed, once again, a higher number of 3-weeks-old cells was related to a lower AS4 (ρ= -0.7787, p= 0.003) (Fig. 12 A). However, mice infected with the shRNA-Smad2 lentivirus, exhibiting a higher number of $BrdU^+$ cells in contrast to the control group (see Results, Ch. 1, Fig 8), revealed a loss of this correlation (Fig. 12 B).

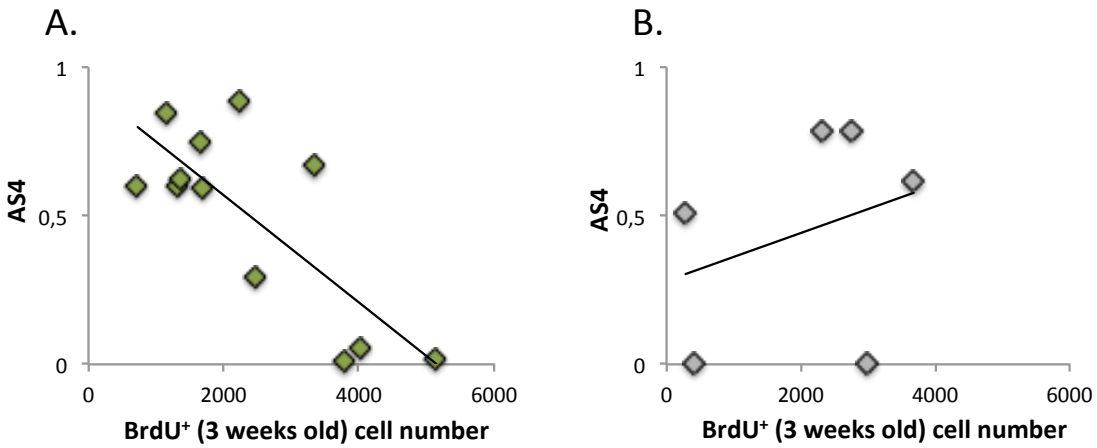

Fig. 12 Correlations between the number of specific immature neuron subpopulations with task acquisition. A. Control, sedentary animals. **B.** In sedentary mice infected with pLVTHM-shRNA-Smad2 lentiviral vector there is not a correlation between AS4 and the number of 3-weeks-old cells.

In control animals, it was also possible to confirm the correlation between the cost in newborn immature neurons to acquire the task and the number of 3-weeks-old cells (ρ= 0.9087, p< 0.001) (Fig. 13). As the number of $BrdU^+$ cells increases, the number of DCX^+/CLR^+ cells needed to achieve the score also increases. In pLVTHM-shRNA-Smad2_SED group this correlation does not exist because some animals score 0 at day 4.

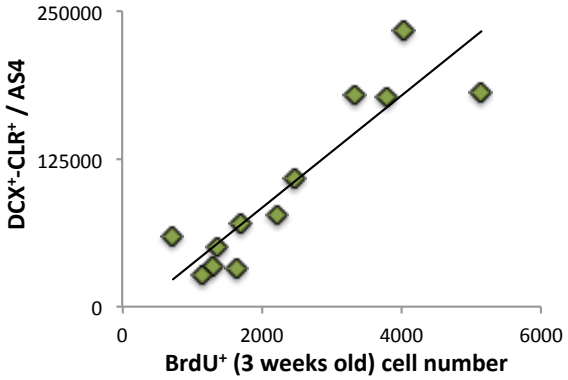

Fig. 13 The positive relationship between neural resources and behaviour in control animals.

Finally, in control mice it was observed the same trend in the correlation between the ratio $BrdU^+/(DCX^+/CLR^+)$ and AS4: the higher the proportion of the 3-weeks-old cells relative to the total immature subpopulation of DCX^+/CLR^+ cells, the lower the AS (ρ= -0.8639, $p< 0.001$) (Fig. 14 A). In the pLVTHM-shRNA-Smad2_SED group, this correlation is also confirmed (ρ= -0.9621, p= 0.002) (Fig. 14 B). However, animals infected with the shRNA-Smad2 construct showed the same amount of immature post-mitotic neurons, but a higher number of 3-weeks-old cells, than the control group (see Results, Ch. 1 Fig. 9 and 10 for immature post-mitotic neurons; Fig. 8, for $BrdU^+$ cell number).

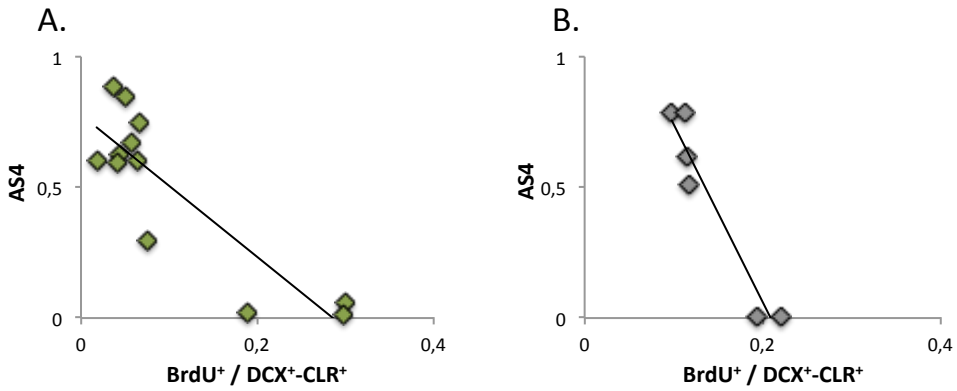

Fig. 14 Negative correlation between the acquisition score at the end of the test and the number of 3-weeks-old cells relative to the DCX^+/CLR^+ subpopulation in control animals **(A)** and in animals operated with the shRNA-Smad2 construct **(B)**.

These last results show that the distinct adult hippocampal neurogenic subpopulations of cells certainly have a role in the execution of a spatial learning task as the Morris Water Maze. If the expression of the *Smad2*

gene is down-regulated, the result is a reshaped structure and composition of the neurogenic population and an altered behavioural outcome.

Discussion

DISCUSSION

The first aim of this thesis consists of exploring the role of *Smad2* in the neuroplasticity processes in the adult dentate gyrus due to its possible implications in the commitment of cell fates. *Smad2* is highly expressed in this neurogenic niche, so it was hypothesized a role for this gene in the modulation of AHN. Furthermore, it was also studied how *Smad2* expression and SMAD2 activity are modulated by exercise and how it affects hippocampal neuroplasticity, not only restricted to neurogenesis. *Smad2* gene is expressed especially by mature and immature neurons in the granule layer. For this reason, to carry out the experiments presented in this study, cells in the dentate gyrus were infected using lentiviral constructs. In fact, the lentivirus is able to infect cells in every stage of cell cycle. Moreover, the expression of shRNA sequence and *Smad2* gene were under the control of constitutive promoters.

To our knowledge, there are not previous studies carried out to directly evaluate the role of *Smad2* gene in the hippocampus of adult animals. Many studies described the role of TGF-β downstream pathway focusing on membrane receptors (He et al., 2014), on *Smad3* (Tapia-González et al., 2013; Muñoz et al., 2016) or using *in vitro* models (Funaba et al., 2002; Ishihara et al., 1994). As *Smad2*-KO organisms show an early embryonic lethality (Nomura and Li, 1998; Waldrip et al., 1998; Heyer et al., 1999; Tremblay et al., 2000; Liu et al., 2016), the most interesting results about the role of *Smad2* in the adult brain were studied with a *Smad2*-CNS-KO model (Wang et al., 2011). This thesis brings new knowledge about the role of *Smad2* at cell level and in the hippocampus network.

1. *Smad2* modulates hippocampal neuroplasticity

A decrease in *Smad2* expression leads to a decrease in the area occupied by inhibitory GAD boutons, resulting in an increase of the ratio vGlut/GAD (see Results, Ch. 1, Fig. 12 A, C and E). So, when there is a decrease in SMAD2, the overall result in the hippocampus is an increase in the percentage of excitatory synapses. It is possible to assume that this change could produce signals inducing, indirectly, hippocampal stem cells to proliferate and this is

demonstrated by the higher number of $pH3^+$ cells observed in animals operated with the shRNA-Smad2 lentivirus (see Results, Ch.1, Fig. 7 A and C). These animals also show a larger SGZ area (see Results, Ch. 1 Fig. 5 C). The decrease of SMAD2 protein not only enhances proliferation, it also induces a more consistent survival of 3-weeks-old cells. A decrease in SMAD2 protein also slows down the differentiation process and this is demonstrated analysing two different kind of parameters: on one hand, the higher number of cells co-expressing DCX and GFP shows how cells silencing *Smad2* remain for a longer period in an immature state (see Results, Ch. 1, Fig. 11 A); in addition, mature neurons, silencing *Smad2*, have a less developed dendritic tree. The arborisation complexity and the number of spines are reduced (see Results, Ch. 1, Fig. 13 A and C; Fig. 14 A, C and E; Fig. 15 A). It is worth of note that cells silencing *Smad2* show particularly shorter tertiary dendrites, representing the branches reaching the molecular layer. These results are indeed very coherent with previously reported data in which the loss of TβRI in progenitor cells, infected with retroviral constructs expressing shRNA against ALK5, affects the survival and maturation of newborn cells in the dentate gyrus, reducing neurogenesis and dendritic processes (He et al., 2014).

When *Smad2* expression is increased, it is possible to observe a change in the previously described scenario. In fact, the over-expression of *Smad2* leads to a decrease in proliferation and in 3-weeks-old cells survival (see Results, Ch.1, Fig. 7 B and D; Fig. 8 B and D). Moreover, the number of GFP^+ cells co-expressing DCX tends to decrease, indicating that cells over-expressing *Smad2* mature quickly or die (see Results, Ch.1, Fig. 11 B). As the total number of the different subpopulations of DCX/CLR cells, as well as the total number of granule cells, does not change (see Results, Ch.1, Fig. 6 B and D; Fig. 10 B, D and F), it is possible to conclude that the over-expression of *Smad2* accelerates the development of cells expressing DCX. However, the over-expression of *Smad2* gene does not enhance the arborisation of the neurons after 3 weeks of lentivirus expression. GFP^+ mature neurons over-expressing *Smad2* present a morphology and a morphometry very similar to the control (see Results, Ch.1, Fig. 13 B and D; Fig. 14 B, D and F; Fig. 15 B). In a previous study (Buckwalter et al., 2006), it was observed that a chronic increase in TGF-β1 reduced the total

number of immature hippocampal neurons and that a TGF-β over-expression decreases hippocampal neurogenesis. It was further showed that an increase in apoptosis was not responsible for this reduction. Instead, it was measured a significant decrease in the proliferation marker Ki67. Altogether, these data suggest that *Smad2* is a player in the adult neurogenesis, acting at many levels: promoting cell's maturation and differentiation, and inhibiting proliferation and survival.

2. A variation in the expression of *Smad2* influences hippocampal-dependent spatial learning and memory

As animals were subjected to an invasive surgical operation, they were tested in an activity cage to ensure the reliability of the behavioural tests. In fact, all the tasks required a certain ability and freedom of movement, so it was necessary to exclude any kind of motor deficit due to the stereotaxic operation. As expected, all the animals were in good health 2 weeks after the lentivirus injections and no differences were found in the activity cage between the experimental groups (see Results, Ch.1, Fig. 16).

The exact functional role of the hippocampus remains a topic of debate. However, the prevailing view is that the dorsal region of the hippocampus is implicated in spatial learning and memory, while the ventral hippocampus mediates anxiety-related behaviours (Fanselow and Dong, 2010). This thesis is focused on these kinds of behaviours, so the Elevated Plus Maze was chosen to test anxiety, while the Morris Water Maze was adopted to test spatial navigation and memory, together with the T-Maze.

The silencing and the over-expression of *Smad2* induced changes that seem not to affect the anxiety state of the animal (see Results, Ch.1, Fig. 17). A more interesting result was obtained testing the animals in a classic MWM: surprisingly, mice infected with the *Smad2* silencing lentivirus performed significantly worst the test (see Results, Ch.1, Fig. 18). Analysing the learning curve, while control animals achieve better results every day, mice operated with the shRNA construct show difficulties in the acquisition phase. The resulting slope is less negative and, at the last day, the performance is significantly worst than the control group. The silencing of *Smad2* does not prevent the learning, but it produces a delay in the acquisition process. It is possible to observe this slight cognitive deficit analysing the probe: when

comparing the mean time spent in the platform quadrant with the mean time spent in the other three quadrants, it is clear that the silencing group learned the task and remember the location of the platform. However, the total time spent in the other quadrants is higher than the mean time spent in the platform quadrant. To further analyse this result, a new group of animals was operated and tested in a different memory test, 3 weeks after the operation. The results obtained from the T-Maze confirm a deficit in memory. In fact, the aim of this test is to verify if the animal remember a place after a training period. As result, when the animal is exposed to a new place, it normally prefers to explore the new one. This result was obtained with the control mice, but not with the mice silencing *Smad2*: they explored the new place for the same amount of time than the previously explored arm of the maze.

The results obtained from the cognitive tests suggested to analyse a possible distinct cells distribution along the rostro-caudal axis. It is remarkable that gene expression in the dorsal hippocampus is highly correlated with cortical regions involved in information processing, while genes expressed in the ventral hippocampus correlate with regions involved in emotion and stress, as amygdala and hypothalamus (Fanselow and Dong, 2010). The dorsal region of the DG appeared to be particularly affected by the silencing of *Smad2*, showing a higher number of proliferating cells and an increase in 3-weeks-old $BrdU^+$ cells (see Results, Ch.1, Fig. 8 E and F). Previous studies tried to describe the correlation between dorsal neurogenesis and learning. For example, in a study by Järlested (Järlested et al., 2013), an induced reduction in cell survival in the dorsal hippocampus did not affect either contextual or cued fear memory. However, other findings suggested that a pool of immature granule cells in the dorsal hippocampus might be responsible for spatial learning and memory (Jinno, 2011). The overall result obtained in this thesis for the learning and memory tests is the consequence of greater changes, involving not only proliferation and survival, but also adjustments in the neuroplasticity of mature neurons. In fact, in the silencing group, the infected mature neurons showed a reduction in the arborisation tree, in particular in the length of the tertiary dendrites and in spines density. It is possible to assume that this dendritic re-shaping is partially responsible of

the result obtained in the learning and memory task. In fact, it is well known that learning accelerates the maturation of the dendritic trees of newborn cells and it promotes their integration into the hippocampal network, depending on the cognitive demand (Tronel et al., 2010). However, on the other hand, one of the requirements for the neuron to process information is the correct development of their dendritic trees, with appropriate dendrites, capable of receiving and integrating complex spatio-temporal informations into synaptic inputs.

3. Effects of exercise on AHN mediated by *Smad2*

Mice operated with the silencing or over-expressing lentivirus show a different modulation of AHN after 2 weeks of physical exercise. The silencing effect seems to be partially reverted and counterbalanced by exercise. Survival of 3-weeks-old neurons is still increased (see Results, Ch.2, Fig. 5 A and C), but there are no differences in proliferation (see Results, Ch.2, Fig. 4 A and C). In fact, also the number of inhibitory and excitatory synapses in the molecular layer is balanced and none prevails upon the other (see Results, Ch.2, Fig. 9 A, C and E). Exercise increases the number of immature neurons and, in those animals silencing *Smad2*, the number of GFP^+ cells co-expressing DCX is higher than the control (see Results, Ch.2, Fig. 8 A). The same effect was observable in the sedentary animals, where the expression of shRNA against Smad2 mRNA decelerated the process of maturation, leaving the infected cells for longer time in an immature state, expressing DCX protein. With this experiment it was possible to confirm the role of *Smad2* in promoting the differentiation and maturation process. Moreover, at a cellular level, mature neurons infected with shRNA-Smad2 still have a less developed arborisation tree and fewer spines, as in the sedentary mice (see Results, Ch.2, Fig. 10, 11 and 12). This result demonstrates that the effects of exercise depend partially on *Smad2*, as a modulation of its expression led to lose some of the positive outcomes normally observed after training and extensively reviewed by Kempermann (Kempermann, 2011): from an increase in the survival of the adult-generated granule cells (Snyder et al., 2009), to an increase in spine density (Glasper et al., 2010).

It can be highly relevant to take into account the hormetic responses to exercise when comparing the results obtained from the sedentary and trained groups (Gradari et al., 2016b). It is well-known that forced treadmill exercise can induce detrimental effects when performed after a deep brain surgery (Jun et al., 2012). While exercise intensity level usually promotes positive changes in neuron morphology, together with anxiolytic and procognitive effects, after a surgery it could produce no changes or changes in the opposite direction. These findings can be easily interpreted in the way that surgery is diminishing the maximum positive response to exercise, and shortening the hormetic zone of exercise biphasic effects (Calabrese, 2008; Gradari et al., 2016b). What is worth noting is the effect of exercise on those mice operated with the over-expressing lentivirus. In this case, the effects of the over-expression are very clear and, in some circumstances, opposite to the silencing effects. First of all, the overall effect in the hippocampus of these mice was a general increase of the inhibitory synapses in the molecular layer (see Results, Ch.2, Fig. 9 B, D and F). There was a decrease in the number of GFP^+ cells over-expressing *Smad2* that co-express DCX (see Results, Ch.2, Fig. 8 B). So, cells seem to mature quickly. This effect was observable also in the sedentary mice, but with exercise it seems more emphasized. In addition, it was possible to note an improved dendritic arborisation with an increased spine density (see Results, Ch.2, Fig. 10, 11 and 12). The morphological results are consistent with a previous work showing that TGF-β promotes *in vitro* neurites sprouting and elongation of cultured rat hippocampal neurons (Ishihara et al., 1994). To explain these results, it was proposed that exercise, increasing blood levels of TGF-β (Das, 2004), activates its receptor more consistently than in sedentary animals. The activation of the receptor leads to SMAD2 phosphorylation and activation as transcription factor (Brown et al, 2007). In this thesis, it was demonstrated that 2 weeks of treadmill increase the level of pSMAD2 in the hippocampus of runner animals (see Results, Ch.3, Fig. 8 B). So, data from this work reveals that *Smad2* over-expression itself does not induced considerable changes because the protein remains in an inactive state, but exercise it is able to increase the level of phosphorylation of the over-expressed protein and to induce the subsequent effects. Altogether, this data confirm a role for *Smad2* in the

maturation process of the hippocampal granule neurons, as well as in the late-stages of neurogenesis and that this role could be modulated by exercise.

4. Exercise influences SMAD2 and affects hippocampal-dependent spatial learning and memory

Runner mice, receiving the silencing lentivirus construct against *Smad2* in the hippocampus, obtained the same scores in the MWM as the control group (see Results, Ch.2, Fig. 15). So, physical exercise seems to revert the deficit in the learning process observed in sedentary animals. Also memory, tested by the probe, did improve. It could be very interesting to compare these results with data from another study analysing the role of TGF-β1 in hippocampal plasticity and memory in wild-type mice (Caraci et al., 2015): in that study, blocking the endogenous TGF-β1 signalling pathway led to an impairment in long term potentiation (LTP) and object recognition. However, the impairment was recovered by administering exogenous TGF-β1. Such results suggest two conclusions: first of all, a role for TGF-β1 pathway in the mechanisms underlying LTP and memory (and, together with our results, a role for *Smad2*); second, that an increase in TGF-β1 signal, obtained here thanks to physical exercise that raises the amount of pSMAD2, could rescue the memory task. On the other hand, in the over-expression group, exercise does not enhance the performance and the same kind of learning curve was obtained in the two groups (see Results, Ch.2, Fig. 16). It is possible to speculate that the overall effect observed in the behavioural tests is not attributable to the morphology of the single-infected cells. In fact, GFP^+ mature neurons silencing *Smad2* show a decrease in their arborisation tree, independently from exercise. But sedentary mice show a cognitive deficiency, while in the trained animals there is a recovery of this deficit. On the other hand, exercise phosphorylates and activates SMAD2 protein improving the dendritic complexity of those cells over-expressing *Smad2*, while without exercise, no differences were observed. Nevertheless, in both groups, sedentary and trained, no differences were observed in the MWM. It is possible to conclude that the behavioural outcomes do not depend from single infected cells, but from general changes occurring in the hippocampus.

5. Molecular regulation of *Smad2* by exercise

Data from this thesis show that exercise needs an intact *Smad2* expression in both immature and mature cells to achieve its optimal effects on hippocampus and behavioural performance. For this reason, it was analysed the response of two weeks of moderate exercise in the modulation of AHN in control animals. The results obtained demonstrate that exercise increases proliferation of neural stem cells, it increases the survival of 2-weeks-old cells and it also increases the number of immature cells. Moreover, proliferation and survival are counterbalanced by an increase in apoptotic events to ensure homeostasis (see Results, Ch. 3, Fig. 2). However, these changes are not sufficient to significantly improve behavioural tests, as EPM and MWM. Runner animals achieve better scores in the MWM, but the learning curve does not diverge from the curve of the control group (see Results, Ch. 3, Fig. 3). These results are in line with previously published works, both from our laboratory (Llorens-Martín et al., 2006; Llorens-Martín et al., 2010) and from other research groups (for example, Liu et al., 2008; Nam et al., 2014), demonstrating that a moderate exercise leads to an improvement in behavioural performance and neurogenesis, and it ensures the reliability of our training protocol to modulate positively AHN (see also Gradari et al., 2016b).

Once established the effect of 2 weeks of treadmill, this thesis demonstrates that *Smad2* is a transcription factor able to modulate adult hippocampal neurogenesis and mature neurons plasticity, and that exercise modifies its expression. So, in order to study the relationship between exercise and *Smad2* gene expression in the hippocampus, it was carried out an epigenetics analysis. Epigenetics represents the interplay between genes and environment. Organisms use complex mechanisms to adapt to changing environment without mutate their genome and DNA methylation was one of the first described epigenetic mechanisms in the hippocampus. Epigenetic mechanisms allow modifications in the genome that may lead to subsequent behavioural manifestations such as learning and memory and emotions (Nestler, 2009). In a previous study, it was demonstrated that 1 week of voluntary exercise elevates BDNF mRNA level and learning and memory performance. This effect was produced by reducing the methylation of CpG in the *Bdnf* promoter (Gomez-Pinilla et al., 2011). So, DNA

methylation plays a crucial role in remodeling chromatin in the brain and may be a crucial step by which exercise regulates gene expression. Dynamic changes in DNA methylation seem to have a role in the regulation of cell cycle and for this reason the methylation level of the CGs regions of *Smad2* were analysed in sedentary and runner mice. Moreover, the DNA methylation level of other stem cell transcription factors was studied in order to have a more complete view of the effect of exercise in the hippocampus. Interestingly, almost all the genes considered in this analysis were in an unmethylated status in sedentary and exercised animals. It means that their expression is not altered by 2 weeks of moderate physical exercise and mechanisms of methylation. However, *Smad2* was hypermethylated in sedentary mice and exercise was able to demethylate the promoter region (see Results, Ch. 3, Fig. 5 and Fig. 6 A). This led to an increase in *Smad2* gene expression in runner animals, but not to an increase in the production of SMAD2 protein (see Results, Ch. 3, Fig. 7 A and 8 A). However, exercise induces the phosphorylation of the protein leading to an increase in the pSMAD2/SMAD2 ratio in runner mice compared to the sedentary group (see Results, Ch. 3, Fig. 8 B). It is not clear why it was not detectable an increase in protein production in response to a greater amount of mRNA, but perhaps it is possible to explain it considering that the synthesis of new SMAD2 proteins is immediately followed by phosphorylation in runner animals. The activity of the phosphorylated proteins could be regulated by processes of protein degradation and this can explain why it was not observed an increase in the total amount of SMAD2 protein.

Another important result was obtained considering *Hdac1* gene that produces a protein forming a co-repressor complex with SMAD2 (Wotton et al., 1999). As *Smad2*, *Hdac1* gene is highly methylated in sedentary mice, while exercise induces demethylation and so an increase in its expression (see Results, Ch. 3, Fig. 6 B and Fig. 7 B). However, 2 weeks of exercise activate a process that leads to regulate the production of HDAC1 protein. Runner mice show a decreasing trend in the amount of HDAC1 protein in the hippocampus (see Results, Ch. 3, Fig. 8 C). An increase in pSMAD2, but a decrease in HDAC1, suggests a decrease in the formation of repressive

transcription complexes as effect of 2 weeks of moderate physical exercise, but to confirm this assumption further analysis are required.

6. The relationship between behaviour acquisition and persistence with the involvement of adult hippocampal neurogenesis

Inter-individual differences in AHN have been closely associated to distinct efficacy in performing tasks. In Results, Chapter 4 (published as Gradari et al., 2016a, see Appendix), it was first analysed the relationship between the performance during the acquisition of a spatial task and the persistence of the acquired behaviour after the removal of the reinforcement, and then it was considered the relationship between these parameters and the morphological changes in adult hippocampal neurogenesis. Finally, all these findings were applied to the histological and behavioural results obtained from the sedentary mice where the silencing of *Smad2* was induced, in order to study the cognitive deficits showed by these animals in the MWM.

No previous direct evidences exist about a direct relationship between the way mice learn a task and the persistence of the acquired behaviour. In both rats and mice, it is well known that the operant conditioning in the MWM, by using a continuous reinforcement paradigm, leads to a rapid acquisition rate and a low persistence in the extinction trials, compared to the conditioning using an intermittent reinforcement protocol, that leads to a slower acquisition rate and to a higher persistence in the unreinforced trials (Dickinson, 1980). As for the relationship between spatial learning and AHN, a high number of works demonstrated a key role for immature newborn neurons in the execution of the water maze. Moreover, the complete removal of adult-born neurons in the DG leads to an impairment in some of the hippocampus-dependent aspects of the test. It is also known that the spatial learning task requires a specific balance between some discrete subpopulations of immature neurons, differing in age and differentiation stage (Dupret et al., 2007). So, different populations with different ages might play distinct roles and could be involved in a different way in the execution of the task. For this reason, in this thesis, it was first compared the performance during the task acquisition with the performance during the unreinforced test.

First of all, it was tested the reliability of the learning curve slope as a valid parameter to analyse behaviour. By using a high number of mice, from different strains and bred in different laboratories, but applying the same test protocol, it was analysed the learning curve parameter. All the animals learnt the task and, analysing the individual scores, it was first discovered that the learning process is well described by an exponential equation. By considering each animal's performance on the basis of this equation, it was possible to describe three different styles, called in this thesis "Learning Profiles" (for definitions, see Materials and Methods, Table 31; Results, Ch. 4 Fig. 2). What is worth of note is that a very similar proportion of control animals performs all the three learning profiles. As all the animals learn to find the platform at the end of the task, but the first day's score depends on whether they found it by chance or not, the curve slope does not represent adequately the learning process of each animal. The only significant prediction is that animals scoring high differences between acquisition day 1 and 2 (profile 3 animals, with a high Early Profile variable), significantly tend to obtain a higher score at the end of the acquisition. However, any other combination of values for Early Profile was not significantly related to the final score at the end of the acquisition. As result, the score at the end of the acquisition process is not directly predictable from the performance at the beginning of the task, except for animals showing the third learning profile. For all these reasons, the learning curve cannot be the best parameter to describe the learning process in a Morris Water Maze.

7. The task acquisition score shows a negative correlation to the persistence in the acquired behaviour

In order to study the persistence behaviour, it was used a MWM protocol with almost no time delay (just 1 h) between the last acquisition trial (day 5) and the next unreinforced trial (the probe test), aiming to maximize the probability of appearance of extinction bursts and novel search strategies after task acquisition in all animals. The unpredictable result obtained was that animals showing better acquisition behaviour, in a continuously reinforced operant conditioning, are more prone to use novel strategies when the task is unreinforced. On the other hand, animals with worst scores at the end of the learning period are more prone to show extinction bursts

in the unreinforced trial. This finding suggests that the best animals acquiring the task spend shorter time in looking for the platform at the learned location when the platform is no longer there (see Results, Ch. 4, Fig. 4 A), pointing to a different behaviour of the animals when they face to a first unexpected trial without reward. As all the animals learnt the task and spent less than 20 s to reach the platform at the end of the acquisition phase, they performed similarly the probe test as a matter of time. However, they displayed different behaviours to obtain the same result: from persisting in searching the platform in the same quadrant, to looking for it in the other three quadrants (novel locations). Probably, the best interpretation for these data is that the efficiency to learn a task and the persistence of the new behaviour after an unreinforced protocol are conflicting-opposing outcomes.

8. The relationship between neural resources and behaviour

The relationship between the neural resources in terms of newborn immature neurons and a given behaviour score represents the "cost" in immature cells to acquire a specific behaviour. One interesting target to compare these ratios is to analyse the influence of precise, discrete, immature known-age cell subpopulations. The results obtained in this thesis are task-specific, as no significant correlations were found between all the cell-related parameters and the scores at the elevated plus maze. A great range of immature cells was analysed: $CldU^+$ (4-weeks old cells), IdU^+ (3-weeks-old cells), $pH3^+$ (mitotic cells in the SGZ at the moment of the sacrifice), DCX^+/CLR^+ (post-mitotic immature differentiating neurons), DCX^+/CLR^- (an heterogeneous subpopulation of newborn cells, including dividing neuroblasts) (see Results, Ch. 4, Fig. 7 D-H), but just the number of some of these subpopulations correlates significantly with changes in behaviour. So, the present results are also population-specific. This finding is consistent with previous works demonstrating that different treatments (such as environmental enrichment) modify the number of surviving neurons without modify all the distinct subsets of immature neurons (for example, Llorens-Martín et al., 2010). In the same way, physical exercise is able to increase the total number of immature neurons although each subpopulation has been shown to correlate differently with the changes in

behaviour. The results shown in this thesis demonstrate that the higher the number of 2- to 3-weeks-old immature neurons in the hippocampal DG of adult mice, the lower the AS (so, the longer the time the animals need to reach the hidden platform at the end of the acquisition phase) (see Results, Ch. 4, Fig. 6 A). Accordingly, these animals also persisted longer in searching for the platform at its former location when tested in the probe trial, immediately after the acquisition phase (see Results, Ch. 4, Fig. 6 B). Conversely, animals with a higher AS (better acquisition performance) and that remained less time in the former quadrant when faced to the absence of the platform, were both more efficient in finding the platform at a new location in the reversal trial and they had fewer 2- to 3-weeks-old immature neurons (see Results, Ch. 4, Fig. 4 B).

In Experiment Neurogenesis, the forced swim test induced a decrease in some immature subpopulations of cells and in the number of proliferating cells (see Results, Ch. 4, Fig. 7 D-H). This change in cell number reflects the result obtained from the EPM: animals subjected to the forced swim test spent less time in the open arms than the control animals (see Results, Ch. 4, Fig. 7 C). However, all the animals performed correctly the MWM: they learned the task and they retained the memory when tested in the probe trial (see Results, Ch. 4, Fig. 7 A and B). What is worth of note, is that some of the animals subjected to the FST had the lowest number of immature cells and the lowest ratio between persistence and acquisition (see Results, Ch. 4, Fig. 10). The biological meaning of these findings is that the proportion of discrete subpopulations of immature neurons is correlated to the relationship between acquisition and persistence of a new behaviour, pointing to different contributions from these subpopulations to the same task.

The MWM is a very complex task and the process involving neurogenesis is indubitable complicated. For example, it was previously demonstrated that the MWM is characterised by different stages and that each phase generates distinct effects on adult neurogenesis (Döbrössy et al., 2003). While the late phase induced proliferation of newborn cells and it increased their survival, the same late phase decreased the number of the previous generated cells and this decline in neurogenesis positively correlated with the learning performance. This study also showed that rats with the highest number of

cells were less competent in acquiring and using spatial information compared to those with less new cells number.

9. The reversal trial and the full extinction performance depend on the way the animal learn the task

Reversal score has been positively correlated with the rate of neurogenesis in some mouse models (Pan et al., 2013), although not specifically with discrete subpopulations of immature neurons, as shown here. So, not all cell subpopulations of AHN are involved with the same role in reversal learning. Similarly, DCX^+ immature neurons are implicated in spatial learning acquisition and reversal, but not with the retrieval of stored long-term memories (Vukovic et al., 2013). This is compatible with the present results, which point to the involvement of discrete subpopulations of immature neurons ($CldU^+$ or IdU^+/DCX^+ cells) as a key influence on acquisition and persistence. Indeed, it is not the total number of a discrete subpopulation of neurons that appears to be relevant for the behavioural outcome, but rather the proportion of those neurons (2- to 3-weeks old) with respect to the entire population of adult-born neurons.

The Full-Extinction experiment demonstrates that mice are able to learn that no reward exists into the pool after only 4 days of extinction trials and independently of their previous quadrant preference during the probe. Anyway, those animals with a higher persistence in searching for the platform in its original location during the first day of extinction, displayed significantly less time in this quadrant at the end of the extinction protocol (see Results, Ch. 4, Fig. 5). All these results suggest that the way the animal applies an information to perform a task is strictly related to the way the animal have previously learned that information.

10. *Smad2* down-expression modulates the relationship between neural resources and behaviour

The injection of shRNA-Smad2 lentivirus inside the hippocampus generated important changes in the histological composition of the region. These changes led to a slight cognitive deficit in spatial learning and memory (see Results, Ch. 1, Fig. 18). The Morris Water Maze protocol used here was a highly hippocampal-dependent procedure: the platform was maintained

hidden in the same position during all the test duration, but the starting point was changed every time. To find the platform, the mouse needed to apply an "allocentric mapping strategy", consisting of learning the positional relationships among multiple independent environmental cues. This strategy is known as a spatial relational memory (Dupret et al., 2008).

What is worth noting is that data from mice receiving the control lentiviral construct showed the same correlations between histology and behaviour found in the control, no operated, animals (see Results, Ch. 4, Fig. 12 A). Despite the surgical operation, in these animals the different cell ratios remained constant and no cognitive deficits were observed. On the other hand, changes induced by the silencing of *Smad2* led to lose the correlation between the number of 3-weeks-old cells and the acquisition score obtained at the end of the task in the MWM (see Results, Ch. 4, Fig. 12 B).

Moreover, in control animals, as the number of 3-weeks-old cells increased, also the number of DCX^+/CLR^+ cells had to increase to achieve the same score (see Results, Ch. 4, Fig. 13). As there were mice expressing the shRNA-Smad2 lentivirus that scored 0 at the fourth day of acquisition (it means that they did not learn at all the task), this previous cited correlation disappeared in the silencing group. However, as the ratio between 3-weeks-old cells and DCX^+/CLR^+ cells increases, the score in spatial learning decreases. This correlation remained valid also for the animals silencing *Smad2* (see Results, Ch. 4, Fig 14). Mice silencing *Smad2* showed a higher number of 3-weeks-old cells, because the decrease in *Smad2* increases the survival of these cells, but there were no changes in the number of DCX^+/CLR^+ cells (see Results, Ch. 1, Fig. 8 A and C; Fig. 9 A, C, E and G). This re-shaped proportion of immature subpopulations demonstrates that it is important the balance between immature cells to obtain certain behavioural outcomes. In particular, it demonstrates how 3-weeks-old cells and DCX^+/CLR^+ subpopulation in the DG are crucial, even if not the only determinant factors, in hippocampal-dependent spatial learning and memory.

In conclusion, it was showed here that *Smad2* signaling contributes to neurogenesis in the adult DG, highlighting its role in plasticity and memory.

Conclusions

Conclusiones

CONCLUSIONS

1. *Smad2* is a modulator of neuroplasticity of mature neurons and it regulates the late-stages of adult hippocampal neurogenesis: *Smad2* does not promote cell proliferation and survival but it induces neuron's maturation and differentiation.

2. A decrease in the expression of *Smad2*, and a 60% decrease in the amount of SMAD2 protein in the adult dentate gyrus, produces a reduction in neuroplasticity and a deficit in hippocampal-dependent spatial learning and memory.

3. Exercise generates *Smad2*-independent and dependent effects, promoting cell proliferation, differentiation and survival, increasing mature neuron's arborisation and improving hippocampal-dependent spatial learning and memory.

4. Exercise modulates the expression of *Smad2* through the epigenetic mechanism of DNA methylation and it induces the activation of SMAD2 protein increasing its phosphorylation.

5. A negative correlation defines the relationship between task acquisition and behaviour persistence: the faster the animals find the water maze platform at the end of the acquisition stage, the less they persist in searching for it at the learned position in a subsequent no-reinforced trial.

6. Specific subpopulations of immature cells (4- and 3-weeks old) in the adult dentate gyrus represent neural resources playing a role in achieving a given score in the hippocampal-dependent spatial learning task.

7. A decrease in the expression of *Smad2* leads to lose the relationship between specific subpopulations of immature cells in the dentate gyrus and spatial learning and memory abilities.

CONCLUSIONES

1. *Smad2* es un modulador de la neuroplasticidad de neuronas maduras que regula las fases tardías de la neurogénesis hipocampal adulta: *Smad2* no promueve la proliferación celular y la supervivencia, sin embargo induce la maduración y diferenciación de las neuronas.

2. Una disminución en la expresión de *Smad2* y una disminución de un 60% en la cantidad de proteína SMAD2 en el giro dentado adulto producen una reducción de la neuroplasticidad y un déficit en el aprendizaje espacial hipocampo dependiente y en la memoria.

3. El ejercicio genera efectos independientes y dependientes de *Smad2*, promoviendo la proliferación celular, la diferenciación y la supervivencia, aumentando la arborización de las neuronas maduras y mejorando el aprendizaje espacial hipocampo dependiente y la memoria.

4. El ejercicio modula la expresión de *Smad2* mediante mecanismos epigenéticos de metilación de ADN e induce la activación de la proteína SMAD2 aumentando su fosforilación.

5. Existe una correlación negativa entre el desempeño en la adquisición de la tarea en el laberinto acuático de Morris y la persistencia de la conducta. Cuanto más rápido los animales encuentran la plataforma en el laberinto en la última fase de adquisición, menos tiempo persistirán en buscarla en la posición aprendida en la siguiente prueba sin refuerzo.

6. Subpoblaciones específicas de células inmaduras (de 4 y 3 semanas de edad) en el giro dentado adulto representan los recursos neurales que juegan un papel fundamental en adquirir una determinada puntuación en el aprendizaje hipocampo dependiente.

7. Una disminución en la expresión de *Smad2* lleva a perder la relación entre específicas subpoblaciones de células inmaduras en el giro dentado y el aprendizaje espacial y la memoria.

Bibliography

BIBLIOGRAPHY

Aguiar AS Jr, Tuon T, Pinho CA, Silva LA, Andreazza AC, Kapczinski F, Quevedo J, Streck EL, Pinho RA (2008). Intense exercise induces mitochondrial dysfunction in mice brain. Neurochem Res vol. 33 (1) pp. 51-58

Aimone JB, Li Y, Lee SW, Clemenson GD, Deng W, Gage FH (2014). Regulation and function of adult neurogenesis: from genes to cognition. Physiological Reviews Vol. 94 no. 4, 991-1026

Arendt T, Holzer M, Stöbe A, Gärtner U, Lüth HJ, Brückner MK, Ueberham U (2000). Activated mitogenic signaling induces a process of dedifferentiation in Alzheimer's disease that eventually results in cell death. Ann N Y Acad Sci vol. 920 pp. 249-55

Bannerman DM, Sprengel R, Sanderson DJ, McHugh SB, Rawlins JNP, Monver H, Seeburg PH (2014). Hippocampal synaptic plasticity, spatial memory and anxiety. Nature Reviews Neuroscience vol. 15 (3) pp. 181-92

Brandt MD, Jessberger S, Steiner B, Kronenberg G, Reuter K, Bick-Sander A, von der Behrens W, Kempermann G (2003). Transient calretinin expression defines early postmitotic step of neuronal differentiation in adult hippocampal neurogenesis of mice. Mol Cell Neurosci vol. 24 (3) pp. 603-13

Broadbent NJ, Squire LR, Clark RE (2004). Spatial memory, recognition memory, and the hippocampus. Proc Natl Acad Sci USA vol. 101 (40) pp. 14515-20

Brown KA, Pietenpol JA, Moses HL (2007). A tale of two proteins: differential roles and regulation of Smad2 and Smad3 in TGF-beta signaling. J Cell Biochem vol. 101 (1) pp. 9-33

Buckwalter MS, Yamane M, Coleman BS, Ormerod BK, Chin JT, Palmer T, Wyss-Coray T (2006). Chronically increased transforming growth factor-beta1 strongly inhibits hippocampal neurogenesis in aged mice. Am J Pathol vol. 169 (1) pp. 154-64

Calabrese EJ (2008). Hormesis and medicine. Br J Clin Pharmacol vol. 66 (5) pp. 594-617

Calonge MJ and Massagué J (1999). Smad4/DPC4 silencing and hyperactive Ras jointly disrupt transforming growth factor-beta antiproliferative responses in colon cancer cells. J Biol Chem vol. 274 (47) pp. 33637-43

Caraci F, Gulisano W, Guida CA, Impellizzeri AAR, Drago F, Puzzo D, Palmeri A (2015). A key role for TGF-β1 in hippocampal synaptic plasticity and memory. Sci Rep vol. 5 pp. 11252

Chalmers KA and Love S (2007). Neurofibrillary tangles may interfere with Smad 2/3 signaling in neurons. J Neuropathol Exp Neurol vol. 66 (2) pp. 158-67

Chang C and Harland RM (2007). Neural induction requires continued suppression of both Smad1 and Smad2 signals during gastrulation. Development vol. 134 (21) pp. 3861-72

Chen Y, Ai Y, Slevin JR, Maley BE, Gash DM (2005). Progenitor proliferation in the adult hippocampus and substantia nigra induced by glial cell line-derived neurotrophic factor. Exp Neurol vol. 196 (1) pp. 87-95

Clark RE, Zola SM, Squire LR (2000). Impaired recognition memory in rats after damage to the hippocampus. J Neurosci vol. 20 (23) pp. 8853-60

Cotman CW and Berchtold NC (2007). Physical activity and the maintenance of cognition: learning from animal models. Alzheimer's & Dementia

Coyle EF (2000). Physical activity as a metabolic stressor. Am J Clin Nutr vol. 72 (2 Suppl) pp. 512S-20S

Das UN (2004). Anti-inflammatory nature of exercise. Nutrition, Volume 20, Issue 3, 323-326

Deng W, Aimone JB, Gage FH (2010). New neurons and new memories: how does adult hippocampal neurogenesis affect learning and memory? Nature Reviews Neuroscience vol. 11 (5) pp. 339-50

Di Guglielmo GM, Le Roy C, Goodfellow AF, Wrana JL (2003). Distinct endocytic pathways regulate TGF-beta receptor signalling and turnover. Nat Cell Biol vol. 5 (5) pp. 410-21

Dickinson A (1980). Contemporary Animal Learning Theory. Cambridge: Cambridge University Press

Döbrössy MD, Drapeau E, Aurousseau C, Le Moal M, Piazza PV, Abrous DN (2003). Differential effects of learning on neurogenesis: learning increases or decreases the number of newly born cells depending on their birth date. Mol Psychiatry vol. 8 (12) pp. 974-82

Dreesen O and Brivanlou AH (2007). Signaling pathways in cancer and embryonic stem cells. Stem Cell Rev vol. 3 (1) pp. 7-17

Drew LJ, Fusi S, Hen R (2013). Adult neurogenesis in the mammalian hippocampus: why the dentate gyrus? Learn Mem vol. 20 (12) pp. 710-29

Dunn NR, Koonce CH, Anderson DC, Islam A, Bikoff EK, Robertson EJ (2005). Mice exclusively expressing the short isoform of Smad2 develop normally and are viable and fertile. Genes Dev vol. 19 (1) pp. 152-63

Dupret D, Fabre A, Döbrössy MD, Panatier A, Rodríguez JJ, Lamarque S, Lemaire V, Oliet SH, Piazza PV, Abrous DN (2007). Spatial learning depends on both the addition and removal of new hippocampal neurons. PLoS Biol vol. 5 (8) pp. e214

Dupret D, Revest JM, Koehl M, Ichas F, De Giorgi F, Costet P, Abrous DN, Piazza PV (2008). Spatial relational memory requires hippocampal adult neurogenesis. PLoS ONE vol. 3 (4) pp. e1959

Encinas JM, Michurina TV, Peunova N, Park JH, Tordo J, Peterson DA, Fishell G, Koulakov A, Enikolopov G (2011). Division-coupled astrocytic differentiation and age-related depletion of neural stem cells in the adult hippocampus. Cell Stem Cell vol. 8 (5) pp. 566-79

Epp JR, Chow C, Galea LA (2013). Hippocampus-dependent learning influences hippocampal neurogenesis. Front Neurosci vol. 7 pp. 57

Ernst C, Olson AK, Pinel JP, Lam RW, Christie BR (2006). Antidepressant effects of exercise: evidence for an adult-neurogenesis hypothesis? J Psychiatry Neurosci vol. 31 (2) pp. 84-92

Fanselow MS and Dong HW (2010). Are the dorsal and ventral hippocampus functionally distinct structures? Neuron vol. 65 (1) pp. 7-19

Fink SP, Mikkola D, Willson JK, Markowitz S (2003). TGF-beta-induced nuclear localization of Smad2 and Smad3 in Smad4 null cancer cell lines. Oncogene vol. 22 (9) pp. 1317-23

Fuentealba LC, Obernier K, Alvarez-Buylla A (2012). Adult neural stem cells bridge their niche. Cell Stem Cell vol. 10 (6) pp. 698-708

Funaba M, Zimmerman CM, Mathews LS (2002). Modulation of Smad2-mediated signaling by extracellular signal-regulated kinase. J Biol Chem vol. 277 (44) pp. 41361-8

García-Capdevila S, Portell-Cortés I, Torras-Garcia M, Coll-Andreu M, Costa Miserachs D (2009). Effects of long-term voluntary exercise on learning and memory processes: dependency of the task and level of exercise. Behav Brain Res vol. 202 (2) pp. 162-70

Glasper ER, Llorens-Martín MV, Leuner B, Gould E, Trejo JL (2010). Blockade of insulin-like growth factor-I has complex effects on structural plasticity in the hippocampus. Hippocampus vol. 20 (6) pp. 706-12

Gomez-Pinilla F, Zhuang Y, Feng J, Ying Z, Fan G (2011). Exercise impacts brain-derived neurotrophic factor plasticity by engaging mechanisms of epigenetic regulation. Eur J Neurosci vol. 33 (3) pp. 383-90

Gomez-Pinilla F and Hillman C (2013). The influence of exercise on cognitive abilities. Compr Physiol vol. 3 (1) pp. 403-28

Gradari S, Pérez-Domper P, Butler RG, Martínez-Cué C, de Polavieja GG, Trejo JL (2016a). The relationship between behavior acquisition and persistence abilities: Involvement of adult hippocampal neurogenesis. Hippocampus Jul;26(7):857-74

Gradari S, Pallé A, McGreevy KR, Fontán-Lozano Á, Trejo JL (2016b). Can Exercise Make You Smarter, Happier, and Have More Neurons? A Hormetic Perspective. Front Neurosci vol. 10 pp. 93

Kaplan S, Odaci E, Canan S, Önger ME, Aslan H, Ünal B (2012). The Disector counting technique. NeuroQuantology 10, 44-53

Kojima S, Vignjevic D, Borisy GG (2004). Improved silencing vector co-expressing GFP and small hairpin RNA. BioTechniques vol. 36 (1) pp. 74-9

He Y, Zhang H, Yung A, Villeda SA, Jaeger PA, Olayiwola O, Fainberg N, Wyss-Coray T (2014). ALK5-dependent TGF-β signaling is a major determinant of late-stage adult neurogenesis. Nat Neurosci vol. 17 (7) pp. 943-52

Heyer J, Escalante-Alcalde D, Lia M, Boettinger E, Edelmann W, Stewart CL, Kucherlapati R (1999). Postgastrulation Smad2-deficient embryos show defects in embryo turning and anterior morphogenesis. Proc Natl Acad Sci USA vol. 96 (22) pp. 12595-600

Howard CV and Reed MG (1998). Unbiased stereology: three-dimensional measurement in microscopy. Bios Scientific, Oxford UK

Ickes BR, Pham TM, Sanders LA, Albeck DS, Mohammed AH, Granholm AC (2000). Long-term environmental enrichment leads to regional increases in neurotrophin levels in rat brain. Exp Neurol vol. 164 (1) pp. 45-52

Isaacson R (1974). The structure of the limbic system. The Limbic System, pp. 1-57

Ishihara A, Saito H, Abe K (1994). Transforming growth factor-beta 1 and -beta 2 promote neurite sprouting and elongation of cultured rat hippocampal neurons. Brain Res vol. 639 (1) pp. 21-5

Järlestedt K, Naylor AS, Dean J, Hagberg H, Mallard C (2013). Decreased survival of newborn neurons in the dorsal hippocampus after neonatal LPS exposure in mice. Neuroscience vol. 253 pp. 21-8

Jinno S (2011). Topographic differences in adult neurogenesis in the mouse hippocampus: A stereology-based study using endogenous markers. Hippocampus May;21(5):467-80.

Jun H, Mohammed Qasim Hussaini S, Rigby MJ, Jang MH (2012). Functional role of adult hippocampal neurogenesis as a therapeutic strategy for mental disorders. Neural Plast vol. 2012 pp. 854285

Kandasamy M, Lehner B, Kraus S, Sander PR, Marschallinger J, Rivera FJ, Trümbach D, Ueberham U, Reitsamer HA, Strauss O, Bogdahn U, Couillard-Despres S, Aigner L (2014). TGF-beta signalling in the adult neurogenic niche promotes stem cell quiescence as well as generation of new neurons. J Cell Mol Med vol. 18 (7) pp. 1444-59

Kandasamy M, Couillard-Despres S, Raber KA, Stephan M, Lehner B, Winner B, Kohl Z, Rivera FJ, Nguyen HP, Riess O, Bogdahn U, Winkler J, von Hörsten S, Aigner L (2010). Stem cell quiescence in the hippocampal neurogenic niche is associated with elevated transforming growth factor-beta signaling in an animal model of Huntington disease. J Neuropathol Exp Neurol vol. 69 (7) pp. 717-28

Kandel ER, Schwartz JH, Jessel TM (2000). Principles of Neural Science. McGraw-Hill, 4th Edition

Kempermann G (2002). Why new neurons? Possible functions for adult hippocampal neurogenesis. J Neurosci vol. 22 (3) pp. 635-8

Kempermann G (2006). Adult neurogenesis: stem cells and neuronal development in the adult brain. Oxford University Press, 426 pagine

Kempermann G (2011). Adult Neurogenesis 2. New York, NY: Oxford University Press.

Kempermann G (2012). New neurons for 'survival of the fittest'. Nat Rev Neurosci. Oct;13(10):727-36.

Kempermann G, Fabel K, Ehninger D, Babu H, Leal-Galicia P, Garthe A, Wolf SA (2010). Why and how physical activity promotes experience-induced brain plasticity. Frontiers in Neuroscience; 4:189.

Kempermann G, Song H, Gage FH (2015). Neurogenesis in the Adult Hippocampus. Cold Spring Harb Perspect Biol

Koehl M, Meerlo P, Gonzales D, Rontal A, Turek FW, Abrous DN (2008). Exercise-induced promotion of hippocampal cell proliferation requires beta-endorphin. FASEB J vol. 22 (7) pp. 2253-62

Kojima S, Vignjevic D, Borisy GG (2004). Improved silencing vector co-expressing GFP and small hairpin RNA. BioTechniques vol. 36 (1) pp. 74-9

Kronenberg G, Reuter K, Steiner B, Brandt MD, Jessberger S, Yamaguchi M, Kempermann G (2003). Subpopulations of proliferating cells of the adult hippocampus respond differently to physiologic neurogenic stimuli. J Comp Neurol vol. 467 (4) pp. 455-63

Leasure J and Jones M (2008). Forced and voluntary exercise differentially affect brain and behavior. Neuroscience

Lee E and Son H (2009). Adult hippocampal neurogenesis and related neurotrophic factors. BMB reports

Lee HG, Ueda M, Zhu X, Perry G, Smith MA (2006). Ectopic expression of phospho-Smad2 in Alzheimer's disease: uncoupling of the transforming growth factor-beta pathway? J Neurosci Res vol. 84 (8) pp. 1856-61

Leuner B, Gould E, Shors TJ (2006). Is there a link between adult neurogenesis and learning? Hippocampus vol. 16 (3) pp. 216-24

Li L and Xie T (2005). Stem cell niche: structure and function. Annu. Rev. Cell Dev. Biol. 21:605-31

Lim DA and Alvarez-Buylla A (2014). Adult neural stem cells stake their ground. Trends Neurosci vol. 37 (10) pp. 563-71

Liu F, Pouponnot C, Massagué J (1997). Dual role of the Smad4/DPC4 tumor suppressor in TGFbeta-inducible transcriptional complexes. Genes Dev vol. 11 (23) pp. 3157-67

Liu L, Liu X, Ren X, Tian Y, Chen Z, Xu X, Du Y, Jiang C, Fang Y, Liu Z, Fan B, Zhang Q, Jin G, Yang X, Zhang X (2016). Smad2 and Smad3 have differential sensitivity in relaying TGFβ signaling and inversely regulate early lineage specification. Sci Rep vol. 6 pp. 21602

Liu YF, Chen HI, Yu L, Kuo YM, Wu FS, Chuang JL, Liao PC, Jen CJ (2008). Upregulation of hippocampal TrkB and synaptotagmin is involved in treadmill exercise-enhanced aversive memory in mice. Neurobiol Learn Mem vol. 90 (1) pp. 81-9

Livak and Schmittgen (2001). Analysis of relative gene expression data using real-time quantitative PCR and the 2(-Delta Delta C(T)) Method. Methods vol. 25 (4) pp. 402-8

Llorens-Martín M, Torres-Alemán I, Trejo JL (2006). Pronounced individual variation in the response to the stimulatory action of exercise on immature hippocampal neurons. Hippocampus 16, 480–490.

Llorens-Martín M, Torres-Alemán I, Trejo JL (2009). Mechanisms mediating brain plasticity: IGF1 and adult hippocampal neurogenesis. Neuroscientist vol. 15 (2) pp. 134-48

Llorens-Martín M, Tejeda GS, Trejo JL (2010). Differential regulation of the variations induced by environmental richness in adult neurogenesis as a function of time: a dual birthdating analysis. PLoS ONE vol. 5 (8) pp. e12188

Lorente de Nó (1934). Studies on the structure of the cerebral cortex. II. Continuation of the study of the ammonic system. Journal für Psychologie und Neurologie

Luo J, Lin AH, Masliah E, Wyss-Coray T (2006). Bioluminescence imaging of Smad signaling in living mice shows correlation with excitotoxic neurodegeneration. Proc Natl Acad Sci USA vol. 103 (48) pp. 18326-31

Luwor RB, Kaye AH, Zhu HJ (2008). Transforming growth factor-beta (TGF-beta) and brain tumours. J Clin Neurosci vol. 15 (8) pp. 845-55

Marosi K and Mattson MP (2014). BDNF mediates adaptive brain and body responses to energetic challenges. Trends Endocrinol Metab vol. 25 (2) pp. 89-98

Marr D (1970). A theory for cerebral neocortex. Proceedings of the Royal Society of B. Volume 176, issue 1043**.**

Massagué J (2000). How cells read TGF-beta signals. Nat Rev Mol Cell Biol vol. 1 (3) pp. 169-78

Massagué J, Seoane J, Wotton D (2005). Smad transcription factors. Genes Dev vol. 19 (23) pp. 2783-810

Mirzadeh Z, Merkle FT, Soriano-Navarro M, Garcia-Verdugo JM, Alvarez-Buylla A (2008). Neural stem cells confer unique pinwheel architecture to the ventricular surface in neurogenic regions of the adult brain. Cell Stem Cell vol. 3 (3) pp. 265-78

Morrens J, Van Den Broeck W, Kempermann G (2012). Glial cells in adult neurogenesis. Glia vol. 60 (2) pp. 159-74

Muñoz MD, Antolín-Vallespín M, Tapia-González S, Sánchez-Capelo A (2016). Smad3 deficiency inhibits dentate gyrus LTP by enhancing GABAA neurotransmission. J Neurochem vol. 137 (2) pp. 190-9

Nam SM, Kim JW, Yoo DY, Yim HS, Kim DW, Choi JH, Kim W, Jung HY, Won MH, Hwang IK, Seong JK, Yoon YS (2014). Physical exercise ameliorates the reduction of neural stem cell, cell proliferation and neuroblast differentiation in senescent mice induced by D-galactose. BMC Neurosci vol. 15 pp. 116

Nestler EJ (2009). Epigenetic mechanisms in psychiatry. Biol Psychiatry vol. 65 (3) pp. 189-90

Nomura M and Li E (1998). Smad2 role in mesoderm formation, left-right patterning and craniofacial development. Nature vol. 393 (6687) pp. 786-90

O'Keefe J and Nadel L (1979). The hippocampus as a cognitive map. Behavioral and Brain Sciences

Olson AK, Eadie BD, Ernst C, Christie BR (2006). Environmental enrichment and voluntary exercise massively increase neurogenesis in the adult hippocampus via dissociable pathways. Hippocampus vol. 16 (3) pp. 250-60

Pan YW, Storm DR, Xia Z (2013). Role of adult neurogenesis in hippocampus-dependent memory, contextual fear extinction and remote contextual memory: new insights from ERK5 MAP kinase. Neurobiol Learn Mem vol. 105 pp. 81-92

Paxinos G and Franklin KBJ (2004). The mouse brain in stereotaxic coordinates. Gulf Professional Publishing

Peake JM, Markworth JF, Nosaka K, Raastad T, Wadley GD, Coffey VG (2015). Modulating exercise-induced hormesis: Does less equal more? J Appl Physiol vol. 119 (3) pp. 172-89

Pérez-Domper P, Gradari S, Trejo JL (2013). The growth factors cascade and the dendrito-/synapto-genesis versus cell survival in adult hippocampal neurogenesis: the chicken or the egg. Ageing research reviews vol. 12 (3) pp. 777-85

Radak Z, Chung HY, Koltai E, Taylor AW, Goto S (2008). Exercise, oxidative stress and hormesis. Ageing research reviews vol. 7 (1) pp. 34-42

Ramsden M, Berchtold NC, Patrick Kesslak J, Cotman CW, Pike CJ (2003). Exercise increases the vulnerability of rat hippocampal neurons to kainate lesion. Brain Res vol. 971 (2) pp. 239-44

Redish AD and Touretzky DS (1997). Cognitive maps beyond the hippocampus. Hippocampus vol. 7 (1) pp. 15-35

Romano MF (2009). Targeting TGFbeta-mediated processes in cancer. Curr Opin Drug Discov Devel vol. 12 (2) pp. 253-63

Schouten M, Buijink MR, Lucassen PJ, Fitzsimons CP (2012). New Neurons in Aging Brains: Molecular Control by Small Non-Coding RNAs. Front Neurosci vol. 6 pp. 25

Shi Y, Wang YF, Jayaraman L, Yang H, Massagué J, Pavletich NP (1998). Crystal structure of a Smad MH1 domain bound to DNA: insights on DNA binding in TGF-β signalling. Cell 94(5):585-94.

Shihabuddin LS, Horner PJ, Ray J, Gage FH (2000). Adult spinal cord stem cells generate neurons after transplantation in the adult dentate gyrus. J Neurosci vol. 20 (23) pp. 8727-35

Snyder JS, Glover LR, Sanzone KM, Kamhi JF, Cameron HA (2009). The effects of exercise and stress on the survival and maturation of adult-generated granule cells. Hippocampus vol. 19 (10) pp. 898-906

Squire LR (1992a). Memory and the hippocampus: a synthesis from findings with rats, monkeys, and humans. Psychol Rev vol. 99 (2) pp. 195-231

Squire LR (1992b). Declarative and non declarative memory: Multiple brain systems supporting learning and memory. Cognitive Neuroscience

Stegmüller J, Huynh MA, Yuan Z, Konishi Y, Bonni A (2008). TGFbeta-Smad2 signaling regulates the Cdh1-APC/SnoN pathway of axonal morphogenesis. J Neurosci vol. 28 (8) pp. 1961-9

Stipursky J, Francis D, Gomes FC (2012). Activation of MAPK/PI3K/SMAD pathways by TGF-β(1) controls differentiation of radial glia into astrocytes in vitro. Dev Neurosci vol. 34 (1) pp. 68-81

Stranahan AM, Khalil D, Gould E (2006). Social isolation delays the positive effects of running on adult neurogenesis. Nat Neurosci vol. 9 (4) pp. 526-33

Suzuki WA and Eichenbaum H (2000). The neurophysiology of memory. Ann N Y Acad Sci vol. 911 pp. 175-91

Tapia-González S, Muñoz MD, Cuartero MI, Sánchez-Capelo A (2013). Smad3 is required for the survival of proliferative intermediate progenitor cells in the dentate gyrus of adult mice. Cell Commun Signal vol. 11 pp. 93

Tomporowski PD (2003). Effects of acute bouts of exercise on cognition. Acta Psychol (Amst) vol. 112 (3) pp. 297-324

Trejo JL, Carro E, Torres-Aleman I (2001). Circulating insulin-like growth factor I mediates exercise-induced increases in the number of new neurons in the adult hippocampus. J Neurosci vol. 21 (5) pp. 1628-34

Tremblay KD, Hoodless PA, Bikoff EK, Robertson EJ (2000). Formation of the definitive endoderm in mouse is a Smad2-dependent process. Development vol. 127 (14) pp. 3079-90

Tronel S, Fabre A, Charrier V, Oliet SH, Gage FH, Abrous DN (2010). Spatial learning sculpts the dendritic arbor of adult-born hippocampal neurons. Proc Natl Acad Sci USA vol. 107 (17) pp. 7963-8

Ueberham U and Arendt T (2013). The Role of Smad Proteins for Development, Differentiation and Dedifferentiation of Neurons. Trends in Cell Signaling Pathways in Neuronal Fate Decision, Dr Sabine Wislet-Gendebien (Ed.), InTech, DOI: 10.5772/54532

Ueberham U, Lange P, Ueberham E, Brückner MK, Hartlage-Rübsamen M, Pannicke T, Rohn S, Cross M, Arendt T (2009). Smad2 isoforms are differentially expressed during mouse brain development and aging. Int J Dev Neurosci vol. 27 (5) pp. 501-10

Ueberham U, Ueberham E, Gruschka H, Arendt T (2006). Altered subcellular location of phosphorylated Smads in Alzheimer's disease. Eur J Neurosci vol. 24 (8) pp. 2327-34

Vaynman S, Ying Z, Gomez-Pinilla F (2004). Hippocampal BDNF mediates the efficacy of exercise on synaptic plasticity and cognition. Eur J Neurosci vol. 20 (10) pp. 2580-90

Wachs FP, Winner B, Couillard-Despres S, Schiller T, Aigner R, Winkler J, Bogdahn U, Aigner L (2006). Transforming growth factor-beta1 is a negative modulator of adult neurogenesis. J Neuropathol Exp Neurol vol. 65 (4) pp. 358-70

Waldrip WR, Bikoff EK, Hoodless PA, Wrana JL, Robertson EJ (1998). Smad2 signaling in extraembryonic tissues determines anterior-posterior polarity of the early mouse embryo. Cell vol. 92 (6) pp. 797-808

Wan YY and Flavell RA (2007). 'Yin-Yang' functions of transforming growth factor-beta and T regulatory cells in immune regulation. Immunol Rev vol. 220 pp. 199-213

Wang L, Nomura M, Goto Y, Tanaka K, Sakamoto R, Abe I, Sakamoto S, Shibata A, Enciso PL, Adachi M, Ohnaka K, Kawate H, Takayanagi R (2011). Smad2 protein disruption in the central nervous system leads to aberrant cerebellar development and early postnatal ataxia in mice. J Biol Chem vol. 286 (21) pp. 18766-74

Wiznerowicz M and Trono D (2003). Conditional suppression of cellular genes: lentivirus vector-mediated drug-inducible RNA interference. J Virol vol. 77 (16) pp. 8957-61

Wotton D, Lo RS, Lee S, Massague J (1999). A Smad transcriptional corepressor. Cell vol. 97 (1) pp. 29-39

Zhong W and Chia W (2008). Neurogenesis and asymmetric cell division. Curr Opin Neurobiol vol. 18 (1) pp. 4-11

Appendix

PUBLICATIONS

Gradari S, Pérez-Domper P, Butler RG, Martínez-Cué C, de Polavieja GG, Trejo JL (2016). The relationship between behavior acquisition and persistence abilities: Involvement of adult hippocampal neurogenesis. Hippocampus Jul;26(7):857-74

Gradari S, Pallé A, McGreevy KR, Fontán-Lozano Á, Trejo JL (2016). Can Exercise Make You Smarter, Happier, and Have More Neurons? A Hormetic Perspective. Front Neurosci vol. 10 pp. 93

Pérez-Domper P, **Gradari S**, Trejo JL (2013). The growth factors cascade and the dendrito-/synapto-genesis versus cell survival in adult hippocampal neurogenesis: the chicken or the egg. Ageing research reviews vol. 12 (3) pp. 777-85